



University  
of Glasgow

Gruenenfelder, Fredrik Ingemar (2012) *Phenotypic analysis of the Plp1 gene overexpressing mouse model #72 : implications for demyelination and remyelination failure*

PhD thesis

<http://theses.gla.ac.uk/3190/>

Copyright and moral rights for this thesis are retained by the author

A copy can be downloaded for personal non-commercial research or study, without prior permission or charge

This thesis cannot be reproduced or quoted extensively from without first obtaining permission in writing from the Author

The content must not be changed in any way or sold commercially in any format or medium without the formal permission of the Author

When referring to this work, full bibliographic details including the author, title, awarding institution and date of the thesis must be given

**Phenotypic analysis of the *Plp1* gene  
overexpressing mouse model #72: Implications  
for demyelination and remyelination failure**

Fredrik Ingemar Gruenenfelder

Dr.med.vet

Submitted in fulfilment of the requirements for the  
Degree of Doctor of Philosophy

College of Medical, Veterinary and Life Sciences  
Institute of Infection, Immunity and Inflammation  
University of Glasgow

February, 2012

©

i

## Abstract

Duplication of the *proteolipid protein (PLP1)* gene, which encodes the most abundant protein of central nervous system (CNS) myelin, is the most common cause of Pelizaeus Merzbacher disease (PMD). Various animal models have been generated to study the effect of *Plp1* gene overexpression on oligodendrocyte and myelin sheath integrity. The #72 line harbours 3 additional copies of the murine *Plp1* gene per haploidic chromosomal set. Homozygous #72 mice appear phenotypically normal until three months of age, after which they develop seizures leading to premature death at around 4 months of age. An earlier study examining the optic nerve showed a progressive demyelination accompanied by marked microglial and astrocytic responses. Using electron microscopy and immunohistochemistry, I demonstrated that initial myelination of the #72 corpus callosum was followed by a progressive demyelination, probably mediated by a distal “dying back” phenomenon of the myelin sheath. No evidence of effective remyelination was observed despite the presence and proliferation of oligodendrocyte progenitor cells (OPCs). A marked increase in density and reactivity of microglia/macrophages and astrocytes, and the occurrence of axonal swellings, accompanied the demyelination. *In situ* and *in vitro* evaluation of adult #72 OPCs provided evidence of impaired OPC differentiation. Transplantation of neurospheres (NS) into adult #72 mouse corpus callosum confirmed that axons were capable of undergoing remyelination. Furthermore, NS transplanted into neonatal CNS integrated into the parenchyma and survived up to 120 days, demonstrating the potential of early cell replacement therapy. Taking advantage of the spatially distinct pathologies between the retinal and chiasmal region of the #72 optic nerve, I evaluated the capability of diffusion weighted MRI to identify lesion type. I found significant differences between #72 and wild type optic nerves, as well as between the two distinct pathological regions within the #72 optic nerve. These results confirm the potential of the #72 mouse to serve as a model to study chronic demyelination. The study also demonstrates the utility of the #72 mouse to evaluate cell transplant strategies for the treatment of chronic CNS white matter lesions and PMD. Additionally, DW MRI has potential as a modality capable of diagnosing myelin-related white matter changes, and may be applicable to the clinical setting.

# List of Contents

List of Contents .....	iii
List of Figures .....	xii
List of Tables .....	xviii
Acknowledgement .....	xxi
1 Introduction.....	1
1.1 Background.....	1
1.2 The central nervous system (CNS).....	2
1.2.1 The neuron.....	3
1.2.2 The axon.....	4
1.2.3 The oligodendrocyte .....	5
1.2.4 The myelin sheath and its adjacent structures .....	5
1.2.5 The oligodendrocyte precursor cell .....	11
1.2.6 The astrocyte .....	12
1.2.7 Microglia .....	13
1.3 Myelination of the CNS.....	16
1.4 The regenerative capacity of the white matter .....	17
1.4.1 Demyelination and remyelination of the CNS .....	18
1.4.2 Successful remyelination is dependent on a finely tuned interaction between oligodendrocyte precursor cell intrinsic and cell extrinsic changes .....	19
1.4.3 The role of OPC intrinsic factors in successful (re)myelination .....	20
1.4.4 Factors in the OPC extrinsic compartment that can disrupt the remyelination process leading to remyelination failure .....	25
1.5 Diseases affecting the myelin sheath .....	30
1.5.1 Models of myelin pathology .....	31
1.5.2 The Leukodystrophies .....	33
1.5.3 Demyelination in <i>Plp1</i> overexpressing mice.....	46

1.6	Use of MRI in diagnosing white matter changes.....	47
1.6.1	The homozygote #72 optic nerve as a model to evaluate the ability of MRI techniques to detect specific white matter pathological states.....	49
1.7	Aim of the thesis .....	50
2	Material and Methods .....	51
2.1	Miscellaneous .....	51
2.2	Mouse breeding.....	51
2.2.1	Animal breeding facilities .....	51
2.2.2	Transgenic mouse lines .....	52
2.2.3	Maintenance of transgenic lines of mice .....	54
2.3	Isolation of nucleic acid .....	59
2.3.1	Tissue biopsy procedure.....	59
2.3.2	Extraction of genomic DNA from tissue.....	59
2.4	PCR Genotyping .....	60
2.4.1	PCR core programme .....	60
2.4.2	Genomic PCR.....	60
2.4.3	DNA electrophoresis.....	61
2.4.4	Identification of CFP expression in Thy-1 CFP mice .....	61
2.4.5	Identification of GFP expression in $\beta$ -actin GFP mice .....	62
2.5	Experimental procedures .....	65
2.5.1	Intraperitoneal injection of 5-bromo-2-deoxyuridine (BrdU) as a marker for cell proliferation.....	65
2.5.2	Cell culture.....	65
2.5.3	Generation of Plp1 Lac-Z expressing neurospheres and generation of $\beta$ -actin GFP expressing neurospheres .....	67
2.5.4	Identification of stereotactic coordinates for corpus callosum cell transplantation .....	69

2.5.5	Surgical procedure and injection of neurospheres into adult homozygote #72 corpus callosum .....	71
2.6	Tissue sampling and processing .....	73
2.6.1	Fixatives .....	73
2.6.2	Fixation technique and processing .....	74
2.6.3	Cryopreservation and sectioning .....	77
2.6.4	Resin processing and sectioning .....	78
2.6.5	Processing of transplanted tissue .....	79
2.7	Staining techniques.....	80
2.7.1	Immunofluorescence .....	80
2.7.2	Light microscopy .....	92
2.7.3	Electron microscopy.....	93
2.8	Morphological studies .....	94
2.8.1	Cell quantification of immunolabelled samples.....	94
2.8.2	Quantification of GFAP positive area in optic nerve after immunolabelling .....	95
2.8.3	Quantification of percentage myelinated axons .....	95
2.8.4	Measurement of cell process length of cultured OPCs.....	96
2.9	Statistical analysis and graphical presentation of the data .....	96
3	The development of the phenotype and pathology of the homozygote #72 corpus callosum .....	97
3.1	Introduction.....	97
3.2	Aims .....	100
3.3	Material and Methods .....	100
3.3.1	Animals.....	100
3.3.2	Intraperitoneal BrdU injection for OPC proliferation studies .....	100
3.3.3	Tissue sampling and processing for histopathological examination. ....	101
3.3.4	Tissue sectioning.....	101

3.3.5	Quantification of percentage myelinated axons .....	101
3.3.6	Markers used for evaluation of the corpus callosum.....	102
3.3.7	Statistical analysis .....	103
3.4	Results .....	104
3.4.1	Extensive myelin degradation was observed in the #72 homozygote corpus callosum .....	104
3.4.2	The corpus callosum is almost completely demyelinated at P120 in the #72 mouse.....	107
3.4.3	Mature oligodendrocytes were present in the demyelinating #72 homozygote corpus callosum .....	111
3.4.4	Oligodendrocyte precursor cells were abundantly present in the #72 corpus callosum.....	113
3.4.5	Characterisation of OPC response during progressive myelin loss ..	116
3.4.6	Astrocytic response during demyelination of the #72 homozygote corpus callosum .....	124
3.4.7	Immune cell response in the #72 homozygote corpus callosum.....	127
3.4.8	Progressive demyelination and inflammation is associated with axonal swelling in the #72 homozygote corpus callosum .....	134
3.4.9	Axonal density in the #72 homozygote was unaltered compared to the wild type corpus callosum.....	137
3.4.10	Demyelination and remyelination failure was not caused by Caspase3 mediated cell apoptosis .....	139
3.4.11	OPC cell differentiation inhibition: an in situ screening of OPC intrinsic and extrinsic factors known to be involved in remyelination failure.....	141
3.5	Discussion .....	151
3.5.1	Progressive demyelination was accompanied by remyelination failure in the #72 homozygote corpus callosum .....	151
3.5.2	Potential inhibitors of OPC differentiation .....	154

3.6	Conclusion.....	161
4	An evaluation of cell intrinsic and cell extrinsic factors that contribute to remyelination failure .....	162
4.1	Introduction.....	162
4.2	Aims of the study .....	165
4.3	Material and Methods .....	166
4.3.1	Mouse colony .....	166
4.3.2	Identification of GFP expression in the <i>β-actin-GFP</i> expressing line.....	166
4.3.3	Isolation and culture of adult and neonate OPCs from the corpus callosum for culture .....	166
4.3.4	Generation of <i>Plp1 Lac-Z</i> and <i>β-actin GFP</i> expressing neurospheres.....	167
4.3.5	Preparation of neurosphere for transplantation.....	167
4.3.6	Adult mice used in the transplant study .....	167
4.3.7	Neonate mice used in the transplant study.....	168
4.3.8	Processing of cell cultures and transplanted tissue .....	168
4.3.9	Measurement of oligodendrocytic processes from co-cultured OPCs.....	168
4.3.10	Statistical analysis .....	169
4.4	Results .....	169
4.4.1	Evaluation of the differentiation potential of OPCs using an <i>in vitro</i> co-culture system.....	169
4.4.2	Evaluating the cell extrinsic compartment: Cell transplantation into demyelinated corpus callosum .....	175
4.4.3	Long term survival and integration of transplanted wild type neurospheres after neonatal cell transplantation into CNS parenchyma.....	185
4.5	Discussion .....	192
4.5.1	Impaired OPC differentiation is age dependent in #72 mouse.....	192
4.5.2	The adult #72 homozygote corpus callosum is permissive for (re)myelination when neurospheres are transplanted. ....	196

4.5.3	Early post natal transplanted gene wild type neurospheres integrate and form a stable myelinating cell population in the #72 CNS - a potential treatment for PMD.....	200
4.6	Conclusion.....	202
5	Evaluation of advanced diffusion weighted magnetic resonance imaging as a molecular probe to distinguish between acute and chronic demyelination in the optic nerve of the #72 mouse.....	204
5.1	Introduction.....	204
5.1.1	The impact of conventional magnetic resonance imaging in diagnosing central nervous system white matter changes.....	204
5.1.2	The use of diffusion weighted imaging of central nervous system white and grey matter in the research and clinical settings .....	205
5.1.3	Diffusion tensor imaging and its application in investigating central nervous system white matter physiology and pathology .....	206
5.1.4	Multiexponential signal decay - an opportunity to differentiate between inflammation with acute demyelination and chronic silent demyelination? .....	210
5.1.5	The #72 mouse optic nerve as a model system in which to assess the potential of DWI to distinguish complete demyelination from inflammatory demyelination.....	212
5.2	The aims of the chapter .....	213
5.3	Material and Methods .....	213
5.3.1	Breeding and identification of homozygote #72 mice .....	213
5.3.2	Coil and sample holder design for mouse optic nerve DWI .....	213
5.3.3	Preparation of optic nerves for DW MRI scan.....	216
5.3.4	Instrumentation .....	219
5.3.5	Scan protocol .....	219
5.3.6	Processing and analysis of DWI data.....	220
5.3.7	Conventional analysis of the data using two <i>b</i> -values only .....	220

5.3.8	Analysis of the data using multiple increasing <i>b</i> -values .....	221
5.3.9	Tissue sampling for histological examination .....	224
5.3.10	Primary antibodies for characterisation of cell types in the optic nerve .....	224
5.3.11	Secondary antibodies .....	224
5.3.12	Quantification of cell densities.....	225
5.3.13	Statistics .....	225
5.4	Results .....	225
5.4.1	Good signal quality was obtained from the scanned optic nerves...	226
5.4.2	Analysis of the data using two <i>b</i> -values .....	226
5.4.3	Analysis of the data using multiple increasing <i>b</i> -values.....	232
5.4.4	Histological examination of optic nerves confirmed the spatially distinct regions of silent demyelination and active inflammatory demyelination in the scanned regions of #72 mouse optic nerves..	239
5.5	Discussion .....	252
5.5.1	Distinct changes in parallel and perpendicular fast and slow diffusion become apparent .....	253
5.5.2	The basis of anisotropic diffusion and the relation of diffusion changes to white matter disease .....	253
5.5.3	Changes in “conventional” DW MRI parameters distinguish lesion types in the optic nerve .....	255
5.5.4	Multiexponential signal decay becomes apparent after applying multiple increasing high <i>b</i> -values to the DWI .....	259
5.6	Conclusion.....	262
6	Final discussion and future experiments.....	264
6.1	The #72 mouse as a model for chronic demyelination .....	265
6.2	<i>In vitro</i> systems to investigate cell intrinsic pathways .....	266
6.3	Evaluation of OPC extrinsic changes in relation to remyelination failure .....	269

6.3.1	The role of the microglial/macrophage response in the pathogenesis of remyelination failure in the #72 mouse .....	269
6.3.2	The extracellular matrix - impact on myelin repair and beyond ....	270
6.4	Axonal pathology as a consequence of <i>Plp1</i> gene overexpression ..	270
6.5	The use of stem cells in long term myelin repair.....	271
6.6	Diffusion weighted imaging in myelin disorders .....	272
6.7	The use of demyelinating models in investigating psychiatric disorders.....	272
6.8	Summary.....	273
7	Appendix.....	274
7.1	Fixatives .....	274
7.1.1	Periodate lysine paraformaldehyde .....	274
7.1.2	4% Paraformaldehyde in PBS .....	274
7.1.3	Karnovsky's modified fixative (paraformaldehyde / glutaraldehyde 4% / 5%).....	275
7.2	Tissue Processing .....	276
7.2.1	Resin processing.....	276
7.3	Staining protocols.....	279
7.3.1	Immunohistochemistry using methanol for cell membrane penetration .....	279
7.3.2	Immunohistochemistry using Triton-X 100 for cell membrane penetration .....	280
7.3.3	X-gal staining.....	280
7.3.4	Staining for electron microscopy .....	281
7.4	Staining solutions .....	282
7.4.1	Methylene blue / azur II .....	282
7.5	Media for cell culture .....	282
7.5.1	Differentiation media with insulin (50 ml).....	282

7.5.2	N1 mix (25ml) .....	282
7.5.3	Neurosphere media (50 ml).....	283
8	Abbreviations .....	284
9	Reference list.....	287

## List of Figures

Figure 1. White matter at a glance.....	15
Figure 2. Organisation of the murine <i>Plp1</i> gene and its major transcription products. ....	35
Figure 3. Schematic representation of the <i>Plp1</i> #72 transgene.....	57
Figure 4. Schematic representation of CFP and GFP transgene constructs. ....	58
Figure 5. Schematic representation of the LacZ transgene construct. ....	58
Figure 6. Representative image of a gel after electrophoresis with twelve PCR products, each from an individual mouse ear sample. ....	63
Figure 7. Identification of CFP expression was made on fresh ear biopsies. ....	64
Figure 8. Identification of the corpus callosal region for histopathological characterisation and potential external modulation. ....	70
Figure 9. Correct needle placement is of major importance to achieve optimal perfusion of the specimen. ....	75
Figure 10. #72 homozygote mice were identified by progressive macroscopic changes in the optic nerve, which correlated with the degree of demyelination. ....	75
Figure 11. Progressive reduction in myelin staining in the #72 corpus callosum. ....	105
Figure 12. Progressive loss of PLP/DM20 staining in the #72 corpus callosum. ....	106
Figure 13. Progressive demyelination follows initial myelination of the #72 homozygote corpus callosum. ....	108
Figure 14. Initial myelination of the #72 mouse corpus callosum was followed by progressive demyelination. ....	109

Figure 15. Demyelination progresses with increasing age in the corpus callosum. ....	110
Figure 16. Mature oligodendrocytes were present at all time points during demyelination. ....	112
Figure 17. NG2+ cells were present in the #72 mouse corpus callosum during all stages of demyelination. ....	114
Figure 18. NG2+ cells in the #72 mouse corpus callosum between P40 and P120. ....	115
Figure 19. PDGFR $\alpha$ positive cells in the demyelinating #72 mouse corpus callosum. ....	115
Figure 20. Cell proliferation occurred in response to demyelination. ....	117
Figure 21. OPC proliferation occurred in association with progressive demyelination. ....	118
Figure 22. All variants of subcellular Olig1 localisation in NG2+ cells were found in the #72 mouse during demyelination. ....	120
Figure 23. Different subcellular Olig1 localisation was observed in NG2 negative cells. ....	121
Figure 24. The subcellular distribution of Olig1 in #72 mouse NG2 +ve cells. ....	123
Figure 25. A progressive astrocytic response accompanied demyelination in the #72 mouse corpus callosum. ....	125
Figure 26. Astrocyte cell density is increased in the #72 mouse corpus callosum. ....	126
Figure 27. A marked increase in microglial/macrophages accompanies progressive demyelination. ....	129
Figure 28. Microglial/macrophage cell density increases progressively in the #72 homozygote corpus callosum. ....	130

Figure 29. Sialoadhesin expressing cells were found in the demyelinating corpus callosum.....	131
Figure 30. The density of activated microglial/macrophages is progressively increased in the #72 mouse corpus callosum. ....	132
Figure 31. T cell infiltration accompanied progressive demyelination and activation of the microglial/macrophage cell population.....	133
Figure 32. Axonal changes increased with progressive demyelination and inflammation. ....	135
Figure 33. Axonal swellings as a sign of axonal injury were increasingly present with progressive demyelination and inflammation.....	136
Figure 34. Axonal density was not reduced in the demyelinated corpus callosum of the #72 mouse. ....	138
Figure 35. Caspase3 mediated cell apoptosis was not detected in the #72 homozygote corpus callosum. ....	140
Figure 36. Activation of the canonical Wnt pathway was present at time points where OPC proliferation was upregulated. ....	143
Figure 37. Axin2 is located in cells originating from the oligodendroglial lineage.....	144
Figure 38. Hyaluronan accumulation was identified in the demyelinated corpus callosum at P120. ....	146
Figure 39. PSA-NCAM expression was detected on astrocytes and not on axons in the #72 mouse corpus callosum.....	148
Figure 40. The microglia/macrophage population did not express D3 in the adult, chronically demyelinated #72 homozygote corpus callosum.....	150
Figure 41. OPCs were successfully isolated from adult corpus callosum using a Percoll® gradient technique. ....	171

Figure 42. Microglial/macrophage contamination could not be prevented when using the Percoll® gradient protocol to purify adult #72 homozygote OPCs. ....	172
Figure 43. The cell process length of adult #72 homozygote OPCs was significantly reduced when compared to the co-cultured wild type OPCs. ....	173
Figure 44. The mean total process length of neonatal #72 and wild type OPCs was not significantly different after 7 days in vitro. ....	174
Figure 45. Pronounced changes in myelin integrity and astroglial, microglial and OPC populations were present in the #72 mouse corpus callosum at P100. ....	176
Figure 46. LacZ transgene expressing neurospheres are multipotent and develop into oligodendrocytes, astrocytes and neurons in vitro.	177
Figure 47. Transplanted neurospheres survived and (re)myelinated axons in the adult chronically demyelinated #72 homozygote corpus callosum. ....	180
Figure 48. Neurospheres formed myelin sheaths after transplantation into the adult #72 corpus callosum. ....	181
Figure 49. Formation of normal compact myelin sheaths 14 days after neurosphere transplantation into #72 homozygote corpus callosum. ....	182
Figure 50. Transplanted neurospheres also differentiated into astroglia...	184
Figure 51. Successful integration, ensheathment/myelination and long term survival of neurospheres after intracerebral transplantation into neonatal #72 homozygote mice. ....	187
Figure 52. A large amount of transplant-derived myelin is present in regions of the adult #72 mouse corpus callosum after transplantation of neurospheres into the neonatal brain. ....	188

Figure 53. The cell density appeared normal in white matter regions where donor cells populated and myelinated the white matter. ....	190
Figure 54. The inflammatory response was reduced in white matter regions if the #72 CNS was populated by transplanted, Plp1 expressing oligodendroglia.....	191
Figure 55. Examples of anisotropic and isotropic diffusion.....	209
Figure 56. Image of the purpose built transmit/receive coil. ....	215
Figure 57. Image of the optic nerve sample holder used for the diffusion weighted imaging experiment. ....	215
Figure 58. Image of the sample holder filled with seven microtubes, each containing one optic nerve or just PBS/Multihance.....	218
Figure 59. Image of a sealed sample holder containing optic nerves ready to be placed into the coil for scanning. ....	218
Figure 60. Illustration of the two components identified after applying the curve fitting routine on the signal decay curve obtained from multiple increasing <i>b</i> -values. ....	223
Figure 61. Good signal to noise ratio was achieved with the purpose built coil. ....	227
Figure 62. Fractional anisotropy was reduced in both #72 optic nerve regions, compared to wild type. ....	228
Figure 63. Mean diffusion was increased in the #72 mouse optic nerve. ...	228
Figure 64. Perpendicular apparent diffusion coefficient was increased in the #72 optic nerve.....	230
Figure 65. Parallel apparent diffusion coefficient was increased in the retinal, but not the chiasmal region of the #72 nerve, compared to wild type.....	231

Figure 66. Biexponential signal decay became apparent with increasing <i>b</i> -values. ....	233
Figure 67. Perpendicular slow diffusion was increased in #72 nerves compared to wild type. ....	235
Figure 68. Parallel slow diffusion was increased in the #72 nerve compared to wild type. ....	236
Figure 69. The contribution of fast diffusion ( $\alpha$ ) was increased in the #72 optic nerve. ....	238
Figure 70. The #72 mouse optic nerve was almost completely demyelinated at P120. ....	241
Figure 71. Cell density was markedly increased in the #72 chiasmal section of optic nerve. ....	242
Figure 72. The density of CD45 +ve microglia/macrophages was increased in the chiasmal portion of the #72 mouse optic nerve. ....	243
Figure 73. The #72 mouse optic nerve was characterised by a marked astrocytosis. ....	244
Figure 74. Mature oligodendrocyte cell density was reduced in #72 mouse optic nerve. ....	245
Figure 75. Oligodendrocyte precursor cell density was elevated in the inflamed demyelinated chiasmal region of #72 optic nerve. ....	246

## List of Tables

Table 1.	Transgenic animals overexpressing <i>Plp</i> genomic transgenes and human cDNA transgenes (Yool, 2000). .....	44
Table 2.	List of primary antibodies used in all studies. ....	87
Table 3.	List of secondary antibodies used in all studies. ....	88
Table 4.	Intranuclear Olig1 was rarely observed in wild type and #72 homozygote NG2 +ve cells.....	122
Table 5.	Summary of diffusion parameters, calculated from two <i>b</i> -values only.....	248
Table 6.	Summary of #72 diffusion parameters calculated from two <i>b</i> -values only.....	248
Table 7.	Summary of the mean perpendicular fast ( $D_{1\perp}$ ) and slow ( $D_{2\perp}$ ) diffusion values including the percentage of diffusion changes ( $\Delta D_{1\perp}$ and $\Delta D_{2\perp}$ ) between the wild type and the #72 optic nerves. ....	249
Table 8.	Summary of the mean perpendicular fast ( $D_{1\perp}$ ) and slow ( $D_{2\perp}$ ) diffusion values in #72 optic nerves.....	249
Table 9.	Summary of the mean parallel fast ( $D_{1\parallel}$ ) and slow ( $D_{2\parallel}$ ) diffusion values including the percentage of diffusion changes ( $\Delta D_{1\parallel}$ and $\Delta D_{2\parallel}$ ) between the wild type and the #72 optic nerves.....	250
Table 10.	Summary of the mean perpendicular fast ( $D_{1\parallel}$ ) and slow ( $D_{2\parallel}$ ) diffusion values in #72 optic nerves.....	250
Table 11.	Summary of the contribution of fast and slow diffusion (in %) in the perpendicular and parallel direction. ....	251
Table 12.	Summary of the contribution of fast and slow diffusion (in %) in the #72 optic nerves.....	251

## Declaration

GFP expressing neurospheres were generated by Mrs Kalliopi Ioannidou. The purpose built coil was designed and manufactured by James Mullin and Dr. William Holmes. The diffusion weighted imaging sequences were programmed by Dr. William Holmes. MatLab® programing for analysis of diffusion values was performed by Dr. Maria Rosario Lopez-Gonzalez.

I, Fredrik Ingemar Gruenfelder, declare that the rest of the work carried out in this thesis is original and was carried out by myself and has not been present for award or degree at any other university.

Some of the results obtained during the research period have been presented in poster or abstract form or in publications and are listed below:

**F.I. Gruenfelder**, T.J. Anderson, J.A. Barrie, R.J.M. Franklin, K-A. Nave, J. Penderis, J.M. Edgar. Abstract and Poster Presentation: Characterisation of persistent demyelination within the corpus callosum of the *Plp1* gene overexpressing mouse. MS Frontiers Conference 2009, Sofitel London Heathrow, United Kingdom

**F. I. Gruenfelder**, W. M. Holmes, M. R. Lopez-Gonzalez, J. A. Barrie, K-A. Nave, T. J. Anderson, J. Penderis, J. M. Edgar. Abstract and Poster presentation: Ex vivo MRI of optic nerve of a mouse model of Pelizaeus-Merzbacher disease Integrative Mammalian Biology Initiative, Glasgow Showcase Symposium 31st March 2010, Wolfson Medical School Building, University of Glasgow, Glasgow United Kingdom

**F. I. Gruenfelder**, W. Holmes, M.R. Lopez-Gonzalez, J. E. Barrie, T. J. Anderson, J. Penderis, J. M. Edgar. Abstract and oral presentation: Can MRI distinguish between inflammatory and non-inflammatory demyelinating lesions along the optic nerve of a mouse model of Pelizaeus-Merzbacher disease? A comparison of histological measures and MRI data. Young Researcher Vision Camp, Castle Wildenstein, Leibertingen, Germany.

Edgar JM, McCulloch MC, Montague P, Brown AM, Thilemann S, Pratola L, Gruenfelder FI, Griffiths IR, Nave KA, Demyelination and axonal preservation in a transgenic mouse model of Pelizaeus-Merzbacher disease. *EMBO Mol Med.* 2010 Feb; 2(2):42-50.

Gruenfelder FI, Thomson G, Penderis J, Edgar JM, Axon-glia interaction in the CNS: what we have learned from mouse models of Pelizaeus-Merzbacher disease, *J Anat.* 2011 Jul;219(1):33-43

## Acknowledgement

I would like to express my gratitude to my supervisor, Dr. Julia Edgar, who has given me great support and guidance during the whole project and has always been approachable and open for discussions and problem solving. Many thanks also go to my second supervisor, Professor Jacques Penderis, who has been the steady centerpoint during my research and has given me enormous support in medical writing.

Special thanks go to my assessor Professor James T. Anderson, who has helped me in adapting from daily clinical routine to laboratory research practice and has guided me professionally through the three years of research.

I also would like to thank my second assessor, Professor Mhairi McRae for some delightful discussion about stroke research and especially about the importance and the joy of a good balanced between work and life.

Special thanks go out to the applied neurobiology lab members:

Dr. Mark McLaughlin and Dr. Paul Montague for challenging and interesting in depth discussion about biochemical and genetics related issues in myelin and transgenic biology, showing me the joy of „a beer and a curry“ in Glasgow and the introduction into Scottish Football including the unforgettable super score board.

Gemma Thomson, my research pal and the „Queen of myelin culture“ for getting across the wonderful and friendly spirit of the west of Scotland and Kalliopi Ioannidou for all her help in cell culture and the enormous support during the last three years.

Mailis McCulloch and Jennifer Barrie for the endless technical and personal support during my research time and daily life in Scotland.

A special note goes to Marie Ward; you are a star, thank you for all your help in the lab and with Lennart.

Dr. Maria del Rosario Lopez-Gonzalez, Dr. William Holmes and Jim Mullin for MRI and mathematical support.

The generous funding of the veterinary postgraduate school, University of Glasgow enabled me to complete this work.

I am very grateful to Professor Klaus-Armin Nave for the support with the #72 mouse line.

A special note goes to Julie and Bruce Gamble, who took wonderfully care of me and supported me during my time here in Glasgow.

Finally special thanks go to my wife, Saskia who kept up with me and my moods during my time in the lab and during writing and friends and family for help and support.

# 1 Introduction

## 1.1 Background

Central nervous system (CNS) myelin is a lipid rich structure synthesised by oligodendrocytes and wrapped around axons in order to reduce transmembrane capacitance and enable saltatory conduction of the electrical potential. This results in a much higher speed of electrical impulse transmission in myelinated compared to non myelinated axons (Frankenhaeuser, 1952). The importance of myelin is illustrated by the devastating consequences of diseases that affect it. The genetic developmental disorders of myelin, such as the leukodystrophies, are progressive and invariably untreatable debilitating diseases (reviewed in Biffi et al., 2011; Schiffmann and Boespflug-Tanguy, 2001; Schiffmann and van der Knaap, 2004). Pelizaeus-Merzbacher disease (PMD), as a specific example of a leukodystrophy, is caused by a mutation in the *PLP1* gene and spans a wide spectrum of clinical severity, ranging from severe, congenital forms which are incompatible with life, to relatively mild forms with a late onset and a normal life expectancy (reviewed in (Seitelberger, 1995; Yool et al., 2000; Hudson et al., 2004). In the severe congenital form of PMD there is a failure to form normal myelin (dysmyelination), whereas in classical PMD there is a failure to maintain myelin (demyelination).

Multiple sclerosis (MS), the archetypical demyelinating disease, is relatively common, especially among Caucasians (reviewed in Noseworthy et al., 2000). Progressive demyelination leads to chronic disability and, in some cases, to premature death. In general, changes in myelin affect the myelin sheath integrity and lead to neurological dysfunction including motor dysfunction, cognitive dysfunction, seizures, mental health impairment and death, depending on the extent of, and the CNS region affected by, the demyelination.

In MS the histopathological changes are not only restricted to the myelin sheath but also involve the axon. Axonal changes may occur concomitant with inflammatory demyelination or later, possibly as a consequence of chronic

demyelination (Bjartmar et al., 2003;Bjartmar and Trapp, 2003;Dutta and Trapp, 2011). Axonal changes may even occur in some primarily dysmyelinating disorders without demyelination (Edgar et al., 2004b;Griffiths et al., 1998; reviewed in Edgar and Garbern, 2004;Nave, 2010a;Nave, 2010b). The involvement of the axon in disorders primarily affecting the myelin sheath highlights the importance of a normal functioning axonal-glia interaction in order to maintain axonal integrity (reviewed in Nave, 2010a;Nave, 2010b;Gruenenfelder et al., 2011).

Remarkable progress has been made in the diagnosis and monitoring of myelin disorders following the development of magnetic resonance imaging (MRI). The non-invasive nature, superior soft tissue resolution and high sensitivity for detecting pathological changes in soft tissues, compared to other imaging modalities, makes MRI a useful tool to investigate white matter changes and progression *in vivo* (reviewed in Ciumas et al., 2008). However the specificity for determining the lesion type is not high with standard MRI sequences and it is currently not possible to distinguish between acute and chronic demyelination (Bitsch et al., 2001). Diffusion tensor imaging (DTI), which measures the directionality of water diffusion in tissue, is influenced by tissue ultrastructure and allows detection of microstructural changes in white matter tracts. If acute inflammatory demyelination could be distinguished from chronic silent demyelination, it would provide the research and clinical community with invaluable information about disease development and therapy response. Only recently a study by (Xie et al., 2010) has attempted to investigate if DTI detects differences between active demyelination with inflammation and chronic silent demyelination, the two hallmarks of MS lesions.

## **1.2 The central nervous system (CNS)**

The white and grey matter of the CNS differs substantially in cell architecture and function. Astroglia, oligodendroglia, oligodendroglial precursor cells (OPCs) and microglia are distributed throughout the grey and white matter, while neuronal cell bodies with dendrites are predominantly located in the grey matter and axons are largely arranged in parallel bundles in the white matter. In the

brain, the grey matter is macroscopically identified as the cortex or, in deeper structures, as nuclei. The white matter is macroscopically present below the cortex or in between the nuclei.

A magnitude of precisely timed neuronal-neuronal interactions are necessary for normal function of the CNS. To maintain the demand for fast and precise communication between neurons, highly organised and rapid propagation of electrical signals along axons is crucial. The rate of propagation of the electrical potential is dependent on both axonal diameter and myelination status. The larger the axonal diameter, the lower its resistance, and the faster electrical impulses are propagated. The evolution of myelin serves to maximise fast conduction of electrical impulses while minimising the amount of space, which is required to contain the millions of nerve fibres that constitute the vertebrate CNS (Rushton, 1951). With myelination of axons, the necessity for large axonal diameters to enable fast electrical potential transmission is overcome. Saltatory conduction is also highly energy efficient, since action potentials need only be generated at the node of Ranvier, and not constitutively as in non myelinated nerves (reviewed in Rosenbluth et al., 1994).

### **1.2.1 The neuron**

The neuron consists of the cell body, dendrites and one or more axons. The neuronal cell body processes signal inputs and generates the electrical potential at the level of the axonal hillock for signal output. The dendrites conduct inputs to the neuronal cell body and the axons conduct outputs from the cell body to other neurons or (in the peripheral nervous system [PNS]) effector organs. Most of the neurons in the CNS are multipolar; in which multiple dendrites and multiple axons are present in one neuron. Communication between neurons is mediated at synapses, a specialised region where the electrical signal is converted into a chemical signal, affecting the post synaptic/effector neuron. The chemical signal binds to receptors on the postsynaptic membrane, which then produce either an excitatory or inhibitory signal in the target neuron. In some cases direct transmission of the electrical signal between the neurons can occur (Blumenfeld, 2002).

### 1.2.2 The axon

The axon is the long extension of the neuronal cell body that allows information to be transferred over long distances. Axons of projection neurons can extend for up to several feet. Axonal diameter varies between axons, with the average diameter in the CNS being around 1 $\mu$ m. In general, the diameter is constant along the entire axon (Friede and Samorajski, 1970), except at nodal regions. The electrical compound potential generated at the axonal hillock is conducted along the axon to the presynaptic membrane (reviewed in Hildebrand et al., 1993; Blumenfeld, 2002). Most CNS axons have a diameter larger than 0.2 $\mu$ m and are myelinated (reviewed in Hildebrand et al., 1993).

The axolemma, or axonal membrane is a lipid bilayer and maintains the resting potential of the axon (reviewed in Hildebrand et al., 1993). The molecules in the axolemma are also responsible for action potential generation and propagation. In the myelinated axon there is an accumulation of electron microscopy (EM) dense structures in the axolemma of the axonal hillock and at the level of the node of Ranvier, which are related to ion channels (Rosenbluth, 2009). Actin filaments located beneath provide support to the axolemma. In the cytosol, there is a dense network of neurofilaments and microtubules (Amos and Amos, 1987). The neurofilaments, which are 10 nm thick unbranched fibres, give the axon structure and stability (Brady et al., 1999). Neurofilaments become phosphorylated during the myelination process and this increases filament spacing, concomitantly increasing axonal diameter. Microtubules are 25nm thick unbranched tubes, consisting of heterodimers of  $\alpha$  - and  $\beta$  tubulin (Brady et al., 1999). Microtubules are utilised by molecular motor proteins for the anterograde and retrograde transport of organelles. This is an important transport mechanism since most of the transcriptional entities of the neuron are located in the cell body or synapses. The axons itself is dependent on the synthesis and transport of cellular products from the cell body. In the cytosol, mitochondria are found along the entire axon and are also transported in both directions on the microtubular system to supply the axon with adenosine triphosphate (ATP).

### 1.2.3 The oligodendrocyte

The oligodendrocyte is a multiprocess-bearing cell that forms the CNS myelin sheath. Oligodendrocytes are located in the grey and white matter, with the highest density in the white matter ranging between 350 - 1000/mm<sup>2</sup>, depending on the white matter tract and the thickness of the tissue section in which density is measured (see [Chapter 5](#) and Al-Saktawi et al., 2003). The oligodendrocyte is metabolically highly active during myelination, and a single oligodendrocyte can synthesise up to 50,000µm<sup>2</sup> of membrane per day (reviewed in Pfeiffer et al., 1993). One single oligodendrocyte can produce and maintain up to 60 individual myelin sheaths (reviewed in Hildebrand et al., 1993). The advantage of myelination is clear (see above). The disadvantage is the vulnerability of the complex myelin sheath to injury (reviewed in Hildebrand et al., 1993).

### 1.2.4 The myelin sheath and its adjacent structures

The myelin sheath is not a continuous structure and multiple myelin sheaths align along one axon. Individual oligodendrocyte processes wrap multiple times around an axonal segment; in some cases up to 160 times (Hildebrand et al., 1993), to form the compact myelin sheath. The lateral and longitudinal dimensions of the myelin sheath segment are directly coupled to the axon diameter. In general this results in a ratio between axon diameter and fibre diameter (G-ratio) of approximately 0.6; the optimal ratio for maximal conduction velocity (Hildebrand and Hahn, 1978). Between each myelin sheath segment there is a gap of 0.8 - 0.9µm, which is referred to as the node of Ranvier (Hildebrand and Waxman, 1984). There are four distinct regions which can be distinguished along a myelinated axonal segment: the internodal segment, the node or Ranvier, the paranode and the juxtaparanode.

The internodal segment is the unit between the lateral edges of each myelin sheath. The length of an internodal segment varies in the CNS but increases in general with larger diameters and ranges between 100 to 1700µm (Hildebrand et al., 1993).

The node of Ranvier, which is not covered by the myelin sheath, contains various voltage gated sodium channels. The node is mainly responsible for the generation of the action potential for the saltatory conduction but also interact with oligodendrocytes and OPCs (reviewed in Salzer, 2003).

The paranode, which is adjacent to the node, constitutes of non-compact myelin loops, which interact with the axolemma. The axolemmal cis complex, which is composed of caspr and contactin, interacts with the glial expressed NF155 and is believed to regulate junction development and stabilisation (reviewed in Salzer, 2003;Nave, 2010a). The interaction between caspr/contactin and NF155 is also believed to influence axon-glial communication (reviewed in Salzer, 2003;Nave, 2010a).

The juxtaparanode mainly harbours voltage gated Kv 1.1/1.2 potassium channels and Caspr2 expressed on the axolemma. The glial expressed Tag-1 protein forms a cis complex with Caspr2. The function of the juxtaparanode is believed to prevent hyperexcitation and backfiring of action potentials (reviewed in Salzer, 2003;Nave, 2010a).

#### **1.2.4.1 Myelin ultrastructure**

The concentric layers of the oligodendrocyte process as it wraps around the axon gives myelin an ordered structure. Between the cytoplasmic surfaces of each wrap, the major dense line forms when cytoplasm is extruded and the myelin sheath compacts. Between the extracellular surfaces of consecutive wraps of compact myelin lies a 2 nm thick space, called the intraperiod line or space. The distance between two adjacent major dense lines is defined as one myelin period and, in CNS tissue processed for EM, measures 15.65nm (Agrawal et al., 2009;Hildebrand et al., 1993;Edgar and Griffiths, 2009). The outermost rim of the oligodendrocyte process is a cytoplasm-filled channel that forms the inner and outer tongues and the paranodal loops of each myelin sheath segment. Together, these constitute non-compact myelin. At the paranode, the myelin sheath is attached by transverse bands to the axolemma (reviewed in Edgar and Griffiths, 2009). Finally, the radial component which appears as a dense

thickening in consecutive intraperiod lines in electron micrographs, spans the whole or part of the compact myelin, and represents the tight junctions (Hildebrand and Mohseni, 2005; Kosaras and Kirschner, 1990).

#### **1.2.4.2 Biochemical composition of myelin**

Biochemical and histochemical analysis of the myelin sheath have identified multiple proteins and lipids. Proteins account for about 30% of the myelin dry mass. The most abundant protein is proteolipid protein (PLP) and its isoform DM20, followed by myelin basic protein (MBP). Less abundant proteins include myelin associated oligodendrocytic basic protein (MOBP), 2'-3'-cyclic nucleotide-3'-phosphodiesterase (CNP), myelin associated glycoprotein (MAG) and Claudin 11. Small amounts of myelin/oligodendrocyte protein (MOG) and oligodendrocyte myelin glycoprotein (OMpg) are also present. Recently a large number of myelin proteins were identified using mass spectrometry (Jahn et al., 2009).

Lipids account for approximately 70% of the dry mass of myelin (Norton, 1984). Four main classes are histochemically identifiable including galactosphingolipids (cerebrosides and their sulphated derivatives, sulfatides); sterols, mainly cholesterol; phospholipids; and plasmalogens (Bosio et al., 1998; Saher et al., 2011).

##### **1.2.4.2.1 *Myelin Proteins***

###### **1.2.4.2.1.1 *Proteolipid Protein/DM20 (PLP/DM20)***

PLP and its isoform DM20 is the major myelin protein in the CNS. Recent proteomics studies suggest that together, PLP/DM20 account for around 17% of all myelin protein (Jahn et al., 2009). PLP and DM20 are predicted to be tetraspan proteins. DM20 differs from PLP in that it lacks 35 amino acids in the second intracellular loop. Prior to myelination, DM20 is the predominant isoform in the CNS. Once myelination is initiated, PLP becomes the predominant form. The role of PLP/DM20 in CNS myelin is still not fully understood, but it has been

shown to be important for formation and maintenance of the intraperiod line of compact CNS myelin (Klugmann et al., 1997) and for the transport of other proteins into compact myelin (Werner et al., 2007). More detail about the proteolipid protein gene structure and function are found in [1.5.2.1 The proteolipid protein gene in the CNS: normal structure, function and the role in the aetiology of Pelizaeus-Merzbacher disease.](#)

#### **1.2.4.2.1.2 Myelin basic protein (MBP)**

MBP is the second most abundant myelin protein. Its relative contribution to the total myelin protein content is about 8% (Jahn et al., 2009). MBP is a cytoplasmic protein mainly located in the major dense line. There are at least five isoforms which become upregulated during myelination (reviewed in Campagnoni and Skoff, 2001). It has been demonstrated that the *Mbp* gene is part of a larger gene complex, the gene of oligodendrocyte lineage (*Golli-Mbp* gene). GOLLI-MBP proteins are only expressed at a low level in the CNS. However GOLLI-MBP products have been found in T-cells and macrophages in the thymus and are believed to play a role in the induction of experimental autoimmune encephalitis (EAE) (reviewed in (Campagnoni and Skoff, 2001). In the CNS, MBP is responsible for the fusion of the two cytoplasmic myelin sheath membrane surfaces, forming the major dense line. MBP has also been demonstrated to stabilise microtubules in differentiating oligodendrocytes (Galiano et al., 2006). Lack of MBP function in the naturally occurring *shiverer* mutant mouse and the Long Evans *shaker* rat (O'connor et al., 1999; Readhead and Hood, 1990) causes severe hypomyelination of the CNS.

#### **1.2.4.2.1.3 Claudin 11/OSP**

Claudin 11 also referred to oligodendrocyte specific protein (OSP) is the third most abundant myelin protein and accounts for about 7% of the total myelin proteins (Bronstein et al., 1997). It is a tetraspan protein and its structure is similar to PLP/DM20. Claudin11 is located between the extracellular surfaces and is detectable as the radial component of the CNS myelin. It is believed that

Claudin11 forms tight junctions and is thought to play a structural role in myelin formation and maintenance (Gow et al., 1999). However, Claudin11 deficient mice, like *PLP/DM20* null mice, morphologically develop a relatively normal myelin sheath. However, *Claudin11\*PLP/DM20* double knockout mice have a severe deficiency in myelin compaction leading to neurological deficits, suggesting an interaction between PLP/DM20 and Claudin11 for myelin compaction (Chow et al., 2005).

#### **1.2.4.2.1.4 2'-3'-cyclic nucleotide-3'-phosphodiesterase (CNP)**

CNP constitutes about 4% of total myelin protein (Jahn et al., 2009). CNP is an enzyme which is expressed in oligodendrocytes from very early in the myelination process. CNP is located in the non-compact myelin, such as the inner and outer tongue, the paranodal loops and, in the PNS, in the Schmitt-Lantermann incisures. However the substrate of CNP has not been found in the CNS and the function of CNP in oligodendrocytes is not clear. Overexpression of CNP impairs distal oligodendrocyte process extension (Gravel et al., 1996). CNP can bind to RNA and suppress translation, indicating that it may be involved in trafficking RNA to the distal oligodendrocyte process (Gravel et al., 2009). *Cnp1* null mice form almost completely normal myelin except for swelling of the inner tongue process of some oligodendrocytes, but develop an early-onset axonopathy (Edgar et al., 2009 and Lappe-Siefke et al., 2003).

#### **1.2.4.2.1.5 Myelin associated glycoprotein (MAG)**

MAG accounts for approximately 1% of total myelin protein (reviewed in Schnaar and Lopez, 2009). MAG is a transmembranous glycosylated protein located in the periaxonal membrane of the oligodendrocyte. MAG is believed to interact with the axon through gangliosides and through the Nogo and p75 receptor on the axolemma. The main function of MAG seems to be in the support of the axo-glial stabilisation and mediates neurofilament phosphorylation (reviewed in (Schnaar and Lopez, 2009). Although MAG is not essential for myelination, a late onset axonopathy has been observed in MAG deficient mice (Fruttiger et al., 1995). Recently MAG was shown to play a role in the molecular organisation of

the node of Ranvier (Marcus et al., 2002). It also inhibits axonal growth after injury (McKerracher et al., 1994). However the role of MAG in axonal regeneration is not fully understood (reviewed in Schnaar and Lopez, 2009).

#### **1.2.4.2.2 Myelin lipids**

Of the four main classes of myelin lipids, galactocerebrosides and cholesterol, have been the focus of in depth investigation and will be briefly presented.

##### **1.2.4.2.2.1 Cerebrosides and sulfatides**

Twenty seven percent of myelin lipids originate from the galactocerebrosides and their sulphated derivatives, the sulfatides (Norton and Cammer, 1984). Galactocerebrosides (GalC) are expressed from the early stages of oligodendrocyte development (reviewed in Pfeiffer et al., 1993). It has been shown that application of antibodies against (GalC) results in a  $Ca^{++}$  influx mediated re-arrangement of microtubules in oligodendrocytes (Dyer and Benjamins, 1988;Dyer and Benjamins, 1990) and inhibit the myelination process *in vitro* and *in vivo* (Fry et al., 1974;Rosenbluth et al., 1994). Mouse models lacking GalC showed that myelin formation takes place without GalC, but the myelin has impaired insulation properties and lacks long term stability (Coetzee et al., 1996).

##### **1.2.4.2.2.2 Cholesterol**

Cholesterol is an important structural lipid in the cell membrane of vertebrates. It contributes to the semi-permeability of cell membranes and influences cell membrane fluidity (Ikonen, 2008). In myelin, cholesterol constitutes about 28% of the lipid content and it is locally synthesised in oligodendrocytes (Morell and Jurevics, 1996;Saher et al., 2005). Mice deficient in cholesterol synthesis in oligodendrocytes manifest hypomyelination of the CNS during post-natal development, leading to tremor, ataxia and in some cases premature death. However, in surviving animals, the phenotype stabilises with age and

myelination returns to more normal levels. The recovery is related to the supply of cholesterol by astrocytes (Saher et al., 2005). Recently the role of cholesterol in lipid raft formation and its interaction with myelin proteins such as PLP has initiated an increased interest in the role of cholesterol in myelin. Lipid rafts are highly motile regions in the cell membrane that are believed to function as platforms for protein interaction and signal transduction (Simons and Ikonen, 1997). These rafts have also been shown to associate with PLP integration into the membrane (Simons et al., 2000). On the other hand, overexpression of the *Plp1* gene results in a sequestration of cholesterol to endosomes/lysosomes and autophagosomes inducing storage disease-like changes (Saher et al., 2011; Simons et al., 2002; Karim et al., 2010).

### 1.2.5 The oligodendrocyte precursor cell

OPCs represent the undifferentiated multipotent cell pool, which develop into myelinating cells during post natal development (Kessarlis et al., 2006). In adult CNS, OPCs are the cells that differentiate into new myelin sheath forming oligodendrocytes after demyelination (2006; Zawadzka et al., 2010). OPCs are dispersed over the entire CNS and constitute, in the rat, approximately 8 - 9% of the glial cell population in white matter and approximately 2 - 3% of the glial cells in grey matter (Dawson et al., 2003). OPCs derive from different regions in the developing CNS. In the spinal cord they originate from the ventral neuroepithelial tube and migrate from there into other spinal cord areas. A recent study showed that the situation in the forebrain is different. Here OPCs populate the forebrain in waves. The first wave originates from the medial ganglionic eminence and the anterior entopeduncular area, the second wave originates from lateral and caudal ganglionic eminence and the third wave from the postnatal neocortex. Only the OPCs originating from the second and third wave persist and supply the region with myelinating oligodendrocytes (Kessarlis et al., 2006).

The morphology of OPCs in the CNS differs during post natal maturation. *In vitro*, at an early stage of development, the cells appear bipolar and are identified by the expression of A2B5 and PDGFR $\alpha$ . In the adult *in vivo*, OPCs are

cells with multiple processes, which express PDGFR $\alpha$  and the chondroitin sulphate proteoglycan NG2. At this stage the OPCs are multipotent and can develop either into oligodendrocytes, astrocytes or neurons (reviewed in Levine et al., 2001; Miron et al., 2011). During myelination OPCs exit the cell cycle and differentiate into oligodendrocytes (Miller, 2002). In adults after chemically induced demyelination, OPCs proliferate, repopulate the demyelinated area and differentiate into myelin forming oligodendrocytes (Zawadzka et al., 2010). Remyelination by OPCs after chemical demyelination is in general very successful but in diseases such as MS, failure of the repair process is commonly observed, and leads to chronic and permanent neuronal dysfunction.

OPCs are not only responsible for (re)myelination. They influence neuronal activity at the node of Ranvier (Butt et al., 1999). OPC processes have also been detected in close proximity to synapses, where they may contribute to synapse remodelling (reviewed in Frohlich et al., 2011). Recently a glutamate mediated interaction between yet unmyelinated axons and NG2<sup>+</sup> cells was demonstrated and is believed to facilitate rapid axono-glia communication initiating myelination (Ziskin et al., 2007). NG2<sup>+</sup> cells are also capable of differentiating into astrocytes, highlighting their stem cell like multipotency (Zhu et al., 2008a).

### **1.2.6 The astrocyte**

Astrocytes are characterised by their star shaped appearance and generally, by expression of glial fibrillary acidic protein (GFAP) (Eng et al., 1971). They can be divided into two main groups; fibrous astrocytes of the white matter and the protoplasmic astrocytes of the grey matter (reviewed in Figley and Stroman, 2011). The function of astrocytes in the CNS is multifaceted. They are involved in electrolyte homeostasis (reviewed in Sofroniew and Vinters, 2010), in the maintenance and function of the blood brain barrier (reviewed in Abbott, 2002), in regulating local blood flow (reviewed in Figley and Stroman, 2011), influencing the generation of synapses and modifying synaptic transmission (Ullian et al., 2001), influencing myelination dynamics (reviewed in Nash et al., 2011) and maintaining an active astrocyte-astrocyte and astrocyte-neuronal

signalling network (reviewed in (Sofroniew and Vinters, 2010;Rusakov et al., 2011). In the white matter astrocytes interact with the oligodendroglia via gap junctions (Nagy et al., 2001) and extend processes to the node of Ranvier (Butt et al., 1994). Astrocytes respond to any kind of tissue damage including demyelination by proliferating and changing morphology, turning into reactive astrocytes (reviewed in Norton et al., 1992).

### **1.2.7 Microglia**

The microglial cells are the resident macrophages of the CNS and are considered to constitute the innate immune system of the CNS. They originate from myeloid precursor cells and populate the CNS during late embryonic development. Approximately 12% of CNS glial cells can be attributed to microglia (reviewed in Walter and Neumann, 2009). In the normal CNS, microglia monitor their environment by continuously scanning to detect pathological changes, without disturbing the cellular network (reviewed in Hanisch and Kettenmann, 2007). As soon as there are abnormal changes in the CNS tissue, such as invasion by microorganism, production of inflammatory cytokines, accumulation of intracellular substances or protein aggregates, microglia change their activity from a surveillance mode to a reactive mode, depending on the severity and duration of the insult. In general, when microglia become 'activated' they change their morphology from small cell bodies with fine processes to swollen cell bodies with shortened and thicker processes. Activation is mainly mediated through activation of Toll-like receptors, through lack of inhibition of receptors or through neurotransmitters, making them respond to known and unknown changes. 'Activated' microglia can interact with other immune cells such as macrophages and T-cells, can exhibit phagocytic activity, for example removing myelin debris after demyelination, secrete pro- or anti-inflammatory substances and can support adult oligodendroglioneogenesis and neurogenesis. In general microglia maintain and restore optimal conditions for normal CNS function (reviewed in Hanisch and Kettenmann, 2007). However microglial activation can also exacerbate and aggravate the disease process.

This exacerbation and aggravation of the disease process has been shown in different models of demyelination where suppression of microglial/macrophage activation led to amelioration of the disease process (Ip et al., 2007;Popovic et al., 2002;Kondo et al., 2011) and highlights the bivalent role of microglia in white matter pathology.

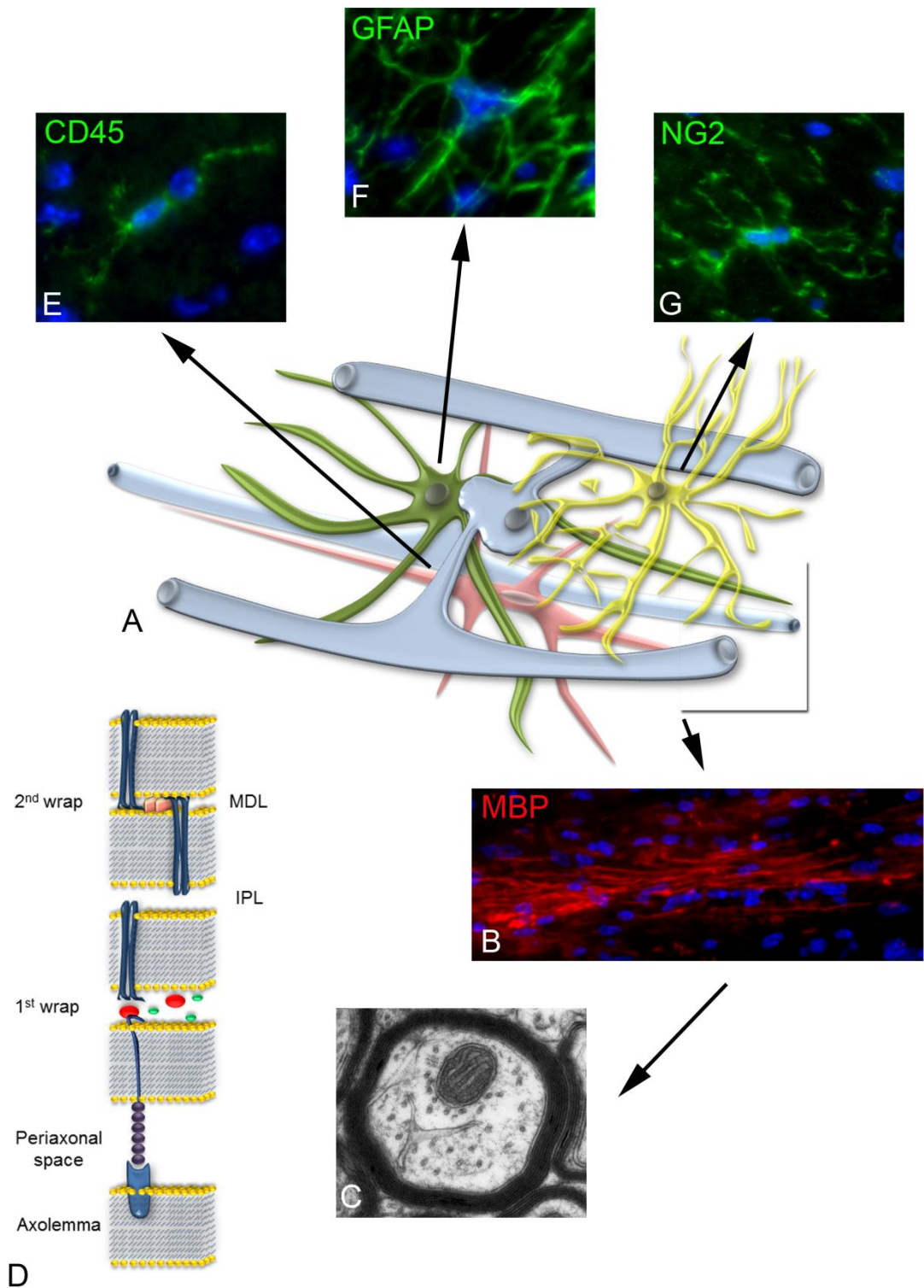


**Figure 1. White matter at a glance.**

Illustration of the architecture of major white matter tracts (A) composed of axons and their myelin sheath (B, C, and D), microglia (E), astroglia (F) and oligodendrocyte precursor cells (G). PLP (blue) and MBP (orange), the two most abundant proteins of CNS myelin, are located in compact myelin. CNP (red) and Sirtuin2 (green) are associated with non-compact myelin. MAG (purple) traverse the periaxonal space and binds to receptors (blue) in the axolemma (MDL: major dense line, IPL: intraperiod line, modified from Gruenfelder et al., 2011).

### 1.3 Myelination of the CNS

Myelination of the mouse CNS mainly occurs during post natal development with peak myelination around P20. The myelination process is largely complete around P60 (Edgar and Griffiths, 2009). However there are some regions, such as the corpus callosum, where on-going myelination into late adulthood is present (see [Chapter 3](#)). The process of myelination is tightly controlled and involves in general all axons larger than 0.2 $\mu$ m in diameter (reviewed in Hildebrand et al., 1993).

The process of myelination, from OPC proliferation to differentiation and formation of the myelin sheath is orchestrated by a precise temporal and spatial interaction of inhibitory and promoting cell intrinsic and extrinsic factors (reviewed in Franklin and ffrench-Constant, 2008; Emery, 2010a). Most of the known OPC extrinsic factors and molecules are expressed on axons and act through axonal glial communication. They are, in general, inhibitors of OPC differentiation and the down-regulation or inactivation of these ligands such as Jagged, PSA-NCAM, NRG1-III or LINGO-1 results in decreased inhibition of OPC differentiation (Charles et al., 2000; Mi et al., 2005; Wang et al., 1998; Emery, 2010a; Flores et al., 2008). Neuronal activity has additionally been identified to induce OPC differentiation and myelination (Barres and Raff, 1993). The influence of neuronal activity on myelination highlights the plasticity of the white matter, which is preserved into adulthood and can be stimulated with specific training (Scholz et al., 2009).

Activation of the canonical Wnt pathway in OPCs is required for OPC proliferation but needs to be downregulated to induce OPC differentiation. Prolonged activation of the Wnt pathway leads to delayed myelination and also delayed remyelination (Fancy et al., 2009).

Cell intrinsic factors involved in the regulation of OPC differentiation include translational, posttranslational and epigenetic mechanisms (Emery, 2010a; Franklin and ffrench-Constant, 2008). For OPC development, normal function of the transcriptional factor Olig2 is crucial and disruption thereof leads

to absence of OPCs in the CNS (Lu et al., 2002 and reviewed in Emery, 2010b). During OPC differentiation other transcription factors such as Olig1, Sox10 and Nkx 2.2 become more important and any disruption thereof impairs the differentiation of OPC into myelin synthesising oligodendrocytes (Emery, 2010b). Recently microRNA has been shown to control OPC differentiation. The transgenically mediated inhibition of the microRNA processing enzyme Dicer1 in cells from the oligodendrocyte lineage, leads to a dysmyelinating phenotype with an elevated OPC pool. OPC differentiation and myelination was reinduced by overexpression of miR-291 and miR-338 which act through silencing the inhibitory factors Sox6 and Hes5 (Zhao et al., 2010).

Finally epigenetic control mechanism involving, for example, histone deacetylases (HDAC1 and 2) influence myelination as well as remyelination. It has been shown that HDACs block Wnt pathway activity believed to inhibit OPC differentiation (Ye et al., 2009).

In contrast to the PNS, where myelination is mainly governed by axonal signals, the myelination process in the CNS is more complex and some of the cell intrinsic and cell extrinsic influences on myelination have been identified. Understanding the molecular changes involved in normal myelination during development could help to investigate the mechanism involved in remyelination and remyelination failure.

#### **1.4 The regenerative capacity of the white matter**

It has been shown that extensive repair can occur after a pathological insult to the myelin sheath where the demyelinated axons become remyelinated (Duncan et al., 2009). The remyelination process in the CNS can be very effective and extensive, leading to a full recovery of the whole demyelinated area. Recently it has been observed that demyelinated regions become repopulated by a specific multipotent cell type, the OPCs. However remyelination often fails especially in MS despite of OPCs being abundantly present in the demyelinated regions (Chang et al., 2002; Goldschmidt et al., 2009; Kuhlmann et al., 2008). These regions often stay demyelinated and secondary axonal changes develop,

possibly as a consequence of failed remyelination. Why the default remyelination process fails with disease chronicity is not understood and research using animal models of demyelination is focusing on this phenomenon in order to understand the development of remyelination failure and to potentially find ways to enhance the regenerative process.

#### **1.4.1 Demyelination and remyelination of the CNS**

Demyelination is the process whereby the myelin sheath breaks down. Demyelination of the CNS occurs in two ways:

- a) Primary demyelination, where pathology mainly affects the myelin sheath, causing a demyelination
  
- b) Wallerian degeneration, where the breakdown of the myelin sheath follows axonal degeneration.

Primary demyelination of the white matter is a common pathology in humans and two major disease groups affect the CNS myelin sheath: inflammation induced primary demyelination, with MS being the most common aetiology, and much less common, demyelination mediated through a genetic defect, such as the leukodystrophies, for example, PMD or Krabbe's disease.

In general, the regeneration potential of the CNS is limited. However, with regard to regeneration of the myelin sheath, it has been shown that remyelination is a highly effective and dynamic process following a demyelinating insult (Blakemore, 1974;Coman et al., 2005;Woodruff and Franklin, 1999;Kuhlmann et al., 2008;Franklin and ffrench-Constant, 2008;Duncan et al., 2009;Miron et al., 2011). It has been demonstrated that OPCs are responsible for remyelination in the adult CNS (Zawadzka et al., 2010). This regenerative capacity of the OPC is believed to be maintained throughout life (reviewed in Franklin and ffrench-Constant, 2008).

This regenerative capacity has also been observed in patients suffering from MS, in that virtually complete restoration of myelin can occur after an acute event (Kuhlmann et al., 2008). However there appears to be a different situation in chronically demyelinated lesions, where the remyelination capacity of OPCs becomes diminished (Goldschmidt et al., 2009).

Chronic remyelination failure is leading to permanent demyelination as seen in chronic MS. The reasons for remyelination failure are not fully understood. However the consequence of this failure is that axonal loss, which is believed to lead to permanent disability and which can be caused by inflammation-mediated demyelination, is also recognised in association with remyelination failure (reviewed in Trapp and Nave, 2008). Consequently, more attention has been given to investigating the axonal glial interaction, and it has been suggested that the axonal loss evident in chronic demyelinated regions is due to the long term loss of trophic factors derived from the myelin sheath (Pohl et al., 2011; reviewed in Bjartmar et al., 2003;Nave, 2010a;Nave, 2010b). Evidence for the trophic supporting role of the myelin sheath has been provided from the study of various genetically modified mouse models (reviewed in Edgar and Garbern, 2004), such as the *Plp1* (Griffiths et al., 1998;Garbern et al., 2002) and *Cnp1* knock out (Lappe-Siefke et al., 2003;Edgar et al., 2009) mice in which axonal degeneration occurs over time despite an abundance of relatively normal myelin. This suggests that biochemically abnormal myelin may even be more detrimental to axonal health, than no myelin (Edgar et al., 2010; reviewed in (Nave, 2010a).

#### **1.4.2 Successful remyelination is dependent on a finely tuned interaction between oligodendrocyte precursor cell intrinsic and cell extrinsic changes**

It has been postulated that for effective remyelination to take place, cell intrinsic and extrinsic factors must interact in a precise spatial and temporal manner (reviewed in Franklin and ffrench-Constant, 2008). Briefly, the initial step after demyelination involves clearance of the affected region of myelin debris by local microglia/macrophages. Normal microglial/macrophage

phagocytic function is an important prerequisite for successful remyelination (Kotter et al., 2001;Pohl et al., 2011). This is followed by OPC migration into the demyelinated area and OPC proliferation, leading to OPC repopulation of the demyelinated area. OPCs must then differentiate into early oligodendrocytes in order to initiate remyelination. Cell processes of the newly formed oligodendrocytes then contact the demyelinated axons, resulting in upregulation of the expression of myelin-related genes (reviewed in Franklin and ffrench-Constant, 2008). Finally, successful restoration of the myelin sheath leads to functional recovery (Duncan et al., 2009).

Given the complexity of the repair process, minimal interference with the process could result in perturbation of the remyelination process, which in the worst case could end in failure of remyelination.

To understand the role of intracellular and extracellular compartments during demyelination and remyelination it is necessary to address the structural and molecular changes within the differentiating OPC intrinsic and extrinsic environment including the astroglia, the microglia and the extracellular matrix. Successful remyelination is mediated by OPCs (Zawadzka et al., 2010). However the mere presence of OPCs within and around the demyelinated lesion is not always sufficient for successful remyelination. This situation has been observed in chronic MS lesions where, despite the presence of OPCs, there is no evidence of remyelination, suggesting that there is a block in OPC differentiation (Kuhlmann et al., 2008). The transition of the OPC from a proliferating to differentiating cell is thought to be a critical point during the remyelination process (reviewed in Fancy et al., 2010;Franklin and ffrench-Constant, 2008).

### **1.4.3 The role of OPC intrinsic factors in successful (re)myelination**

#### **1.4.3.1 Intrinsic control of the cell cycle is crucial for OPC differentiation**

As previously stated, a crucial factor in initiating (re)myelination is the differentiation of OPCs to young oligodendrocytes. This starts with the OPCs exiting the cell cycle. Depending on the dominance of cell cycle promoters or

inhibitors, the OPC will either continue to proliferate and go through another cell cycle, or will exit the cell cycle and start to differentiate into a non-dividing oligodendrocyte. Cell cycle arrest in OPCs depends on a decrease in cyclin-dependent kinase (CDK), with mainly CDK2 and p27Kip-1, which is part of the retinoblastoma (Rb) pathway, as the main regulator (reviewed in Casaccia-Bonofil and Liu, 2003). Additionally, the p53 pathway influences the cell cycle, especially during the differentiation step. The NH<sub>2</sub>-terminus of p53 appears to be important for the development of the cytoskeleton during differentiation, whereas the COOH-terminus of p53 affects exit from the cell cycle (reviewed in Casaccia-Bonofil and Liu, 2003).

#### **1.4.3.1.1 *Wnt pathway activity interacts with the timing of OPC proliferation and differentiation***

As described in Section ([1.3 Myelination of the CNS](#)), the Wnt pathway plays a regulatory role in the induction of OPC differentiation during development (Fancy et al., 2009), but also during remyelination (Fancy et al., 2009). Constitutive activation of the Wnt pathway in mice led to delayed but normal myelination during development and delayed remyelination after chemical demyelination (Fancy et al., 2009). It has been suggested that delayed differentiation, during myelin repair, may lead to incomplete or failed remyelination by missing the narrow time window for the proliferating OPC's to respond to parameters favouring remyelination (Fancy et al., 2009). Further evidence for a regulatory role for the Wnt pathway came from a study showing that suppression of the Wnt pathway, mediated through Axin2 stabilisation, a negative feedback regulator of the Wnt pathway, resulted in enhanced remyelination capacity of OPCs in mice (Fancy et al., 2011).

#### **1.4.3.1.2 *The Notch pathway and remyelination***

The role of the Notch pathway in remyelination is controversial. It has been postulated that Notch1 signalling is involved in the precise timing of the myelination process during development. The effect appears to depend on the

involvement of either the canonical or non-canonical pathway. Blocking of Notch1 receptor stimulation may therefore contribute to remyelination failure in MS (Blaschuk and French-Constant, 1998). However, blocking the canonical Notch1 pathway in young and adult mice did not influence the remyelination rate after chemically induced demyelination in mice (Stidworthy et al., 2004). However, remyelination failure in chronically demyelinated MS lesions, in which Notch1 receptors were saturated with Contactin and therefore activated, was not attributed to Notch pathway activation, but rather to a failure of nuclear translocation of the intracellular non-canonical Notch1 domain (Nakahara et al., 2009). On the other hand, during white matter development and myelination, inhibition of Notch1 through the canonical pathway resulted in impaired OPC differentiation, leading to an increase in prematurely differentiated immature oligodendrocytes (Genoud et al., 2002).

Together, these data show that the Notch signalling pathway can act as an inhibitor or promoter depending on activation pathway, suggesting that Notch signalling plays a regulating role in remyelination kinetics and is not just an inhibitor of OPC differentiation during remyelination (Fancy et al., 2010).

#### **1.4.3.1.3 *The activation of Neuregulin1/ErbB signalling in remyelination is important but not crucial***

In the PNS axonal expressed Neuregulin1-III (NRG1-III) ligands control almost the entire myelination process by binding to glial ErbB2/ErbB3 receptors, which upregulate myelin gene expression through a phosphatidylinositol-3-kinase (PI3K) mediated activation of Akt1/mTor (Michailov et al., 2004). In contrast, in the CNS the role of axonal NRG1-III ligands is not crucial for successful myelination (Brinkmann et al., 2008; Flores et al., 2008). However, transgenic mice with continuous activation of the Akt1 pathway develop a hypermyelination of the CNS (Flores et al., 2008; Brinkmann et al., 2008). Although the Akt1/mTor pathway is involved in myelin gene upregulation and formation of the myelin sheath, the importance of this pathway for successful remyelination is not clear.

#### 1.4.3.1.4 *The spatial and temporal interaction between transcription factors is crucial for successful remyelination*

Recently, the role of transcription factors in the remyelination process has gained increased attention. As previously discussed, during developmental myelination, oligodendrocyte specific transcription factors such as Olig1, Olig2, Nkx 2.2 and Sox10 are responsible for OPC development, differentiation, myelination and survival. It has also been shown that in adult CNS transcription factors are involved in OPC proliferation and differentiation mandatory for successful remyelination (Kuspert et al., 2011).

Accurate subcellular localisation of the basic helix-loop-helix (bHLH) transcription factor Olig1 is crucial for (re)myelination. In normal mice, transient intranuclear translocation of transcription factor Olig1 occurs during remyelination following chemically induced demyelination. In the Olig1 knock out mouse, in which developmental myelination occurs normally, remyelination is severely impaired after chemical demyelination (Arnett et al., 2004). In contrast, overexpression of Olig1 in transgenic mice had no enhancing effect on developmental myelination (Maire et al., 2010). However the influence of Olig1 overexpression during remyelination has not been examined. Another bHLH transcription factor, Olig2 regulates OPC and motoneuron specification during embryonic development (Lu et al., 2002). Olig2 knock-out mice display a severe reduction of OPCs and motoneurons and do not survive post-natally making it impossible to evaluate the influence of absent Olig2 in myelination and remyelination (Lu et al., 2002). Furthermore, transplantation of transfection induced Olig2 overexpressing human stem cells into *shiverer* mouse brain resulted in increased differentiation and MBP expression by transplanted OPCs (Maire et al., 2009; Maire et al., 2010). This suggests that increasing Olig2 expression increases OPC proliferation and differentiation and that manipulating Olig2 levels could potentially enhance remyelination.

However, Olig2 does not function in isolation. During remyelination, increased Olig2 expression is always linked to Nkx 2.2 expression in differentiating OPCs. A delay in co-expression leads to a reduced remyelination, indicating that the combination of Olig2/Nkx 2.2 expression is critical for the remyelination process (Fancy et al., 2004; Kitada and Rowitch, 2006; Othman et al., 2011).

Furthermore, Olig2 regulates Sox10 expression, ensuring OPC survival and acting as a direct promoter of myelin gene expression (Stolt et al., 2002; Finsch et al., 2008; Kuspert et al., 2011).

In summary, the temporally and spatially regulated action of transcription factors is crucial for (re)myelination and only minor disruption can have severe consequences for the repair process.

#### **1.4.3.2 Epigenetic influences on (re)myelination**

The deacetylation of histones by HDAC, an important intracellular epigenetic control mechanism of gene expression, modulates the remyelination capacity of the white matter. In the case of OPCs, the HDACs positively influence remyelination by blocking the function of molecules such as Tcf4, Sox2, Hes5 and Id4, which are thought to inhibit OPC differentiation (Shen and Casaccia-Bonofil, 2008). The reduction of HDAC in mice, especially HDAC1 and HDAC2, causes the level of the intracellular inhibitory molecules for OPC differentiation to be elevated. The negative effect on remyelination capacity in the absence of HDAC1/2 is mediated through the absence of a competing interaction with Tcf4 function, which plays a central part of the Wnt pathway.

Briefly multiple intracellular signalling pathways involved in changing cell status from a proliferating one to a differentiating one play a pivotal role during myelination and remyelination and knowledge of specific cell intrinsic interactions provides an opportunity to manipulate these factors in favour of the remyelination process.

#### **1.4.4 Factors in the OPC extrinsic compartment that can disrupt the remyelination process leading to remyelination failure**

##### **1.4.4.1 Mitogens and differentiation factors act through specific cell receptors on OPCs**

Although OPC intrinsic factors are mandatory for successful (re)myelination, a permissive environment for OPC differentiation and myelin sheath formation is of equal importance. A variety of OPC extrinsic factors can have a stimulatory or inhibitory effect on either proliferation or differentiation.

Mitogens such as PDGF, basic FGF, BDNF and NT3 are responsible for OPC proliferation (reviewed in Casaccia-Bonofil and Liu, 2003) and for increasing the number of OPCs. In order to differentiate into new, non-dividing oligodendrocytes, OPCs must exit the cell cycle. Extracellular factors such as TGF- $\beta$ , cAMP and thyroid hormone enhance OPC differentiation (reviewed in Casaccia-Bonofil and Liu, 2003). However, it is not only mitogens and differentiating inducing molecules that are important, mandatory receptors on the OPC membrane such as the Erb family, and integrins are required for successful (re)myelination (reviewed in Casaccia-Bonofil and Liu, 2003; Taveggia et al., 2010).

##### **1.4.4.2 The influence of the extracellular matrix on the remyelination process**

The composition of the extracellular matrix substantially influences the generation of new oligodendrocytes (reviewed in Franklin and ffrench-Constant, 2008). For example hyaluronan, a glycosaminoglycan composed of glucuronic acid and N-acetylglucosamine, impairs OPC differentiation (Back et al., 2005). The accumulation of high molecular weight (HMW) hyaluronan has been found to negatively impact the activation and differentiation of OPCs in chemically induced and demyelinated lesions *in vitro* in a model of chronic demyelination and in chronic MS biopsy samples (Back et al., 2005). Recently it was

demonstrated that the blocking mechanism of hyaluronan on OPC differentiation is mediated by binding of low molecular weight (LMW) hyaluronan to Toll-like receptor 2 (TLR2) on OPCs. Hyaluronidase, expressed on OPCs, locally breaks down the HMW to LMW hyaluronan and is responsible for the accumulation of LMW hyaluronan (Sloane et al., 2010).

Another inhibitory molecule that accumulates in chronic MS lesions is Semaphorin 3A (Williams et al., 2007a). Semaphorin 3A is synthesised by microglia, astroglia and/or a subset of cells belonging to the oligodendroglial lineage (Williams et al., 2007a). The receptor NP-1, to which Semaphorin 3A binds, is expressed on OPCs. Recent *in vitro* and *in vivo* work showed that Semaphorin 3A acts as an inhibitor of OPC differentiation (Syed et al., 2011).

#### **1.4.4.3 Inhibition of the initial axonal glial contact impairs the remyelination process**

Initiation of myelination is dependent on glia-axonal interaction and it has been suggested that polysialation of the neural cell adhesion molecule (PSA NCAM) on axons may play a role in inhibiting remyelination after demyelination (Charles et al., 2002). PSA NCAM is present on astrocytes and axons during CNS development and is involved in O-2A cell migration *in vitro* (Wang et al., 1996) and axonal growth *in vitro* (Doherty et al., 1990). In the mature CNS, PSA NCAM is no longer expressed on axons (Charles et al., 2002), but it is re-expressed in chronic MS lesions, possibly impairing remyelination (Charles et al., 2002). The contact-mediated inhibitory effect of PSA NCAM results in OPC differentiation failure and a lack of myelin forming oligodendrocytes (Taveggia et al., 2010).

Structural integrity of the axon is also likely to be crucial for remyelination. Of interest, there is evidence that the length of time axons remain demyelinated does not impact on the remyelination potential of the demyelinated axons (Setzu et al., 2004).

#### **1.4.4.4 Astroglia, microglia/macrophages and inflammation influence remyelination**

The important role of macrophages in remyelination was demonstrated by experimental depletion of macrophages, using clodronate-liposome, after demyelination in experimental animals. This led to reduced levels of growth factors, insulin growth factor 1 (IGF-1) and transforming growth factor B1 (TGF-1), and had a negative impact on OPC recruitment into the demyelinated region (Kotter et al., 2001;Kotter et al., 2005).

The important role of the phagocytic activity of macrophages is demonstrated by the observation that the accumulation of myelin debris products impairs remyelination by inhibiting OPC differentiation (Kotter et al., 2006;Syed et al., 2008).

##### **1.4.4.4.1 *Microglial activation and inflammation can stimulate or inhibit the remyelination process***

The role of inflammation during the remyelination process is controversial. In rodents, zymosan, a TLR2 binding glycan, induces an acute inflammation which causes transplanted OPC to myelinate retinal axons more efficiently (Setzu et al., 2006). It has also been shown that a saline mediated acute inflammation induced after transplantation of OPCs into the chronically demyelinated dorsal columns of *taiep* rats had a beneficial effect on transplanted OPCs to effectively remyelinate the chronically demyelinated regions (Foote and Blakemore, 2005a).

On the other hand, minocycline induced suppression of microglial activation in Long Evans shaker rats leads to enhanced function and survival of transplanted OPCs. This observation suggests that fully activated microglia, characterised by expressing MHCII and iNOS and by secretion of cytokines and active phagocytosis, may contribute to the non-permissiveness for remyelination by making the environment detrimental for transplanted OPCs (Zhang et al., 2003).

Furthermore, studies using genetically induced models of demyelination and experimental autoimmune encephalitis showed that suppressing microglial activation ameliorates progressive demyelination (Ip et al., 2007; Popovic et al., 2002).

#### **1.4.4.4.2 Astrocytes - promoter or inhibitor?**

Astroglia also have an ambiguous role during (re)myelination. Remyelination, induced by injection of OPCs and Schwann cells into a chemically and radiation induced astroglia-free demyelinated lesions *in vivo*, was more effective than remyelination after transplantation into a demyelinated area containing astrocytes. This implies a negative influence of the endogenous astroglia on the remyelination capacity (Blakemore et al., 2003). Reactive astrocytes secrete hyaluronan, which inhibit OPC differentiation (Back et al., 2005; Sloane et al., 2010) (see section [1.4.4.2 The influence of the extracellular matrix on the remyelination process](#)). On the other hand, using an EAE model, it was demonstrated that astrocytes in the demyelinated lesions secrete substances such as insulin-like growth factor binding protein 2 (IGFBP-2) which helps to target insulin-like growth factor 1 (IGF-1) to insulin-like growth factor receptor 1 (IGFR-1) expressing oligodendrocytes, essentially having a promoting effect on the newly formed oligodendrocytes to remyelinate (Liu et al., 1994). Furthermore a bivalent role during the remyelination process has been postulated since astrocytes may amplify the damage caused by inflammation mediated through TNF- $\alpha$ . This may lead to repulsion and apoptosis of OPCs. On the other hand the astrocytes facilitated debris clearance, attracted OPCs to the demyelinated region and promoted OPC differentiation by secretion of IL-6 related cytokines (reviewed in Williams et al., 2007b)

#### **1.4.4.5 Thyroid hormone**

Thyroid hormone is known for its positive effect on cell metabolism. Various experimental studies focussing on myelin repair and on functional recovery after spinal cord injury have shown the positive effect of T3, the biologically active

form of thyroid hormone. Acute and also chronic illness has been shown to cause the phenomenon of a non-thyroidal illness syndrome (NTIS) (reviewed in Papanicolaou, 2000). To date the NTIS is believed to be elicited by a combination of systemically suppressive effects on thyroid hormone synthesis and locally on thyroid hormone metabolism and transport. Of interest in the complex aetiology of NTIS are for example tanycytes, which are located on the floor of the third ventricle. The tanycytes respond to acute and chronic illness with local upregulation of deiodinase 2 (D2) which controls the secretory activity of thyroid releasing hormone (TRH) producing cells in the periventricular nuclei (reviewed in Herwig et al., 2008). The upregulation of D2, which is responsible for converting T4 to T3, causes a local hyperthyroidism inhibiting TRH secretion and elicits a centrally mediated systemic hypothyroidism.

An effective local regulator of active thyroid hormone levels in tissue is the deiodinase 3 (D3), which inactivates T4 and T3, locally depriving the tissue of active T3, despite thyroid levels being normal (reviewed in Visser et al., 2011). D3 is expressed on neutrophilic granulocytes and macrophages and is believed to be involved in the development of NTIS in inflammatory diseases (Boelen et al., 2005). Finally T3 has to be actively transported into the cell by active transporters such as monocarboxylase transporters (MTC). In the CNS, MTC8 is the major intracellular transporter for T3 and abnormal function and distribution has been reported to cause PMD like disease development (Vaurs-Barriere et al., 2009). All of these components have been described to be involved in the development of NTIS. The positive effect on remyelination activity observed after application of high T3 doses in different models of EAE may be explained by overriding a potential local tissue hypothyroidism mediated through inflammation, by saturating the D3 activity and by optimising the impaired intracellular transport by artificially elevating the T3 concentration in tissue.

#### **1.4.4.6 Age as an ubiquitous negative factor for remyelination capacity**

Increasing age negatively influences both remyelination promoting cell intrinsic and cell extrinsic factors. Simultaneous expression of Nkx2.2/Olig2, which is important for OPC differentiation and remyelination, diminishes with age (Fancy

et al., 2004). Also the HDAC1 and 2 activity becomes reduced with age, leading to reduced suppression of myelin suppressing pathways, thereby slowing down the remyelination process (Shen et al., 2008;Ye et al., 2009). Aging also affects phagocytic activity, delaying myelin clearance and consequently leading to inefficient remyelination (Kotter et al., 2005; reviewed in Neumann et al., 2009).

## 1.5 Diseases affecting the myelin sheath

The myelin sheath in the CNS can be affected by various diseases leading to two main forms of pathology:

- 1.) Dysmyelination, in which myelin formation and/or structure is perturbed
- 2.) Demyelination, in which there is destruction of the myelin sheath.

The archetypal disease of white matter in humans is MS, which classically leads to widespread formation of demyelinated patches in the white matter. Some demyelinated lesions remyelinate and some develop into chronically demyelinated lesions (reviewed by Agrawal and Yong, 2007; Noseworthy et al., 2000). Another group, where an initial dysmyelination may be followed by demyelination, has a genetically determined background such as in Pelizaeus Merzbacher diseases (Hudson et al., 2004; Garbern, 2007), Krabbe's disease (Duffner et al., 2009), adrenoleukodystrophy (Moser et al., 2005), metachromatic leukodystrophy (Gieselmann, 2008) and Alexander's disease (Johnson and Brenner, 2003). Other reasons, such as metabolic disturbances, toxins, radiation, vascular events or chemotherapy induced demyelination, have been also been described (reviewed in Schmähmann et al., 2008).

In acute diseases affecting the white matter, remyelination with complete restoration of neurophysiological function may occur. However in MS or in genetically induced demyelination, the repair process often fails and, with time, an accumulation of chronically demyelinated regions eventually leads to permanent neurological dysfunction (Kuhlmann et al., 2008). The reason why remyelination fails, and the regenerative process stops, is a major research

area. Classically, the experimentally induced autoimmune encephalitis (EAE) model has been used to study the immunological component of demyelination (Swanborg, 1995). In contrast, the regenerative capacity of white matter, is often studied using chemically induced demyelination. Genetically determined models can also be used to investigate remyelination failure in the absence of an overt immune component.

### 1.5.1 Models of myelin pathology

*In vitro* and *in vivo* models of demyelination are routinely used to investigate remyelination biology and pathology (Fressinaud, 2005; Thomson et al., 2006; Woodruff and Franklin, 1999; Zhang et al., 2011). *In vitro* and *ex-vivo* models such as cell and tissue culture are useful in the study of remyelination biology with respect to the fact that they are easily manipulated, imaged and assessed. The main disadvantage is that they never reflect the *in situ* situation properly. For example, they are generally generated from embryonic or early post-natal tissue and, due to their limited lifespan, cannot be used to reproduce chronic demyelination. Ideally remyelination should be studied *in situ*, either in an animal model or in humans. For studying white matter biology and pathology *in situ*, a prominent white matter tract without neuronal cell bodies is preferred. The long dorsal columns of spinal cord, the optic nerve and the corpus callosum fulfil these criteria. The advantage of the corpus callosum is that it is a large but anatomically confined myelinated white matter tract in the CNS that is readily accessible *in vivo* and in which manipulation does not usually result in substantial clinical deficits.

There are three pathologically distinct groups of animal models that have become useful in investigating myelin pathology:

- 1.) Inflammatory mediated models of demyelination such as the experimental allergic encephalitis (EAE) or the Theiler's murine encephalomyelitis virus (TMEV) models (reviewed in Dal Canto et al., 1995; Swanborg, 1995). EAE, which can be induced in a wide spectrum of experimental animals such as rodents (Swanborg, 1995), pigs (Feng et al., 2009) and non-human

primates (D'Intino et al., 2011), has provided valuable insight into the aetiology of immune mediated demyelination and proved to be invaluable for the development and evaluation of effective immune modulatory drugs that have been used in the treatment of MS (reviewed in Lublin, 2005;Agrawal and Yong, 2007;Korniychuk et al., 2007)

- 2.) Genetically modified models of dysmyelination and demyelination such as the *Plp1* gene related models of the leukodystrophies (reviewed in Yool et al., 2000), the *Mbp* related *shiverer* (Readhead and Hood, 1990) or the newer models of genetically inducible demyelination (Pohl et al., 2011) have highlighted the importance of normal axonal glial interaction (Anderson et al., 1998;Edgar et al., 2002;Edgar et al., 2004b;Edgar et al., 2009;Edgar et al., 2010;Griffiths et al., 1998;Lappe-Siefke et al., 2003; reviewed in Gruenenfelder et al., 2011) and the influence of myelin proteins on myelin sheath integrity (reviewed in Griffiths et al., 1995b), demyelination (Anderson et al., 1999;Inoue et al., 1996b;Mastronardi et al., 1993;Readhead et al., 1994;Kagawa et al., 1994) and remyelination impairment (Ma et al., 2006).
- 3.) The third group consists of chemically induced models of demyelination such as focal injection of ethidium bromide (Blakemore, 1982) or lysolecithin (Hall, 1972) or systemic application of cuprizone (Blakemore, 1974). Chemically induced models, especially the focally demyelinated models, have been extremely helpful in identifying and analysing the endogenous remyelination process in the CNS (Woodruff and Franklin, 1999).

The focus of this study is the homozygous *Plp1* gene overexpressing mouse model, line #72, a mouse model of Pelizaeus-Merzbacher disease. Previous studies have demonstrated changes in the myelin development in spinal cord and optic nerve (Anderson et al., 1998;Edgar et al., 2010) and recently, using a combination of DTI measures and histopathology have provided evidence for widespread hypomyelination in the adult brain (Ruest et al., 2011). However, a complete characterisation of the temporal progression of myelin pathology and associated changes has not been undertaken other than in the optic nerve.

## 1.5.2 The Leukodystrophies

The leukodystrophies represent a relatively rare group of diseases affecting the white matter. So far, more than 40 leukodystrophies with various genetic causes have been identified and only a few will be mentioned. The most common leukodystrophy is the X-linked adrenoleukodystrophy in which an accumulation of very long chain fatty acids is associated with neuroinflammation and demyelination (Schiffmann and van der Knaap, 2004). Other leukodystrophies include metachromatic leukodystrophy, in which deficiency in arylsulfatase A leads to a slowly progressive demyelination (reviewed in Gieselmann, 2008; Kohler, 2010) and globoid cell leukodystrophy (Krabbe's disease), which is caused by a deficiency in the enzyme galactosylceramide beta-galactosidase leading to a demyelination (Kohler, 2010). Haematopoietic stem cells transplantation in X-ALD (Cartier et al., 2009) and Krabbe's disease has led to post natal improvement in treated children. However reports of rapid deterioration in older children and adolescents with Krabbe's disease has raised questions about the long term efficacy of the treatment (Duffner et al., 2009). Finally, Pelizaeus Merzbacher disease (PMD) and the allelic disorder Spastic Paraplegia type 2 (SPG2), in which the genetic defect lies in the *PLP1* gene, (reviewed in Yool et al., 2000) will be described in more detail.

### 1.5.2.1 The proteolipid protein gene in the CNS: normal structure, function and the role in the aetiology of Pelizaeus-Merzbacher disease

#### 1.5.2.1.1 *The PLP1 gene*

The *PLP1* gene encodes the major tetraspan transmembranous proteolipid protein and its isoform DM20. The gene is X-linked and is located on a single locus at Xq21.33-22 in man (Mattei et al., 1986). The *PLP1* gene is expressed in mature oligodendrocytes, but other CNS cells such as specific neurons in the olfactory bulb, hippocampus and cerebellum may also express *PLP1/Plp1* (Bongarzone et al., 1999). Outside the CNS *PLP1/Plp1* gene expression is also found in Schwann cells, lymphoid tissue, spleen and cardiac myocytes (Puckett

et al., 1987;Campagnoni et al., 1992;Voskuhl, 1998). The size of the *PLP1* gene is approximately 17 kb and contains eight exons and seven introns (Diehl et al., 1986;Macklin et al., 1987;Bongarzone et al., 1999). The gene contains three polyadenylated sites and two translation initiation codons (Griffiths et al., 1995a). Exon 1 contains the major translation initiation codon (Yool, 2000). The second translation initiation codon lies on exon 1.1 (Bongarzone et al., 1999). Exon 7 encodes the carboxy terminus and the entire 3'UTR (Macklin et al., 1987;Yool, 2000). Two major protein isoforms (PLP [30 kDa] and DM20 [26.5 kDa]) and two minor isoforms (srPLP and srDM20; in mice) are generated through alternate splicing of the primary transcript ([Figure 2](#)). Recently two exons in intron1 were identified on the human *PLP1* gene, possibly leading to the expression of three more isoforms (Sarret et al., 2010). Between species there is a high level of sequence conservation. Comparing the protein coding region between man and rodents the identity reaches 100%. The non-coding and regulatory regions are also highly conserved, with the upstream regulatory and the 5' non-coding region of the mouse gene having a 92% homology with the human gene (Macklin et al., 1987). The high level of conservation within the protein coding region point to strict regulatory control is vital for normal gene function (Yool, 2000).

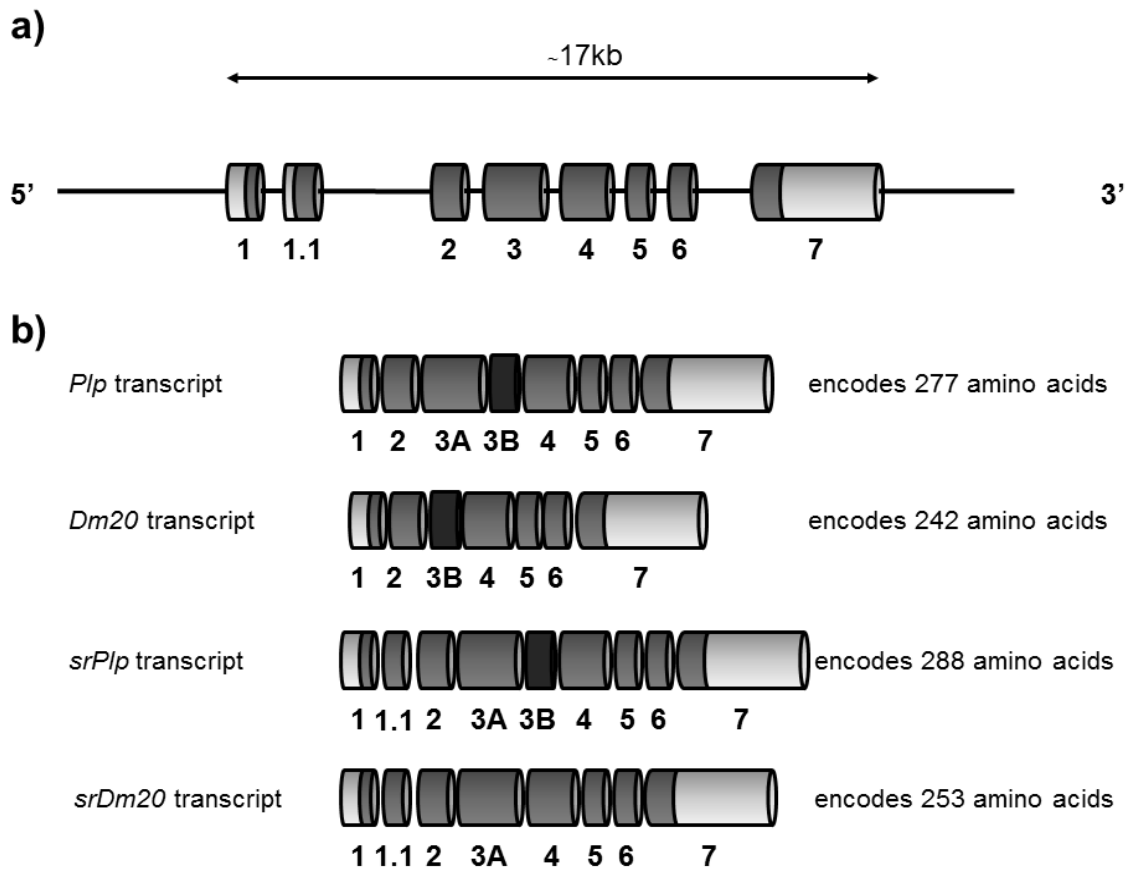


**Figure 2. Organisation of the murine *Plp1* gene and its major transcription products.**

Chromosomal arrangement of the *Plp1* gene (a). Four major products are generated from the *Plp1* gene, the two most abundant transcripts *Plp* and *Dm20*, followed by the two less frequently transcribed *srPlp* and *srDm20* (b) (Yool, 2000).

#### 1.5.2.1.2 *Regulation of the Plp1 gene expression*

Expression of the *Plp1* gene is controlled mainly at the level of gene transcription and the protein production mirrors transcription levels (Cook et al., 1992). Promoter and enhancer regions have been identified on intron 1 and as little as 225bp of the promoter region is sufficient to induce oligodendrocytic specific *Plp1* expression (Cambi and Kamholz, 1994). Interestingly the *Plp1* gene transcripts are expressed parallel to the *Mbp* gene transcripts, which indicates that these two genes share a common controlling pathway (Cook et al., 1992).

#### 1.5.2.1.3 *Posttranscriptional modification and regulation*

Both *Plp* and *Dm20* share the same pre-mRNA and are produced through alternate splicing of the pre-mRNA. *Dm20* mRNA differs from the *Plp*-mRNA by the exclusion of exon 3b (Nave et al., 1987b). The expression pattern of the two isoforms is spatially and temporally distinct (Levine et al., 1990). *Dm20* dominates premyelination, but by the time of maximal *Plp1* gene expression, *Plp* supersedes *Dm20* and becomes the predominant form in the oligodendrocyte.

The two minor isoforms, *srPlp* and *srDm20* show a similar splice site within exon 3 but additionally retain exon 1.1 (Bongarzone et al., 1999). More *Plp* isoforms have been detected recently but the role of these isoforms has not yet been clarified (Jahn et al., 2009; Sarret et al., 2010).

#### 1.5.2.1.4 *Plp1 gene expression during development*

In the mouse *Plp* expression can first be detected post-natally between P0 and P2. The myelination pattern of the CNS follows that of *Plp* upregulation, starting at the medulla and progressing rostrally to the cerebrum and caudally to the spinal cord (Verity and Campagnoni, 1988). At peak myelination, which is around 22 days post natal in the mouse, *Plp* expression is at its highest level and then drops to approximately 60% (Sorg et al., 1987). *Dm20* transcripts on the other hand can be first detected at day 9.5 of embryonic development and DM20

protein is first detected at E12 in the basal plate of the diencephalon and caudal hypothalamus (Spassky et al., 1998). From there, these cells populate the major white matter tracts. DM20 expressing cells belong to the oligodendrocyte precursor population and later develop into myelin synthesising oligodendrocytes (Dickinson et al., 1996). Post-natally *Dm20* expression is observed in close relation to *Plp* expression and maximally reaches 50% of the *Plp* mRNA level (Nave et al., 1987b).

#### **1.5.2.1.5    *The PLP/DM20 protein***

PLP is a transmembranous hydrophobic tetraspan myelin protein, which is composed of 276 amino acids. PLP is located in the lipid bilayer of the myelin sheath membrane. DM20, which contains 35 amino acids less than PLP, has a similar location in the cell membrane. The *Plp* and *Dm20* mRNA are translated in the rough endoplasmatic reticulum and the proteins are transported through the secretory pathway to the myelin sheath membrane where they become integrated into the lipid bilayer (Gow et al., 1994). There are only two post-translational modifications of the protein; removal of the amino terminal located methionine and acylation, reviewed in (Yool, 2000).

The six cysteine residues of the PLP protein (four in DM20) are acetylated with long chain fatty acids, mainly palmitic, oleic, palmitoleic and stearic acids (Bizzozero and Lees, 1999). The acylation of PLP renders the protein more hydrophobic and influences the protein conformation.

#### **1.5.2.1.6    *The function of PLP and DM20 in the CNS***

To date the precise function of PLP/DM20 has still not been fully elucidated. The abundance and transmembranous configuration of PLP in the myelin sheath membrane suggests that PLP has a structural function and provides the compaction and stability to the myelin sheath (Boison et al., 1995). *Plp1* gene mutants often show a hypomyelination and an altered myelin periodicity, especially as condensed intraperiod lines (Duncan et al., 1987;Yool, 2000).

Furthermore PLP/DM20 mediates the provision of trophic support for axons. Mice containing a *Plp1* null allele myelinate relatively normally but develop a late onset axonal pathology, suggesting a supportive role of glial cells for axonal integrity (Griffiths et al., 1998). The PLP protein structure also shows similarities to ion channel proteins and *in vitro* data suggests that PLP isoforms may act as ionophores (Diaz et al., 1990; Mobius et al., 2008).

DM20 is expressed during embryonic development and also during myelination. The presence of *Dm20* transcripts in a subset of OPCs during embryonic development suggests that DM20 is involved in embryonic oligodendrocyte development (Dickinson et al., 1996). However, *Plp1* knockout mice are not deficient in oligodendrocytes.

#### 1.5.2.2 Pelizaeus-Merzbacher disease

PMD (OMIM 312080) and the allelic form SPG2 (OMIM 312920) are X-linked, recessive leukodystrophies caused by mutations in the *PLP1* gene. The severity of the disease is to some extent dependent on the precise mutation (Cailloux et al., 2000; Garbern, 2007). So far over 100 different mutations in the *PLP1* gene have been identified, including duplication of the gene, null mutation and various missense mutations (Hudson et al., 2004). The clinical signs include nystagmus, psychomotor developmental retardance, stridor, spasticity, cerebellar symptoms, mental deterioration, seizures and optical atrophy (Seitelberger, 1995). The marked spectrum of clinical severity of the disease has led to the classification of the PMD into three main categories (Seitelberger, 1995):

- 1.) Type I, which is the connatal form with early onset and rapid progression leading to death within the first two years of life
- 2.) Type II, which is the classical form with an early onset and slow progression with a survival rate up to 40 + years

3.) Type III, which is an intermediate form between Type I and II, with survival rates up to early adolescence

The variety of mutations in the *PLP1* gene causing PMD may explain, in part, the clinical spectrum of disease severity, ranging from severe lethal to mild, late onset forms (reviewed in Koeppen and Robitaille, 2002).

The pathology of PMD consists of a generalised, symmetric hypomyelination of the CNS with reduced numbers of oligodendrocytes and a dense fibrillary astrocytosis. Regions with myelin patches are sometimes present and macroscopically visible. Neuronal architecture appears normal. Ultrastructurally the compaction and lamellar order of the myelin sheath may appear abnormal. The PNS is unaffected and myelinates normally. In the acute congenital form the CNS is severely hypomyelinated (Seitelberger, 1995).

Due to the X-linked mode of inheritance, males are predominantly affected and females act, in general, as unaffected carriers. However juvenile (Hodes et al., 1995) and adult (Hodes et al., 1997) PMD has also been observed in females. Due to random X-inactivation in females, female carriers are chimeric at the *PLP1* locus. Most females do not develop clinical disease despite 50% of oligodendrocytes potentially being affected by the mutation. The observation made in *jimpy* mice, where the genetically altered oligodendrocytes die during post natal development (Kagawa et al., 1994) and are replaced by the oligodendrocytes expressing the wild type *Plp1* gene, may provide an explanation. Whether the situation is similar in humans is unknown, but assuming so the survival of individual cells most likely depends on the nature of the mutation (Koeppen and Robitaille, 2002), since cells harbouring a mild mutation are more likely to survive than those with a severe mutation (Edgar et al., 2002).

#### **1.5.2.2.1 Genetic basis of *PLP1* gene related disorders in man**

The first *PLP1* gene abnormalities leading to PMD to be identified were point mutations (Gencic et al., 1989; Hudson et al., 1989; Trofatter et al., 1989). To

date more than 100 point mutations causing PMD have been identified (reviewed in Woodward, 2008; Garbern et al., 1999). Recently, *PLP1* deletion or loss of function (Raskind et al., 1991) and *PLP1* gene duplication (Inoue et al., 1999) has been linked to PMD (Inoue et al., 1996a). *PLP1* gene duplication accounts for 60 - 70% of PMD cases (Sistermans et al., 1998). Duplication (or occasionally, triplication) of the *PLP1* gene is probably caused by unequivocal sister chromatid exchange during meiosis in the male (Inoue et al., 1999; Mimault et al., 1999; Yool et al., 2000).

From the disease severity point of view the missense mutations, which result in non-conservative amino acid substitution, often cause the most severe form of PMD, whereas *PLP1* gene duplication in general causes a moderate form and in the case of *PLP1* gene deletion or loss of function mutations, a mild form of PMD (reviewed in Woodward, 2008). The effect of *PLP1* gene overexpression or deletion further suggests that altered gene regulation plays a role in the PMD pathogenesis. In short, gain of function or cytotoxic effects of PLP are believed to be largely responsible for early, more severe forms with dysmyelination, whereas loss of function is seen in relation with the later milder forms, where mainly CNS and PNS demyelination is observed (reviewed in Woodward, 2008).

Presumptive diagnosis of PMD is made based on clinical signs and white matter changes detected on MRI. Final diagnosis can often be achieved with specific genetic tests. Since most of the cases are caused by *PLP1* gene overexpression, interface fluorescence *in situ* hybridisation (FISH) technique (Woodward et al., 1998) is the first choice to apply on suspected PMD cases. If FISH turns out to be normal, *PLP1* gene sequencing is used to identify mutations (reviewed in Woodward, 2008). However in about 20% of all suspected PMD cases no abnormalities are detected, which suggests that either changes in regulatory sequences or other loci can cause PMD (reviewed in Woodward, 2008).

### 1.5.2.3 Plp1 gene related disease in animals

#### 1.5.2.3.1 *Plp1* gene mutation in animals

*Plp1* gene mutations has been described in various species such as the mouse (*Plp<sup>jp</sup>* (Nave et al., 1987a), *Plp<sup>jp-4</sup>* (Pearsall et al., 1997), *Plp<sup>jp-msd</sup>* (Gencic and Hudson, 1990), *Plp<sup>jp-rsh</sup>* (Schneider et al., 1992)), the rat (*Plp<sup>md</sup>* (Boison and Stoffel, 1989; Duncan et al., 1987)), the dog (*Plp<sup>sh</sup>* Nadon et al., 1990) and the rabbit (*Plp<sup>dt</sup>* (Tosic et al., 1994), Table 1).

The *jimpy* mouse harbours a point mutation in intron 4 of the *Plp1* gene leading to aberrant RNA processing by disrupting the 3' acceptor splice site, which leads to a deletion of exon 5. This produces a truncated protein with a novel cysteine rich carboxy terminus (Nave et al., 1987a). The other mutants harbour *Plp1* gene point mutations, which lead to amino acid substitutions.

Most of these mutants develop a severe hypomyelination of the CNS, often accompanied by a loss of oligodendrocytes, microglial proliferation (Vela et al., 1996) and astrocytic hypertrophy (Billings-Gagliardi et al., 1995; Harsan et al., 2007). Clinically, the affected animals develop tremors, ataxia and seizures and in general die prematurely (Thomson et al., 1997). However, *rumpshaker* mice show a mild phenotype with a normal life span (Griffiths et al., 1990; Thomson et al., 1997; Edgar et al., 2004a). Nevertheless, the clinical course depends on the genetic background of the mouse (Al-Saktawi et al., 2003).

Although profoundly hypomyelinated, some axons still contain a myelin sheath. The ultrastructure of these myelin sheaths in mutants is often abnormal, apparent as thin and loosely compacted sheaths. In the *md* rat for example, the intraperiod line becomes condensed, which leads to a measurable reduction in the periodicity from 11 nm in the wild type to 9 nm in the *md* rat (Duncan et al., 1987).

The reason for the hypomyelination in the *jimpy* mouse, the *msd* mouse or the *md* rat is considered to be the result of an increased apoptosis of mature

oligodendrocytes, although the numbers of immature oligodendrocytes is normal (Gow et al., 1998;Nadon and Duncan, 1995;Skoff, 1995;Cergnet et al., 2001). The situation in the *shaking pup* dog appears to be different, where the oligodendrocytes remain immature and fail to myelinate (Nadon and Duncan, 1996).

Different studies have focused on the intracellular effects of abnormal *Plp1* gene function due to point mutations (Gow et al., 1998;Southwood et al., 2002;McLaughlin et al., 2007; reviewed in Woodward, 2008). In the variants caused by missense mutations of the *Plp1* mouse/rat gene the mutant PLP appears to accumulate in rough endoplasmatic reticulum and Golgi vesicles causing endoplasmic reticulum stress, which activates the unfolded protein response (UPR) and eventually leads to oligodendrocytic death (Cergnet et al., 2001; reviewed in Woodward, 2008). Mutated PLP protein appears to be poorly tolerated by the oligodendrocyte and apoptosis appears to be the main mechanism preventing the synthesis of a potentially abnormal myelin sheath.

#### **1.5.2.3.2 *Transgenic animals***

#### **1.5.2.3.3 *Plp1 gene deletion, null alleles and knock out models***

In models with *Plp1* gene deletion or loss of function, myelin development initially appears normal. However, with age a progressive axonopathy develops. The late onset of axonal degeneration is believed to be caused by disrupted axonal glial interaction resulting from a lack of PLP/DM20 (Griffiths et al., 1998;Yool, 2000).

These observations further highlight the multifaceted effects of *Plp1* gene mutations and that PLP does not only play a structural role in myelin sheath, but is also involved in axono-glial interactions and oligodendrocyte-mediated axonal support.

#### 1.5.2.3.4 *Plp1* gene overexpressing animals

*PLP1* gene duplication is considered to be the major cause of PMD (Sistermans et al., 1998) and is characterised by a dysmyelination of the CNS (Seitelberger, 1995). So far, no spontaneous model with *Plp1* gene overexpression has been described. There are three transgenic engineered mouse models overexpressing the entire *Plp1* gene, the 4e (Kagawa et al., 1994) the #66 and the #72 (Readhead et al., 1994) mouse model, each with different numbers of extra copies of the *Plp1* gene ([Table 1](#)). The extra copies, including all the exonic sequences linked to 5' and 3' gene flanking sequences of the murine *Plp1* gene, were inserted by pronuclear microinjection and randomly integrated into the genome (Readhead et al., 1994;Kagawa et al., 1994). The 4e contain 2 (Kagawa et al., 1994), the #72 contain 3 (Readhead et al., 1994) and the #66 contain 7 extra *Plp1* gene copies (Readhead et al., 1994) per haploid genome. All three homozygote models develop hypomyelination with associated tremors and seizures (Inoue et al., 1996b;Readhead et al., 1994;Anderson et al., 1999;Kagawa et al., 1994). However the severity of the phenotype is markedly different; the homozygous 4e and #66 develop early clinical signs and die around 60 days of age whereas the homozygous #72 shows a slower disease progression in which clinical signs appear later and die around 120 days of age. The mRNA level in these animal models does not correlate with the number of *Plp1* gene copies and some of these transgenes are probably less effectively transcribed than others (Kagawa et al., 1994;Inoue et al., 1996b;Readhead et al., 1994).

Hemizygotes from all three lines, on the other hand, appear to develop normally and produce similar levels of myelin compared to the wild type. With age, a progressive demyelination of the CNS becomes apparent in the hemizygotes (Inoue et al., 1996b;Anderson et al., 1998;Ma et al., 2006). The demyelination is accompanied by axonal changes such as axonal swellings, which are mainly present in tracts with small diameter fibres.

Transgenic animals, which overexpress only *Dm20* have also been generated (Johnson et al., 1995;Mastronardi et al., 1993). These mice also develop a late onset demyelination with age and the disease severity is dependent on the level of *Dm20* overexpression. There appears to be no correlation between the level of *Dm20* overexpression and DM20 protein levels (Johnson et al., 1995).

Line	Source	Structural gene unit	Haploid copy number	Reference
#66	Mouse	7 exons / 6 introns	7	(Readhead et al., 1994)
#72	Mouse	7 exons / 6 introns	3	(Readhead et al., 1994)
4e	Mouse	7 exons / 6 introns	3	(Kagawa et al., 1994)
<i>Plp</i> Tg1	Human	<i>Plp</i> - cDNA	30	(Nadon et al., 1994)
<i>Dm20</i> Tg2	Human	<i>Dm20</i> - cDNA	?	(Nadon et al., 1994)
ND3a	Human	<i>Dm20</i> - cDNA	17	(Mastronardi et al., 1993)
ND4	Human	<i>Dm20</i> - cDNA	70	(Johnson et al., 1995)

Table 1. Transgenic animals overexpressing *Plp* genomic transgenes and human cDNA transgenes (Yool, 2000).

#### **1.5.2.3.5 Pathogenesis in *Plp1* gene overexpression**

The situation in *Plp1* overexpressing mouse models is different to that in the point mutations. With low *Plp1* gene copy numbers, relatively normal myelination takes place during post natal development and the formed myelin appears ultra-structurally normal. However with increasing numbers of copies of the *Plp1* gene, the CNS pathology becomes more severe, with marked dysmyelination occurring during post natal development (Kagawa et al., 1994;Anderson et al., 1998;Anderson et al., 1999;Readhead et al., 1994). The homozygous #72 mouse, which is the subject of this PhD thesis, with 3 extra copies of *Plp1* gene per haploid, has a relatively mild degree of dysmyelination in development that is followed by progressive demyelination, at least in the optic nerve (Anderson et al., 1998;Anderson et al., 1999;Edgar et al., 2010;Inoue et al., 1996b). The effect on disease severity of *Plp1* gene overexpression is not only dependent on the numbers of *Plp1* gene extra copies but most likely also on modifying loci (Inoue et al., 1999). A prominent astrogliosis and microglial response have also been described in relation to *Plp1* gene overexpression (Ma et al., 2006;Tatar et al., 2010) and has been suggested to contribute to the progression and severity of the demyelination process (Ip et al., 2007;Ip et al., 2006).

#### **1.5.2.3.6 Biochemical changes related to *Plp1* gene overexpression**

A study investigating the biochemical effect of *Plp1* gene overexpression in cell lines has shown substantial disruption in myelin protein transport and distribution (Simons et al., 2002). The overexpression of *Plp1* leads to accumulation of PLP and cholesterol in late endosomes and lysosomes (Simons et al., 2002). In PLP overexpressing cells, sphingolipids become missorted from their normal location in the Golgi apparatus (Simons et al., 2002).

Using spinal cord and brain from a *Plp1* gene overexpressing mouse model (line #66), Karim et al. showed that PLP/DM20 accumulates in the cell body and is reduced in myelin (Karim et al., 2007). This study also reported that the

overexpression of the *Plp1* gene significantly reduced MBP steady state levels in myelin, emphasizing that overexpression of the *Plp1* gene causes an imbalance in the assembly of myelin components (Karim et al., 2007). Further *in vitro* and *in vivo* investigation of oligodendrocytes from homozygous #66 and #72 mice confirmed the perturbed trafficking and assembly of PLP/DM20 into myelin and lipid rafts. Ultra structural investigation showed an increase of autophagosomes, which are thought to function as a storage vehicle for over synthesised PLP/DM20, in oligodendrocytes. The severity of the ultra-structural changes in the oligodendrocyte cell body was gene dose dependent (Karim et al, 2010).

The biochemical changes in myelin in the *Plp1* gene overexpressing mouse models are believed to result in disturbed myelin formation, leading to perturbation of myelin and oligodendrocyte development (Readhead et al., 1994;Kagawa et al., 1994;Inoue et al., 1996; Simons et al., 2002:Karim et al., 2007, Karim et al, 2010). The different biochemical and morphological changes that are evident suggest that disruption of normal protein distribution leads to impaired cell function and results in abnormal morphological development.

### 1.5.3 Demyelination in *Plp1* overexpressing mice

*Plp1* overexpression has an adverse effect on normal myelin maintenance, which over time leads to instability of the myelin sheath, progressive demyelination, an inflammatory response and axonal changes (Inoue et al., 1996b;Kagawa et al., 1994;Anderson et al., 1999;Edgar et al., 2010;Readhead et al., 1994). The findings of some studies using transgenic models with a low number of *Plp1* gene extra copies or just overexpression of *Dm20* gene, suggest that these mouse models may mimic chronic MS demyelinated lesions and might provide new insights into the development of remyelination failure (Ma et al., 2006;Mastronardi et al., 1993). So far no detailed description of the temporal and spatial pathological development and progressive demyelination in *Plp1* gene overexpressing mouse models has been published, except in the optic nerve (Edgar et al., 2010), although other studies have shown that the spinal cord is demyelinated in older mice (Inoue et al., 1996b;Kagawa et al., 1994;Anderson et al., 1998;Readhead et al., 1994). The spontaneous demyelination and the

development of chronic demyelinated regions are of high interest. Major intracranial white matter tracts, such as the corpus callosum, have been shown to have reduced myelin content in the adult #72 mouse (Ruest et al., 2011) and hemizygote 4e model (Ma et al., 2006), but the development of the pathological process in these two models has not been described to date. Considering the myelin phenotype in these animals, the relative clinical normality of the #72 mice up to 90 days is remarkable. After 90 days the mice show a subtle tremor and generalised mild ataxia with seizures, which eventually leads to premature death. The relatively late development of clinical deficits suggests that post natal development is largely normal but is followed by apparently progressive clinical signs, suspicious of a progressive demyelination, presumably without repair.

## **1.6 Use of MRI in diagnosing white matter changes**

One of the difficulties in monitoring the progression of white matter lesions *in vivo* (including the effect of any intervening therapy) has been visualising the CNS. In the past the full distribution and extent of the pathology was only evident at the point of necropsy. With the advent of advanced imaging modalities including magnetic resonance imaging (MRI), the diagnosis and monitoring of white matter lesions *in vivo* has become possible. In the case of multiple sclerosis, MRI has resulted in improved accuracy of diagnosis, localisation and monitoring of the course of white matter pathology (Ciumas et al., 2008; Fox, 2008). Repeated MRI allows mapping of lesion distribution and provides the ability to compare temporal changes in lesion size and location. One major disadvantage of conventional MRI sequences in the characterisation of white matter pathology is the inability to distinguish between different pathological changes, in particular between areas of acute active inflammation with ongoing demyelination and inactive, chronically demyelinated areas (Fox, 2008; Inglese et al., 2005b; Inglese et al., 2005a). A modality capable of distinguishing these two different stages of white matter pathology would have a major impact on monitoring disease development, treatment regime and accurate prognosis for the affected patient and would also allow better monitoring of experimental models of demyelination.

Advanced MRI techniques such as magnetisation transfer imaging (MTI), magnetic resonance spectroscopy (MRS) and diffusion weighted MRI (DW MRI) are being used to detect pathological changes in relation to the myelin sheath (reviewed in Zivadinov and Cox, 2007). The most commonly used technique in clinical settings is MTI, which is based on the interaction between unbound free protons in water and protein bound molecules (reviewed in Horsfield, 2005). MTI has proven useful in evaluating lesion type in MS and EAE and correlations have been found with regard to lesion development (reviewed in Horsfield, 2005; Zivadinov and Cox, 2007). However, not only myelin, but also inflammation, is responsible for protein-proton interaction and the value of MTI in distinguishing inflamed from non-inflamed demyelinating lesions is therefore still speculative.

Magnetic resonance spectroscopy has mainly been used in neurodegenerative disorders (reviewed in Zivadinov and Cox, 2007). MRS in MS has not yet been used extensively, but it has been demonstrated that inflammation correlates with increased choline, lactate and lipid peaks, whereas axonal damage correlates with an increased N-acetylaspartate (NAA) peak. MRS is considered to be helpful in detecting axonal damage and could become valuable in specifically detecting progressive axonal degeneration (reviewed in Zivadinov and Cox, 2007).

The DW MRI technique utilises the movement of molecular water within the tissue. The motion of water molecules is caused by the natural phenomenon of random thermal motion of molecules, also referred to as Brownian motion (reviewed in Mori and Zhang, 2006; Zivadinov and Cox, 2007). In pure water, the water molecules can move around freely. Water molecules in tissue, however, are restricted in movement, with this restriction depending on the composition of the surrounding tissue. Cell type, cell number, cell integrity and extracellular composition all contribute to the water diffusivity. White matter is a complex network composed of axons, myelin sheaths and the associated supporting cell populations of oligodendrocytes, astrocytes, microglia, trafficking immune cells and OPCs. All these cells could potentially influence the Brownian motion of water molecules. In normal tissue axons have the most pronounced effect on water diffusivity (Basser and Pierpaoli, 1996; Beaulieu and Allen, 1994; Beaulieu, 2009; Zivadinov and Cox, 2007), but myelin and, in all probability, the density of

the supporting cell population also contribute substantially to the direction of water diffusivity. Since axons in specific tracts are arranged in a parallel fashion, DTI becomes useful for fibre tract examination and tracking. In these white matter tracts, the parallel nature of the nerve fibres leads to a net movement of water molecules parallel to the axonal alignment and this can be detected and measured by DTI sequences (Alexander et al., 2007). The high sensitivity of the sequence for water molecule diffusion may also be used to identify pathological states of white matter or pathological process interfering with the normal course of water diffusion along axons (Laule et al., 2007). However, distinguishing between chronic demyelination and active inflammation with ongoing demyelination has not been fully elucidated.

#### **1.6.1 The homozygote #72 optic nerve as a model to evaluate the ability of MRI techniques to detect specific white matter pathological states**

Ideally a mouse model in which an inflamed demyelinated and a chronic non-inflamed “silent” demyelination exists simultaneously along one major white matter tract would be used to evaluate the sensitivity of novel MRI techniques to detect different white matter lesion types. The adult #72 homozygote optic nerve, with spatially distinct regions of active and complete demyelination (Edgar et al., 2010), is as an ideal model to evaluate MTI, MRS or DW MRI.

## 1.7 Aim of the thesis

The study aims are

- 1.) To describe the temporal histological changes in white matter elements in the corpus callosum in the #72 mouse model in order to understand the nature and progression of the pathology that leads to profound hypomyelination in this model.
- 2.) To evaluate changes in OPC intrinsic and extrinsic factors in relation to the reduced myelin content using *in vivo* and *in vitro* strategies.
- 3.) To use the optic nerve of the #72 mouse model of PMD to test if DW MRI techniques can distinguish between specific white matter lesion types.

The results of these three chapters will be critically assessed and future areas, where the findings can be integrated and which could induce new work, will be discussed in the final discussion of the thesis.

## **2 Material and Methods**

### **2.1 Miscellaneous**

All experiments were carried out according to the guidelines laid out in the Animals Scientific Procedures Act under a project license from the UK Home Office, and were approved by the local Ethics and Welfare review panel of the Faculty of Veterinary Medicine, University of Glasgow.

Inorganic chemicals were of molecular biology grade and were sourced from Sigma or VWR. Solutions were sterilised as appropriate. Bulk solutions were autoclaved using a stovetop steam autoclave (Prestige classic steam autoclave 2100, Prestige Medical UK). Small volumes and fluids that could not be autoclaved were either filter sterilised through a 0.2µm filter (Minisart Plus filter, Sigma Aldrich 17823K) in a sterile laminar flow hood (Biogen) or UV sterilised, where each sample was placed in a UV steriliser for twelve minutes. Gloves, eye protection and protective clothing were worn when appropriate. Fixatives, volatile liquids and toxic powders were prepared in a specifically designated fume cupboard.

Details of the preparation of fixatives, stains, buffers, staining and processing protocols can be found in the Appendix and are cross referenced by page number in this section.

### **2.2 Mouse breeding**

#### **2.2.1 Animal breeding facilities**

Mice were bred in designated animal breeding facilities, Biological Services, Faculty of Veterinary Medicine, University of Glasgow. Picorna virus and murine hepatitis virus infections have occurred in the past within the unit and both are known to be associated with neurological disease in mice (Fujiwara, 1994;Lipton

et al., 1994). During the period of the study, there was no evidence of clinical disease. The wild type mice did not show the phenotype and pathology seen in the transgenic mice.

## **2.2.2 Transgenic mouse lines**

### **2.2.2.1 The *Plp1* transgenic overexpressing #72 transgenic mouse line**

#72 transgenic mice were generated by (Readhead et al., 1994). A rat *Plp1* cDNA probe was used to isolate the murine *Plp1* gene from a cosmid library. The isolated murine *Plp1* gene was used to generate a purified 26.6 kb *Cla*I fragment that contains the transgene construct including 3.5 kb of the PLP 5' regulatory region and a transgene unique T7 promoter at the PLP 3' region. To generate transgenic mice, pronuclear microinjection into BDF2-fertilized ova of the transgene cassette was performed. Two transgenic lines were produced containing intact *Plp1* transgenes, the #66 and the #72 line. These two lines were assessed by southern blotting, estimating seven copies in the #66 line and three copies in the #72 line per haploid genome. The transgene cosegregated in subsequent generations in an autosomal inheritance pattern suggestive of tandem integration at autosomal sites (Readhead et al., 1994). In our study we only used the #72 line on a C57BL/6N (Charles River) background, containing 6 extra copies of the *Plp1* gene in the homozygote mouse ([Figure 3](#)).

### **2.2.2.2 The *Plp1* transgenic and cyan fluorescing protein (Thy-1 CFP) expressing mouse line**

Mice expressing cyan fluorescence protein (CFP) under the *Thy1* reporter gene (B6.Cg-Tg(Thy1-CFP)23Jrs /J) produced by (Feng et al., 2000) were introduced into the *Plp1* transgenic #72 mouse line on a C57BL/6N background and bred for more than six generations. In the CNS, *Thy1* is mainly expressed in neurons. The CFP gene has been inserted into the *Thy1.2* gene excluding part of exon 2 and 4, completely excluding exon 3 and the flanking introns of exon 3 (Caroni,

1997;Feng et al., 2000). The product was introduced by pronuclear microinjection into fertilised oocytes obtained from mating C57BL/6J with CBA hybrids (Feng et al., 2000). Although *Thy1* is expressed in most neurons (Kollias et al., 1987;Vidal et al., 1990), it has been observed that in the transgenic *Thy1 CFP* mice generated by Feng et al., the CFP expression is limited to a certain subset of neuronal cells. About 25 different founder lines have been described so far (Feng et al., 2000). The reason for the variable expression pattern in the different lines is not clear but is thought to most likely be due to genetic, epigenetic and stochastic components on transgene expression in relation to the insertion site of the *CFP* transgene copies (Feng et al., 2000). However, the CFP expression from a specific line does not vary in the following generations (Feng et al., 2000). In our *Thy 1-CFP* expressing mouse line, only a subset of motor and sensory neurons express CFP. Therefore not all axons in the corpus callosum express CFP. CFP is located unbound in the cytoplasm and is distributed in neuronal cell bodies, axons and dendrites (Feng et al., 2000). The fluoroescing protein tends to accumulate in axonal swellings, which are early changes in axonal pathology. Therefore, CFP expressed in axons can be used as a sensitive marker for early axonal changes.

The newly created mouse line carries the *Plp1* transgene and the *Thy1-CFP* transgene (*CFP+ / Plp1+*). Only CFP positive male mice were used in the current study. The group of neurons expressing CFP can be readily detected under epifluorescence microscopy without further processing. Due to the fluorescence microscope filters used in the Olympus IX-70, CFP appears green instead of blue. To increase the probability of producing homozygous *Plp1* overexpressing and CFP positive samples for transplantation studies the *CFP+ / Plp1+* line was mated with a homozygote #72 mouse ([Figure 4](#)).

### 2.2.2.3 The green fluorescent protein ( $\beta$ -actin GFP) expressing mouse line

The GFP expressing mouse line containing the reporter gene *GFP*, was generated by (Ikawa et al., 1995). The GFP transgene was linked to the chicken  $\beta$ -actin promoter possessing a cytomegaly virus enhancer (Ikawa et al., 1995). The GFP construct was introduced by microinjection into male pronuclei of B6C3F1

fertilized oocytes. The resulting offspring expressed GFP under a *β-actin* promoter. In the cell, GFP is located unbound in the cytoplasm (Ikawa et al., 1995) and is detected under UV light without additional processing. *In vivo* GFP positive pups can be detected easily by exposing them to ultraviolet (UV) light, where the pups display green fluorescence ([Figure 4](#)).

#### **2.2.2.4 The Plp1-LacZ fusion protein transgenic mouse line**

Mice harbouring a *Plp1-LacZ* fusion gene were generated by (Wight et al., 1993). The *Plp1-LacZ* transgene contains the proximal 2.4 kb of 5'-flanking *Plp* DNA, exon1, intron 1 and the first 37bp of exon 2 ligated to a *trpS-LacZ* fusion gene and SV-40 polyadenylation signal. The transgene was introduced by pronuclear microinjection into BDF2 fertilised mouse oocytes (Wight et al., 1993). The resulting transgene product is a protein where  $\beta$ -galactosidase is fused to 13 amino acids from the NH<sub>2</sub>-terminal of PLP and is only expressed when PLP expression occurs. The fusion of  $\beta$ -galactosidase with the thirteen amino acids from the NH<sub>2</sub>-terminal of PLP is sufficient for the transgene product to be integrated into the myelin sheath (Wight et al., 1993) and is a marker of myelin sheaths ([Figure 5](#)).

#### **2.2.3 Maintenance of transgenic lines of mice**

The *Plp1* overexpressing #72, *Thy-1 CFP/Plp1*, *β-actin GFP* and *Plp1-LacZ* lines of transgenic mice were maintained by creating colonies of transgene positive animals with a C57BL/6N background.

##### **2.2.3.1 Maintenance of the #72 mouse line**

For the histopathological evaluation of the #72 corpus callosum and the MRI study, non-litter mate #72 hemizygote mice on a C57BL/6N (Charles River) background were bred to generate homozygote, hemizygote and wild type offspring. Only homozygote and wild type mice were used for the experiments.

For the cell intrinsic and cell extrinsic pathway evaluation experiments, cell culture experiment and the transplant study, homozygote *Plp1* gene overexpressing #72 males were mated with homozygote *Plp1* gene overexpressing #72 females to generate homozygote samples and wild type males were mated with wild type females to generate wild type samples.

To identify homozygote #72 mice at an early stage (P30) to establish the specific homozygote #72 lineage, genotyping using quantitative real time PCR to ascertain gene copy number and therefore identification of homozygote animals was outsourced to Embark Scientific. To confirm that the line contained the *Plp1* transgene, amplification by PCR was performed as described below. At regular intervals, breeding mice from this line were killed by a schedule 1 method and the optic nerves were dissected and examined to confirm that the line was homozygous for the transgene. The optic nerve of homozygous mice appears relatively transparent compared to the nerve of wild type or hemizygous mice

#### **2.2.3.2 Maintenance of the CFP+/Plp1+ mouse line**

For histopathological evaluation of the axons in the #72 mouse during demyelination and after transplantation of neurospheres, the *CFP Thy-1* mice were crossed with transgene positive #72 mice with a C57BL/6N background (Charles River) for at least six generations. The newly created mouse line was a carrier of the *Plp1* transgene and the *Thy1-CFP* transgene (*CFP+/Plp1+*). For the transplant study, the *CFP+/Plp1+* line was always mated with a known homozygote #72 mouse in order to increase the probability of producing homozygote *Plp1* overexpressing and CFP fluorescing samples. Only CFP and *Plp1* transgene positive male mice were used for this specific study.

#### **2.2.3.3 Maintenance of the GFP expressing mouse line**

For generation of a *GFP* expressing mouse line, a male mouse expressing the reporter gene *GFP* was crossed with a wild type female from the #72 line with a C57BL/6N (Charles River) background. For generation of GFP expressing

neurospheres and GFP expressing OPCs only *GFP*<sup>+</sup> #72 wild type male pups were used.

#### **2.2.3.4 Maintenance of the LacZ expressing mouse line**

In order to generate neurospheres, expressing  $\beta$ -galactosidase under the *Plp1* promoter, P1 pups from -homozygous *Plp1-LacZ* mice on a C57BL/6 background were used.

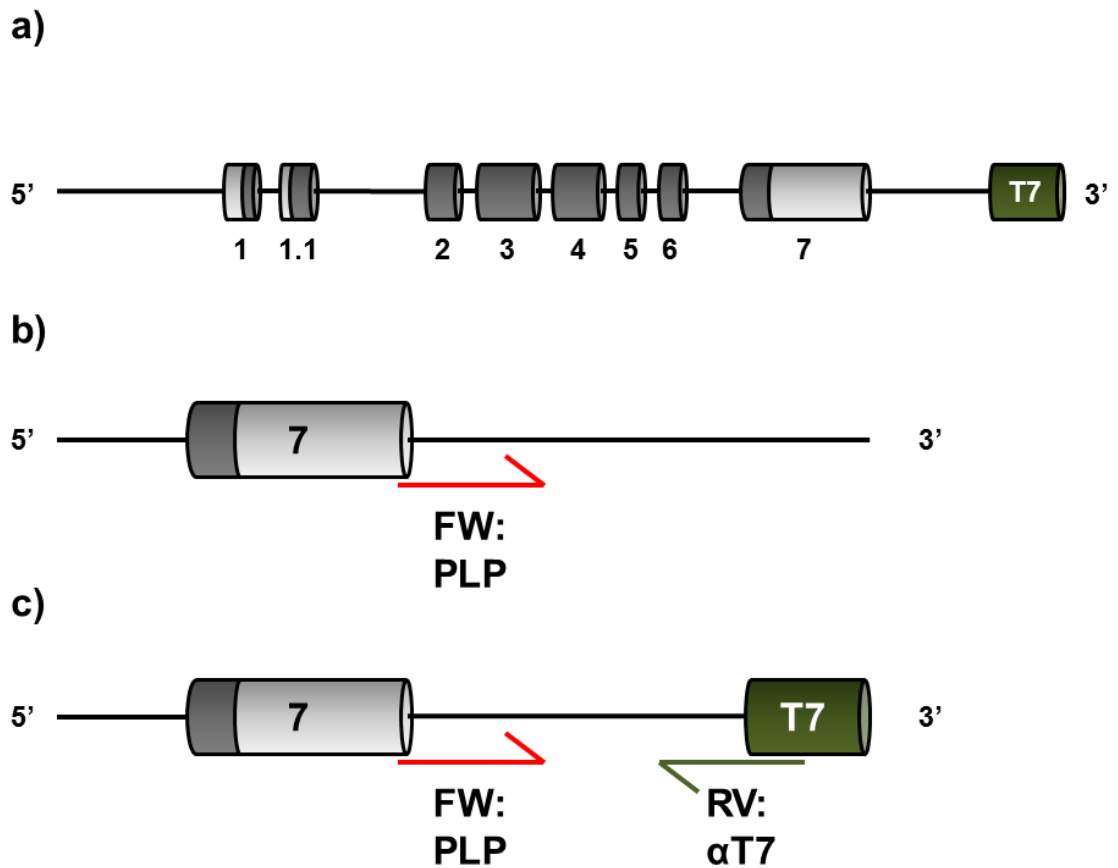


**Figure 3. Schematic representation of the *Plp1* #72 transgene.**

a) Genomic organization of the transgene construct. The *Plp1* exons are depicted as numbered cylinders, dark grey regions represent the coding regions. The transgene specific T7 promoter is shown as a green cylinder

b) Endogenous *Plp1* allele of a wild type mouse lacking the transgene specific T7 promoter. The *Plp* primer (red arrow) binds to the *Plp1* gene. However as the T7 promoter is absent, the reverse T7 primer cannot bind to the DNA, accordingly no PCR product can be amplified.

c) The 3' end of *Plp1* transgene with the T7 promoter. The *Plp1* primer (red arrow) and the T7 primer (green arrow) will generate a PCR product of approximately 400bp readily detectable by ethidium bromide gel electrophoresis (modified from Yool, 2000).

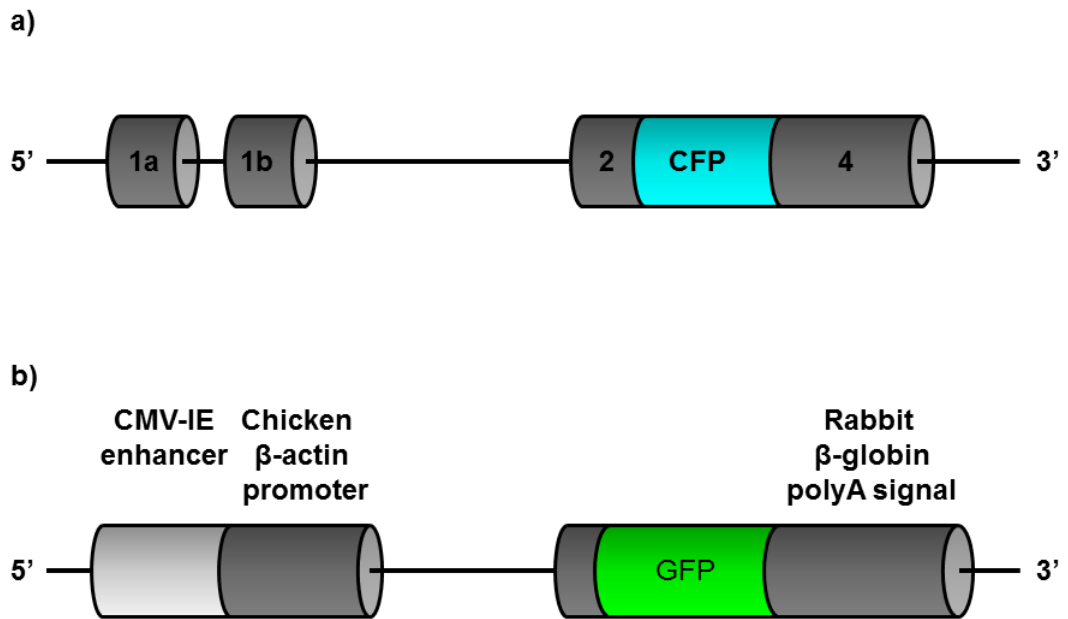


**Figure 4. Schematic representation of CFP and GFP transgene constructs.**

a) Schematic representation of *CFP Thy1* transgene. Exons are numbered and are coloured in dark grey and the CFP gene in turquoise. The CFP gene was inserted into the *Thy1.2* gene as a construct comprising part of exon 2 and full length exon 4 (Caroni, 1997; Feng et al., 2000).

b) Schematic representation of *GFP B-actin* transgene. Expression of the GFP *B-actin* transgene is driven by a combination of two regulatory elements comprising a cytomegaly virus (CMV-IE, light grey cylinder) enhancer and a chicken - *B-actin* promoter (dark cylinder). A rabbit *B-globin* polyadenylation signal (dark grey) is inserted in the 3' end of the *GFP* transgene (Ikawa et al., 1995).

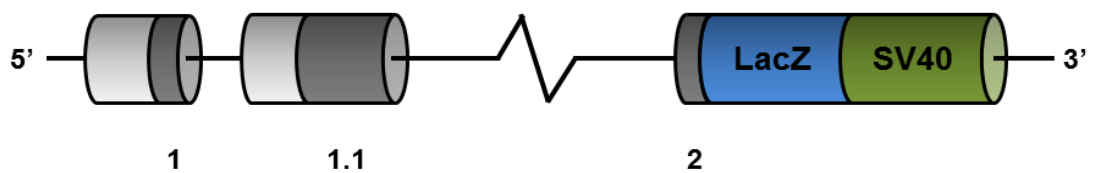


**Figure 5. Schematic representation of the LacZ transgene construct.**

The construct contains exon 1, intron 1 and the first 37bp of exon 2 followed by the LacZ gene linked to a SV40 polyadenylation signal (Wight et al., 1993). Coding regions are in dark grey, LacZ transgene in blue and the SV40 polyA signal in green (modified from Yool, 2000).

## **2.3 Isolation of nucleic acid**

### **2.3.1 Tissue biopsy procedure**

Ear biopsies for DNA extraction were taken using an ear punch, transferred into an Eppendorf tube and stored at -20°C. In the case of CFP expressing animals, fresh ear biopsies were used for CFP evaluation. Tissue from tail biopsies were placed in an Eppendorf tube, stored at -20°C and later used for DNA extraction. The ear biopsies were performed in a systematic manner so that the location of the ear punch was also used for animal identification ([Figure 5](#)).

### **2.3.2 Extraction of genomic DNA from tissue**

DNA was extracted from ear or tail biopsies using 100µl of 50mM sodium hydroxide (Fisher, 1310-73-2). The tissue was lysed on PHC-3 thermal cycler (Techne) for 90 minutes at 95°C, then cooled to 4°C and neutralised using 10µl Tris buffer, pH 5.0 per sample (Truett et al., 2000).

## 2.4 PCR Genotyping

### 2.4.1 PCR core programme

Amplifications for genotyping were performed on a Perkin Elmer DNA thermal cycler

1) Initial cycle	denaturing temperature	94°C	3min
	annealing temperature	58°C	1min
	extension temperature	72°C	2min
2) Step cycle (35 cycles)	denaturing temperature	93°C	40sec
	annealing temperature	58°C	1min
	extension temperature	72°C	30sec
3) Final cycle	denaturing temperature	93°C	40sec
	annealing temperature	58°C	1min
	extension temperature	72°C	2min

### 2.4.2 Genomic PCR

All plastic ware was UV treated prior to use and the work surface was wiped with 70% ethanol. A commercially available polymerase chain reaction assay (RedTaq, Sigma, R2523) was used to amplify the transgene specific product in the #72 mouse. 25 µl PCR reactions were carried out in 0.1 ml PCR tubes containing 12.5 µl RedTaq with MgCl<sub>2</sub>, 0.5 µl *Plp1* primer (concentration:300nM in sterile pure H<sub>2</sub>O), 0.5 µl T7 primer (concentration:300nM in sterile pure H<sub>2</sub>O), 10.5 µl sterile pure H<sub>2</sub>O and 1 µl of lysed tissue solution. The transgene specific marker, the T7 promoter, is attached at the 3' end of the transgenic cassette. The T7 primer (αT7 5' GCA-TAA-TAC-GAC-TCA-CTA-TAG-GGA-TC 3') recognising the T7 promoter region and the *Plp1* primer (PLP 5' CAG-GTG-TTG-AGT-CTG-ATC-TAC-ACA-AG 3') recognising a specific region at the 5' end of the

murine *Plp1*-gene produce a PCR product of approximately 400bp from the transgene (Readhead, 1994).

### 2.4.3 DNA electrophoresis

Routine analysis of PCR products was performed on a 2% agarose gel in tris acetate ethylene-di-amine-tetra-acetate (TAE) buffer. Gels were made from ultra-pure, electrophoresis grade agarose (Invitrogen, 15510-027) dissolved by heating in 1x TAE buffer. Ethidium bromide (from a stock of 5mg/ml) was added to the cooling gel to give a final concentration of 0.5µg/ml. 10µl of the PCR product was loaded in each well. A one kb DNA ladder (Invitrogen, 15615-016) was used as a control for the PCR product size. In each gel a positive, a negative and a H<sub>2</sub>O control sample were run. PCR products were run for 25 minutes at 70 volt. The PCR product of approximately 400bp was visible under UV light ([Figure 6](#)). The test was qualitative and only detected the presence or absence of the *Plp1*-transgene. Gels were viewed with an ultraviolet trans illuminator (Fotoprep I, Fotodyne Inc.). Gels were recorded using a digital Camera (Kaiser RA1 CCD) and a video graphic thermal printer (Sony UP-890CE). For colour photographs a Canon G4 Powershot digital camera was used and the images were stored digitally ([Figure 6](#)).

### 2.4.4 Identification of CFP expression in Thy-1 CFP mice

CFP positive mice were identified by evaluation of fresh ear biopsies under fluorescence microscopy (Olympus IX70). The filter available was a FITC filter, which excites at 450nm and makes the CFP appear green. Samples containing green fluorescing axons in the pinna were regarded as a positive. Questionable and non-fluorescing tissue was regarded as negative ([Figure 7](#)).

#### **2.4.5 Identification of GFP expression in $\beta$ -actin GFP mice**

GFP positive mice were identified by exposing the new born litter to a handheld UV lamp in a dark room. GFP positive pups could readily be identified by green fluorescence of their skin.

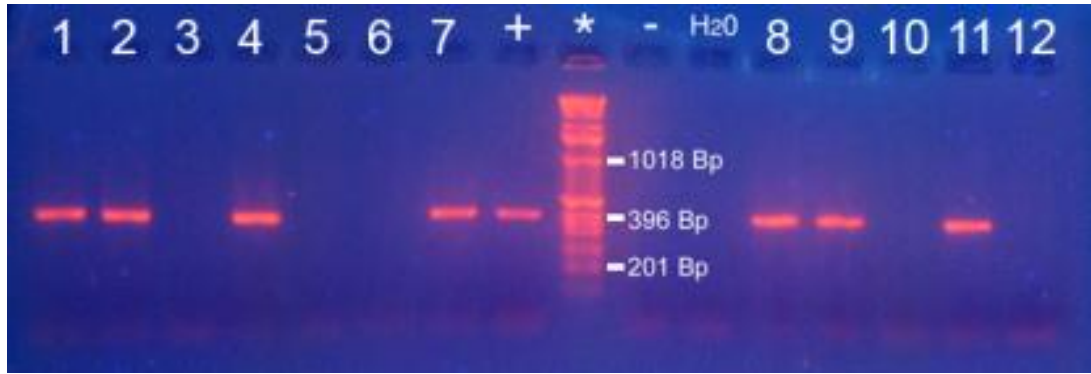


**Figure 6. Representative image of a gel after electrophoresis with twelve PCR products, each from an individual mouse ear sample.**

A 1 kb DNA ladder (asterisk) was used to confirm the correct size of the PCR product (400bp). One positive sample (+), one negative sample (-) and a water sample (H<sub>2</sub>O), were used as controls. Lanes 1-7 and 8-12 contain test samples. Transgene positive samples are identified by the presence of a fluorescent band at the level around 400bp. Transgene negative samples have complete absence of a band.

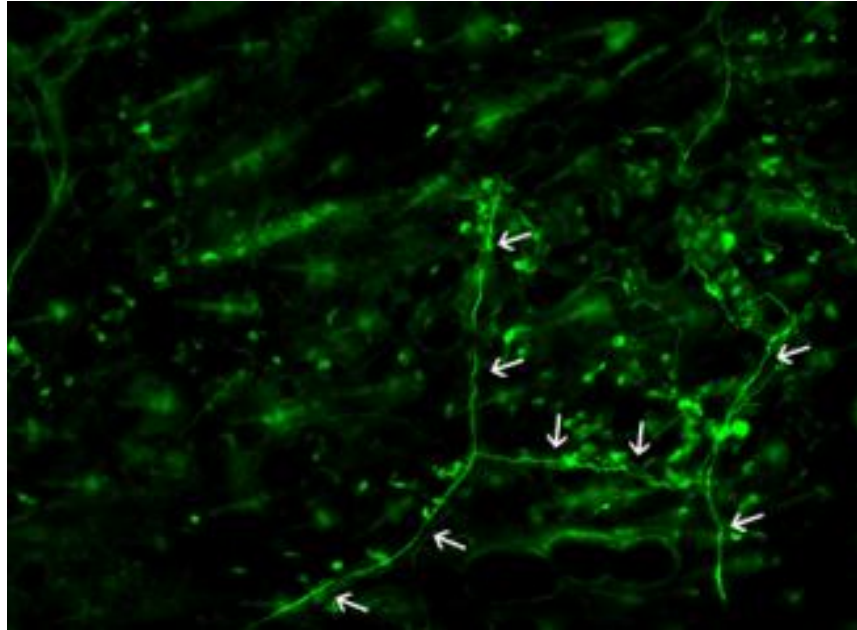


**Figure 7.** Identification of CFP expression was made on fresh ear biopsies. Image of a pinna from a CFP expressing mouse as seen under epifluorescent microscopy (Olympus IX-70, x10). The axons in the pinna of a CFP expressing mouse are visible as green fine lines running across the pinna (arrows).

## 2.5 Experimental procedures

### 2.5.1 Intraperitoneal injection of 5-bromo-2-deoxyuridine (BrdU) as a marker for cell proliferation

To evaluate cell proliferation a single intraperitoneal injection of 50µg/gram body weight 5-bromo-2-deoxyuridine (BrdU) (Sigma, B5002) was performed one hour prior to euthanasia.

### 2.5.2 Cell culture

#### 2.5.2.1 Isolation of adult OPCs from corpus callosum for culture

For each OPC co-culture experiment, OPCs were isolated from two adult wild type GFP expressing corpus callosa and from two adult #72 homozygote corpus callosa. The isolated wild type OPCs were mixed with the isolated homozygote #72 OPCs at the same density immediately before plating down on poly-L-lysine coated glass coverslips.

To isolate adult OPCs, P120 homozygote #72 and wild type GFP expressing mice were killed using CO<sub>2</sub>. Decapitation and collection of the head into a sterile Petri dish was performed after spraying the head with 70% ethanol. Using sterile instruments, the brain was removed from the skull cavity and placed into a sterile Petri dish containing 500µl of cold Leibovitz's L15 with L-glutamine and without phenol red (L15, Gibco, 21083-027). The meninges were carefully removed before isolating the corpus callosum from each brain. Two dissected corpus callosa were placed on a sterile Petri dish and cut into 1mm<sup>3</sup> pieces. The cut tissue was transferred into a small sterile bijoux filled with 3ml HBSS (Sigma, H-4891) solution containing 0.125% trypsin (Sigma, T-3924). 30µl of DNase (50mg/ml, Sigma, DN25-100mg) was finally added to 3ml of HBSS/Trypsin solution and incubated for 90 minutes in 5% CO<sub>2</sub> at 37°C

After 90 minutes the tissue digestion was stopped by adding 100µl of heat inactivated foetal bovine serum (HIFBS) (Invitrogen, 10082147) per 1ml solution. The cell emulsion was then transferred into a 15ml tube using a curved, flame polished glass pipette and filled with L15 containing 10% HIFBS and centrifuged at 1000 rpm for 10 minutes at room temperature. The supernatant was removed and the remaining pellet was resuspended in 2ml of L15 containing 10% HIFBS and triturated at least 6 times or until no tissue chunks were visible through a flame polished, bent glass pipette on ice.

After trituration, the cell suspension was diluted to a total volume of 6.5ml using L15 containing 10% HIFBS in which 65µl of DNase (50mg/ml) was added. A 90% Percoll® (Sigma, 4937) solution was obtained by adding an appropriate volume of 10x Dulbecco's phosphate buffered saline (Gibco, 14200-067) to Percoll®. 3ml of the 90% Percoll® solution was added to the cell suspension and gently mixed. The solution was then transferred into an Oakridge tube and centrifuged at 30000g at 4°C for 30 minutes. After the centrifugation the myelin layer sitting on top of the gradient and some of the Percoll® gradient were removed until approximately 1 - 1.5cm above the red blood cell layer. The OPCs were then harvested immediately above the red blood cell layer. The OPC suspension was then diluted in a minimum of 5ml of L15 containing 10% HIFBS before centrifugation at 1000rpm for 10 minutes at room temperature. The excess fluid was removed and the pellet was resuspended in 100µl of L15 containing 10% HIFBS. 10µl of the cell suspension was mixed with 10µl trypan blue and placed into a haemocytometer for cell counting. Following the cell count the remaining suspension was diluted to a concentration of  $10^5$  cells/100µl. The high cell count was chosen because test runs demonstrated that adult OPCs appeared to have a high rate of cell death *in vitro*. Before plating the OPCs on poly-L-lysine coated 12mm diameter glass coverslips, *Plp1* transgenic and GFP wild type OPCs were mixed together in equal numbers for co-culture and plated down at a concentration of  $10^5$  cells/coverslip. Three coverslips were contained in one Petri dish of 3cm diameter.

Purification of P5 old OPCs was performed using the same technique as for the purification of adult OPCs. However, since young OPCs can be expected to be more robust in relation to the isolation process, less cell death can be expected

during the *in vitro* experiment, the number of cells plated down in young animals was reduced to 30,000 to 40,000 cells/coverslip.

#### **2.5.2.2 Maintenance of the OPC culture**

The OPC cell culture was maintained in 5% CO<sub>2</sub> at 37°C for seven days. Differentiation medium ([7.5 Media for cell culture](#)) was used to feed the cells during the experiment. Every second day, 480µl of media was removed from the Petri dish containing the three coverslips and replaced by 520µl of fresh differentiation media.

#### **2.5.3 Generation of Plp1 Lac-Z expressing neurospheres and generation of β-actin GFP expressing neurospheres**

Neurospheres carrying the *LacZ* reporter gene under the control of *Plp1* gene promoter (Wight et al., 1993) or the *GFP reporter gene under the β-actin promoter* (Okabe et al., 1997) were generated from *LacZ* or *GFP* expressing mice. These mice were wild type at the *Plp1* locus.

Post-natal day 0 or 1 (P0 and P1) animals were sacrificed using isofluorane. The brain was removed from the calvarium and transferred into a Petri dish containing neurosphere (NS) medium ([7.5 Media for cell culture](#)). The brain was cut in half in the sagittal plane. The meninges, the ependymal intraventricular layer, brainstem, midbrain and olfactory bulb were removed. The striatum was then isolated, transferred into a separate Petri dish containing NS medium and cut into small pieces. The tissue was triturated with a bent, flame-polished glass pipette using an automatic pipette until a single cell suspension was achieved. The single cell suspension was then transferred into a T25 flask containing 5ml of NS medium. The cells were triturated twice to achieve even dispersion throughout the medium. One microliter of epidermal growth factor (EGF, stock concentration 20ng/ml, Gibco, 13247-010) per 5ml NS medium was added to the flask and incubated at 37°C in 5% CO<sub>2</sub>.

Every second day, depending on cell growth, 2 - 4ml of medium was removed and replaced by 5 - 10ml fresh NS medium. For every 5ml of fresh NS media, 1 $\mu$ l (stock concentration 20ng/ml) of EGF was added to the flask. Each week the neurospheres were passaged into a new flask. The flask size used during NS culture was dependent on cell proliferation, but in general the cell suspension was put into a T75 flask after one week in culture, containing a minimum of 20ml of NS media. Neurospheres were removed for transplantation between the second and the fourth passage, depending on the neurosphere density in the flask.

#### **2.5.3.1 Preparation of neurosphere for transplantation into homozygote #72 mice**

On the day of transplantation 10 - 20ml of neurosphere medium containing *LacZ* expressing neurospheres and 10 - 20ml of neurosphere medium containing *GFP* expressing neurospheres (the volume was dependent on the actual neurosphere density in the flask, based on a required density of approximately 50,000 cells/ml) were mixed together and centrifuged at 1000r.p.m. for 5 minutes. The supernatant was then removed and the cell pellet was resuspended in 1ml 1x L15 and placed in an Eppendorf tube. The cell suspension was then triturated with a flame polished glass pipette until no cell clusters were visible to the naked eye.

At this stage 10 $\mu$ l of cell suspension was removed and mixed with 10 $\mu$ l trypan blue to evaluate the viability of the cells and perform an approximate cell count. The remaining cell suspension was centrifuged at 1000r.p.m. for five minutes, the supernatant removed and finally resuspended in 20 - 30 $\mu$ l ice cold L15, forming a visible, dense neurosphere cell mass, which corresponded to at least 50000 cells/ $\mu$ l. The Eppendorf tube containing the cell suspension was then stored on ice until immediately before intraparenchymal injection.

To evaluate the viability and potency of the neurospheres, neurospheres that were surplus to requirements following transplantation were diluted in plating medium at the end of the transplantation procedure, plated down on poly-l-

lysine covered coverslips and cultured for three days in the differentiation media used for oligodendrocyte precursor cell culture.

#### **2.5.4 Identification of stereotactic coordinates for corpus callosum cell transplantation**

Two areas of the corpus callosum were selected for transplantation based on the results from the histopathological study of the homozygote #72 corpus callosum. The areas of interest chosen were 0.5mm parasagittal to the midline, at the level at which the fimbria hippocampi merged with the corpus callosum (Figure 8). The selected regions were stereotactically accessible and could safely be used for the intraparenchymal injections cells. The stereotactic coordinates for the selected regions of the corpus callosum were then determined from a stereotactic atlas of the mouse brain (Paxinos and Franklin, 2001). The coordinates of the first injection site were -0.58mm caudal to the Bregma point 0, 0.5mm lateral to the midline suture and 1.5mm ventrally to the brain surface. The second injection site coordinates are -1.34mm caudal to Bregma point 0, 0.5mm lateral to the midline suture and 1.5mm ventrally from the brain surface. To avoid extensive haemorrhage the injection site was adjusted intra-operatively to avoid large meningeal vessels. The accuracy of the coordinates was confirmed prior to the start of the study on the basis of test injections with toluidine blue into freshly euthanized animals.

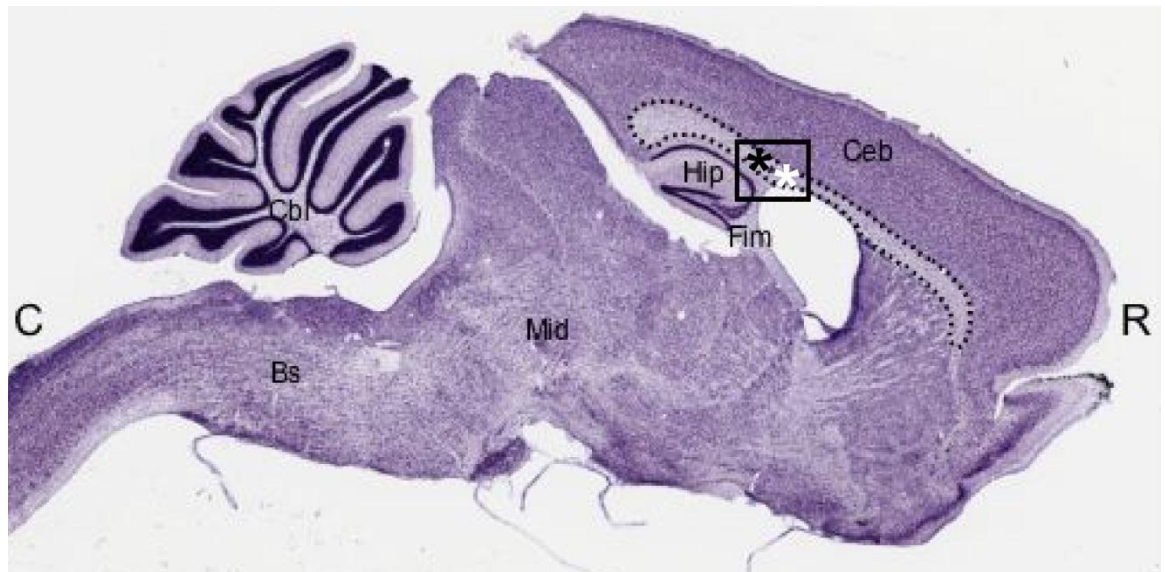


**Figure 8. Identification of the corpus callosum region for histopathological characterisation and potential external modulation.**

Parasagittal view of a mouse brain. The corpus callosum is delineated with dotted lines. The area of interest is where the fimbria merges with the corpus callosum (square) and the two potential injection sites are marked with a black and a white star. (R: rostral, C: caudal, Ceb: Cerebrum, Hip: Hippocampus, Fim: Fimbria, Mid: Midbrain, Bs: Brainstem, Cbl: Cerebellum. Nissl stain. Image taken from <http://brainmaps.org/HBP-JPG/8/m17b.jpg>).

#### **2.5.4.1 Identification of injection sites for homozygote #72 P1 neonates**

Four injection sites were chosen to allow even distribution over the two cerebral hemispheres. Two injections were made into the rostral part of the cerebrum, immediately right lateral and left lateral to Bregma point 0. Two injections were made into the caudal part of the cerebrum, immediately right and left lateral to where the midline suture crosses the caudal suture line. A waterproof mark was set 1.5mm proximal to the needle tip in order to have a constant injection depth in each mouse brain.

#### **2.5.5 Surgical procedure and injection of neurospheres into adult homozygote #72 corpus callosum**

Anaesthesia was induced with isoflurane and maintained at 2% isoflurane, 30% O<sub>2</sub> and 70% NO<sub>2</sub> during the whole procedure. The anaesthetised animal was fixed in a rodent stereotactic frame with a mouse face mask and non-traumatic ear bars. Presurgical subcutaneous injection of 0.3ml carprofen (Rimadyl® large animal injection solution, Pfizer; diluted in 1:100 sterile H<sub>2</sub>O to a concentration of 0.5mg/ml) was administered to each mouse for pain management. Longitudinal incision of the skin was performed from the rostral aspect of the frontal bone to the caudal aspect of C1. The skull was exposed and prepared for the craniectomy.

The margins of the craniectomy window were made along the following anatomical hallmarks: The starting point was at Bregma point 0. A rostro-lateral drill line was continued along the rostral suture line for approximately 5mm. A medial drill line was continued along the midline suture for approximately 7.5mm, terminating just rostral to the occipital protuberance. The midline suture line was included in the drill line. A caudo-lateral drill line was continued till 5mm lateral to the end point of the medial drill line. The craniectomy was completed by connecting the rostro-lateral and the caudo-lateral points, forming a square shaped bone flap. During drilling, sterile NaCl was used to cool the drill bit and the bone.

Once the bone had been thinned along the entire drill line, the skull bone was penetrated along the drill lines using a fine dental hook. The bone flap was removed, exposing the right lateral cerebral hemisphere and the intact dorsal sagittal sinus. A glass capillary was connected to a microinfusion pump (CellTram Oil manual piston pump, Eppendorf). The air in the capillary was removed completely and L15 was drawn up to form a barrier between the oil from the microinjection system and the cell suspension. At least 2 $\mu$ l of neurosphere suspension with a minimum density of 50,000 cells/ $\mu$ l was transferred into the glass capillary. The glass capillary containing the neurospheres was placed at Bregma 0, touching the brain in order to calculate the stereotactic coordinates for the two previously defined injection sites. At each injection site the dura was pierced with a sharp, bent 25G needle tip before advancing the glass capillary into the parenchyma. Once the capillary reached the injection site, the glass capillary was advanced for another 0.5mm, left in place for 1 minute and then retracted to the calculated injection site where the injection of the cell suspension commenced ([Figure 8](#)). The total volume injected at each site was 1 $\mu$ l with an injection rate of 0.1 $\mu$ l/min. After the injection was finished, the needle was left in place for 5 minutes, then slowly retracted and removed from the brain.

After finishing the two injections, the surgical site was moistened and closed by suturing the skin using 5-0 absorbable Vicryl (Ethicon) with a cutting needle.

Before recovering the mouse from anaesthesia, a subcutaneous injection of 0.5ml 0.85% NaCl was given.

For continuous pain management, Rimadyl® was added to the drinking water to a concentration of 0.05mg/ml for three days.

#### **2.5.5.1 Injection of neurospheres into neonate homozygote #72 mice**

The entire litter was removed from the mother prior to surgery to minimise the risk of rejection, afterwards. Anaesthesia was induced by putting the pups into a box containing 5% isoflurane and O<sub>2</sub> for approximately 30 - 45 seconds. The pups

were then placed under the operating microscope. The head was manually fixed and a 5µl Hamilton syringe (Hamilton 65RN, 7633-01) was used to inject the neurospheres. At each injection site, after advancing the needle through the skin and soft skull into the brain parenchyma to a depth of 1.5mm, 0.5µl of the neurosphere cell suspension was injected slowly. A total of 2µl of neurosphere suspension was injected into each pup. The injections were made free handed under visual control. After injection, the pups were left to recover in a heated recovery box before returning them to their mother.

## **2.6 Tissue sampling and processing**

### **2.6.1 Fixatives**

#### **2.6.1.1 Periodate - lysine - paraformaldehyde (PLP) fixative**

PLP fixative (McLean and Nakane, 1974; [7.1.1 Periodate lysine paraformaldehyde](#)) was used for preservation of all the tissue used in the descriptive histopathological study of the corpus callosum and in the *in situ* evaluation of the cell intrinsic and cell extrinsic compartments in remyelination failure.

#### **2.6.1.2 4% paraformaldehyde in PBS**

4% paraformaldehyde in PBS ([7.1.2 4% Paraformaldehyde in PBS](#)) was used for preservation of the tissue used for the MRI experiment. All cell culture and cell transplantation samples were also preserved in 4% paraformaldehyde before immunohistochemical evaluation. Tissue where PSA-NCAM and hyaluronan markers were used, were also fixed in 4% paraformaldehyde. All CFP positive mice were preserved in 4% paraformaldehyde.

### **2.6.1.3 Karnovsky's modified fixative (paraformaldehyde / glutaraldehyde 4%/5%)**

Karnovsky's modified fixative ([7.1.3 Karnovsky's modified fixative \(paraformaldehyde / glutaraldehyde 4% / 5%\)](#)) was used for preservation of tissue destined for resin embedding and electron microscopy evaluation.

## **2.6.2 Fixation technique and processing**

### **2.6.2.1 Cardiac perfusion**

Mice over 10 days of age were euthanized in a CO<sub>2</sub> chamber. Mice under 10 days of age were euthanized using Isoflurane. All mice older than 20 days were fixed via cardiac perfusion. This was performed as follows: once the mice were dead they were pinned down to a cork board. The thorax was opened to expose the heart and the right atrium was incised to allow blood, saline and fixative to escape. Intracardiac injection of 20ml 0.85% saline was performed through a 25 gauge 1.5 inch hypodermic needle into the left ventricle ([Figure 9](#)). Once all the blood was flushed out of the circulatory system, 2 x 10 - 20ml (depending on the mouse size) of fixative was injected into the left ventricle.

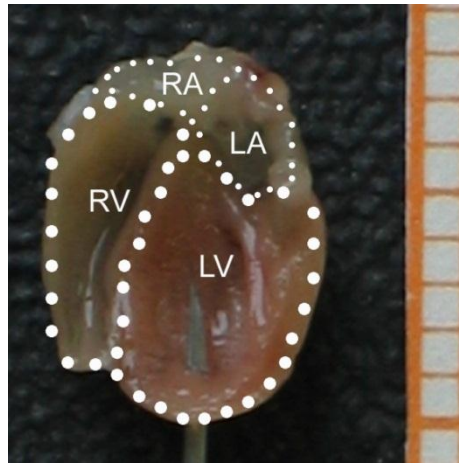


**Figure 9. Correct needle placement is of major importance to achieve optimal perfusion of the specimen.**

Image of a midaxial section through a fixed mouse heart showing the correct positioning of the needle for optimal tissue perfusion. After correct placement of the needle into the left ventricle, injection of 0.8% NaCl was followed by the injection of the fixative solution, allowing even distribution into all organs supplied by the left ventricular system. The fixative returned to the heart via the right atrium, which was incised to allow drainage of excess fluid from the circulatory system (LV: left ventricle, LA: left atrium, RV: right ventricle, RA: right atrium, scale square 1 x 1mm)

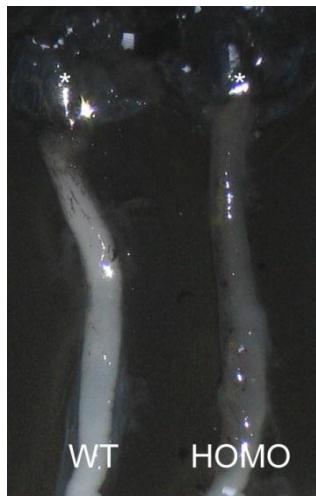


**Figure 10. #72 homozygote mice were identified by progressive macroscopic changes in the optic nerve, which correlated with the degree of demyelination.**

Image of a wild type and a homozygote optic nerve at P120 extending from the sclera (\*) caudally to the chiasm (6.4x magnification). The optic nerves have been dissected and removed from their calvaria. The wild type optic nerve (WT), which appeared opaque and was clearly distinguishable from the #72 homozygote mouse optic nerve, which became, with progressive demyelination, increasingly translucent (HOMO). With experience the changes could be detected as early as P40. In general the changes were readily identifiable from P60 onwards.

### **2.6.2.2 Tissue dissection**

Tissues were harvested using a low power dissection microscope and microsurgical tools. Skin and muscles were removed from the head and from the dorsal part of the spinal cord. The calvarium was opened and the bone removed. Dorsal laminectomy of the entire spinal column was performed. After removing the meninges, the spinal cord was transected and separated from the brain at the atlanto-occipital level. The brain was gently removed from the calvarium. The optic nerves were cut at the caudal level of the optic tracts and were gently removed from the brain tissue leaving the optic chiasm intact. The brain was then removed and the visual system, including the caudal part of the optic tracts and the eye balls, was removed from the calvarium as a single unit. The spinal cord was completely removed from the spinal canal. An approximately 1cm long proximal section of the sciatic nerve was also removed after blunt exposure.

The following tissues were collected and frozen: longitudinal sections of the brain, transverse sections of the brain where the rostral 5mm of the brain was removed using a brain matrix, longitudinal sections of optic nerve including the optic tract, transverse sections of the retinal, chiasm and optic tract portion of the optic nerve, longitudinal and transverse sections of cervical spinal cord at C1 - C3 level and lumbar spinal cord at L4 - L6 level. Spleen, liver and distal colon for positive controls for various antibodies were also removed from the abdominal cavity.

### **2.6.2.3 Morphological identification of homozygote *Plp1* gene overexpressing #72 mice**

Homozygote animals become clinically apparent at around P90, with affected animals becoming increasingly more ataxic, demonstrating a mild body tremor and also developing generalised tonic-clonic seizures. However the homozygote status of an animal was definitively confirmed at the point of dissection by evaluating the optic nerves. From P40 on, the optic nerves from homozygote *Plp1* transgene overexpressing #72 mice were macroscopically distinguishable from the wild type, as progressive demyelination resulted in the optic nerves

turning gradually more translucent ([Figure 10](#)). The optic nerves from hemizygote mice were indistinguishable from the wild type. Since the PCR technique utilised in this study could only confirm the presence of the *Plp1* transgene the presence of macroscopic changes in the optic nerve was used to distinguish between hemizygote and homozygote specimens.

#### **2.6.2.4 Processing of fixed tissue and storage**

PLP or 4% paraformaldehyde fixative perfused tissue was immediately dissected after perfusion and post fixed in in the same fixative for 2 hours. In the case of CFP expressing tissue the tissue was immediately dissected after perfusion and post fixed in 4% paraformaldehyde for 20 minutes only. The tissue was then placed in 0.1 M Glycine (Sigma, 7126-1kg) for 10 minutes to suppress auto fluorescence originating from paraformaldehyde.

After fixation in PLP fixative or 4% paraformaldehyde the tissue was cryoprotected in 20% sucrose and then frozen in OCT (Sakura, 4583). The frozen OCT blocks were then wrapped in wax film and stored at either -20°C -80°C until further processing. Tissue fixed with modified Karnovsky's fixative was dissected within 7 days and stored in fixative at 4°C until processing.

#### **2.6.3 Cryopreservation and sectioning**

##### **2.6.3.1 Cryopreservation of fresh neural tissue**

Fresh, unfixed brain and optic nerve tissue for B-cell immunostaining (see [Table 2](#)) was collected immediately after euthanasia. The tissue was suspended in an OCT compound filled, self-built aluminium container and frozen in 2-methylbutane (Isopentane, Fisher, 78-78-4) cooled to at least -80°C in liquid nitrogen. The frozen OCT blocks were wrapped in Nescofilm (Carl Roth, 2569.1) and stored at -20°C or -80°C until further processing.

### **2.6.3.2 Cryopreservation of fixed material**

The following tissues were collected and frozen for immunohistochemistry: longitudinal and transverse sections of the brain, longitudinal sections of the optic nerve and the optic tract, transverse sections of the retinal, chiasmal and optic tract portion of the optic nerve, longitudinal and transverse sections of cervical spinal cord at C1 - C3 level and lumbar spinal cord at L4 - L6 level. After perfusion the tissue was cryoprotected by immersing the tissue into 20% sucrose in PBS for 24 hours and freezing in OCT as described above. The frozen OCT blocks were wrapped in Nescofilm and stored at -20°C or -80°C until further processing.

### **2.6.3.3 Sectioning of cryopreserved tissue**

Cryopreserved tissue was sectioned on an OTF cryostat (Bright Instruments) at 10 - 30µm thickness. The sections were mounted on poly-l-lysine coated slides, left for 2 hours at room temperature to dry and attach to the slide, then stored at -20°C or -80°C.

### **2.6.4 Resin processing and sectioning**

For resin embedding only neural tissue from mice processed with Karnovsky's modified fixative were used. The Lynx microscopy tissue processor (Leica) automated the dehydration and resin infiltration process ([7.2.1 Resin processing](#)).

After processing, the tissue was placed in resin filled rubber moulds and left overnight in an incubator at 60°C for polymerisation. Resin blocks were cut on an ultratome (Ultracut-E, Reichert Jung). For light microscopy 1µm thick sections were produced using a glass knife. The sections were then placed on plain slides, covered and sealed with glass coverslips using DPX (BDH, 36029417).

For electron microscopy 70nm thick sections were produced using a diamond knife. The sections were mounted on 200-mesh 3.06mm diameter copper grids.

## **2.6.5 Processing of transplanted tissue**

### **2.6.5.1 Tissue sampling and processing for $\beta$ - galactosidase staining and immunohistochemistry after cell transplantation**

Fourteen days after cell transplantation, the mice were euthanized using a CO<sub>2</sub> chamber. Intracardiac perfusion of 0.85% saline was followed by 4% paraformaldehyde perfusion to achieve optimal tissue fixation. The brain was then dissected and transferred into a mouse brain matrix and cut into 1 mm thick slices. In transplants where neurospheres containing the *LacZ* or *GFP* reporter gene were injected simultaneously, only the sections containing green cells were further processed. To identify the sections containing GFP +ve cells, fluorescence microscopy (Olympus IX-70) was used. To visualise *LacZ* reporter gene containing neurospheres, the whole brain section was processed using the X-gal method ([7.3.3 X-gal staining](#)).

### **2.6.5.2 Tissue sampling and processing for electron microscopy after cell transplantation**

Samples used for electron microscopy (EM, Joel 100CX) evaluation were collected after perfusion. Samples containing green fluorescing cells or samples with blue sections in the corpus callosum after X-gal staining were selected for EM evaluation. The brain slices containing GFP positive or blue cells were then immersed overnight in 4% formaldehyde / 5% glutaraldehyde. Before EM processing, the brain samples were trimmed to approximately 20mm<sup>3</sup> large pieces, containing corpus callosum and part of the injection tract. The prepared tissue samples were then embedded into resin blocks.

## 2.7 Staining techniques

### 2.7.1 Immunofluorescence

#### 2.7.1.1 Immunohistochemical markers

##### 2.7.1.1.1 *Primary antibodies used in the study*

The origin, titres and the host for specific antibodies are described in [Table 2](#).

##### 2.7.1.1.2 *A2B5*

A2B5, an early surface marker for oligodendrocyte precursor cells (Schnitzer and Schachner, 1982) was used to identify undifferentiated OPCs in vitro.

##### 2.7.1.1.3 *Adenomatous polyposis coli (APC)*

Adenomatous polyposis coli (APC, CC1) is a protein involved in tumour suppression and cell division. The antibody against APC recognises the adenomatous polyposis coli protein and, in the CNS, is a specific marker for mature oligodendrocytes (Bhat et al., 1996). Antibodies against APC were used to label mature oligodendrocytes.

##### 2.7.1.1.4 *Axin2*

Axin2 is a protein involved in the Wnt pathway. It serves as a negative feedback regulator like Axin1. However unlike Axin1, which is constitutively present at low levels, Axin2 is only expressed when the Wnt pathway is upregulated (Fancy et al., 2009). Antibody against Axin2 was used to identify cells where the Wnt pathway was activated.

#### **2.7.1.1.5 5 - Bromo - 2 - deoxyuridine (BrdU)**

5 - Bromo - 2 - deoxyuridine (BrdU) is an analogue to thymidine and is incorporated, when present, into the DNA during the S-phase. Antibody against BrdU was used to label dividing cells incorporating BrdU.

#### **2.7.1.1.6 Caspase3**

Antibody against Caspase 3, which is an enzyme from the cysteine aspartic acid proteases involved in cell apoptosis pathway (Denault and Salvesen, 2002), was used to evaluate the effect of *Plp1* gene overexpression on cell apoptosis *in situ*.

#### **2.7.1.1.7 Inflammatory cell population**

The following antibodies were used to characterise the inflammatory population: Antibodies against CD169, which is a marker for activated macrophages (Perry et al., 1992). CD3, which labels T-cells (Tsoukas et al., 1987). CD45, which is expressed on all nucleated haematopoietic cells and is used as a panleukocytic marker (Huntington and Tarlinton, 2004). CD45R, a marker for identifying B-cells (Coffman, 1982).

#### **2.7.1.1.8 Type 3 deiodinase (D3)**

Type 3 deiodinase (D3) is an intracellular enzyme expressed in various cell types such as neurons, neutrophils, macrophages, monocytes (reviewed in Visser et al., 2011). Antibody detecting Type 3 deiodinase (D3) (a gift from Dr. T. Visser) was used to identify D3.

#### **2.7.1.1.9 *Glial fibrillary acidic protein (GFAP)***

Glial fibrillary acidic protein (GFAP) is a structural intracellular protein in astrocytes (Bignami et al., 1972). Antibody against glial fibrillary acidic protein (GFAP) was used to label the astrocytic population.

#### **2.7.1.1.10 *Green fluorescing protein (GFP)***

Depending on the associated promoter, the GFP is linked to specific cell lines, allowing the cell lines to be traced due their expression of GFP (Feng et al., 2000). A GFP antibody, which recognises GFP and CFP was used to enhance the fluorescence of GFP and CFP in the tissue.

#### **2.7.1.1.11 *Hyaluronan binding protein (HABP)***

Hyaluronic acid, a glycosaminoglycan in the extracellular matrix, is believed to have a negative influence on OPC differentiation after demyelination (Back et al., 2005) The biotinylated hyaluronic acid binding protein, was used to label hyaluronic acid in the CNS.

#### **2.7.1.1.12 *Myelin basic protein (MBP)***

Myelin basic protein (MBP) is one of the major myelin proteins in mature myelin. MBP is synthesised in free ribosomes in the oligodendrocytic processes and becomes incorporated into the myelin sheath soon after synthesis (Colman et al., 1982). Antibody against MBP was applied to evaluate for the presence of myelin in the white matter.

#### **2.7.1.1.13 *Chondroitin sulphate proteoglycan NG2***

NG2 is a single spanning membranous chondroitin sulphate proteoglycan, which is expressed on residing OPCs (Nishiyama et al., 2009). Antibody against NG2 was used to label oligodendrocyte precursor cells

#### **2.7.1.1.14 *O4 sulfatides***

O4 is an antigen of the O family, which are sulfatides located in the cell membrane. O4 is expressed at most stages of oligodendrocyte development and is detectable from early OPCs up to mature oligodendrocytes in culture (Sommer and Schachner, 1981). Antibody against O4 was applied during living cell culture experiments to label the cells belonging to the oligodendrocytic lineage.

#### **2.7.1.1.15 *Basic Helix-Loop-Helix transcription factors Olig1 and Olig2***

Olig1 and Olig2 are basic Helix-Loop-Helix (bHLH) transcription factors expressed in OPCs and oligodendrocytes. (Lu et al., 2002). Antibodies detecting Olig1 and Olig2 were used to characterise the response of adult OPCs during the development of chronic demyelination.

#### **2.7.1.1.16 *Platelet derived growth factor receptor alpha (PDGFRa)***

Platelet derived growth factor receptor alpha (PDGFRa) is expressed on developmental and adult OPCs from a relatively early time point (Pringle et al., 1992). Antibody detecting PDGFRa (gift from Dr. C. Heldin) was used to identify OPCs.

#### **2.7.1.1.17 *Proteolipid protein / DM20***

PLP/DM20 is the major myelin protein. It is a tetraspan protein located in the cell membrane. Antibody against the PLP-C terminal recognises the carboxy

terminus of the PLP protein isoforms and was used to label PLP and DM20 (Fanarraga et al., 1992) in order to identify wild type and transgenic PLP.

#### **2.7.1.1.18 *Polysialation of the neural cell adhesion molecule (PSA NCAM)***

Polysialation of the neural cell adhesion molecule (PSA NCAM) on axons has been suggested to play a role in inhibiting remyelination after demyelination (Charles et al., 2002). PSA - NCAM antibody was used to assess if axonal surface expression was altered.

#### **2.7.1.1.19 *SMI31 and SMI32***

In the CNS axons, neurofilaments are structural proteins important for cell structural integrity, axonal and dendritic growth (reviewed in Lee and Cleveland, 1994; Grant and Pant, 2000). SMI-31 antibody recognises the phosphorylated neurofilaments, whereas SMI-32 antibody recognises non phosphorylated neurofilaments. These two markers were used to label axons.

#### **2.7.1.1.20 *Secondary fluorescent antibodies***

All secondary fluorescent antibodies were raised in goat and their specific binding affinities to primary antibodies are listed in [Table 3](#).

For green fluorescence, secondary antibodies labelled with fluorescein isothiocyanate (FITC), with an excitation spectrum peak at 491nm and emission spectrum peak at 521nm, or labelled with Alexa Fluor (AF488, Invitrogen, A-11008), with an excitation spectrum peak at 495nm and emission spectrum peak at 519nm, were used.

For red fluorescence, secondary antibodies labelled with sulforhodamine 101 acid chloride (Texas Red, TxR) with an excitation spectrum peak at 589nm and emission spectrum peak at 615nm were used.

#### **2.7.1.1.21 Nuclear stain**

4',6-diamidino-2-phenylindol (DAPI), a blue fluorescent nuclear stain, strongly binds to double stranded DNA, with a preference for binding at AT cluster sites, and has an excitation spectrum peak at 358nm and emission spectrum peak at 461nm (Kubista et al., 1987). DAPI was used to counterstain the cell nucleus in cryosections.

Primary Antibody	Host	Manufacturer Cat. Nr.	Dilution	Method
A2B5	Mouse IgM		1:3	live
APC (CC1)	IgG2b	Abcam ab16794	1:100	DV
Axin2	Rabbit IgG	Abcam ab32197	1:100	0.5% Triton X
BrdU	Mouse IgG1	Sigma B8434	1:500	HCl
Caspase 3	Rabbit IgG	Cell Signaling #9661	1:4000	Methanol
CD169	Rat IgG2a	Serotec MCA884	1:100	Methanol
CD3	Rat IgG1	Serotec MCA1477T	1:100	Methanol
CD45	Rat IgG	AbD Serotec MCA1388	1:600	Methanol
CD45R	Rat IgG2a	BD Pharmingen 550286	1:100	Fresh frozen
D3 (676)	Rabbit IgG	Gift from Dr. T Visser	1:1000	0.5% Triton X
GFAP	Mouse IgG1	Sigma G3893	1:1000	Methanol
GFP	Rabbit IgG	Abcam ab290	1:1000	Methanol
HABP	Biotinylated Protein	Seikagaku 400763	2µg/ml	Methanol
MBP	Rat IgG	Serotec MCA4095	1:500	Methanol
NG2	Rabbit IgG	Millipore AB5320	1:150	Methanol or 0.5% Triton X
O4	Mouse IgM	Gift from Dr. I Sommer	1:5	Live
Olig-1	Mouse IgG2b	Millipore	1:1000	0.5%

Primary Antibody	Host	Manufacturer Cat. Nr.	Dilution	Method
		MAB5540		Triton X
Olig-2	Rabbit IgG	Millipore AB9610	1:500	0.5% Triton X
PDGFRa2	Rabbit IgG	Gift from Dr C. Heldin	1:500	Methanol
PLP-C term	Rabbit IgG	Groome 226/7	1:600	Methanol
PSA (E-NCAM)	Mouse IgM	Millipore MAB5324	1:500	Methanol
SMI-31	Mouse IgG1	Convance SMI31-R	1:1500	Methanol
SMI-32	Mouse IgG1	Convance SMI32-R	1:1500	Methanol

**Table 2. List of primary antibodies used in all studies.**

Secondary Antibody	Manufacturer / Cat Nr.	Dilution
Goat anti Rat IgG FITC	Southern Biotech / 1050-02	1:50
Goat anti Mouse IgG FITC	Southern Biotech / 1034-02	1:30
Goat anti Mouse IgG1 FITC	Southern Biotech / 1070-02	1:80
Goat anti Mouse IgG2a FITC	Southern Biotech / 1080-02	1:25
Goat anti Mouse IgG2b FITC	Southern Biotech / 1090-02	1:100
Goat anti Mouse IgM FITC	Southern Biotech / 1021-02	1:50
Goat anti Rabbit IgG FITC	Southern Biotech / 4050-02	1:80
Goat anti Rabbit IgG AF488	Invitrogen / A11008	1:1000
Goat anti Rat IgG TxR	Southern Biotech / 1050-07	1:50
Goat anti Mouse IgG TxR	Southern Biotech / 1034-07	1:50
Goat anti Mouse IgG1 TxR	Southern Biotech / 1070-07	1:75
Goat anti Mouse IgG2b TxR	Southern Biotech / 1090-07	1:70
Goat anti Mouse IgM TxR	Southern Biotech / 1021-07	1:50
Goat anti Rabbit IgG TxR	Southern Biotech / 4050-07	1:100
Extravidin FITC	Sigma / E2761	1:75
DAPI	Sigma / D1306	1:1500 (1 min)

**Table 3. List of secondary antibodies used in all studies.**

### **2.7.1.2 Immunohistochemistry protocol using methanol to permeabilise cell membranes**

Immunohistochemistry was performed on PLP fixative and 4% paraformaldehyde fixed tissue. After thawing, the slides containing the sections were immersed in PBS for 10 minutes to remove the OCT embedding. Cell permeabilisation was performed by immersing the sections in -20°C methanol (Fisher, 67-56-1) for 10 minutes. After permeabilisation the sections were washed twice in PBS for ten minutes. Blocking of non-specific binding of secondary antibodies was performed using PBS containing 10% normal goat serum (NGS, Sigma G9023) was applied to the sections for 1 hour. After removing the excess fluid from the sections, the primary antibody was applied overnight at 4°C in PBS containing 10% NGS. After washing the sections three times in PBS for 10 minutes the secondary antibody was applied in PBS containing 10% NGS for one hour at room temperature and then again washed three times in PBS for ten minutes. For nuclear staining, 4'-6-Diamidino-2-Phenylindole (DAPI, Sigma, 32670) in PBS was applied for one minute. The samples were washed in PBS and running water for 5 minutes and mounted in glycine / PBS. The coverslips were sealed using nail varnish.

### **2.7.1.3 Immunohistochemistry protocol using Triton-X 100 to permeabilise cell membranes**

Immunohistochemistry was performed on PLP and 4% paraformaldehyde fixed tissue. After thawing, the sections were immersed in PBS for 10 minutes to remove the OCT embedding. Cell permeabilisation was performed by applying Triton-X 100 (Sigma, 9002-93-1) for one hour at various concentrations (0.2 - 0.5% in 10% NGS) to the sections. This procedure also served to block non-specific binding of secondary antibodies. After removing the excess from the sections, the primary antibody was applied overnight at 4°C in PBS containing 0.2 - 0.5% Triton-X and 10% NGS. The following day the sections were washed three times in PBS for 10 minutes followed by application of the secondary antibody in PBS containing 0.2 - 0.5% Triton-X and 10% NGS for one hour at room temperature.

The final steps, including nuclear staining and mounting, were performed as previously described.

#### **2.7.1.4 Immunohistochemistry protocol using the DV method**

Immunohistochemistry staining for APC (CC1) (see table for origin and dilution) was performed on PLP and 4% paraformaldehyde fixed tissue. After thawing, the sections were immersed in PBS for 10 minutes to remove the OCT embedding. Cell permeabilisation was performed by applying DV solution for one hour to the sections. This procedure also served to block non-specific binding of secondary antibodies. After removing the excess from the sections, the primary antibody was applied over night at 4°C in DV solution. The following day the sections were washed three times in PBS for 10 minutes followed by application of the secondary antibody in DV solution for one hour at room temperature. The final steps including nuclear staining and mounting were performed as previously described.

#### **2.7.1.5 Hydrochloric acid immunohistochemistry protocol for BrdU staining**

Double labelling of PDGFR $\alpha$  positive cells and BrdU positive cells on tissue fixed with PLP fixative was performed as follows: The staining protocol for the first antibody (OPC marker PDGFR $\alpha$ ) has been previously described. After completion of the PDGFR $\alpha$  staining the slides were immersed in 50% ethanol / 50% glacial acetic acid (see Appendix) for ten minutes and then in 50% hydrochloric acid containing 1% Triton-X 100 (see Appendix) for ten minutes. The slides were washed three times in PBS for ten minutes. Antibody against BrdU in PBS containing 1% Triton-X 100 and 10% NGS was applied overnight at 4°C to the PBS washed slides. The unbound BrdU antibody was then removed by immersing the slides three times in PBS for 10 minutes. The secondary antibody recognising the BrdU antibody was applied for 2 hours at room temperature. The subsequent steps were as described for the PLP fixative fixed tissue staining protocol.

#### **2.7.1.6 Immunohistochemistry protocol on unfixed, fresh frozen tissue**

Fresh frozen samples for staining with the B-cell marker CD45R were thawed and processed unfixed. The primary antibody was applied for one hour at room temperature. The samples were then fixed for 10 minutes in 4% paraformaldehyde before applying the secondary fluorescent antibody or before applying other primary antibodies. The subsequent steps were as described above.

#### **2.7.1.7 Immunohistochemistry protocol on live culture**

Live staining to identify OPCs and oligodendrocytes was performed on adult OPC cultures using the markers O4 or A2B5. The coverslips were washed three times in DMEM at 37°C for ten minutes. The antibody against A2B5 or O4 were suspended in DMEM, applied to the coverslips, and incubated for 1 hour at 37°C in a 5% CO<sub>2</sub> atmosphere. The coverslips were then washed three times in DMEM at 37°C for ten minutes and once in PBS at 37°C before fixing the cells in 4% paraformaldehyde at room temperature for ten minutes. After fixation the methanol protocol was used for application of the subsequent second primary antibodies.

#### **2.7.1.8 Immunohistochemistry protocol of fixed cultured cells**

After fixation, the coverslips were washed three times in PBS then the secondary fluorescent antibody in DMEM was applied for one hour at room temperature. The coverslips were then washed three times in PBS and the cells were permeabilised in methanol for 10 minutes at -20°C. After 3 washes in PBS 10% normal goat serum in PBS for applied for one hour. In coverslips where O4 antibody was applied to label the OPCs, the second primary antibody used was against GFP. In coverslips where antibody against O4 was not used, either an antibody against MBP (Table 2) or an antibody against PLP (Table 2) was combined with the GFP antibody. After incubation of the second primary antibody, the coverslips were washed in PBS and the second fluorescent antibody was applied (Table 3). Finally, after washing in PBS, the cell nuclei

were stained using DAPI (Table 3). Coverslips were then briefly washed in PBS and water before mounting and sealing the coverslips on a microscope slide.

### **2.7.1.9 Immunofluorescence of transplanted tissue**

The following antibodies were used to label the transplanted cells. An antibody against GFP was used to identify the cell population originating from GFP expressing neurospheres. An antibody against MBP was used to identify myelin sheaths. To identify the astrocytic population, an antibody against GFAP was used. To identify the microglial population CD45 and CD169 antibodies were used. For nuclear staining, 4'-6-Diamidino-2-Phenylindole (DAPI) was applied. Secondary antibodies used in this study were FITC labelled antibodies for GFP detection and TxR labelled antibodies to label the antibodies against MBP, GFAP, CD45 and CD169. Dilution and origin of the primary and secondary antibodies and DAPI are listed in Tables 2 and 3.

### **2.7.2 Light microscopy**

#### **2.7.2.1 X-gal staining of *Plp1 LacZ* expressing samples**

X-gal staining was performed on 4% paraformaldehyde fixed tissue either as a whole mount tissue or on 10µm thick frozen sections. After fixation, the transplanted brain was cut into 2mm thick axial sections using a 1mm step brain matrix (Harvard Apparatus, 62-0050). The sections were then briefly washed in PBS followed by 1M MgCl<sub>2</sub> for 10 minutes on ice. The tissue was then immersed into detergent solution for another 10 minutes on ice, followed by the application of X-Gal staining solution ([7.3.3 X-gal staining](#)) over night at room temperature. The reaction product after X-Gal treatment of tissue containing β-galactosidase is 5-bromo-4-chloro-3-indolyl β-D-galactoside, which is a blue product visible to the naked eye. The sections were then washed in and immersed in 20% sucrose for 24 hours, immersed in OCT and frozen and stored as described above.

Alternate 10 and 20µm thick mounted cryosections from NS transplanted brains were taken for β-galactosidase staining.

#### **2.7.2.1.1 *Tissue sampling and processing for β - galactosidase staining and immunohistochemistry of P1 injected homozygote #72 mice***

Following the cell transplantation two mice were euthanized on each of the following days post cell transplantation: day 7, 14, 35, 80 and 120. The mice were euthanized using a CO<sub>2</sub> chamber. The procedure for fixation and processing of the tissue was identical to that previously described.

#### **2.7.2.1.2 *Methylene blue / azur II***

For light microscopy, resin sections were stained with methylene blue (VWR, 340484B)/ azur II (VWR, 340064Y) ([7.4.1 Methylene blue / azur II](#)). Sections were placed on a hot plate (60°C) and flooded with stain. Once the rim of the stain solution appeared golden the sections were washed in running water. The sections were mounted in DPX (BDH, 360 294 17) after drying overnight on a hot plate (60°C).

### **2.7.3 Electron microscopy**

#### **2.7.3.1 Tissue sampling and processing for electron microscopy of P1 injected homozygote #72 mice**

Samples for electron microscopic (EM) evaluation were collected at P7, P14, P21, P40, P80 and P120 after intracardiac perfusion with 4% PF. Post fixation was performed by immersion in 4% formaldehyde / 4% glutaraldehyde for one week.

Before EM processing, the brain samples were cut to approximately 10mm<sup>3</sup> large pieces, containing the corpus callosum and part of the injection tract. The

prepared tissue samples were then embedded into resin blocks ([7.2.1 Resin processing](#)).

For EM evaluation resin blocks were trimmed and the brain samples were cut into 1µm thick sections for myelin sheath evaluation of the transplantation site using toluidine blue. After methylene blue/azur II evaluation, 60µm thick sections of the areas containing myelin (presumed to be from the transplanted cells) were cut for EM evaluation.

Uranyl acetate (AGAR Scientific, R1260) and lead nitrate (VWR, 290384R) was used to stain the copper grid mounted thin resin sections ([7.3.4 Staining for electron microscopy](#)).

## **2.8 Morphological studies**

### **2.8.1 Cell quantification of immunolabelled samples**

Quantification of cells was performed on 10µm thick axial cryosections from the corpus callosum, retinal and chiasmal portion of optic nerve. Sections were placed on slides at 100µm intervals to avoid counting the same cell twice.

Immediately after staining, images from the area of interest were taken using an Olympus IX70 microscope, QImcam Fast digital camera (Qimaging Surrey, Bcm Canada) and Image ProPlus 6.0 software (Media Cybernetic, Silver Spring, MD, USA).

The cells positive for the immunohistochemical marker of interest were counted manually in a defined area of interest using Image ProPlus 6.0 software. For the immunohistochemical marker, the area of interest in the corpus callosum was 20515.176µm<sup>2</sup>. In the optic nerve the area of interest was 28060.455µm<sup>2</sup>. DAPI was used to identify the nucleus for calculating the total cell density using the automatic cell count function in Image ProPlus 6.0. The area of interest in the corpus callosum and optic nerve for DAPI positive cells nuclei was 6986.3584µm<sup>2</sup>.

The cells were included in the cell count if they were lying within the area of interest. Cells crossing the top (north) and the right (east) side border were also included. Cells crossing the bottom (south) and left (west) side border were excluded from the cell count.

### **2.8.2 Quantification of GFAP positive area in optic nerve after immunolabelling**

In the optic nerve the GFAP area was measured using a semi-automated programme in ImagePro 6.0. A minimum of six images per optic nerve were used. Briefly, the images were opened in ImagePro 6.0. A copy of the original was made and converted into a black and white image, where fluorescent areas appear white. The original image was used as a template for manual segmentation of the black and white image until the white area was judged to match the fluorescent area of the original image. An area of interest (AOI) of  $16397.771\mu\text{m}^2$  was applied to the image and the area occupied by white pixels within the AOI was then automatically calculated, giving the area occupied by GFAP in  $\mu\text{m}^2$  per  $\mu\text{m}^2$  of the total AOI. For each optic nerve the measurement was then used to calculate the area occupied by GFAP per  $\text{mm}^2$ .

### **2.8.3 Quantification of percentage myelinated axons**

Images obtained from electron microscopy were used to calculate the percentage of myelinated axons within the region of interest in the corpus callosum. Eight images were randomly taken from the mid corpus callosum at 8000x magnification using a film camera system (JOEL 100CX). After developing the film negatives were scanned (EPSON Perfection 3200 PHOTO) and evaluated in ImagePro 6.0. Axonal numbers were manually counted using an area of interest of  $45.166\mu\text{m}^2$ . Myelinated axons and non myelinated axons were counted after placing a grid square over the digital image, from which to select fibres for counting. All fibres lying under an intersection were only counted once. The percentage of myelinated axons was calculated in relation to myelinated and non myelinated axons, after placing a counting grid over the digital image. All

axons lying beneath the grid lines were counted and designated as myelinated or non myelinated

#### **2.8.4 Measurement of cell process length of cultured OPCs**

To evaluate and quantify the morphological changes of OPC differentiation *in vitro*, 6 semi randomly chosen fields per coverslip were photographed using phase microscopy and fluorescence microscopy (Olympus IX-70, x200 magnification). The reason why the photographing process was not performed in a completely random fashion was the low yield of cells on the coverslips. Wild type differentiating OPCs were distinguished from homozygote OPCs by the presence of GFP. Semiautomatic tracing of OPC processes were performed in ImageJ® using the NeuronJ® plug-in on phase microscopy images.

### **2.9 Statistical analysis and graphical presentation of the data**

In the histopathological study an unpaired t-test was used to analyse the cell count, axonal count and percentage myelinated area data. In the MRI study an unpaired and paired t-test was used to analyse the histological and diffusion data. In the cell culture study an unpaired t-test was used to compare the process length. Statistical significance was set at  $p < 0.05$  throughout the study.

Cell density and axonal density were always presented as the count per  $\text{mm}^2$ . The percentage of myelinated axons was displayed as a proportion relative to the total axonal count. Area occupied by GFAP was presented as the area of GFAP in  $\mu\text{m}^2$  per  $1000000\mu\text{m}^2$ .

Statistical analysis and the graphical presentation of data were performed using GraphPad Prism 4®.

Specific Materials and Methods are described in [3.3 Material and Methods](#), [4.3 Material and Methods](#) and [5.3 Material and Methods](#).

## 3 The development of the phenotype and pathology of the homozygote #72 corpus callosum

### 3.1 Introduction

The *Plp1* gene overexpressing mouse (homozygous; line #72) model of PMD due to gene duplication appears phenotypically normal during development and in early adulthood. At around 3 months of age however, mice develop a mild ataxia and exhibit seizure activity, particularly if disturbed. The generalised ataxia becomes progressively more pronounced, a very mild whole body intention tremor develops and the seizure activity increases. Mice rarely live beyond 4 months of age and death probably occurs as a consequence of prolonged seizure activity, which most likely causes a cardio-respiratory arrest.

Diffusion magnetic resonance imaging of the brain of 4 month old #72 mice demonstrated widespread changes in diffusion parameters in all major white matter tracts (Ruest et al., 2011). Quantification of myelination in three of these tracts, the anterior commissure, hippocampal fimbria and the mid corpus callosum, demonstrated that there was an almost complete lack of myelin sheaths. In the absence of an early clinical phenotype, the paucity of myelin sheaths at this age probably reflects a loss of previously formed myelin rather than a complete failure of developmental myelination. Indeed, both the optic nerve (Edgar et al., 2010) and the spinal cord (Anderson T.J. PhD thesis; Anderson et al., 1998) are well myelinated in the young #72 homozygote mouse.

As described in Chapter 1, the myelin sheath, which surrounds axons in the CNS white matter can be successfully restored by endogenous OPCs, following injury (Zawadzka et al., 2010). The repair mechanisms that restore the myelin sheath are highly effective and full restoration often follows a demyelinating event. However, for reasons that are not fully understood, this repair process is not universal. Various models of dysmyelination and demyelination have been used to investigate (re)myelination biology and pathology and some of these models have been presented in Chapter 1. So far the most common model used in

demyelination research is the immune mediated inflammatory disease model of experimental autoimmune encephalitis (EAE). Although this model has facilitated the identification of immune mediated pathways in demyelination and has also helped to develop drugs to treat MS, it is not a particularly useful model with which to examine the (re)myelination biology, since the background on which repair must take place is hostile. The *Plp1* gene overexpressing mouse model, where the phenotype develops spontaneously, and in which the immune response is mild may represent a better model to investigate (re)myelination biology. Therefore it is of interest to know if the paucity of myelin sheaths in the P120 #72 homozygote mouse represents a failure of developmental myelination and/or a failure of repair following demyelination.

The corpus callosum is commonly used in the investigation of white matter development, myelination, remyelination biology and the pathology thereof. It is a large intracranial white matter structure, divided into five major regions; the rostrum, the genu, the midbody, the isthmus and the splenium (Highley et al., 1999). As a pure white matter structure, it comprises axons, oligodendrocytes, OPCs, astrocytes, microglia and trafficking immunological cells and few, if any, neuronal cell bodies. The neurophysiological function of the corpus callosum is to conduct electrical signals between the cortical neurons of two hemispheres for interhemispherical communication (Zarei et al., 2006). In mice, approximately 60 -70% of the axons are myelinated (Xie et al., 2010). A study by (Olivares et al., 2001) showed that the percentage of myelinated axons is similar across species such as rats, rabbits, cats, dogs, cows, horses and macaque. However other studies show a variation between species that, in reality, is probably due to the investigation of different corpus callosal regions and different time points at which myelination was evaluated (Sturrock, 1980;Looney and Elberger, 1986). Therefore, given the region and time dependent differences in myelin composition within the corpus callosum it is essential to characterise and specify the specific region to be examined.

There are some major advantages that make the corpus callosum an ideal structure to investigate (re)myelination biology and pathology. Individual regions are easily identifiable in histological samples and with newer *in vivo* techniques such as magnetic resonance imaging. This has the advantage that myelination

changes and white matter responses to pathological impacts along the corpus callosum can be investigated over time *in vivo* (Harsan et al., 2006;Harsan et al., 2010). Secondly, the development of the corpus callosum has been extensively described in mouse (Ozaki and Wahlsten, 1998) and the time point of myelination in various species is known (Olivares et al., 2001). Thirdly, the size of the corpus callosum facilitates the implantation of cells for transplantation studies and the structure can be reached with minimally invasive surgical techniques using stereotactic equipment for *in vivo* transplantation experiments.

A disadvantage of the corpus callosum, however, is the high number of small diameter axons. Fibers with a diameter below 0.2 $\mu$ m do not become myelinated (reviewed in Hildebrand et al., 1993). However, external manipulation (specific training) or compensation of lost neuronal function by another area of the brain could induce small fibre growth. If the fibre diameter grows above 0.2 $\mu$ m, myelination will commence. If this is the case, the change in myelination would not be due to remyelination but to myelination. In this specific situation, it is nearly impossible to distinguish between these two entities, new myelin formation or remyelination.

## 3.2 Aims

The overall aim of this Chapter was to characterise the white matter changes leading to the paucity of myelin and apparent lack of repair in the corpus callosum in the #72 homozygote mouse

The specific aims were to:

- 1.) Examine and quantify myelination in the corpus callosum at various ages up to P120
- 2.) Describe and quantify accompanying changes in neighbouring white matter cells, including oligodendrocyte precursor cells
- 3.) Examine and characterise OPC intrinsic and OPC extrinsic factors that could contribute to myelin pathology

## 3.3 Material and Methods

### 3.3.1 Animals

Mice used in this study were the *Plp1* overexpressing transgenic mouse (#72), generated by (Readhead et al., 1994) and the *Thy1*-cyan fluorescent protein (CFP) (B6.Cg-Tg(*Thy1-CFP*)23Jrs/J) expressing mouse model produced by (Feng et al., 2000). Animals were killed and tissue was collected at P40, P60, P90 and P120. Further details are provided in [2 Material and Methods](#).

### 3.3.2 Intraperitoneal BrdU injection for OPC proliferation studies

To label cells in the s-phase of the cell cycle, one single intraperitoneal injection of BrdU (50µg/g) was administered one hour prior to euthanasia, at 12.00 midday ± 2 hours. BrdU in sterile saline, which was stored in aliquots at -20°C, was warmed to room temperature before injecting. Sometimes BrdU

precipitated in the solution and was therefore vortexed to dissolve the BrdU before injecting.

### **3.3.3 Tissue sampling and processing for histopathological examination**

After euthanasia, intracardiac injection of 0.85% saline followed by fixative was performed. The choice of the fixative was based on which histological technique followed. Detailed description of the fixatives and the techniques are listed in Chapter 2 and the Appendix. Samples used for B-cell evaluation were directly frozen after 0.85% saline injection without fixation.

### **3.3.4 Tissue sectioning**

For immunohistochemical evaluation, 10µm thick tissue sections were prepared with a cryotome at -22°C, from frozen samples embedded in OCT. From each animal, a minimum of 80 sections were cut and mounted, consecutively, onto 10 slides, such that each slide contained a series of sections, each separated by 100µm from the next. For light and electron microscopic evaluation, the tissue was moulded into resin blocks and cut into 1µm and 60 nm thick sections, respectively. Immunohistochemistry was performed on fixed or unfixed frozen sections, depending on the primary antibody used. Details of staining protocols, primary and secondary antibodies and concentrations used are listed in ([Chapter 2 Table 2 & Table 3](#)).

### **3.3.5 Quantification of percentage myelinated axons**

Electron microscopy (EM) images were taken at 8000x magnification. The EM images were scanned and imported into Image ProPlus 6.0 software. Axonal density was calculated from six randomly taken images per animal, of the mid corpus callosal region using a rectangular area of interest (AOI: 47.269µm<sup>2</sup>). All axons in the AOI were counted except those touching its southern and western borders of the AOI.

To calculate the percentage of myelinated axons, a grid comprising 4 bisecting lines was applied to the rectangle AOI. The myelination status of all axons lying under any of the digital lines was assessed and the percentage of myelinated axons was calculated. Details of the quantification procedure are found in ([2.8 Morphological studies](#)).

### **3.3.6 Markers used for evaluation of the corpus callosum**

#### **3.3.6.1 Characterisation of myelin integrity and identification of cells originating from the oligodendroglial lineage**

To identify the myelin integrity, antibodies against MBP and PLP/DM20 were used. For ultrastructural evaluation of the myelin sheath, resin sections were evaluated using light microscopy on methylenblue/azur II stained sections and using electron microscopy. Mature oligodendrocytes were identified using an antibody against APC (CC1). For identification of OPCs, antibodies against PDGFR $\alpha$  and NG2 were used. To characterise OPC proliferation, an antibody against BrdU was used in combination with an antibody against PDGFR $\alpha$ . For evaluation of OPC differentiation, an antibody against Olig1 was used in combination with an antibody to NG2 ([Table 2](#) and [Table 3](#)).

#### **3.3.6.2 Identification extraglial changes**

The astrocytic population was identified using an antibody to GFAP. Immune cells, including B-cells, T-cells and microglia/macrophages were identified using antibodies against CD3, CD45R and CD45 and CD169, respectively.

To identify axonal changes antibody SMI32, that recognises non-phosphorylated neurofilament, was used. In *Thy1-CFP / Plp1* transgenic mouse, where CFP accumulates in axonal swellings, an antibody against GFP was used to enhance the CFP fluorescence.

To examine the Wnt pathway in cells from the oligodendrocytic lineage, an antibody against Axin2 in combination with an antibody against Olig1 was used. To characterise deiodinase 3 (D3) expression in microglia/macrophages an antibody against D3 was used in combination with an antibodies against CD45.

To investigate PSA NCAM expression in demyelinating corpus callosum an antibody against PSA NCAM was used.

The biotinylated hyaluronic acid binding protein (HABP) was used to identify the presence of hyaluronan in the extracellular matrix of the corpus callosum ([Table 2](#) and [Table 3](#)).

### **3.3.6.3 Cell quantification**

Immediately after staining, two images of the corpus callosum, parasagittal to the midline and dorsal to the lateral ventricle, were taken from each brain section at x400 magnification, using an Olympus IX70 microscope with a QIcam Fast digital camera. A maximum of 20 images and minimum of 6 images from each mouse were available for cell quantification. The micrographs were opened in Image ProPlus 6.0 software and an area of interest (AOI: 20515.176 $\mu$ m<sup>2</sup>) was applied manually on each image covering the corpus callosum only. All cells, which were fully or partially located in the AOI, were counted except the cells touching the southern and the western borders of the AOI. The cell density per mm<sup>2</sup> was then calculated based on the cell count from a minimum of 6 AOIs.

### **3.3.7 Statistical analysis**

The unpaired student t-test was used to compare the cell count and percentage of myelinated axons between the wild type and the #72 homozygote. Statistical analysis was performed using GraphPad Prism 5®.

## 3.4 Results

### 3.4.1 Extensive myelin degradation was observed in the #72 homozygote corpus callosum

To globally assess myelin integrity over time, cryostat sections containing the mid corpus callosum were labelled with antibodies against MBP ([Figure 11](#)) and PLP/DM20 ([Figure 12](#)) and examined by fluorescence microscopy. At P40, staining appeared similar in the #72 homozygote compared to the wild type. With time, a progressive reduction in MBP and PLP/DM20 staining was observed in the #72 mouse, reaching a minimum at P120, the oldest age examined. This staining pattern suggests that there is a progressive degeneration of myelin in the corpus callosum. The intense, patchy staining in some regions of the #72 mouse corpus callosum ([Figure 11](#) and [Figure 12](#)) probably represents increased penetration of antibodies into the degenerating myelin sheaths. PLP/DM20 was found in cell bodies as well as in myelin sheath-like structures and a substantial number of PLP/DM20 positive cells were present at the time point of complete demyelination (Insert [Figure 12](#)).

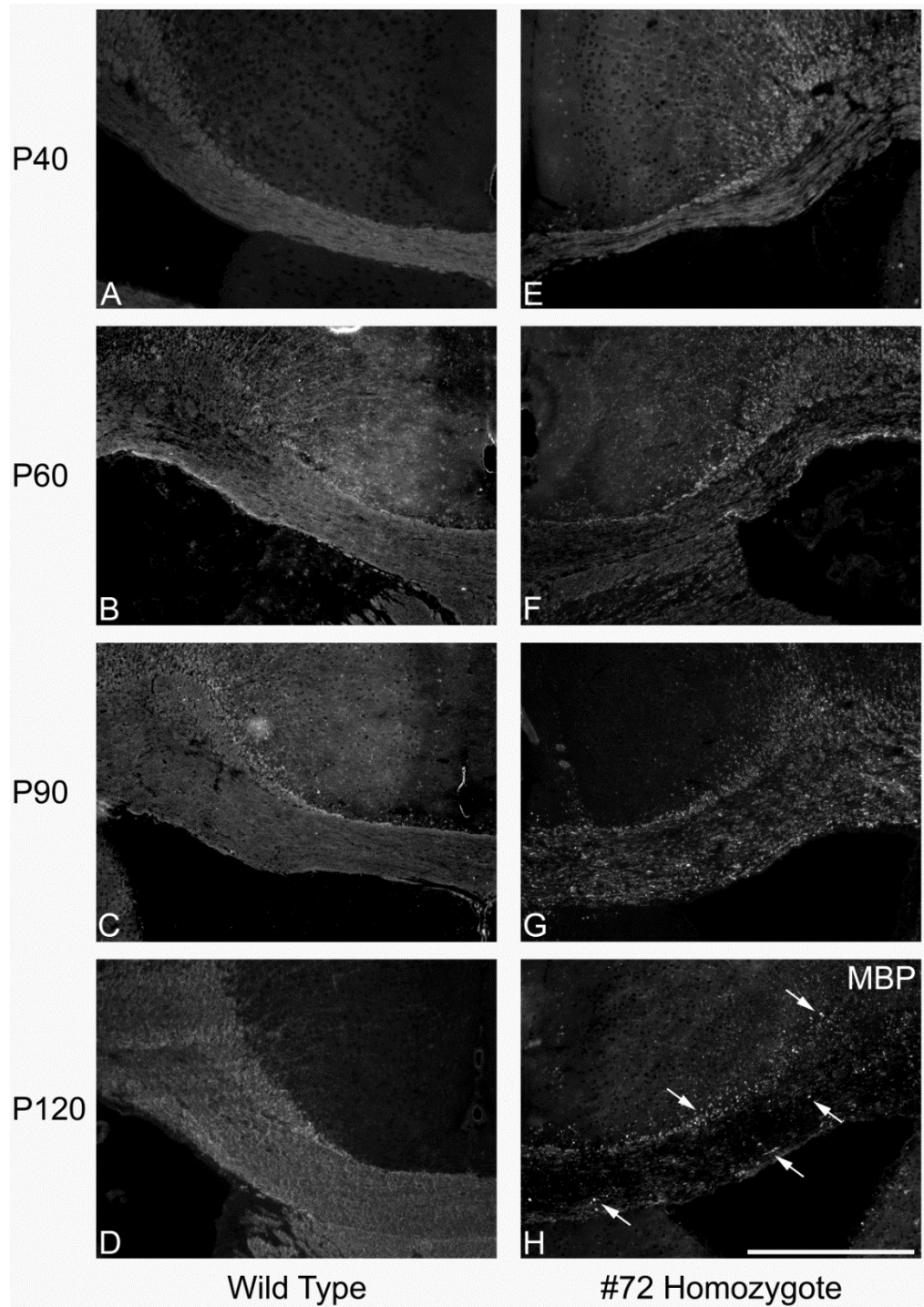


**Figure 11. Progressive reduction in myelin staining in the #72 corpus callosum.**

Micrographs of MBP stained sections through the corpus callosum of wild type (A - D) and #72 mice (E - H; x100, scale bar 400 $\mu$ m) between P40 and P120. At P40 MBP staining in the #72 corpus callosum appeared similar to the wild type. MBP staining diminished with increasing age. The patchy appearance of the staining probably reflects the binding of the antibody to myelin breakdown products. Auto fluorescent lipofuscin (arrows) was present and contributed to the staining pattern.

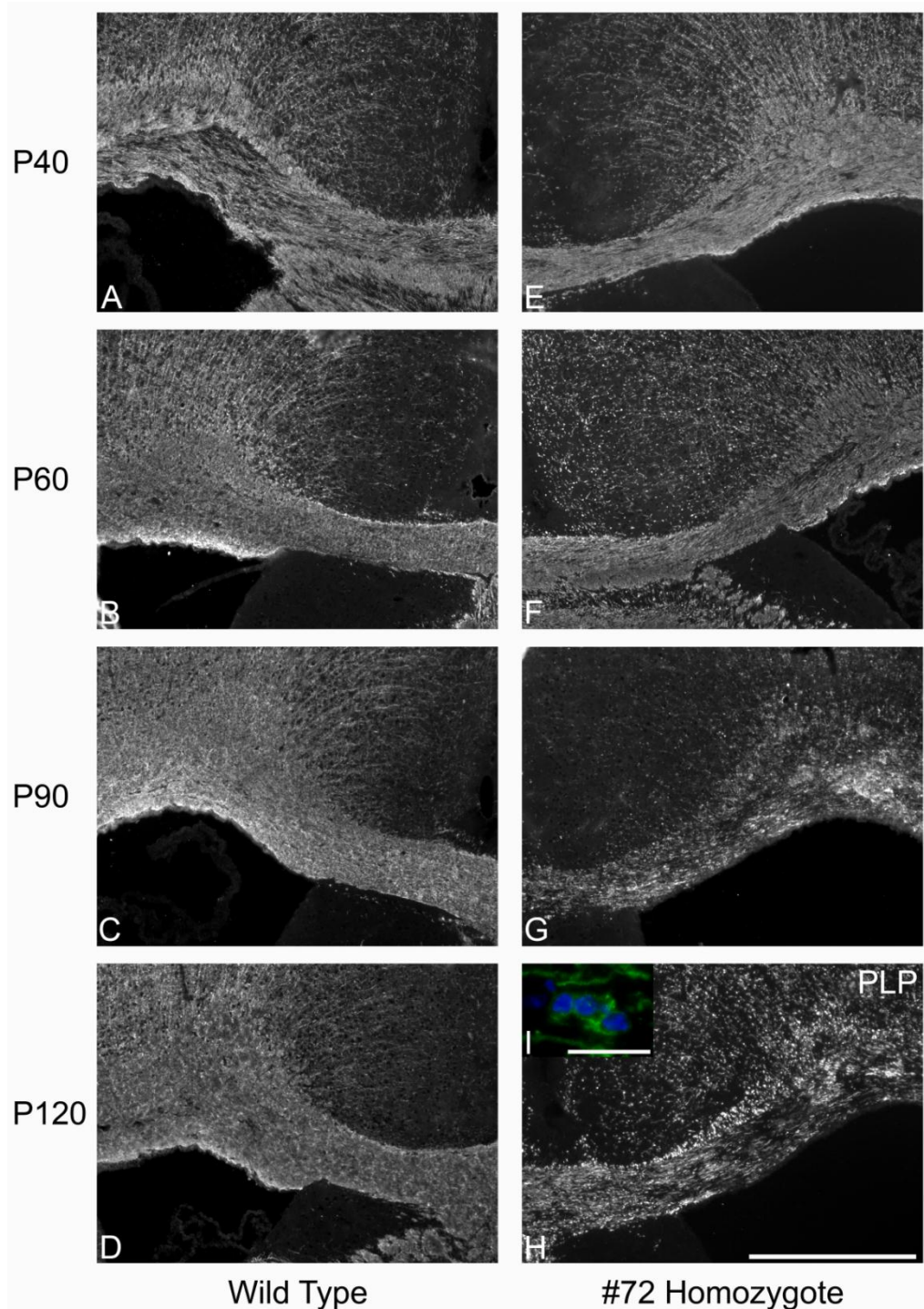


**Figure 12. Progressive loss of PLP/DM20 staining in the #72 corpus callosum.**

Micrographs of PLP/DM20 stained sections through the corpus callosum of wild type (A - D) and #72 mice (E - H; x100, scale bar 400µm) between P40 and P120. The progressive reduction in PLP/DM20 staining followed a comparable pattern when MBP was used as a marker. The myelin status at P40, in the #72 mouse was comparable to the wild type. Later, a progressive loss of PLP/DM20 staining was observed. The paucity of staining appeared less severe with the antibody recognising PLP/DM20 compared to staining with antibody to MBP. This was due to the presence of PLP/DM20 in cell bodies (I, x400, scale bar 25µm).

### **3.4.2 The corpus callosum is almost completely demyelinated at P120 in the #72 mouse**

For qualitative and quantitative assessment of myelination, resin sections were examined using light and electron microscopy. Light microscopy revealed comparable amounts of myelin in the corpus callosum of P40 #72 and the wild type mice. Subsequently, there was a progressive reduction in myelin volume, until demyelination was virtually complete at P120 ([Figure 13](#)). Electron microscopy demonstrated normal appearing myelin sheaths in the #72 mouse corpus callosum ([Figure 14](#)). The percentage of myelinated axons was calculated from electron micrographs. A significant reduction in the percentage of myelinated axons was observed in the #72 mouse compared to the wild type at P60, P90 and P120, with a virtually complete absence of myelinated axons at P120 ([Figure 15](#)).

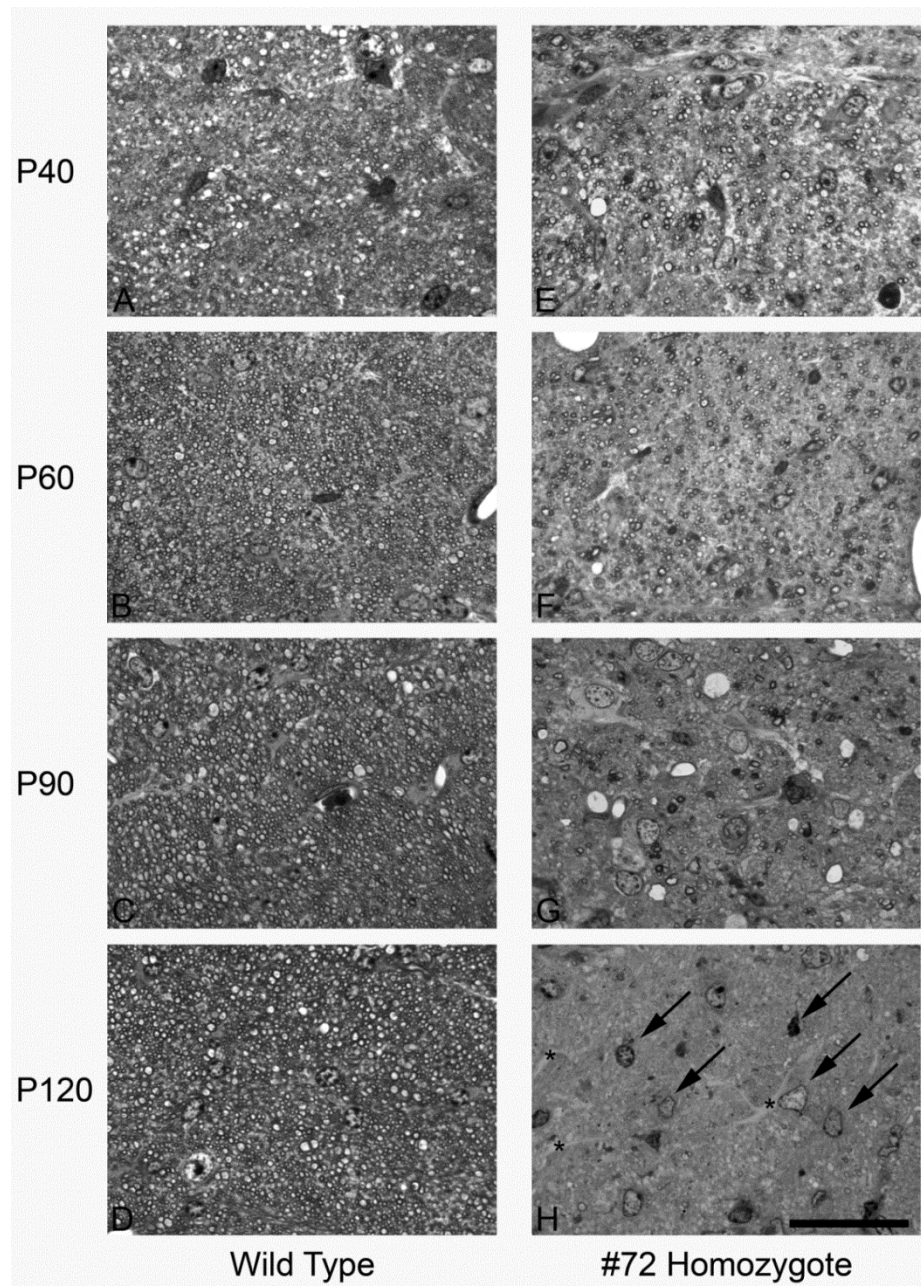


**Figure 13. Progressive demyelination follows initial myelination of the #72 homozygote corpus callosum.**

Methylene blue / azur II stain of the mid corpus callosum between P40 and P120 in wild type (A - D) and #72 mice (E - H, x1000, scale bar 40  $\mu$ m). At P40, myelin volumes appeared similar in the #72 mouse compared to the wild type mouse. With increasing age, the amount of myelin appeared to increase in the wild type showing that myelination of the corpus callosum continued into adulthood. In contrast, in the #72 mouse, the corpus callosum became progressively demyelinated between P60 (B, F), P90 (C, G) and P120 (D, H). There was an almost complete absence of myelinated axons at P120. At this age cell nuclei (black arrows) appeared more numerous in the #72 mouse compared to the wild type and numerous large astrocytic processes (asterisk) were also observed.

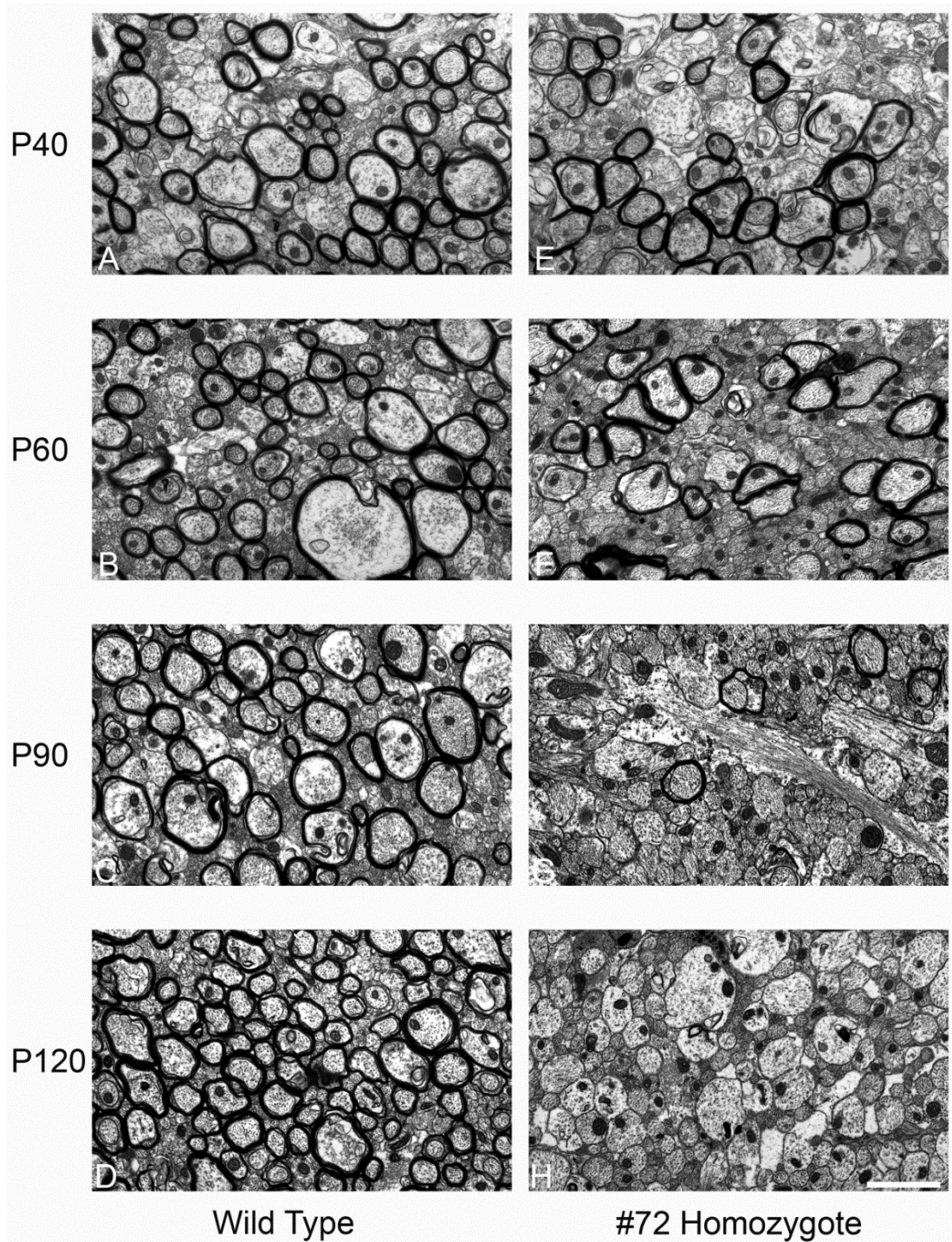


**Figure 14. Initial myelination of the #72 mouse corpus callosum was followed by progressive demyelination.**

Electron micrographs of the corpus callosum between P40 and P120 in wild type (A - D) and #72 mice (E - H, x8000, scale bar 2  $\mu$ m). At P40, myelin volume in the #72 mouse corpus callosum appeared similar to that in the age-matched wild type mouse. The myelin that was present in the #72 mouse had a morphologically normal appearance. At subsequent time-points, the proportion of myelinated axons appeared to decrease progressively from P60 till P120, by which time the corpus callosum was almost completely demyelinated.

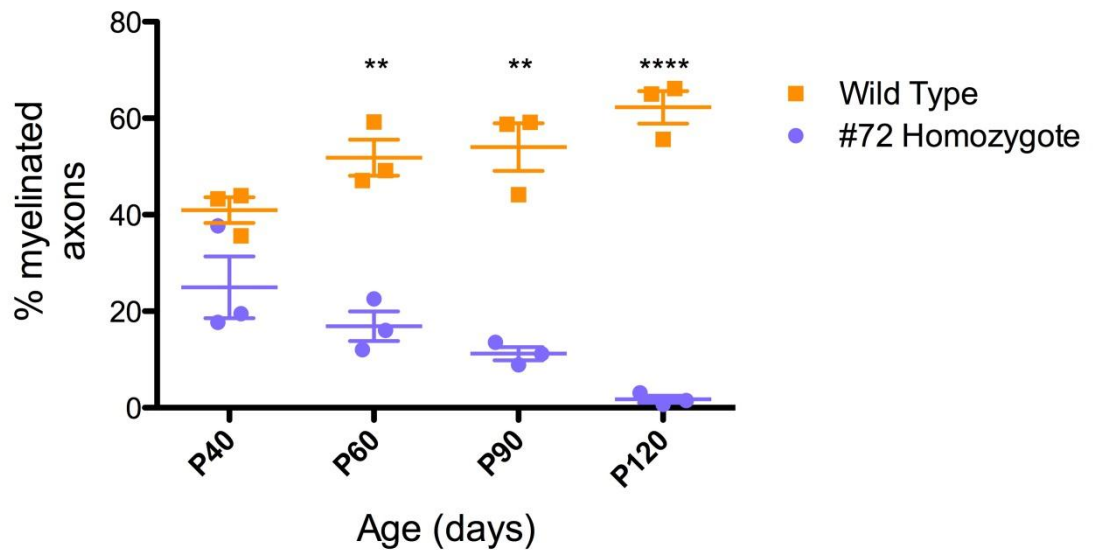


**Figure 15. Demyelination progresses with increasing age in the corpus callosum.**

N=3 (for each given time point and genetic background), adding up to a total number of 24 quantified specimens. Bars display s.e.m. There is a progressive loss of myelin sheaths with time in the #72 mouse corpus callosum, leading to a significant reduction in the percentage of myelinated axons in the #72 mouse corpus callosum compared to wild type, at P60, P90 and P120. At P40 the percentage of myelinated axons was similar in the #72 mouse compared to the wild type mouse, suggesting that developmental myelination is relatively normal in #72 mouse corpus callosum (\*\*:  $p < 0.01$ , \*\*\*\*:  $p < 0.0001$ ).

### **3.4.3 Mature oligodendrocytes were present in the demyelinating #72 homozygote corpus callosum**

To determine if demyelination in the #72 homozygote corpus callosum was accompanied by a loss of mature oligodendrocytes, an antibody to APC, a marker for mature oligodendrocytes, was used. At all time points investigated, APC positive oligodendrocytes were present ([Figure 16](#)). The distribution of oligodendrocytes in the #72 mouse corpus callosum was comparable to the wild type. Even at P120, when the corpus callosum was completely demyelinated, APC positive cells were present. This suggests that myelin degeneration in the #72 mouse is not entirely due to oligodendroglial cell death.

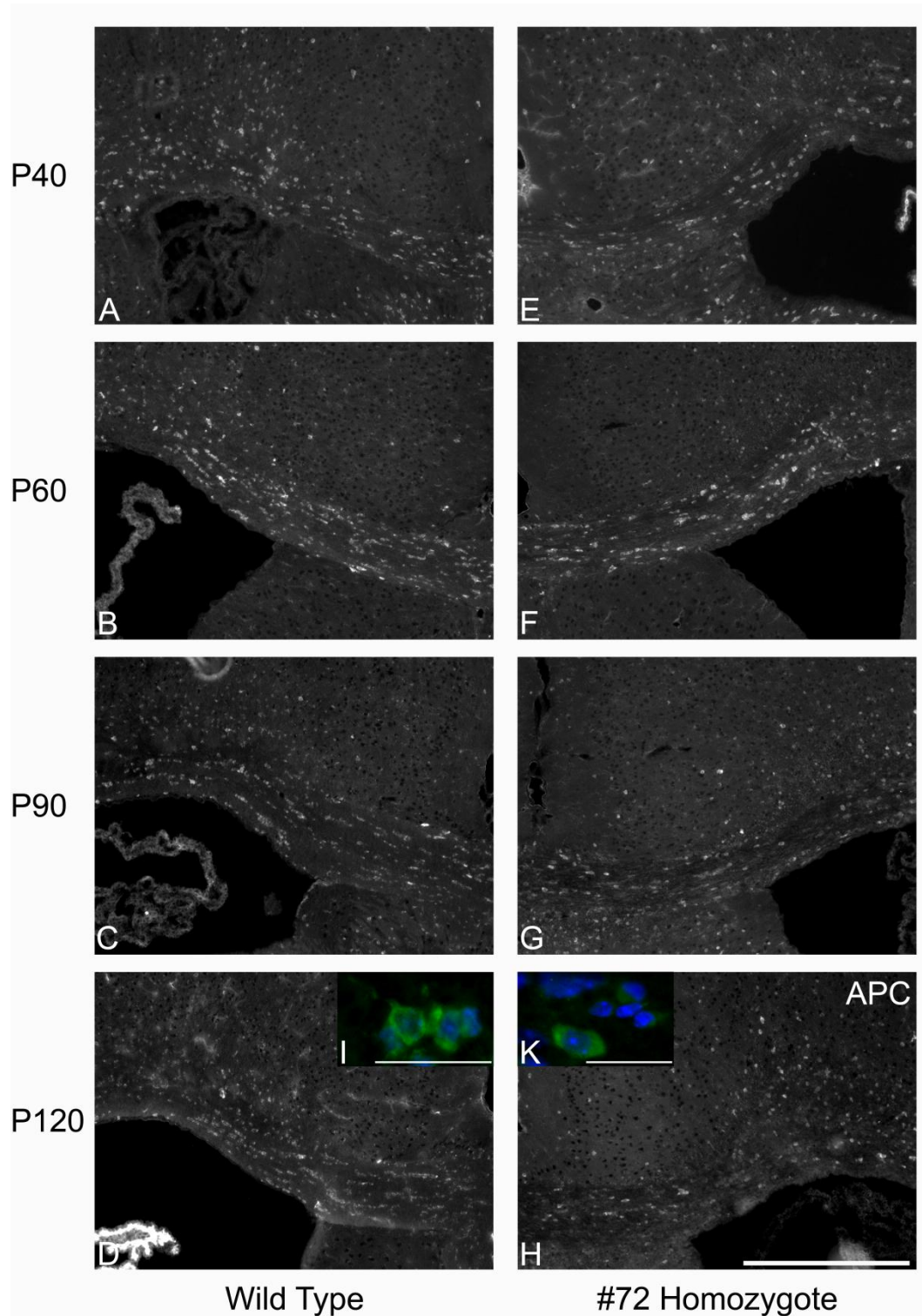


**Figure 16. Mature oligodendrocytes were present at all time points during demyelination.**

Micrographs of wild type (A - D, I) and #72 mouse (E - H, x100, scale bar 400 $\mu$ m; K, x400, scale bar 25 $\mu$ m) corpus callosum labeled with an antibody to APC (CC1), between P40 and P120. The distribution of mature oligodendrocytes appeared similar in the #72 mouse compared to the wild type. Despite progressive demyelination, mature oligodendrocytes were present in the corpus callosum, suggesting that the demyelination is not caused by primary oligodendrocyte cell death.

In summary, these studies demonstrate that there is a slowly progressing demyelination in the #72 mouse corpus callosum with no evidence of effective remyelination. Since, in rodents, remyelination is usually a default response to demyelination, I went on to examine various factors that could contribute to remyelination failure, such as the presence and response of OPCs and the astroglial and the microglial response in the #72 mouse.

#### **3.4.4 Oligodendrocyte precursor cells were abundantly present in the #72 corpus callosum**

OPCs are responsible for regenerating myelin sheaths in the CNS after a demyelinating event (Zawadzka et al., 2010). In the context of the progressive demyelination of the #72 homozygote corpus callosum and in the absence of effective remyelination, I examined the oligodendroglial lineage.

To determine if OPCs were present in the demyelinating corpus callosum, OPC markers NG2 (Figure 17) and PDGFR $\alpha$  were used to label and to quantify the OPC population ([Figure 18](#) & [Figure 19](#)). In the #72 mouse corpus callosum, NG2 and PDGFR $\alpha$  +ve cells were present at all time points examined, at a similar density to the wild type. The NG2 +ve cell density was significantly elevated at P120 in the #72 mouse, compared to the wild type.

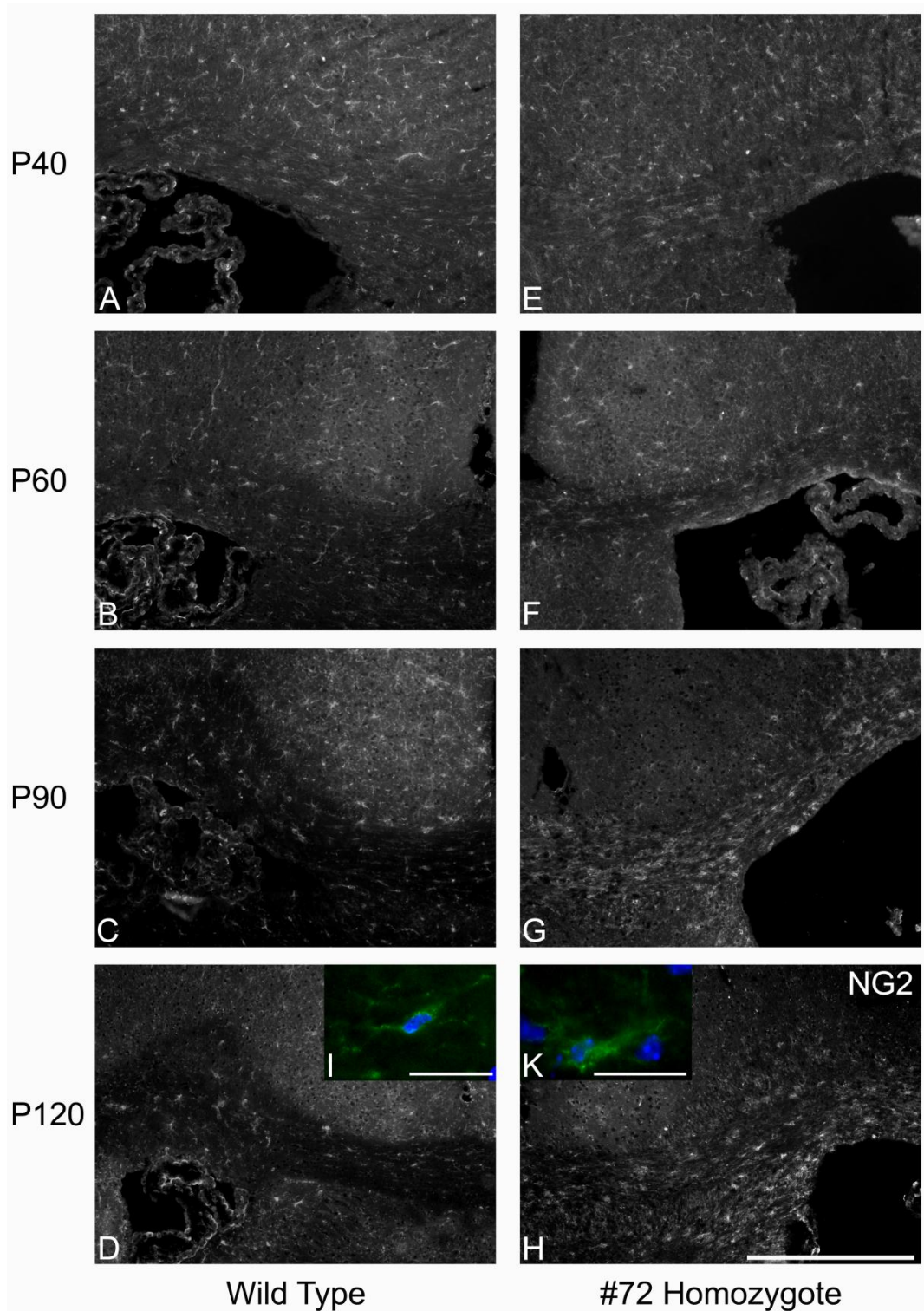


**Figure 17. NG2+ cells were present in the #72 mouse corpus callosum during all stages of demyelination.**

Micrographs of sections stained for NG2, between P40 and P120, in wild type (A - D) and #72 mouse (E - H, x100, scale bar 400µm) corpus callosum. At all time points during the progressive demyelination, NG2 +ve cells were present in the #72 homozygote corpus callosum. The density appeared similar to the wild type. The NG2 cell processes appeared thicker and more branched in the #72 mouse (K) compared to the wild type (I, x400, scale bar 50µm).

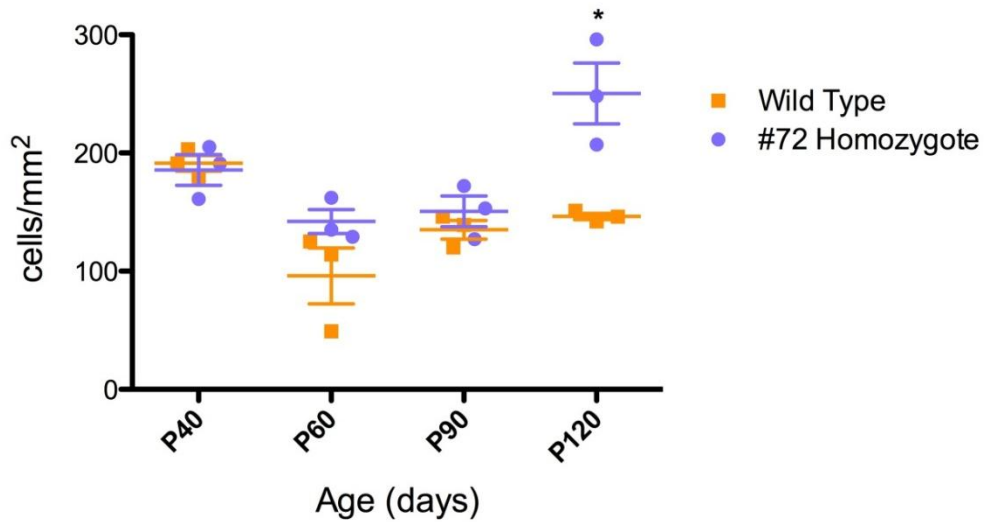


**Figure 18. NG2+ cells in the #72 mouse corpus callosum between P40 and P120.**

Graph illustrating the NG2 +ve cell density between P40 and P120 in wild type and #72 mice. N=3 (for each given time point and genetic background), adding up to a total number of 24 quantified specimens. Bars display s.e.m. Mean NG2 cell density was similar in the #72 mice compared to the wild type up to P90. At P120, when demyelination is complete, there was a significant increase in NG2 +ve cell density in the #72 mice compared to wild type (\*:  $p < 0.05$ ).

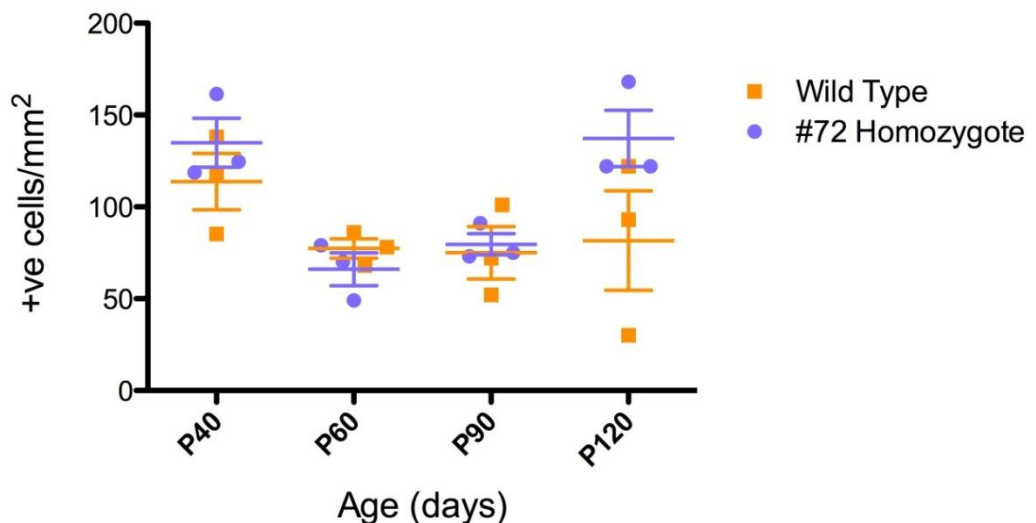


**Figure 19. PDGFRα positive cells in the demyelinating #72 mouse corpus callosum.**

Graph illustrating PDGFRα +ve cell density in the wild type and #72 mouse corpus callosum between P40 and P120. N=3 (for each given time point and genetic background), adding up to a total number of 24 quantified specimens. Bars display s.e.m. There was no significant difference in the density of PDGFRα +ve cells in the #72 mouse corpus callosum compared to the wild type. The PDGFRα +ve cell density was, in both wild type and #72 mouse corpus callosum, lower compared to the NG2 +ve cell population.

In short although progressive extensive demyelination occurs during adulthood in the #72, OPCs are abundantly present at all time points. Despite the abundant OPC population there was no evidence of an effective attempt at remyelination and the question therefore arises of how the OPCs respond to the demyelination.

### **3.4.5 Characterisation of OPC response during progressive myelin loss**

#### **3.4.5.1 Waves of OPC proliferation occurred during progressive demyelination**

To study the proliferation activity of OPCs in the #72 corpus callosum, one single intraperitoneal injection of the thymidine analogue Bromodeoxyuridine (BrdU) was performed one hour prior to euthanasia. BrdU is incorporated into replicating DNA during the s-phase of the cell cycle and can be used to identify proliferating cells. For quantification of OPC proliferation the sections were double labelled with antibodies against PDGFR $\alpha$  and BrdU ([Figure 20](#)).

Initially the PDGFR $\alpha$ /BrdU +ve cell density was similar in #72 and wild type mice. There was a continuous decline in PDGFR $\alpha$ /BrdU +ve cell density in the wild type after P40 up to P120. In the #72 corpus callosum the PDGFR $\alpha$ /BrdU +ve cell density initially followed a similar decline between P40 and P60. However there was a significant increase in PDGFR $\alpha$ /BrdU +ve cell density at P90 in the #72 compared to the wild type. This was followed by a decline in BrdU/PDGFR $\alpha$  +ve cell density at P120, when the cell density again appeared similar to wild type ([Figure 21](#)).

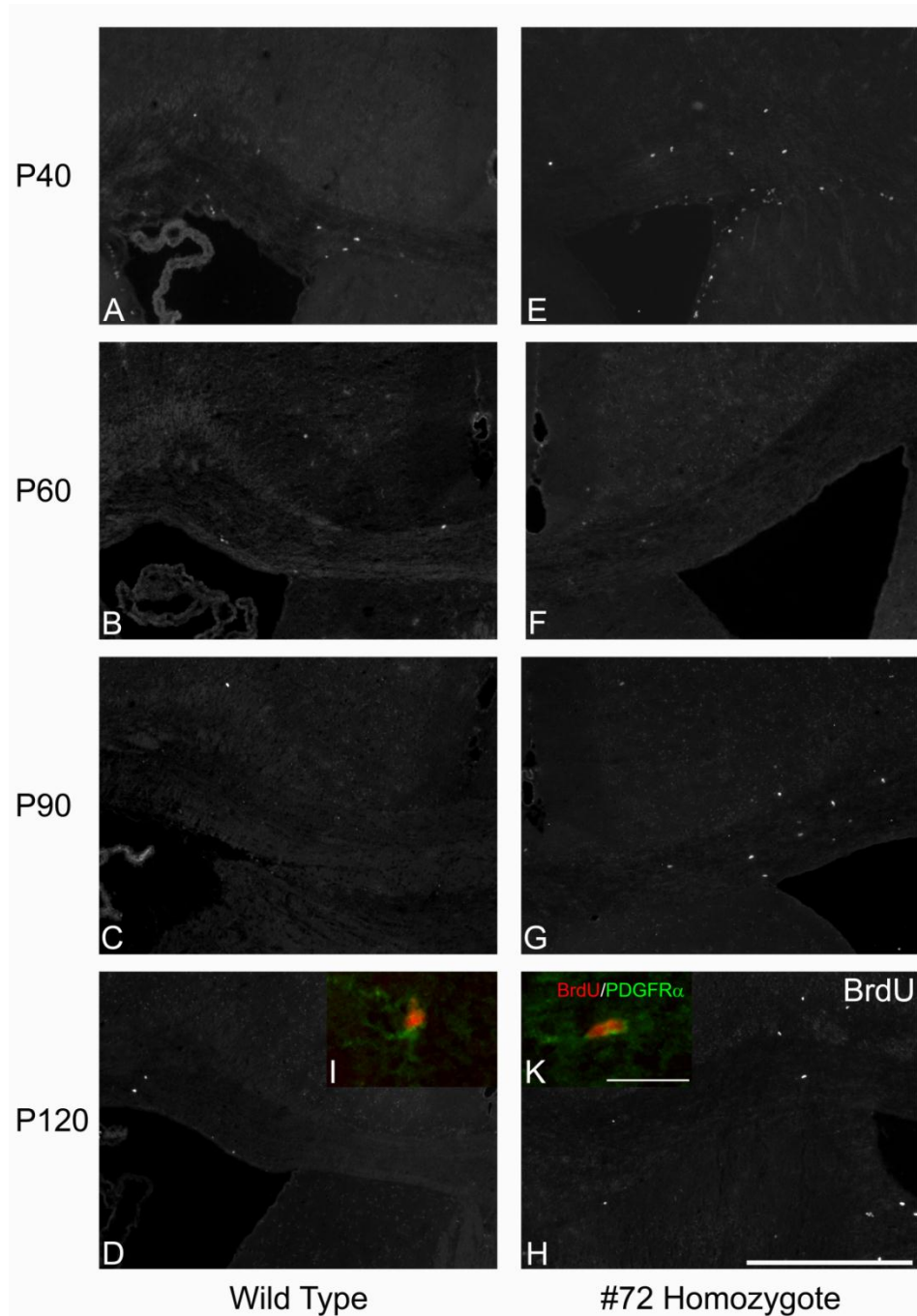


**Figure 20. Cell proliferation occurred in response to demyelination.**

Micrographs of BrdU +ve cells in the corpus callosum between P40 and P120 in wild type (A - D) and #72 homozygote mice (E - H, x100, scale bar 400µm). Initially at P40 and P60 BrdU +ve cells were present in a comparable fashion between the wild type and #72 homozygote mice. However there was a marked increase in BrdU +ve cells in the #72 homozygote compared to the wild type at P90. At P120 the quantity of BrdU +ve cells appeared similar in the #72 and wild type mice. Some of these BrdU +ve cells were PDGFR $\alpha$  +ve, suggesting that OPC proliferation occurs during demyelination (I, K, x400, scale bar 25µm).

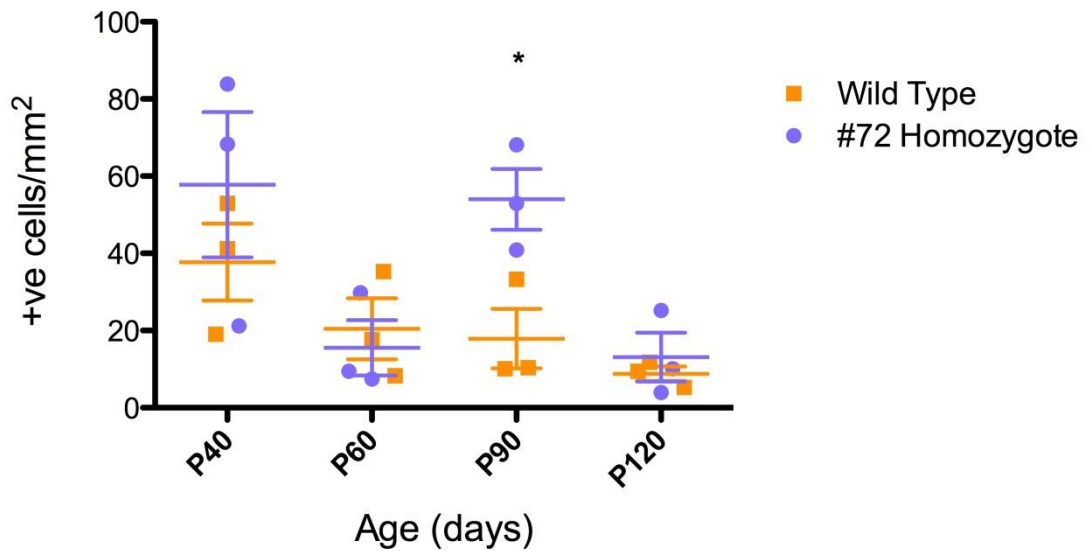


**Figure 21. OPC proliferation occurred in association with progressive demyelination.**

Graph illustrating the OPC proliferation in wild type and #72 homozygote mouse during progressive demyelination. N=3 (for each given time point and genetic background), adding up to a total number of 24 quantified specimens. Bars display s.e.m. In order to focus on OPC proliferation only BrdU/PDGFR $\alpha$  +ve cells were counted. Initially the OPC proliferation was similar in both the wild type and the #72 mouse. Proliferation was higher at this age compared to older ages, probably reflecting ongoing myelination. There was a reduction in PDGFR $\alpha$ /BrdU +ve cell density at P60 in both the wild type and #72 mouse, followed by a significant increase in PDGFR $\alpha$ /BrdU +ve cells, suggesting an increased OPC proliferation at P90 in the #72 mouse. By P120, the proliferative pool was similar to the wild type.

### 3.4.5.2 OPC differentiation is virtually absent in the demyelinated #72 corpus callosum

Since proliferation of the OPCs take place in response to progressive demyelination in the #72 corpus callosum, the next step was to identify the differentiation status of the OPCs during progressive demyelination. It has been shown that the basic Helix-Loop-Helix (bHLH) transcription factor Olig1 is required during remyelination and that the absence of Olig1 leads to remyelination failure (Arnett et al., 2004). For remyelination to be successful OPCs must differentiate into oligodendrocytes. The change in subcellular distribution of Olig1, which has been shown to be a translocation of Olig1 from cytoplasm into the nucleus during OPC differentiation, can be used to characterise the status of OPCs during demyelination and remyelination (Arnett et al., 2004; Kitada and Rowitch, 2006). To investigate if Olig1 translocates to the cell nucleus in OPCs in the #72 homozygote corpus callosum, the subcellular localisation of Olig1 in NG2 cells was analysed and quantified. NG2 +ve cells with (i) intranuclear, (ii) intranuclear and cytoplasmic, (iii) partial intranuclear and cytoplasmic or (iv) cytoplasmic Olig1 localisation were identified ([Figure 22](#)). NG2 +ve cells that were negative for Olig1 as well as Olig1 +ve cells that were negative for NG2 were also observed. P3 #72 mice had the expected intranuclear Olig1 expression during early neonatal development ([Figure 23](#)). In adult animals, only extremely rare NG2 +ve /intranuclear Olig1+ve cells were found in either wild type or the #72 mice ([Table 4](#)). In fact almost half of all NG2 +ve /Olig1 +ve cells in wild type and #72 mice had a pure cytoplasmic localisation of Olig1 ([Figure 24](#)).

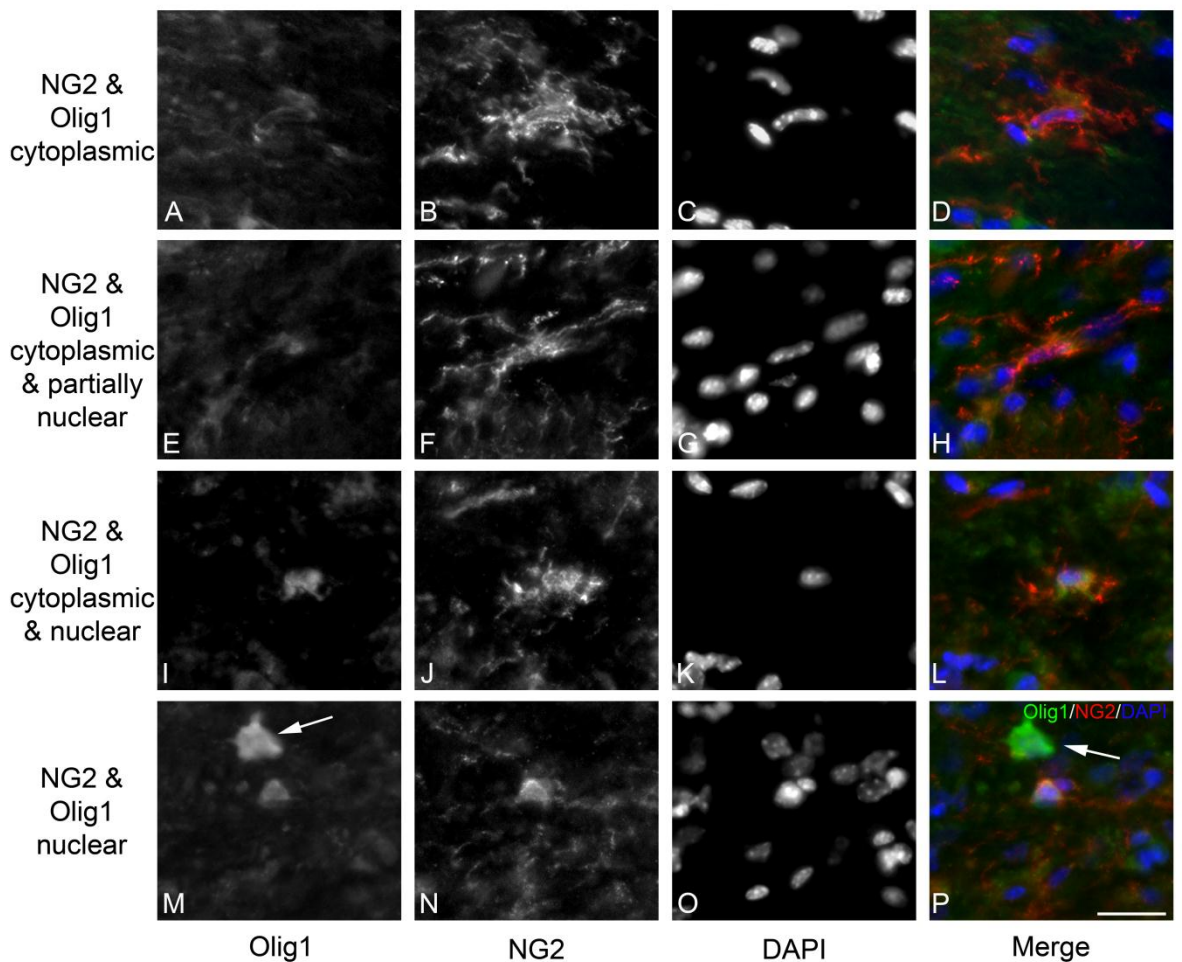


**Figure 22. All variants of subcellular Olig1 localisation in NG2+ cells were found in the #72 mouse during demyelination.**

Micrographs from #72 corpus callosum showing NG2 +ve cells with cytoplasmic localisation of Olig1 (A - D), with cytoplasmic and partially nuclear localisation of Olig1 (E - H), with cytoplasmic and nuclear localisation of Olig1 (I - L) and with nuclear localisation of Olig1 (M - P, x400, scale bar 25µm). This indicates that all stages of OPC proliferation and differentiation were present in the #72 homozygote mouse. Note that combined cytoplasmic and nuclear Olig1 is also present in NG2 negative cells (arrow).

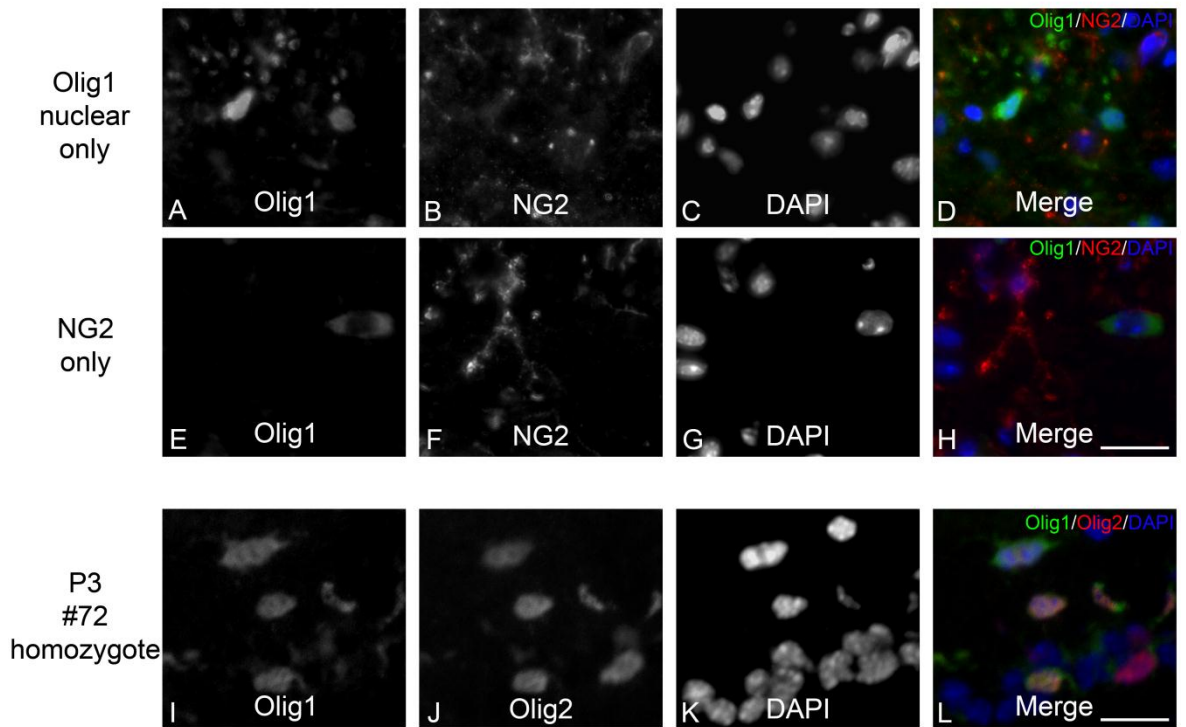


**Figure 23. Different subcellular Olig1 localisation was observed in NG2 negative cells.**

Micrographs from #72 corpus callosum. NG2 negative cells with nuclear localisation of Olig1 were also detected (A - D). There were also a few NG2 +ve cells, which were Olig1 negative. In the same image there is a cytoplasmic Olig1 only positive cell, which is most likely a mature oligodendrocyte (E - H x400, scale bar 25µm). This shows that not only in OPCs but also in other cells the subcellular localisation of Olig1 can vary. In order to verify the sensitivity of the Olig1 antibody to penetrate intranuclear, tissue from P3 #72 homozygote mice was used where intranuclear localisation of Olig1 in Olig2 positive cells is expected to be present. Intranuclear localisation of Olig1 in Olig2 positive cells was detected in developing #72 homozygote corpus callosum (I - L, x400, scale bar 25µm). This is in agreement with observations described in the literature.

	NG2 & Olig1 intranuclear		NG2 & Olig1 cytoplasmic		NG2 & Olig1 intranuclear & partial cytoplasmic		NG2 & Olig1 intranuclear & cytoplasmic	
	Mean (%)	S.E.M	Mean (%)	S.E.M	Mean (%)	S.E.M	Mean (%)	S.E.M
WT P40	0.32	±0.32	63.347	±2.025	24.393	±5.272	11.94	±6.793
#72 P40	0	0	38.69	±2.38	50.29	±3.965	11.02	±3.154
WT P60	0.347	±0.347	51.293	±6.947	41.347	±4.394	7.013	±2.825
#72 P60	1.367	±0.803	34.137	±6.332	44.803	±6.345	19.693	±2.788
WT P90	1.170	±1.170	57.933	±7.153	30.563	±4.632	10.333	±4.535
#72 P90	0	0	47.277	±3.078	48.79	±3.987	3.933	±1.695
WT P120	0	0	49.373	±2.187	49.787	±2.11	0.477	±0.477
#72 P120	0	0	45.673	±4.014	50.905	±4.328	3.423	±0.965

**Table 4. Intranuclear Olig1 was rarely observed in wild type and #72 homozygote NG2 +ve cells.**

N=3 (for each given time point and genetic background), adding up to a total number of 24 quantified specimens. Olig1 was mainly found in the cytoplasm or in mixed cytoplasmic and nuclear locations. The population with mixed subcellular localisation of Olig1 were most likely proliferating OPCs.

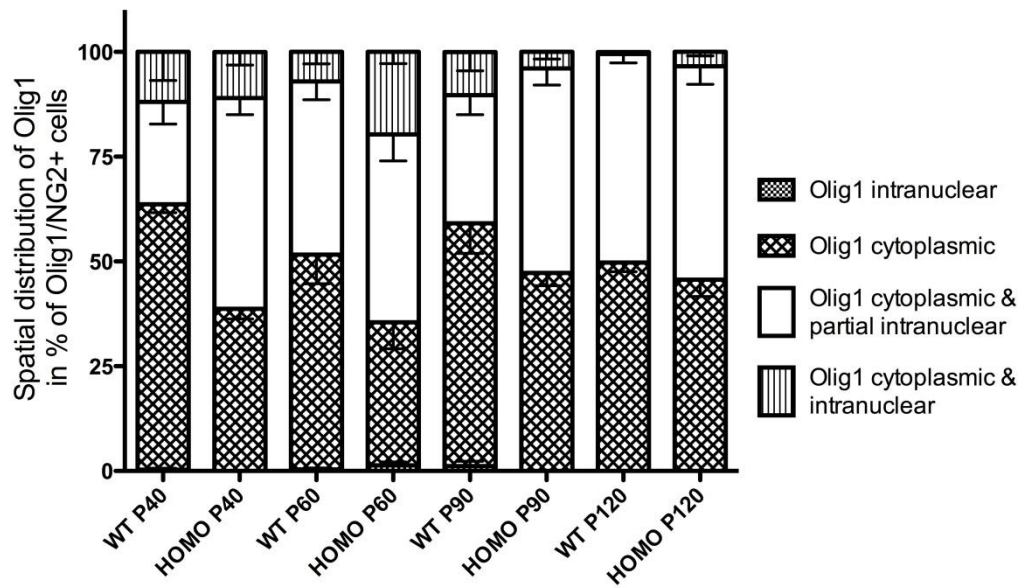


**Figure 24. The subcellular distribution of Olig1 in #72 mouse NG2 +ve cells.**

Graph representing the percentage of subcellular localisation of Olig1 in NG2 +ve cells. N=3 (for each given time point and genetic background), adding up to a total number of 24 quantified specimens. Bars display s.e.m. In NG2 +ve cells in the #72 mouse, Olig1 was mainly localised in both cytoplasm and nucleus. Only a very few NG2 +ve cells had a uniquely intranuclear localisation of Olig1.

### 3.4.6 Astrocytic response during demyelination of the #72 homozygote corpus callosum

In general, astrocytes react to demyelination by proliferation and activation (reviewed in (Moore et al., 2011a;Ayers et al., 2004). The role of astrocytes in demyelinating pathology is controversial. Both beneficial (Franklin et al., 1991;Liu et al., 1994;Moore et al., 2011b) and inhibitory (Back et al., 2005;Blakemore et al., 2003;Su et al., 2011) roles in remyelination has been reported reviewed in (Nash et al., 2011). To characterise the astrocytic response during demyelination in the #72 mouse, an antibody to GFAP was used ([Figure 25](#)). GFAP +ve cell density was increased in the #72 homozygote compared to the wild type at all ages examined. Significant increase was observed ( $p<0.05$ ) from P60 onwards and increased with the severity of demyelination ([Figure 26](#)).

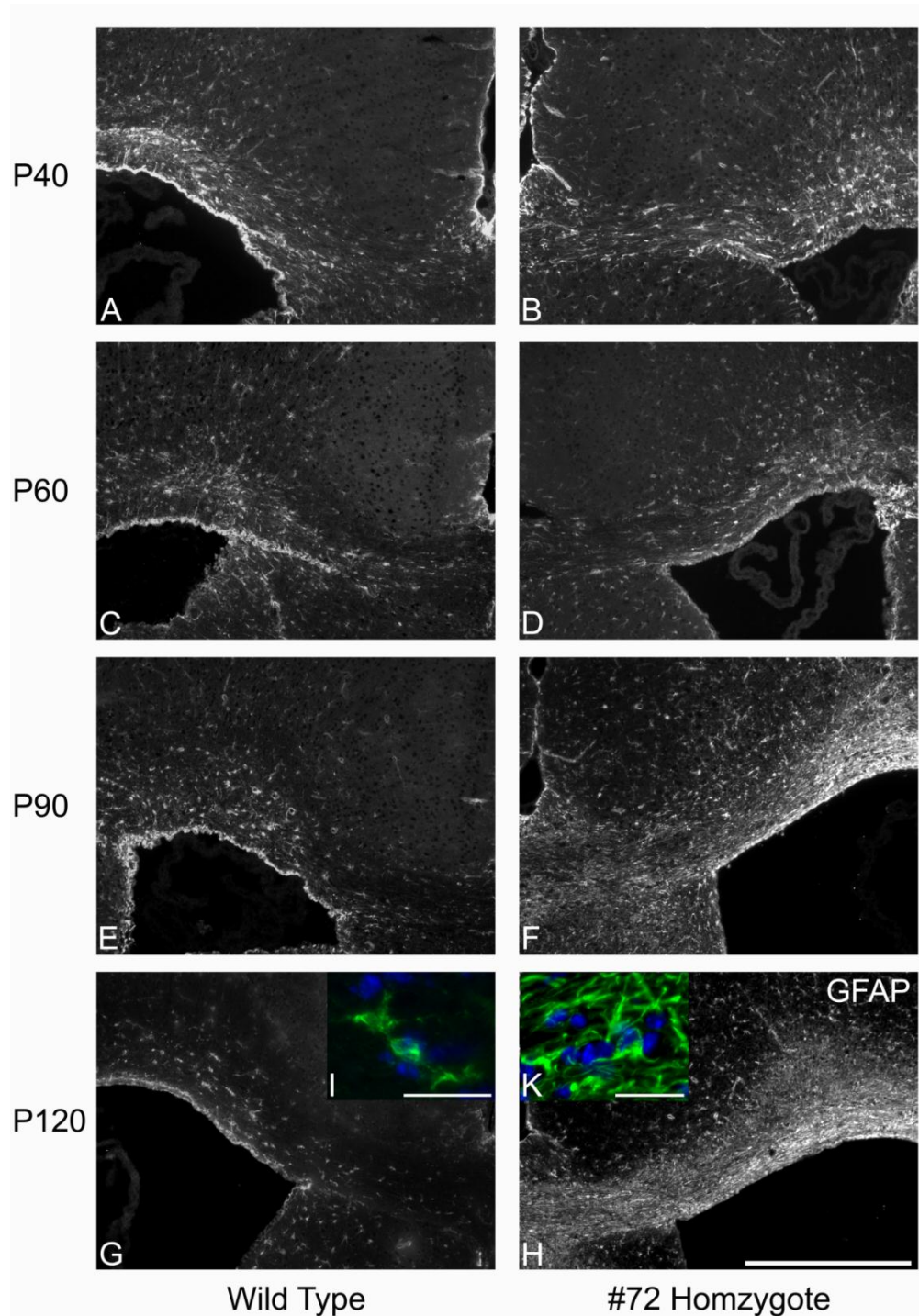


**Figure 25. A progressive astrocytic response accompanied demyelination in the #72 mouse corpus callosum.**

Micrographs of sections stained for GFAP, between P40 and P120, in wild type (A - D) and #72 mouse (E - H, x100, scale bar 400 $\mu$ m) corpus callosum. At P40 the density of astrocytes was similar in #72 and wild type mice. From P60 onwards, the astrocyte density was significantly increased in the #72 mouse corpus callosum compared to the wild type. Astrocyte morphology changed with progressive demyelination. In the #72 mouse, astrocyte processes appeared thicker and more branched (K, magnification x400, scale bar 25 $\mu$ m) than in wild type mice (I, x400, scale bar 25 $\mu$ m).

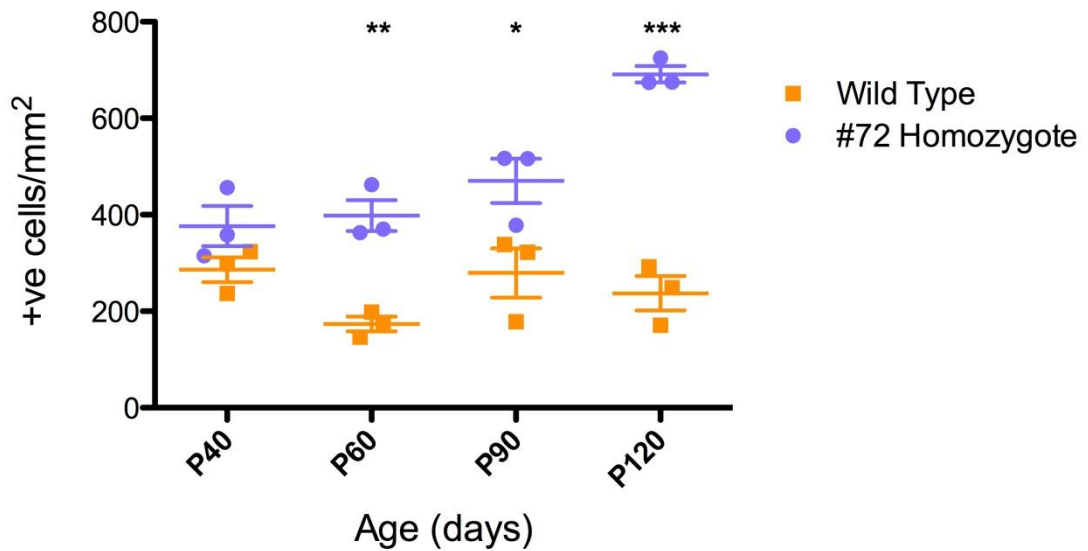


**Figure 26. Astrocyte cell density is increased in the #72 mouse corpus callosum.**

Graph illustrating the astrocytic cell density during progressive demyelination in the #72 mouse corpus callosum. N=3 (for each given time point and genetic background), adding up to a total number of 24 quantified specimens. Bars display s.e.m. The astrocyte density in the #72 mouse is comparable to the wild type at P40. A progressive increase in astrocyte cell density was present after P40, with a particularly steep increase between P90 and P120. Cell density was significantly increased in the #72 mouse, compared to wild type, at P60, P90 and P120. (\*:  $p < 0.05$ , \*\*:  $p < 0.01$ , \*\*\*:  $p < 0.001$ ).

### 3.4.7 Immune cell response in the #72 homozygote corpus callosum

#### 3.4.7.1 Progressive demyelination is accompanied by an increase in CD45 and CD169 positive cell population

The microglial/macrophage population has been shown to undergo marked upregulation (Tatar et al., 2010) and to contribute to the progression in demyelination (Ip et al., 2006; Ip et al., 2007) in *Plp1* gene overexpressing mice (line #66). In context with remyelination, inflammation has been shown to have a promoting effect on remyelination efficacy (Foote and Blakemore, 2005a; Setzu et al., 2006). Also the phagocytic activity of microglia/macrophages is beneficial for remyelination (Kotter et al., 2006; Merson et al., 2010). On the other hand microglia mediated inflammation can also be cytotoxic, which can cause unspecific severe tissue damage also on remyelination capable OPCs (Merson et al., 2010).

The pan leukocytic marker CD45 was used to characterise the microglia/macrophage population during demyelination in the #72 mouse corpus callosum. In the normal CNS there are only a few trafficking T and B cells so the majority of CD45+ cells are microglia. Most of the CD45 +ve cells were dendritic in appearance, resembling microglial cells ([Figure 27](#)). Only a few cells lacked processes, suggesting they were lymphocytes (arrows in [Figure 27](#)). Therefore the vast majority of CD45+ve cells most likely were microglial/macrophages. The density of CD45+ve cells was significantly increased from P60 onwards in the #72 homozygote corpus callosum compared to the wild type, and increased in proportion to the severity of demyelination ([Figure 28](#)).

Not only the increase in density of microglia but also their state of activation, which can be identified by the expression of the macrophage restricted adhesion molecule sialoadhesin (CD169), has been shown to be involved in the demyelination process and the development of axonal pathology. Knock out of sialoadhesin (CD169) expression on microglia/macrophages in a different *Plp1* overexpressing mouse model, (line #66) ameliorated demyelination and axonal

damage (Ip et al., 2007). Activated microglia also secrete TNF $\alpha$  (reviewed in Merson et al., 2010), and may induce OPC apoptosis, which leads to a reduction in OPCs and therefore may have a negative influence on remyelination capacity (Mi et al., 2011). CD169 is normally not expressed on microglia and it is thought that CD169 expressing cells in the CNS are recruited from the periphery to the damaged CNS (Perry et al., 1992). However, activation of residential microglia/macrophages occurs in relation to pathological processes in the CNS and (Ip et al., 2007) suggested that at least some of the CD169+ cells in *Plp1* overexpressing mice CNS are resident microglia (Ip et al., 2007).

In the #72 homozygote corpus callosum, CD169 expression was observed after P60 and markedly increased up to P120 ([Figure 29](#) and [Figure 30](#)). CD169+ cells were also present in the choroid plexus and blood vessels as would be expected ([Figure 29](#) arrows and arrowheads) and were only occasionally present in the wild type corpus callosum at any of the time points examined.

Edgar et al (2010) showed that B cells are rare and that there are only a few T cells in the #72 mouse optic nerve (Edgar et al., 2010). In this study, B-cells were absent in the P120 #72 mouse corpus callosum (data not shown). Infiltrating T cells have been reported to contribute to the demyelination and axonal pathology in *Plp1* gene overexpressing mice (Ip et al., 2006). To investigate if T-cells were present during demyelination in the #72 homozygote corpus callosum, CD3, a marker for T-cells, was examined. A small number of CD3+ve cells were present during the later stages of demyelination ([Figure 31](#)).

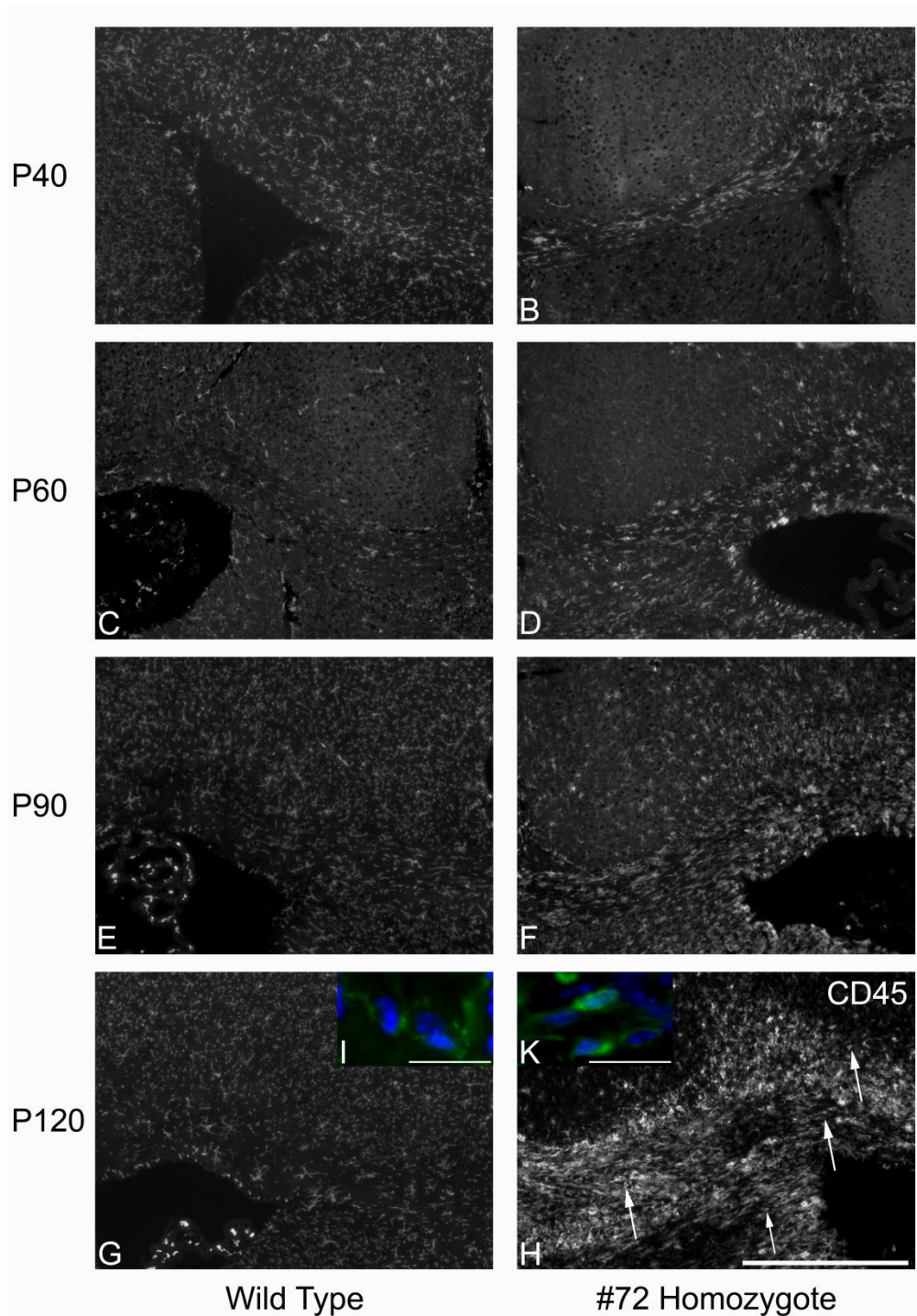


**Figure 27. A marked increase in microglial/macrophages accompanies progressive demyelination.**

Micrographs of CD45 +ve cells in the corpus callosum at P40, P60, P90 and P120 in wild type (A - D) and #72 (E - F; x100, scale bar 400µm) mice. An obvious increase in the density of CD45 positive cells is evident in the #72 mouse compared to the wild type. Morphologically the CD45+ cells in the #72 mouse appeared altered, having thicker and shorter processes (K, x400, scale bar 25µm) than wild type cells (I, magnification x400, scale bar 25µm). At P120 a few cells with a rounded morphology, resembling B or T lymphocytes, were present in the #72 mouse (arrow).

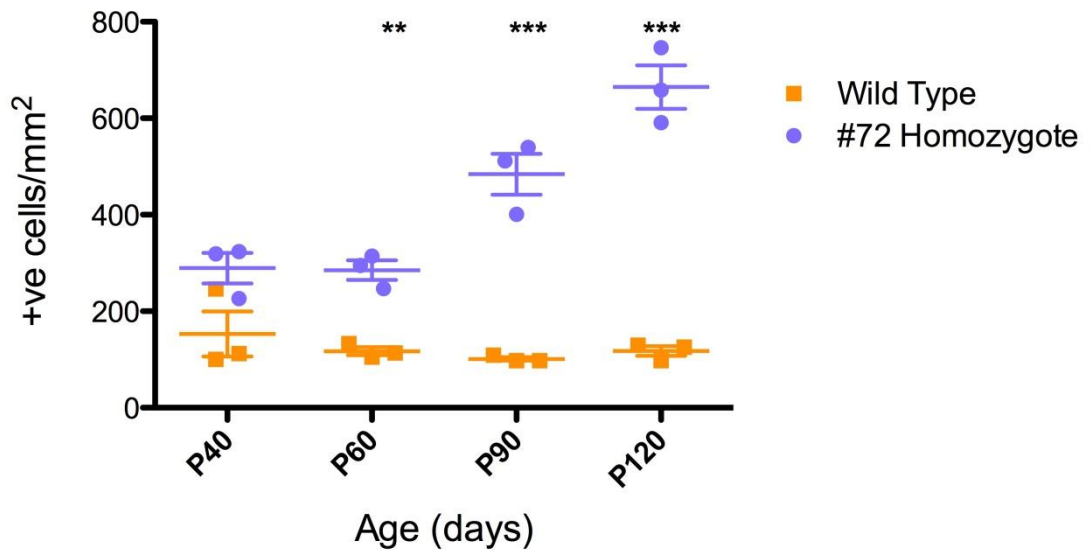


**Figure 28. Microglial/macrophage cell density increases progressively in the #72 homozygote corpus callosum.**

Graph illustrating the microglial/macrophage cell density changes during progressive demyelination. N=3 (for each given time point and genetic background), adding up to a total number of 24 quantified specimens. Bars display s.e.m. The microglial/macrophage cell density was increased in the #72 homozygote corpus callosum compared to wild type, from P60 and progressively increased up to P120, when demyelination of the corpus callosum was virtually complete. (\*\*:  $p < 0.01$ , \*\*\*:  $p < 0.001$ ).

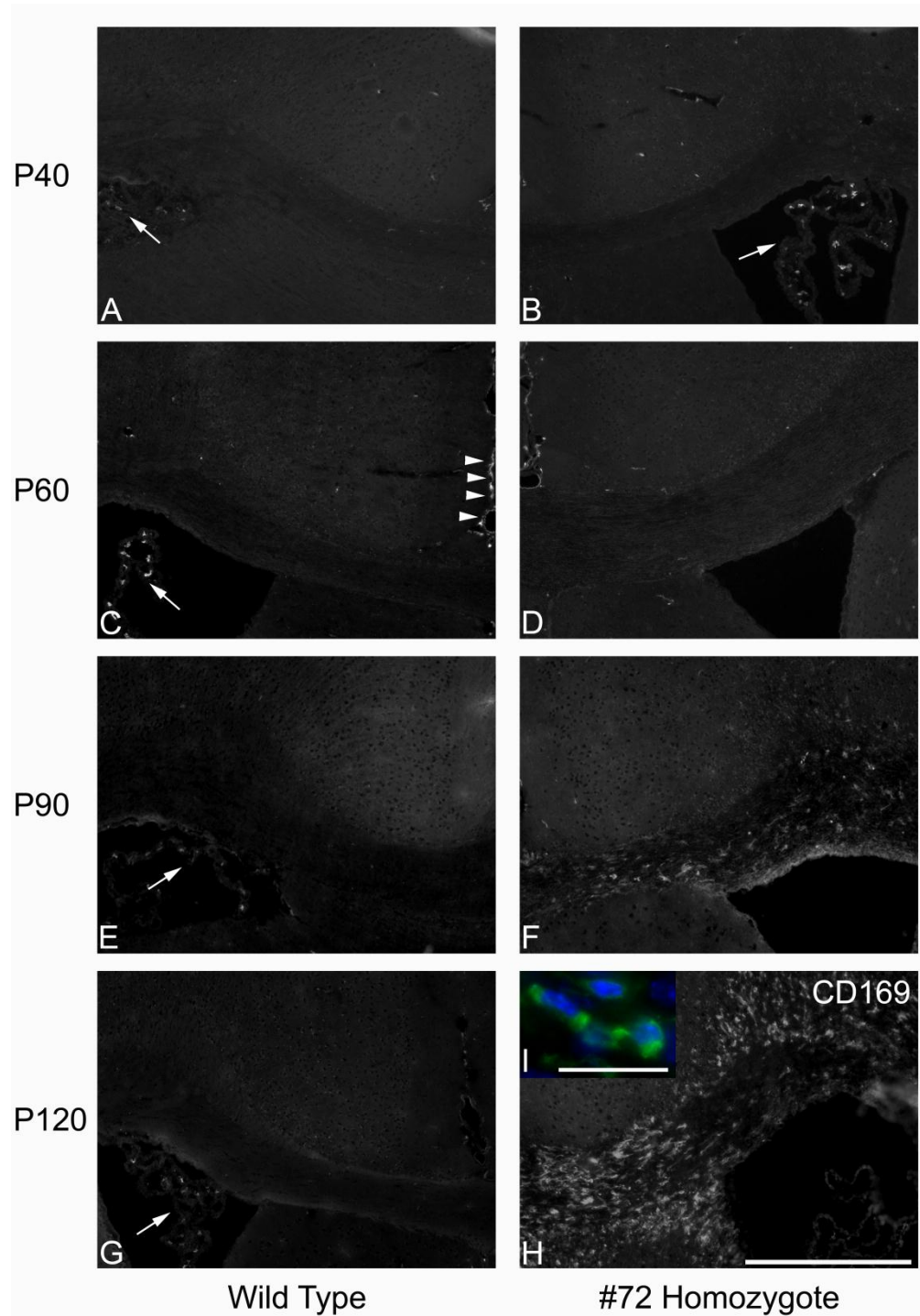


**Figure 29. Sialoadhesin expressing cells were found in the demyelinating corpus callosum.**

Micrographs of CD169 +ve cells in the corpus callosum between P40 and P120, in wild type (A - D) and #72 mice (E - F; x100, scale bar 400um). At all time points in the wild type mice and up to P60 in the #72 mouse corpus callosum there were only occasional CD169 +ve cells detected. At P90 and P120, several CD169 +ve cells were observed in the #72 mouse corpus callosum. CD169 +ve cells were present in wild type and #72 mouse choroid plexus (arrows) and blood vessels (arrowheads). CD169 expression was detected on both the cell body and on cell processes (I, x400, scale bar 25µm).

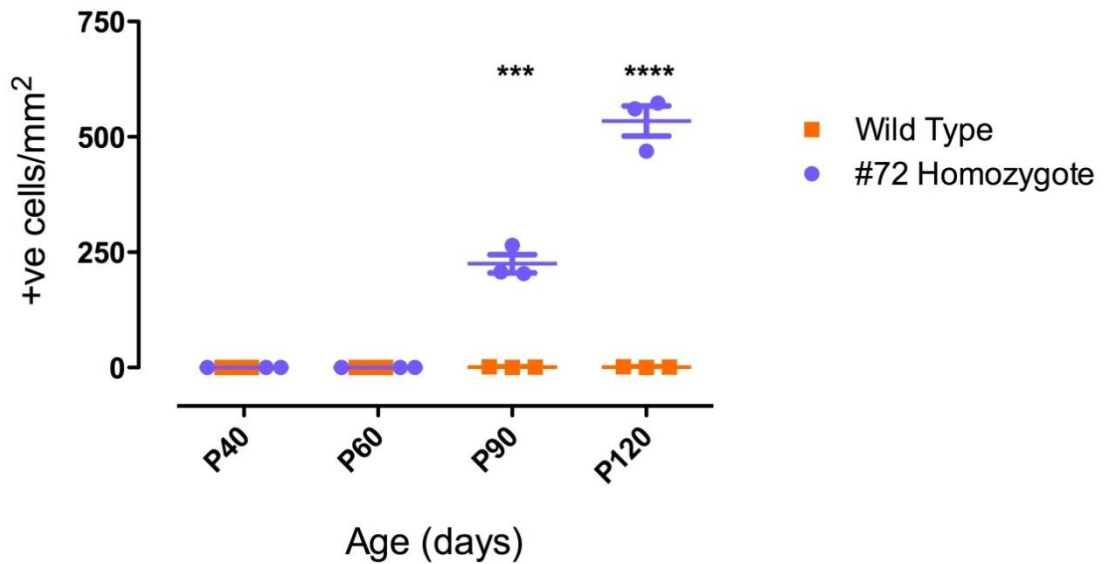


**Figure 30. The density of activated microglial/macrophages is progressively increased in the #72 mouse corpus callosum.**

Graph illustrating CD169 +ve cell density changes during progressive demyelination. N=3 (for each given time point and genetic background), adding up to a total number of 24 quantified specimens. Bars display s.e.m. CD169+ve cells were observed in the corpus callosum after P60 and the CD169 cell density increased between P90 and P120, corresponding with the severity of demyelination (\*\*\*:  $p < 0.001$ , \*\*\*\*:  $p < 0.0001$ )

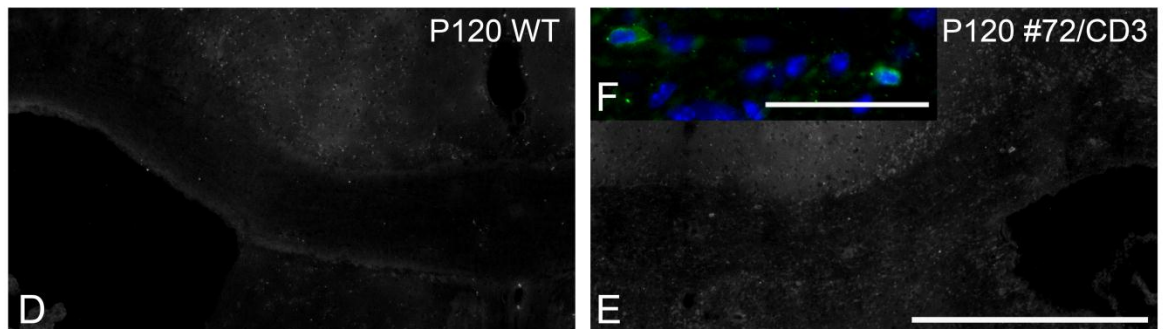
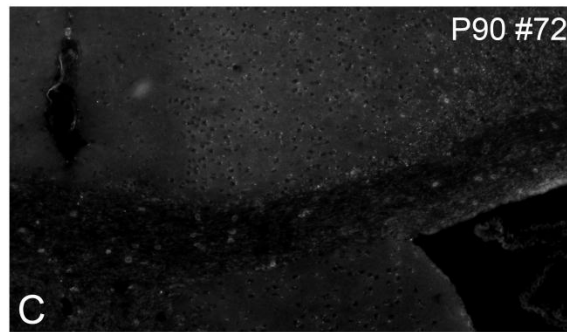
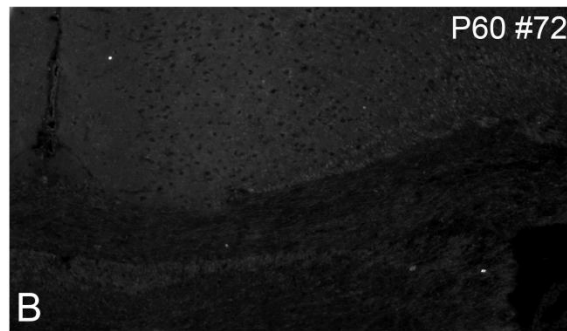
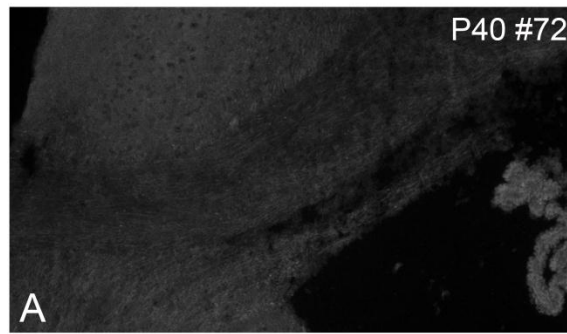


**Figure 31. T cell infiltration accompanied progressive demyelination and activation of the microglial/macrophage cell population.**

Micrographs of CD3+ve cells in the corpus callosum, between P40 and P120, in #72 (A, B, C, E) and wild type mice (D, x100, scale bar 400 $\mu$ m). CD3+ve cells were only observed at P90 and P120 (F, x400, scale bar 50 $\mu$ m), suggesting that the T cell infiltration succeeded the earliest stages of demyelination.

### 3.4.8 Progressive demyelination and inflammation is associated with axonal swelling in the #72 homozygote corpus callosum

Axonal damage and neuronal degeneration is considered to be the main cause of permanent disability in multiple sclerosis (reviewed in Bjartmar and Trapp, 2001). Dystrophic axons are also believed to become non permissive for remyelination (reviewed in Franklin and ffrench-Constant, 2008) and may contribute to remyelination failure. A previous study from (Edgar et al., 2010) showed the presence of axonal swellings in the inflamed, demyelinating chiasmatal region of #72 homozygote mouse optic nerve.

To test if axonal swellings occur in the #72 homozygote corpus callosum I used an antibody to SMI32 that labels non-phosphorylated neurofilaments. Prior to myelination, axonal neurofilaments are largely non-phosphorylated (Brady et al., 1999;Petzold, 2005). Myelination is accompanied by increased phosphorylation of neurofilaments and increase in axonal diameter. Following demyelination, neurofilaments become dephosphorylated (Trapp et al., 1998). Antibodies that recognise non-phosphorylated neurofilaments are routinely used to identify axonal changes in relation to demyelination. At P40, SMI32 staining appeared similar in the #72 mouse compared to the wild type. However, at P120 SMI32 staining appeared markedly increased in the #72 mouse, compared to the wild type ([Figure 32](#)).

To visualise morphological changes in axons, a *Thy-1 / CFP* expressing mouse was crossed with the #72 homozygote mouse to create homozygous *Plp1* overexpressing mice that were hemizygous for the transgenic *Thy-1 / CFP* gene, as described in Chapter 2. Using CFP as a sensitive marker of axonal changes, axonal swellings appeared to be increasingly prevalent in the homozygote #72 mice corpus callosum from P90 onwards ([Figure 33](#)).

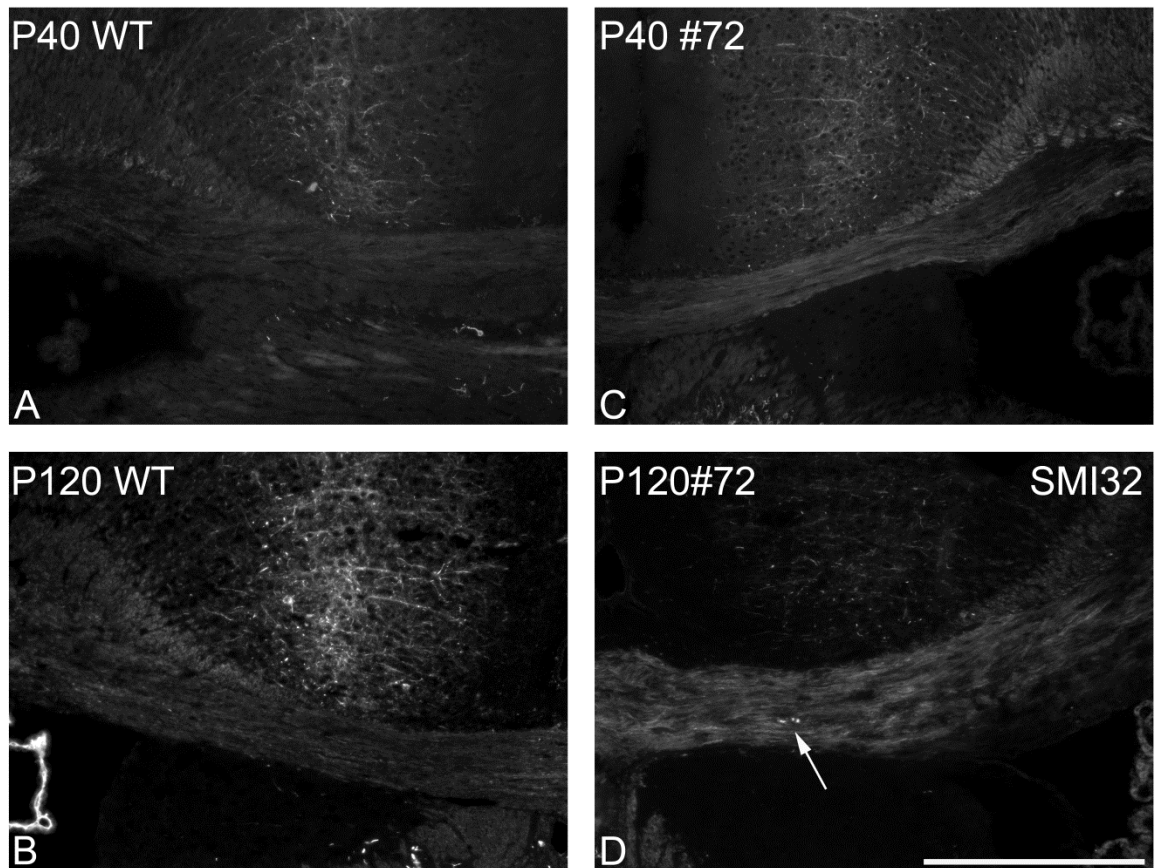


**Figure 32. Axonal changes increased with progressive demyelination and inflammation.**

Micrographs of sections stained using antibody to SMI32 in the corpus callosum of P40 and P120 wild type (A, B) and #72 (C, D, magnification x100, scale bar 400 $\mu$ m) mice. SMI32 labels non-phosphorylated neurofilaments and is a useful marker of pathology in the adult. Axons positive for SMI32 were more prevalent in the #72 mouse than in the wild type, at P120. An SMI32 +ve axonal swelling was observed occasionally (arrow).

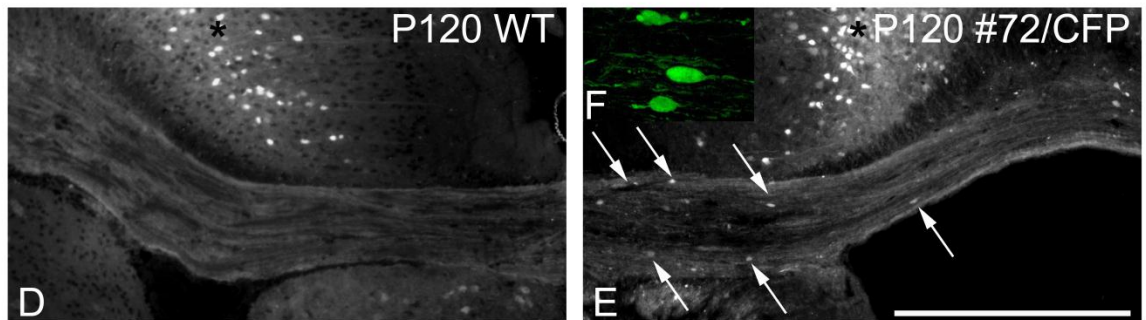
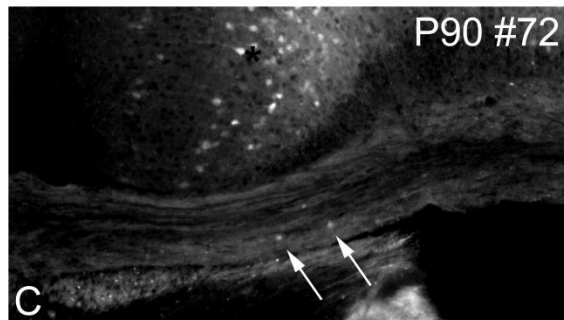
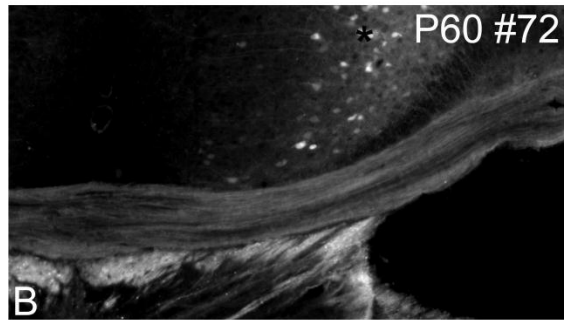
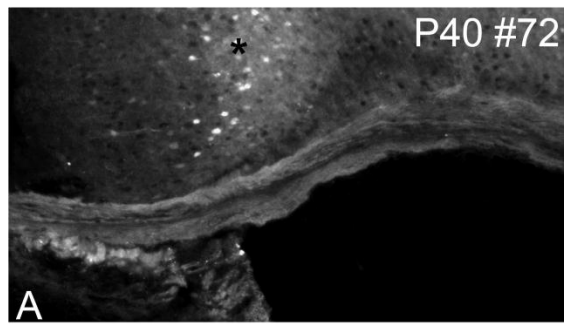


**Figure 33. Axonal swellings as a sign of axonal injury were increasingly present with progressive demyelination and inflammation.**

Micrographs of CFP +ve axons in the corpus callosum of P40 to P120 #72 (A, B, C, E) and P120 wild type mice (D, x100, scale bar 400µm). CFP is expressed in a subset of sensory and motor neurons and is located in the cytoplasm (black asterisk). Visualisation of GFP analogues is a more sensitive marker of axonal swellings (arrows) than antibody staining (Bridge et al., 2009). A number of axonal swellings (K, confocal image, x670) were present after P90 in the #72 mouse.

### **3.4.9 Axonal density in the #72 homozygote was unaltered compared to the wild type corpus callosum**

Demyelination and associated processes, such as inflammation, can lead to axonal changes resulting in permanent axonal loss. To determine if axonal loss could contribute to the failure of remyelination in the #72 homozygote corpus callosum, electron micrographs were used to calculate axonal density. The axonal density decreased slightly with increasing age in wild type and in the #72 homozygote corpus callosum. However, there was no significant difference in axonal density in the #72 homozygote corpus callosum compared to wild type, at any of the ages examined ([Figure 34](#)).

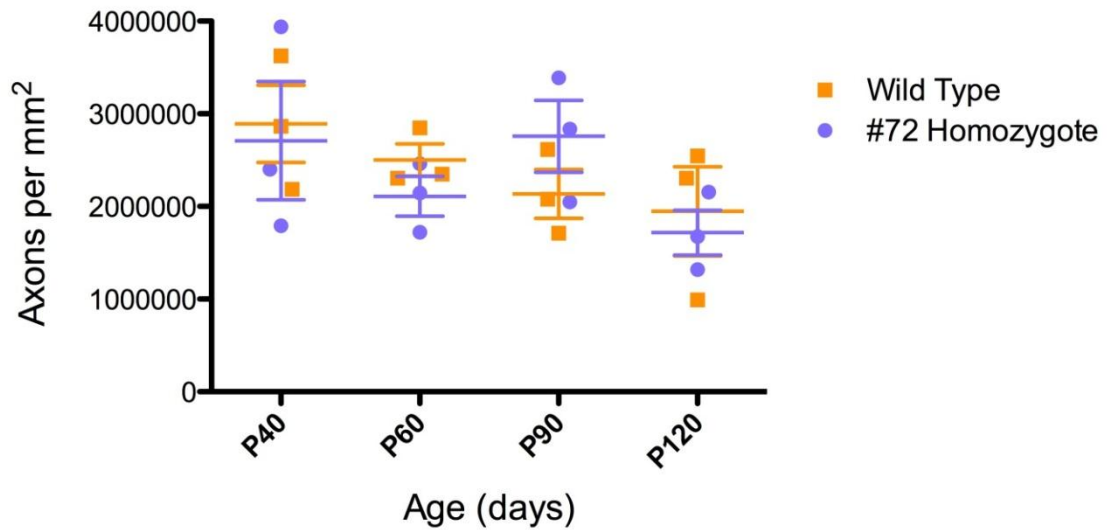


**Figure 34. Axonal density was not reduced in the demyelinated corpus callosum of the #72 mouse.**

Graph of axonal density in the wild type and #72 mouse corpus callosum. N=3 (for each given time point and genetic background), adding up to a total number of 24 quantified specimens. Bars display s.e.m. There was no significant difference in axonal density in the #72 mouse corpus callosum compared to the wild type, at any of the time points examined.

## Demyelination and remyelination failure was not caused by Caspase3 mediated cell apoptosis

In dysmyelinating mutants such as the *jimpy* mouse (Gow et al., 1998; Cerghet et al., 2001), the *rumpshaker* mouse (McLaughlin et al., 2007) or the *msd* mouse (Gow et al., 1998), the mutated PLP/DM20 accumulates in the cell body and causes an unfolded protein reaction (UPR) causing a Caspase12 mediated cleaved Caspase3 induction, leading to cell apoptosis. However it has also been shown that in another *Plp1* gene overexpressing mouse model (line #66) the degree of cell apoptosis is less severe than for example in the *jimpy* mouse (Cerghet et al., 2001). A recent study has shown that inflammation induces Caspase3 mediated OPC apoptosis by DR6 activation, which is highly expressed on immature OPCs leading to impaired remyelination capacity (Mi et al., 2011). Antibody against cleaved Caspase3 was used to characterise cell apoptosis mediated through Caspase3 signalling ([Figure 35](#)). Caspase3 +ve cells were scarce at all time points examined in the #72 homozygote corpus callosum, indicating that if cell apoptosis was present it is not Caspase3 mediated.

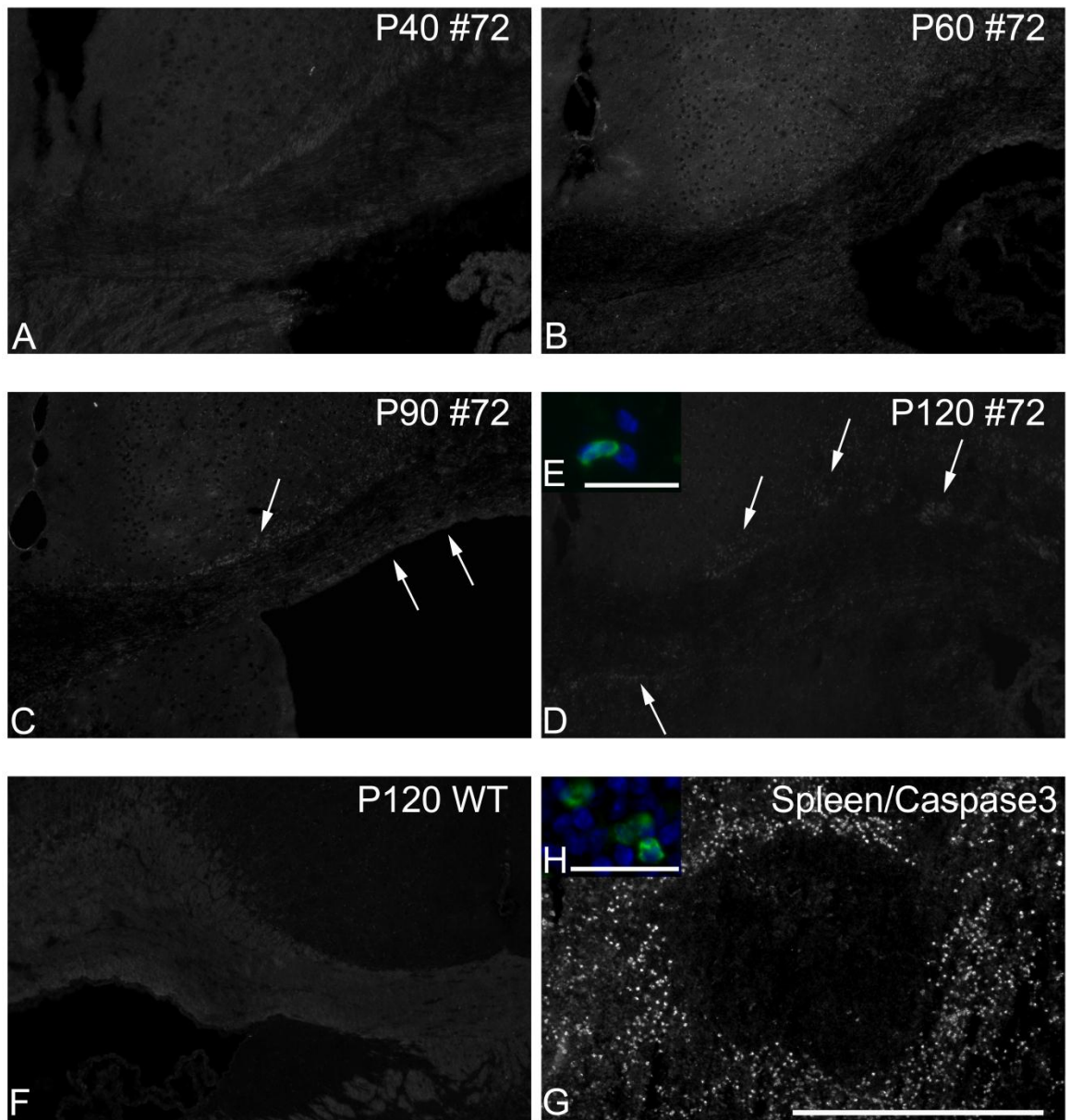


**Figure 35. Caspase3 mediated cell apoptosis was not detected in the #72 homozygote corpus callosum.**

Micrographs of Caspase3 +ve cells in the corpus callosum between P40 and P120 in #72 homozygote mice (A - E), at P120 in wild type mice (F) and in spleen (G, x100, scale bar 400µm, H, x400, scale bar 50µm). Caspase3 positive cells were only rarely observed in the #72 mouse (E). Lipofuscin (arrows) contributes to the fluorescent signal in the #72 mouse.

### **3.4.10 OPC cell differentiation inhibition: an in situ screening of OPC intrinsic and extrinsic factors known to be involved in remyelination failure**

Multiple OPC intrinsic and extrinsic factors have been identified to interact during the complex remyelination process after demyelination. It has been stated that only a slight interruption in any of these finely tuned interactions during the remyelination processes can eventually lead to remyelination failure (reviewed in Franklin and French-Constant, 2008). In my study I focused on a few potential factors, such as prolonged Wnt pathway activation, accumulation of hyaluronan, polysialation of neural cell adhesion molecule and local thyroid hormone regulation which have been described to alter remyelination capacity.

#### **3.4.10.1 There is no evidence that OPC cell differentiation is inhibited by abnormal Wnt pathway activation**

The activation of the Wnt pathway has been shown to play a pivotal role in coordinating remyelination after demyelination. During the OPC recruitment and proliferation phase, the Wnt pathway is activated. For OPC differentiation on the other hand, the Wnt pathway needs to be deactivated. It has been shown that in the case of prolonged Wnt pathway activation, remyelination after chemically induced demyelination is delayed (Fancy et al., 2009). It has been hypothesized that if the delay is prolonged, the narrow temporal window during which the demyelinated area is favourable for remyelination may be missed, potentially leading to remyelination failure (Fancy et al., 2009).

To investigate the possibility that abnormal activation of the canonical Wnt pathway contributes to OPC differentiation block in the #72 mouse corpus callosum, antibody labelling of Axin 2 was undertaken. Axin2 provides negative feedback of the Wnt pathway and is only expressed when the pathway is activated. At P40 and P90, when BrdU +ve OPC density was elevated, Axin2 +ve cells were present. At P60 and P120, where BrdU +ve OPC density was low, Axin2 was not detected ([Figure 36](#)). This is compatible with the Wnt pathway being

active during OPC proliferation phase. Double labelling with Olig1 confirmed that most of the Axin2 positive cells were of oligodendroglial lineage ([Figure 37 A - D](#)). Incidentally, Axin2 staining also co-localised with axonal swellings ([Figure 37 E - H](#)).

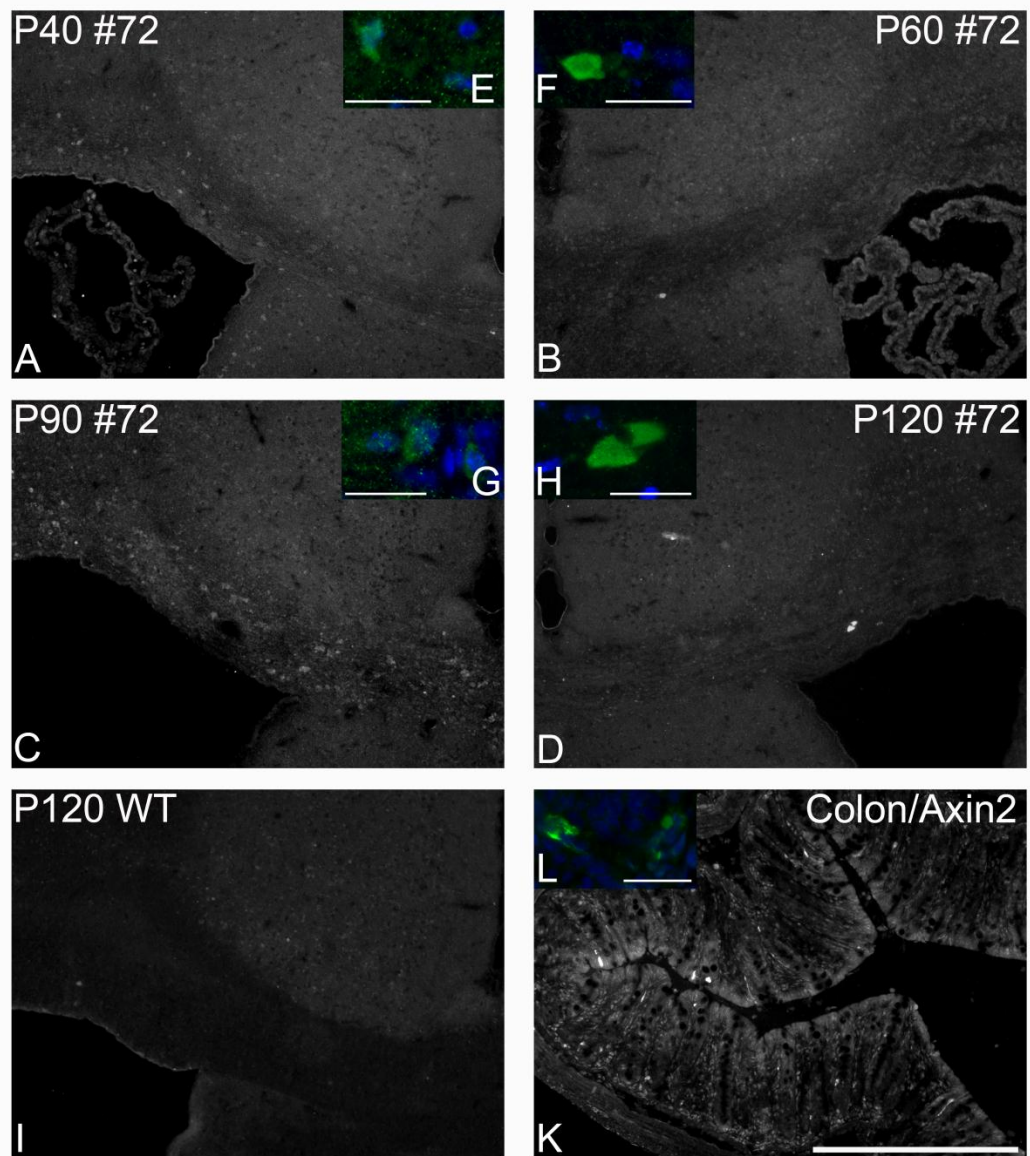


**Figure 36. Activation of the canonical Wnt pathway was present at time points where OPC proliferation was upregulated.**

Micrographs of #72 (A - D) and wild type (I) corpus callosum and colon (K, x100, scale bar 400µm), stained using antibody to Axin2. In the #72 corpus callosum, a higher proportion of Axin2 positive cells were present at P40 and P90 compared to P60 and P120 as well as to the wild type. Axin2 localisation was intranuclear (E) or cytoplasmic (G). Axin2 positive structures that were not related to cell nucleus resembled axonal swellings. (F, H, x400, scale bar 25µm).

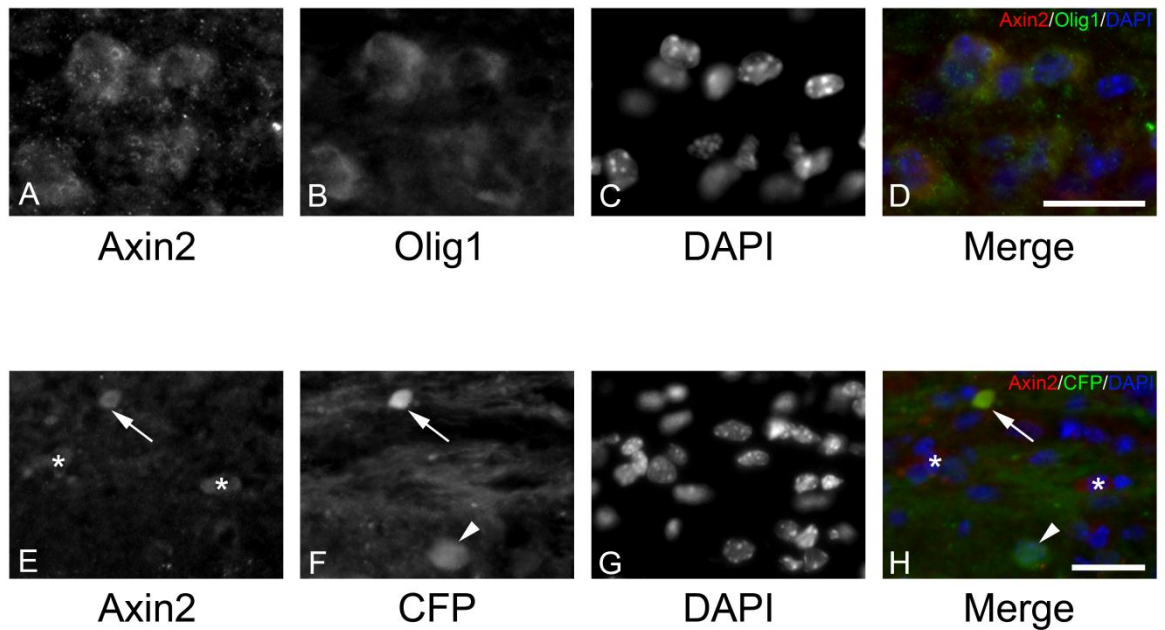


**Figure 37. Axin2 is located in cells originating from the oligodendroglial lineage.**

Micrographs of #72 corpus callosum at P90. Double labeling with Olig1 (A - D) showed that Axin2 positive cells expressed Olig1, indicating that the Wnt pathway is active in cells of the oligodendroglial lineage, during demyelination. Since the Axin2 structures, which could not be correlated with a nucleus, resembled axonal swellings, Axin2 expression in the Thy-1-CFP was investigated. (E -F, x400, scale bar 25 $\mu$ m) Axin2 staining overlapping with CFP in axonal swellings (arrows). Neuronal cell bodies (arrowhead), which were filled with CFP, were Axin2 negative, showing that Axin 2 labeling was not due to unspecific binding of Axin2 to CFP. There were also Axin2 positive cells that were negative for CFP (asterisk) that had a similar morphology to the Olig1/Axin2 positive cells in the #72 homozygote corpus callosum.

#### **3.4.10.2 Accumulation of hyaluronan was present at the end stage of demyelination in the #72 homozygote corpus callosum**

Hyaluronan, which is secreted by astrocytes in chronic demyelination, is a potent inhibitor of OPC maturation and contributes to remyelination failure in chronic demyelinated lesions (Back et al., 2005). The inhibitory effect being mediated through TLR2 receptors on OPCs (Sloane et al., 2010). To test if hyaluronan was expressed in the extracellular matrix I used a biotinylated hyaluronan binding protein (bHABP). At P60, when demyelination is commencing, there was no evidence of hyaluronan expression in the #72 homozygote corpus callosum, similar to wild type. At P120 an accumulation of hyaluronan was identified in the #72 homozygote corpus callosum. To rule out non-specific binding with myelin debris a double stain with MBP showed that HABP did not bind to myelin debris ([Figure 38](#)).

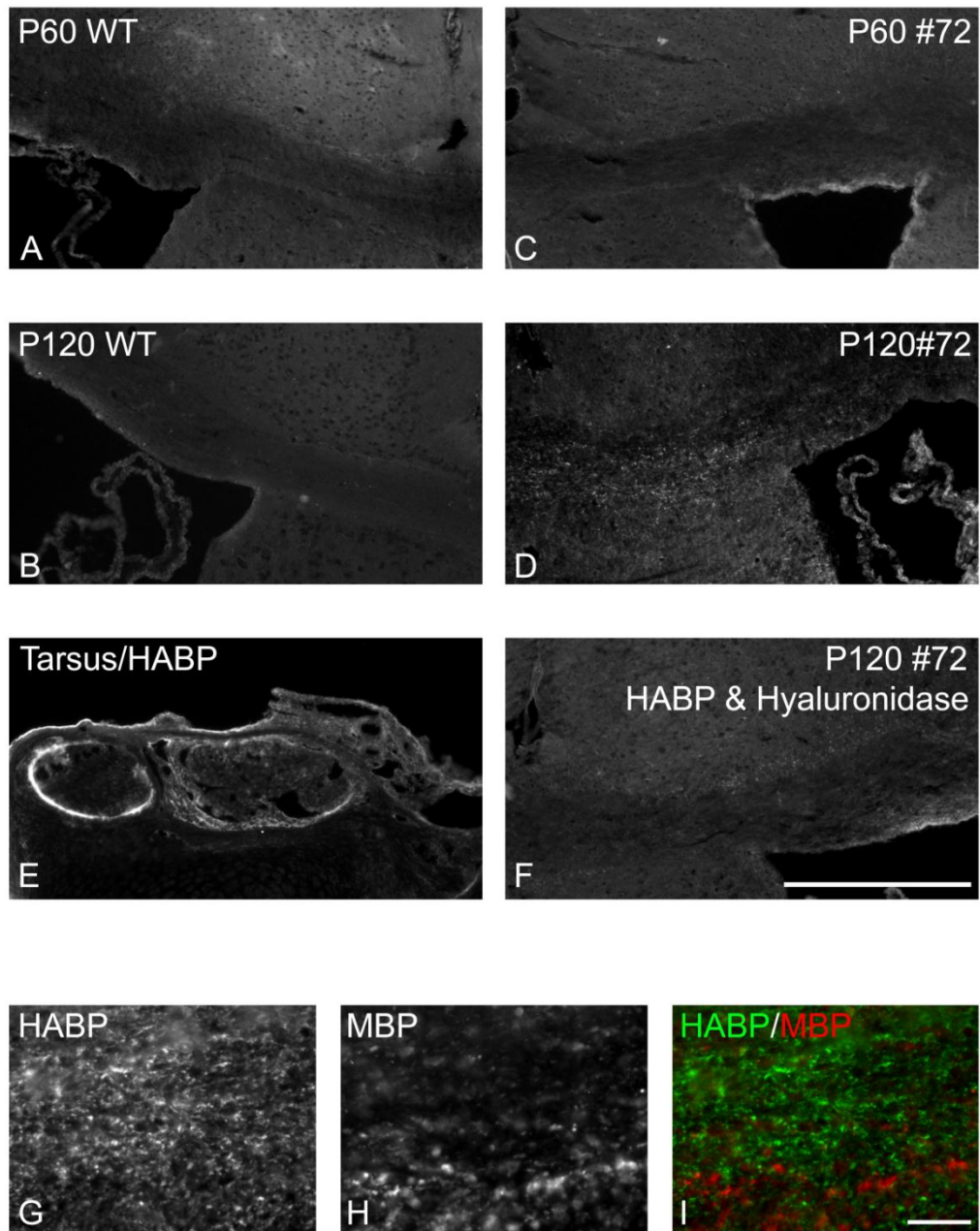


**Figure 38. Hyaluronan accumulation was identified in the demyelinated corpus callosum at P120.**

Micrographs showing the hyaluronan labelling of wild type (A, B) and #72 mouse corpus callosum (C, D). At P60, when demyelination commenced, the distribution of hyaluronan in the #72 homozygote appeared similar to the wild type. An increase in hyaluronan expression was observed at P120 in the #72 mouse and could potentially contribute to the OPC differentiation block. Tarsus was used as a positive control (E) The specificity of hyaluronan binding protein (HABP) was tested using tissue incubated with bovine hyaluronidase (F, x100, scale bar 400 $\mu$ m). To confirm that HABP was not binding to myelin debris, double labelling using HABP and an antibody to MBP was performed (G - I, x400, scale bar 25 $\mu$ m). The HABP positive structures did not co-label with myelin debris, stressing the specificity of the HABP to bind to hyaluronan.

### **3.4.10.3 Poly-sialated neural cell adhesion molecule (PSA-NCAM) expression was identified on astrocytes but not on axons in the chronically demyelinated #72 homozygote corpus callosum**

The polysialation of NCAM on axonal surfaces has been shown to inhibit the initiation of contact between OPC and unmyelinated axons. During development, PSA-NCAM plays a key role in regulating the precise timing of myelination and the expression of PSA-NCAM on axons is not detected after myelination commences (Coman et al., 2005). In pathology, such as in chronic MS, re-expression of PSA-NCAM on demyelinated axons has been detected and it is thought to prevent remyelination by inhibiting the initial axonal glial contact which is needed to initiate remyelination after demyelination (Charles et al., 2002). Antibodies against PSA-NCAM were used to examine the polysialation of NCAM on axons in the chronic demyelinated #72 homozygote corpus callosum. At P120, axons did not express PSA-NCAM, suggesting that is unlikely to be involved in the inhibition of myelination. However PSA-NCAM expression was detected on spindle shaped cells, which were also positive for GFAP ([Figure 39](#)).

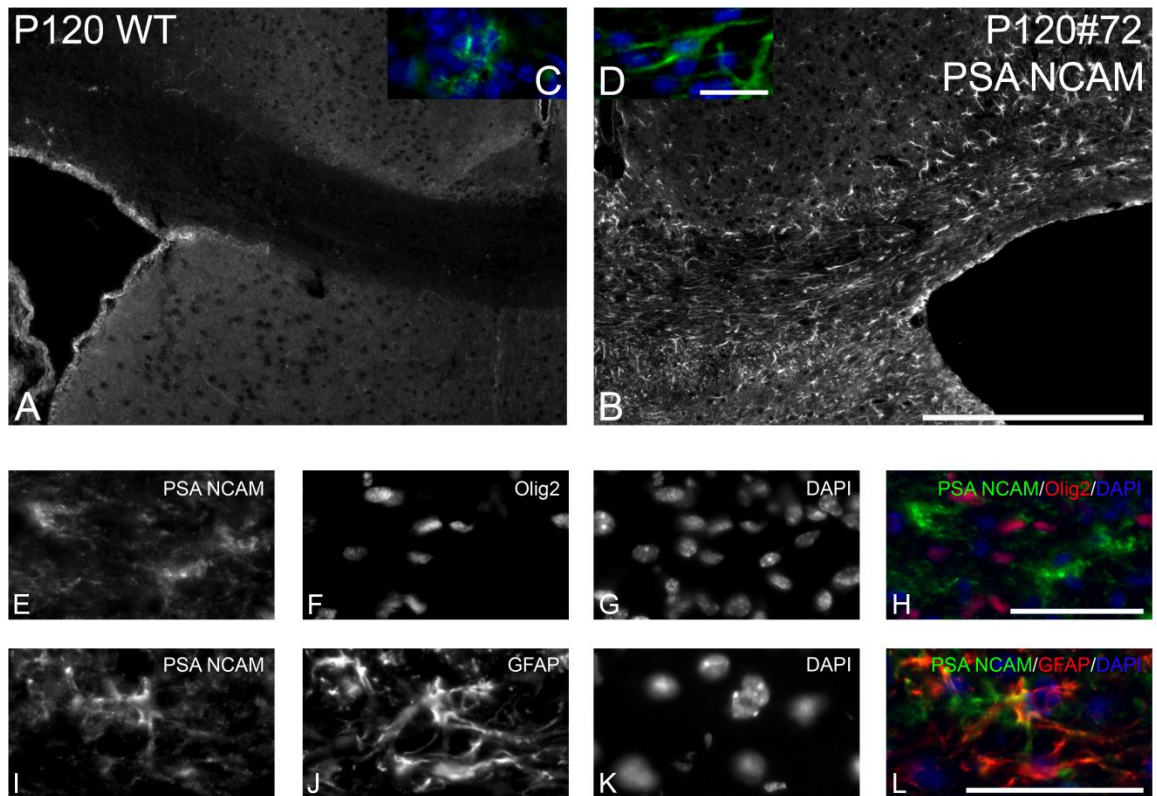


**Figure 39. PSA-NCAM expression was detected on astrocytes and not on axons in the #72 mouse corpus callosum.**

Micrographs from wild type (A) and #72 mouse corpus callosum (B, x100, scale bar 400 $\mu$ m) at P120. A few PSA-NCAM +ve cells were present in the P120 wild type corpus callosum (C). In contrast, the #72 mouse corpus callosum contained a marked number of PSA-NCAM positive cells (D, magnification x400, scale bar 25 $\mu$ m). Double labelling with PSA-NCAM and Olig2 to label oligodendroglia (E - H, x400, scale bar 50 $\mu$ m) or with PSA-NCAM and GFAP (I - L, x400, digitally magnified, scale bar 50 $\mu$ m) to label astrocytes, showed that most of the PSA-NCAM positive cells were GFAP +ve, suggesting that these cells are reactive astrocytes.

#### **3.4.10.4 Deiodinase 3 expression was not detected on activated microglial cells in chronic demyelinated corpus callosum at P120**

The enzyme deiodinase 3, which converts T4 to reverse T3 (rT3) or T3 to T2 and therefore inactivates thyroid hormone activity, is believed to be responsible for tightly regulating the local concentration of active T3 in tissue (Bates et al., 1999). It is believed that, especially in the case of inflammation, increased D3 expression can cause local tissue specific hypothyroidism, which has negative effects on cell metabolism and repair. Since there is chronic inflammation with activation of microglia in the #72 homozygote mouse model, a potential expression of D3 on activated microglia/macrophages could contribute to the remyelination failure. To characterize D3 expression in the #72 corpus callosum, in this case mainly microglia/macrophages during chronic demyelination, an antibody to D3 in combination with antibody to CD45 were used. D3 was not detected by immunohistochemistry in the adult #72 mouse corpus callosum ([Figure 40](#)).

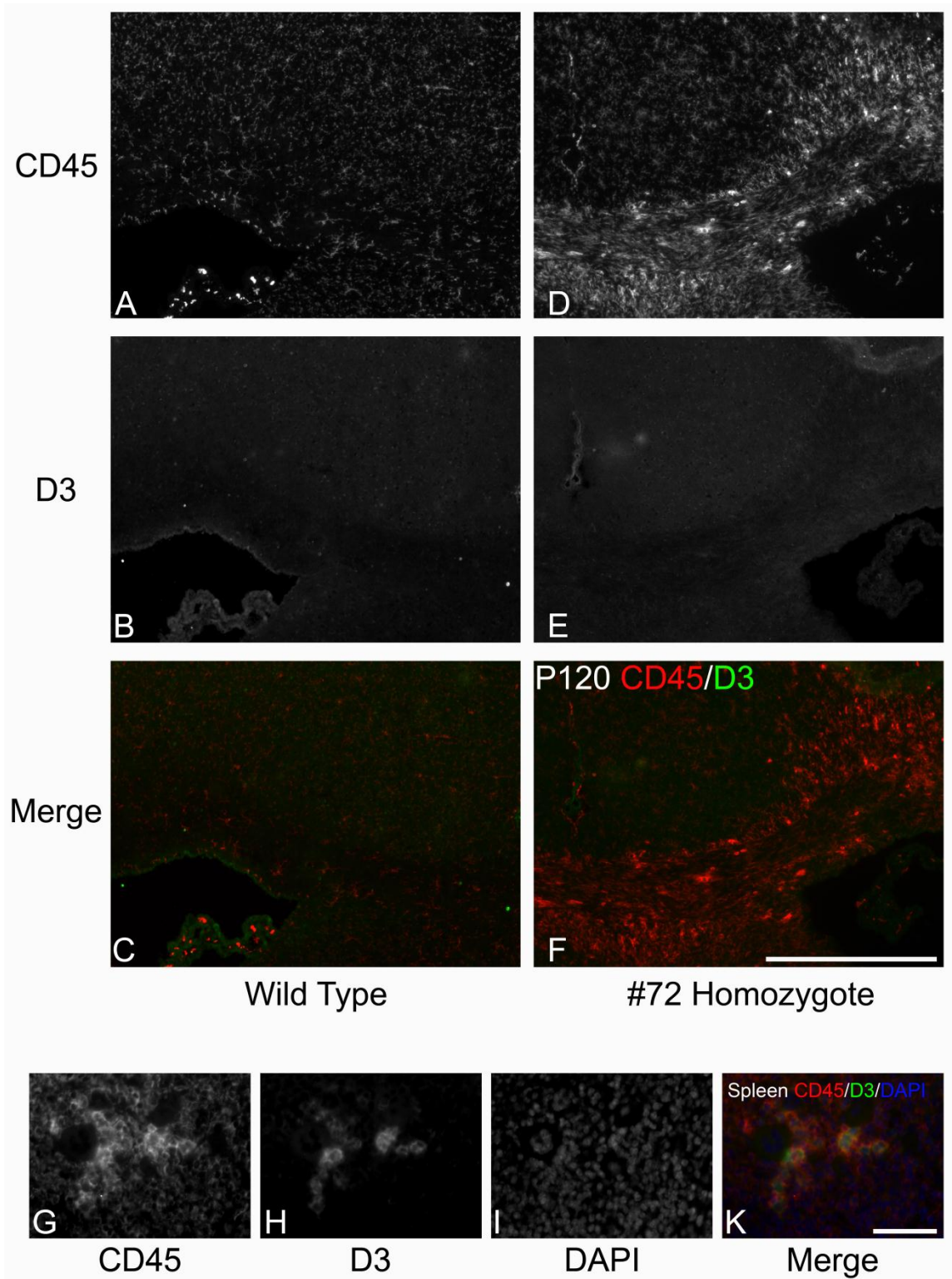


**Figure 40. The microglia/macrophage population did not express D3 in the adult, chronically demyelinated #72 homozygote corpus callosum.**

Micrographs of wild type (A - C) and #72 homozygote (D - F, x100, scale bar 400µm) corpus callosum. Spleen was used as a positive control tissue (G - K, x400, scale bar 50µm). The CD45 positive cell population in the #72 homozygote corpus callosum did not express D3.

## 3.5 Discussion

### 3.5.1 Progressive demyelination was accompanied by remyelination failure in the #72 homozygote corpus callosum

The data presented in this chapter demonstrates that myelination in the corpus callosum of the homozygous *Plp1* overexpressing mouse (#72 mouse) proceeds relatively normally initially, but is followed by a progressive, non-remitting, demyelination, starting after P40 and terminating in virtually complete demyelination by P120. Demyelination is accompanied by activation of microglia/macrophages and astrocytes and by the infiltration of a small number of T cells. Axonal densities are unaltered, but in older mice, there is some evidence of axonal injury. These pathological changes, which are probably present throughout the brain as suggested by DTI findings (Ruest et al., 2011), account for the clinical signs observed in these mice.

While it has previously been shown that demyelination is a characteristic of the optic nerve and spinal cord of various lines of *Plp1* overexpressing mice (Anderson et al., 1998; Edgar et al., 2010; Ma et al., 2006), the evolution of demyelination has not been reported, except in the case of the #72 mouse optic nerve (Edgar et al., 2010). Therefore the nature and evolution of the degenerative and reparative processes are not known.

Furthermore, despite the suggestion that in the hemizygous *Plp1* transgenic mouse “remyelination intermingles with myelin destruction/degeneration” and that in older mice “most axons are demyelinated ... with no signs of remyelination...” (line 4e of Ma et al., 2006) there is actually no evidence in the literature (including publications cited by Ma) to show that this is actually the case. Indeed the only evidence presented to support the assertion that remyelination fails in line 4e is a single high power image showing a marked reduction in PLP staining in the optic nerve of that model.

In the present study, a progressive demyelination in the absence of effective remyelination was demonstrated unequivocally, using a combination of immunofluorescence, light microscopy and EM. The initially formed myelin appeared morphologically normal, showing that during early post natal development, #72 OPCs are capable of appropriately myelinating axons. The inability to effectively (re)myelinate axons developed later on during the disease process.

#### **3.5.1.1 Demyelination in the #72 mouse corpus callosum**

Demyelination was not accompanied by an apparent decrease of mature oligodendrocytes, suggesting that the degenerative process in the #72 mouse represents a dying-back of the genetically defective oligodendrocyte, as suggested previously by (Anderson et al., 1998), which may be related to (i) an intrinsic instability of the biochemically abnormal sheath (Karim et al., 2007) as well as (ii) secondary immune reactions (Ip et al., 2006; Ip et al., 2007). In my study a marked increase and activation of microglia together with a subtle but definite elevation of intraparenchymal T cells accompanied the progressive demyelination, suggesting that secondary immune reactions also contribute to the demyelination in the #72 mouse, although leukodystrophies are classically considered to be non-inflammatory demyelinating diseases.

Severe gliosis with astrocytic activation has also been reported to damage myelin and oligodendrocytes by secretion of TNF $\alpha$  (Selmaj and Raine, 1988; reviewed in Nash et al., 2011). Since there is a considerable astrocytic response accompanying demyelination in the #72 corpus callosum, the progression of the demyelination could also be mediated through the marked astrocytic response.

#### **3.5.1.2 The response of OPCs to demyelination**

It is notable that developmental myelination proceeds almost normally, demonstrating that juvenile #72 OPCs are myelination competent in contrast to

the situation in the adult, where there is no evidence of a remyelination attempt during progressive demyelination.

OPCs, as identified using antibodies to NG2 and PDGFR $\alpha$ , were present in the corpus callosum during the entire period of demyelination. Using BrdU labelling of proliferating cells, I showed that OPCs responded to demyelination by proliferating. Surprisingly however, this did not lead to a marked increase in OPC densities, suggesting that either immature OPCs undergo apoptosis or that OPC proliferation is not extensive enough. OPC numbers were similar to those in the wild type mouse, except that at P120, where the density of NG2 +ve cells was increased in the #72 mouse. However, no such change was observed in the PDGFR $\alpha$  population and the NG2 data must be regarded with caution since NG2 antibodies show unspecific binding to pericytes and a subset of macrophage like cells (MacFadyen et al., 2007;Matsumoto et al., 2008). NG2 +ve cells have also been shown not only to develop into oligodendroglia but also into astroglia, and neurons, which suggests that not all NG2 +ve cells are *per se* OPCs (Zhu et al., 2008b;Zhu et al., 2008a;Nishiyama et al., 2009). Nonetheless, this data suggests that repair in the #72 mouse is not due to the complete absence of OPCs, and the increase in OPC proliferation at P90 suggests that the cells respond to the demyelinating stimulus.

In MS lesions, remyelination sometimes fails despite OPCs being present (Wolswijk, 1998;Chang et al., 2002;Back et al., 2005;Kuhlmann et al., 2008). To determine if a differentiation block contributes to remyelination failure in the #72 mouse, I analysed OPC characteristics during demyelination by characterising the subcellular localisation of Olig1 in NG2+ cells. It has previously been demonstrated that the localisation of Olig1 during myelination and remyelination is a useful indicator of the developmental stage of the OPCs (Arnett et al., 2004;Kitada and Rowitch, 2006). Notably, the translocation of Olig1 from the cytoplasm to the cell nucleus is a prerequisite for (re)myelination (Arnett et al., 2004). In the demyelinating #72 mouse, there was an almost complete absence of pure intranuclear Olig1 in NG2+ cells, suggesting that the differentiation of OPCs into myelinating oligodendrocytes is either not initiated by the OPC or is inhibited.

In both the #72 and wild type mouse, a relatively large proportion of NG2 +ve cells had a cytoplasmic Olig1 localisation. This type of cell was only rarely observed in a recent detailed study focusing on the subcellular localisation of Olig1 (Kitada and Rowitch, 2006). However the study by Kitada and Rowitch focused on OPCs in the spinal cord but not on intracranial white matter structures raising the possibility that corpus callosal OPCs may behave differently from spinal cord cells. Notably, both dys- and demyelination have been observed preferentially in the corpus callosum in some mice (Kassmann et al., 2007; Taveggia et al., 2008).

In short it appeared that the final step in myelin repair, the OPC differentiation, was blocked in the #72 mouse, contributing to remyelination failure.

### **3.5.2 Potential inhibitors of OPC differentiation**

The final step, where OPC differentiate into oligodendrocytes, has been suggested to be the most vulnerable step during the entire remyelination process and often minimal disturbances at this time point leads to remyelination failure (reviewed in Franklin and ffrench-Constant, 2008). Based on the previous findings in this study, OPC differentiation block also seems to lead to remyelination failure in the #72 mouse and the question now arises why OPC differentiation is impaired in the adult #72 mice. Recently, different intrinsic and extrinsic factors, such as canonical Wnt pathway signalling (Fancy et al., 2009), inhibited axonal glial contacts (Charles et al., 2002; Coman et al., 2005) or changes in the extracellular matrix (Back et al., 2005), have been identified to specifically block OPC differentiation during remyelination after demyelination and were further subject to this study.

#### **3.5.2.1 OPC intrinsic factor**

The study by (Fancy et al., 2009) showed that the canonical Wnt pathway is active during OPC proliferation but needed to be downregulated for successful OPC differentiation. The study also showed that prolonged activation of the

canonical Wnt pathway lead to delayed myelination and impaired remyelination capacity after chemically induced demyelination (Fancy et al., 2009).

In the #72 mouse, the Wnt pathway activation pattern corresponded to the proliferation study using BrdU. Initially at P40, the Wnt pathway activity was similar in the #72 homozygote compared to the wild type, most likely reflecting developmental myelination activity. The peak, which was observed in P90 old #72 mice and not in the wild type, was believed to be an OPC proliferation response to the ongoing demyelination. Double labelling with Olig1 confirmed that most of the Axin2 positive cells were from the oligodendroglial lineage. At P120, when demyelination was virtually complete and remyelination would be expected, Axin2 expression was rare, suggesting that the Wnt pathway was not active at the point of virtually complete demyelination. The results suggested that an abnormal Wnt pathway activity was not involved in the development of an absent remyelination response. However the weakness in this study was that the conclusion was based only on Axin2 staining and the described canonical Wnt pathway expression pattern needs to be confirmed by identifying other Wnt pathway induced proteins such as Tcf4 and by proving the increase in Axin2 using western blot techniques. Also the effect of pharmacological manipulation of the canonical Wnt pathway as described in (Fancy et al., 2011) had not been performed and may provide further information about the influence of the Wnt pathway in the #72 mouse on remyelination failure.

Interestingly in this study I identified the presence of Axin2 in axonal swellings. The reason for Axin2 expression in the swellings is not understood and has not been previously reported to my knowledge. The presence of Axin2 in axonal swellings may be due to either accumulation of Axin2 in the swellings as a result of disturbed axonal transport or it may be explained by an upregulation of the Wnt pathway in axons as a response to axonal damage or demyelination.

With regard to abnormal Wnt pathway activation, age has been shown to influence the canonical Wnt pathway by reduced HDAC1 and HDAC2 function, leading to impaired OPC recruitment and differentiation, which had a reductive effect on remyelination efficacy (Sim et al., 2002). However the #72 homozygote model does not live much longer than 4 months. Despite this, when looking at

the successful initial myelination during post natal development, which is then followed by remyelination failure during adulthood, a discrepancy between neonate and adult OPCs seems to be present. Although repeated focal chemical injury to normal CNS is known not to negatively influence the remyelination capacity (Penderis et al., 2003), this does not reflect a pathology affecting the entire CNS. OPCs can migrate from unaffected areas to affected areas. The majority of the OPCs will therefore not be subject to repeated injury. A continuous injury, at least *in vitro*, to the total OPC population has shown to have a marked negative impact on the remyelination capacity (Fressinaud, 2005) and reflects probably better the situation in the #72 mouse. Chronic environmental changes accompanying the progressive demyelination in the #72 corpus callosum could cause sustained injury to the total intracranial OPC pool, suggesting that repeated chronic injury may impair the remyelination capacity of #72 OPCs with time.

#### **3.5.2.2 OPC extrinsic factors**

When looking at the histopathological changes in the cell population of the #72 corpus callosum during demyelination, some of the observed changes may be responsible for interfere with OPC differentiation.

Mature oligodendrocytes, which are still abundantly present despite complete demyelination of the #72 corpus callosum, are known to be unable to remyelinate the demyelinated axons. The presence of mature oligodendrocytes in demyelinated areas potentially may inhibit OPC migration into the demyelinated lesions (Keirstead and Blakemore, 1997). The mature oligodendrocytes present in the #72 may therefore contribute to low OPC migration into demyelinated regions, which may lead to insufficient numbers of OPCs to maintain effective remyelination.

Marked increase in, and activation of, the microglia/macrophage population has been shown to accompany the progressive demyelination in the #72 corpus callosum. Microglial activation has been proven to aggravate the demyelination and to be involved in the development of axonal pathology (Popovic et al.,

2002;Ip et al., 2006;Howell et al., 2010). However, in correlation to remyelination the microglia/macrophage cell population has been shown to positively influence the remyelination process (Arnett et al., 2003;Neumann et al., 2009). In general, acute inflammation and activation of the microglia/macrophage population, even when superimposed on chronic demyelinated tissue (Foote and Blakemore, 2005a), has been shown to have a beneficial effect on remyelination (Setzu et al., 2006;Kondo et al., 2011). Even in MS, the presence of activated microglia/macrophages enhanced the remyelination capacity (Patani et al., 2007). This remyelination enhancing effect is believed to be mediated through phagocytic activity (Kotter et al., 2001) and secretion of promoting substances such as TNF $\alpha$  (Arnett et al., 2001), which is secreted by activated microglia (reviewed in Merson et al., 2010). However, TNF $\alpha$  seems to play a controversial role in the remyelination process. An inhibitory effect mediated through LPS activated microglia secreting TNF $\alpha$  has also been observed to have a negative impact on remyelination capacity *in vitro* (Miller et al., 2007). The negative effect of microglial activation, which leads to increased OPC apoptosis, appears mainly to depend on the differentiation status of OPCs. More mature OPCs, which are differentiating towards oligodendrocytes show less apoptosis compared to the immature OPCs, where apoptosis was increased after microglial activation (Miller et al., 2007). These findings were in agreement with a recent study of (Mi et al., 2011), which has shown that immature OPC express death receptor 6 (DR6), a receptor from the TNF family, and activation of this receptor mediates Caspase3 induced cell apoptosis (Mi et al., 2011). Since TNF $\alpha$  induced apoptosis of OPCs is mediated through Caspase3, it is questionable if a negative effect mediated through TNF $\alpha$  is present in the #72 corpus callosum, where Caspase3 mediated apoptosis could not be detected at any time point in this study. However, in the *Plp1* gene overexpressing mouse models, sialoadhesin expressing microglia/macrophages definitively aggravates demyelination (Ip et al., 2007) and may still negatively impact remyelination through another unknown mechanism.

Another role of the present inflammation in the #72 corpus callosum may be the influence of inflammatory cells on local tissue thyroid homeostasis mediated through D3. Treatment with relatively high doses of the active thyroid hormone T3 have been shown to have an enhancing effect on remyelination after demyelination (Harsan et al., 2008;D'Intino et al., 2011). As previously

mentioned, deiodinases control tissue specific thyroid hormone levels, where D3 is responsible for inactivation of the thyroid hormone (Huang, 2005). Increased expression of D3 has been reported in experimentally induced focal chronic inflammation (Boelen et al., 2005) and in an EAE model on macrophages and granulocytes (Boelen et al., 2009). The upregulation of D3 can lead to a local, or in severe cases, to a general non-thyroid induced hypothyroidism leading to a reduced cell metabolism and consequently to an impaired tissue repair. So far D3 expression on activated microglia has never been described and in this study D3 expression on the activated microglia was examined.

In the #72 homozygote mouse the expression of D3, which could potentially lead to a restricted availability of T3 for the OPCs to differentiate during demyelination, was not present in the corpus callosum. Local T3 depletion causing a local hypothyroid state in white matter therefore seemed unlikely to play a role in the development of remyelination failure in the #72 homozygote mouse. However, if D3 expression was below the detectable level for the antibody, final proof that D3 is not involved in the development of remyelination failure in the #72 brain would be gained by the measurement of #72 CNS D3 activity.

The progressive astrocytic response which is observed in context with the progressive demyelination in the #72 corpus callosum may also influence OPC differentiation. The astrocytic population is also considered to play an ambivalent role by influencing remyelination both negatively (Blakemore et al., 2003; Su et al., 2011) and positively (Liu et al., 1994; Moore et al., 2011a; Franklin et al., 1991). The interaction of the astrocytes with OPCs is regulated by the direct effect of promoting molecules such as IGF-1 (Liu et al., 1994) or inhibitory molecules such as hyaluronan (Back et al., 2005; Sloane et al., 2010) or the ambivalent TNF $\alpha$  (Su et al., 2011). Astrocytes can also indirectly interact with other cells such as microglia or neurons, which then secrete substances, such as FGF-2 (reviewed in Moore et al., 2011a), influencing OPC development. Hyaluronan is certainly present during the late stage of demyelination at P120 in the #72 corpus callosum.

Hyaluronan is known to inhibit remyelination *in vitro* and *in vivo* (Back et al., 2005) and is mediated through activation of toll like receptor 2 expressed on OPCs. For hyaluronan mediated activation of the TLR2 receptor, the presence of the adaptor molecule MyD88 is required (Sloane et al., 2010). Unlike previously described, it is not the high molecular weight hyaluronan which causes the inhibitory effect, but through low molecular weight hyaluronan oligomers, which are generated by hyaluronidase expressed on OPCs (Back et al., 2005; Sloane et al., 2010). There is an obvious accumulation of hyaluronan present in the #72 homozygote corpus callosum compared to the wild type and which could potentially contribute to the remyelination failure. When looking at the cellular changes in the #72 tissue, the astrocytes are probably the source of hyaluronan. However, the HABP used in this study did not distinguish between high or low molecular weight hyaluronan. Also the amount of hyaluronan was not quantified by western blotting and the expression of TLR2 receptors as well as the presence of MyD88 was not investigated.

Another alteration in the #72 corpus callosum extracellular matrix was the persistence of myelin breakdown products up to P120. Accumulation of myelin debris in demyelinated regions has been shown to inhibit OPC differentiation (Kotter et al., 2006). The OPC inhibition can be overcome by pharmacological induction of Fyn Rho and PKC signalling (Baer et al., 2009). In the #72 mouse, a substantial amount of myelin debris was present at the time of complete demyelination and could therefore potentially contribute to OPC differentiation block.

Finally the observed axonal changes and their influence on the remyelination process also need to be addressed in the #72 mouse, which potentially can have a negative effect on remyelination. In the adult *Plp1* overexpressing #66 and #72 mice, inflammation and activation of microglia have also been suggested to cause axonal damage (Ip et al., 2006; Ip et al., 2007; Edgar et al., 2010) and dystrophic or destroyed axons are believed not to become remyelinated. In general after pure demyelination without axonal loss an increase in axonal density would be expected. However the glial response could fill the gap caused by demyelination. Since extensive axonal loss would cause a decrease in axonal

density the comparable axonal density between wild type and #72 homozygote suggests that extensive axonal loss is not present.

Because of the difficulties to establish axonal numbers in the corpus callosum due to its size and its spatial variability of axonal number, I decided to calculate axonal density of the selected corpus callosum region. The use of axonal density in screening and evaluating axonal loss, however, is problematic because axonal loss may not be reflected properly by changes in axonal density. The insensitivity of axonal density to evaluate axonal loss is caused by the influence of extra axonal structures on axonal density. Demyelination will cause an increase in axonal density by the loss of the space expanding property of the myelin sheath. On the other hand the astrocytic response may fill the space for the lost myelin sheath. Stereological estimation, which is used to estimate entities of large dimensional samples based on the information from lower dimensional samples, could solve the problem of evaluating axonal numbers within the corpus callosum.

However, axonal injury, mainly axonal swellings, were observed during the late stages of demyelination in the #72 homozygote corpus callosum. Axonal changes are believed to render damaged axons non-permissive for remyelination (reviewed in Franklin and French-Constant, 2008) and therefore extensive axonal damage may contribute to remyelination failure. Axonal swellings may also inhibit the initial axon-glia contact required to initiate remyelination. In order for OPCs to myelinate axons they must engage with the naked axon. Integrin signalling between the oligodendrocyte and the axon (Camara et al., 2009; Laursen et al., 2009) and axonal electrical activity (Zalc and Fields, 2000) are important modulators of the early events of myelination in the CNS. Extreme distention of the axonal membrane at the site of axonal swelling could potentially have a bearing on both of these factors.

The importance of the initial engagement of demyelinated axons with OPCs can also be seen in context with re-expression of PSA NCAM on axons. In chronic MS tissue, PSA NCAM expression on demyelinated axons was suggested to contribute to the remyelination failure by blocking this crucial initial contact between OPCs and axons and therefore causing a block of OPC differentiation and contributing to the failure of remyelination (Charles et al., 2002).

In the #72 homozygote corpus callosum, PSA NCAM was not detected on demyelinated axons. However at P120, astrocytes expressed PSA NCAM, which has been reported to occur on activated astrocytes (Massaro, 2002;Massaro et al., 2002). In this study the PSA NCAM positive astrocytes were considered to be reactive astrocytes and were only found at P120.

### 3.6 Conclusion

The pathological development of the demyelination and remyelination failure has now been described in detail in the #72 mouse. The characterisation of the corpus callosum is a prerequisite for the transplantation studies that follow in Chapter 4. Future experiments will involve the investigation of the role of the cell intrinsic and cell extrinsic compartment in the development of the remyelination failure. The cell intrinsic and cell extrinsic compartment preferably should be tested individually. The possibility to isolate and culture OPCs *in vitro* gives an opportunity to investigate the cell intrinsic compartment without influence of the cell extrinsic compartment. *In vivo* experiments using cell transplantation or pharmacological intervention will give the opportunity to evaluate the influence of cell extrinsic and to a certain extent the cell intrinsic compartment in the development of remyelination failure.

## 4 An evaluation of cell intrinsic and cell extrinsic factors that contribute to remyelination failure

### 4.1 Introduction

In [Chapter 3](#) I showed that after initial myelination of the corpus callosum, a spontaneous progressive demyelination followed. Despite the fact that OPCs were present in the demyelinating environment, there was no evidence of successful remyelination. This was somewhat unexpected, since, with relatively normal myelin formation during development, a certain remyelination capacity during the advanced disease process might have been expected. The histological studies described in [Chapter 3](#) indicated that both OPC intrinsic and OPC extrinsic factors could potentially be implicated in remyelination failure. In this chapter I use cell culture and cell transplantation to address these issues more directly.

For remyelination to occur successfully, cell intrinsic and extrinsic factors must interact together in a precise spatial and temporal manner (reviewed in (Franklin, 2002; Franklin and ffrench-Constant, 2008; Peru et al., 2008)). Briefly, microglia/macrophages first clear the affected region of myelin debris (Kotter et al., 2001). OPCs then migrate into the demyelinated area, where they proliferate leading to repopulation of the demyelinated area (Foote and Blakemore, 2005b). Following repopulation, the OPCs differentiate into early oligodendrocytes (Shen et al., 2008). The newly formed oligodendrocyte processes contact the demyelinated axons after which the upregulation of myelin related genes in the contacting OPC are induced (Coman et al., 2005). Finally, the restoration of the myelin sheath leads to functional recovery (Duncan et al., 2009; reviewed in Franklin and ffrench-Constant, 2008). Given the complexity of the repair process, dysregulation of intracellular or extracellular signalling can perturb the finely balanced remyelination process, which in the worst case could end in the failure of remyelination.

Remyelination failure as a consequent of *Plp1* gene overexpression has been investigated in another model, the 4e mouse line (Ma et al., 2006). In that study it was suggested that a combination of OPC intrinsic and OPC extrinsic abnormalities led to remyelination failure. However, demyelination and remyelination were only assumed in this mouse model and only a very limited histological assessment of the OPC extrinsic compartment were performed *in situ*. Adult OPC differentiation was only evaluated *in vitro* and was considered to be normal.

The complex interaction between the cell intrinsic and cell extrinsic pathways during remyelination makes it difficult to evaluate the two compartments individually *in vivo*. To investigate the role of cell intrinsic factors in OPC differentiation, *in vitro* systems possess the advantage that the extrinsic influence (i.e. potentially inhibitory factors in the *in vivo* environment) on OPC differentiation and maturation can be eliminated. To date the differentiation potential of young and adult #72 mouse brain derived OPCs has not been evaluated *in vitro*.

The OPC extrinsic compartment consists of multiple different cellular components, which have been shown to interact with the remyelination process such as axons (Charles et al., 2002;Coman et al., 2005;Piaton et al., 2010;Zalc and Fields, 2000), astroglia (Blakemore et al., 2003;Liu et al., 1994), microglia and trafficking immune cells (Foote and Blakemore, 2005a;Kotter et al., 2001;Kotter et al., 2005;Arnett et al., 2003) as well as the extracellular matrix (Arnett et al., 2001;Back et al., 2005). To assess the role of the extrinsic compartment in remyelination failure in the #72 mouse, these components should be left as unaltered as possible. One way to study the extrinsic compartment is to perform *in vivo* transplantation experiments in the demyelinated region. Transplantation of myelination competent cells such as neurospheres into demyelinated areas can be used to evaluate the permissiveness of the environment for remyelination (Foote and Blakemore, 2005a;Blakemore et al., 2003;Setzu et al., 2006;Zhang et al., 2003). The (re)myelination capacity of transplanted neuronal stem cells or glial progenitor cells have been shown in various dys- and demyelinating animal models (Edgar et al., 2004a;Fukuhara et al., 2006;Mothe and Tator, 2008;Pluchino et al.,

2003;Windrem et al., 2008;Zhang et al., 2003) with successful, long lasting, stable chimerisation of the CNS leading, in some cases, to phenotypic normalisation of affected animals (Windrem et al., 2008).

So far, cell transplant experiments aiming to evaluate the influence of the cell extrinsic compartment in chronically demyelinated white matter on remyelination failure has not been conducted in the #72 homozygote mouse model.

## 4.2 Aims of the study

The overall aim of the work presented in this Chapter was to determine if OPC intrinsic and/or environmental factors contribute to remyelination failure in the #72 homozygote mouse. We used the corpus callosum, a major white matter tract where the pathology has been described in detail in Chapter 3, to address the role of the cell intrinsic compartment and the cell extrinsic compartment in remyelination failure in this model.

Specifically the aims were:

1. To determine if adult #72 homozygote OPCs are capable of differentiating normally if removed from demyelinated environment
2. To determine if the #72 homozygote corpus callosum is permissive for (re)myelination

To elaborate these two problems, the following experimental methods were used:

- 1.) A co-culture system of isolated, adult #72 homozygote and wild type OPCs, where the differentiation of the cells can occur in the absence of confounding environmental factors.
- 2.) Transplantation of wild type neurospheres into a predefined region of the adult #72 homozygote corpus callosum to evaluate if the cell extrinsic compartment is permissive for remyelination by myelination competent cells.
- 3.) Injection of wild type neurospheres into P1 #72 homozygote mice to test the proof-of-principle that normal neurospheres can survive, integrate into the #72 homozygote CNS, replace the genetically altered oligodendroglial cells and generate stable myelin, essentially rescuing the #72 homozygote mouse phenotype.

## 4.3 Material and Methods

### 4.3.1 Mouse colony

Homozygote male #72 mice expressing *GFP* under the  $\beta$ -actin promoter and mice harbouring a *Plp1-LacZ* fusion gene were used in the cell culture and cell transplant experiments. Technical details, generation and maintenance of the different mouse lines are described in Chapter [2.2 Mouse breeding](#).

### 4.3.2 Identification of GFP expression in the *B-actin-GFP* expressing line

In the *B-actin-GFP* expressing mouse model GFP is, amongst other cells, also present in epithelial cells. GFP positive pups can therefore be identified by simply exposing them to a handheld UV light in darkness. In these circumstances, green fluorescence is visible to the human eye. Further details are found in Chapter [2.2 Mouse breeding](#).

### 4.3.3 Isolation and culture of adult and neonate OPCs from the corpus callosum for culture

Preliminary studies of isolating OPCs using a Percoll® gradient showed that, especially when using adult #72 homozygote corpus callosum, contamination by microglia was unavoidable. To expose the wild type and #72 homozygote OPCs to the same *in vitro* environment I cultured wild type and #72 OPCs and contaminating microglia together.

For each OPC co-culture experiment, OPCs were isolated from two adult GFP expressing and two adult #72 homozygote corpus callosa. The same number of isolated wild type cells (mainly OPCs) and isolated #72 homozygote cells (mainly OPCs and microglia/macrophages) were mixed together immediately before plating down on poly-L-lysine coated glass coverslips. The same procedure was

also followed when performing this experiment using neonate OPCs. The isolation procedure and maintenance of the culture is described in Chapter [2.2 Mouse breeding](#).

#### **4.3.4 Generation of *Plp1 Lac-Z* and *B-actin GFP* expressing neurospheres**

As described in Chapter 2, neurospheres carrying the *LacZ* or GFP reporter genes under the control of *Plp1* (Wight et al., 1993) and  $\beta$ -actin promoter (Okabe et al., 1997), respectively, were generated from transgenic mice. These mice were wild type at the *Plp1* locus. Detailed information about neurosphere generation can be found in Chapter [2.5.3 Generation of \*Plp1 Lac-Z\* expressing neurospheres and generation of \*B-actin GFP\* expressing neurospheres](#).

#### **4.3.5 Preparation of neurosphere for transplantation**

On the day of transplantation the neurospheres were prepared for transplantation as described in [Chapter 2.5.3.1 Preparation of neurosphere for transplantation into homozygote #72 mice](#).

#### **4.3.6 Adult mice used in the transplant study**

Male #72 homozygote mice at P100 were used in the transplantation experiment. As previously described in [Chapter 3 The development of the phenotype and pathology of the homozygote #72 corpus callosum](#), the corpus callosum is almost completely demyelinated at this stage. After transplantation, mice were kept for 14 days then the brains were processed for immunofluorescence, histological and ultrastructural analysis as described in Chapter [2.6 Tissue sampling and processing](#); [2.7 Staining techniques](#). As a control, an adult male *shiverer* mouse was transplanted at the same time. The CNS of adult *shiverer* mice is permissive to myelination by transplanted neurospheres (J.M. Edgar personal communication). None of the mice were immunosuppressed. Details of the surgical procedure, including the Bregma coordinates, are described in Chapter

### [2.5.5 Surgical procedure and injection of neurospheres into adult homozygote #72 corpus callosum.](#)

#### **4.3.7 Neonate mice used in the transplant study**

One day old (P1) neonatal #72 homozygote male pups were used for injection of wild type neurospheres into the forebrain parenchyma at four locations. Details of the surgical procedure are described in [Chapter 2.5.5.1 Injection of neurospheres into neonate homozygote #72 mice.](#)

#### **4.3.8 Processing of cell cultures and transplanted tissue**

Processing of cell cultures and the transplanted tissue for light microscopy, epifluorescence microscopy and electron microscopy are described in Chapter 2 (2.7 Staining techniques). Antibodies against O4, GFP, MBP, PLP, NG2, PDGFR $\alpha$ , GFAP, CD45, CD169 were used in this study. Protocols and antibody dilutions are described in Chapter 2 ([Table 2](#) & [Table 3](#)) and in [Chapter 7 Appendix](#).

#### **4.3.9 Measurement of oligodendrocytic processes from co-cultured OPCs**

In this study the measurement of oligodendrocyte process length was used as a parameter for OPC differentiation *in vitro* using NeuronJ (Meijering et al., 2004), a plugin program in ImageJ. The culture experiment was repeated 3 times using adult cells and twice using neonatal cells. A total of 234 wild type and 49 #72 homozygote cells were measured in the experiment using adult OPCs. A total of 145 wild type and 166 #72 homozygote cells were measured in the experiment using neonatal OPCs. The mean of the mean total process length per cell from all wild type OPCs was compared with the mean of the mean total process length per cell from all the #72 homozygote OPCs. Details of the procedure can be found in Chapter 2 (2.5.2 Cell culture).

#### 4.3.10 Statistical analysis

An unpaired Student's t-test was used to analyse the data obtained from the cell culture experiment. Statistical analysis was made in GraphPad Prism 5®.

### 4.4 Results

#### 4.4.1 Evaluation of the differentiation potential of OPCs using an *in vitro* co-culture system

To determine if remyelination failure in the #72 mouse is due to an intrinsic defect in the adult OPCs, I removed these cells from a potentially inhibitory environment and analysed their potential to differentiate *in vitro*, in comparison to wild type OPCs.

##### 4.4.1.1 Contamination of activated microglial cells was unavoidable when using a Percoll® gradient to isolate OPCs from #72 homozygote brain tissue

Preliminary experiments evaluating the OPC purification technique using a Percoll® gradient showed that cells expressing PDGFR $\alpha$  and O4 were present after one day *in vitro*. This demonstrated that OPCs were successfully isolated using this technique ([Figure 41](#)). However, a second population was present in even greater numbers. Immunostaining with an antibody to sialoadhesin (CD169), a macrophage restricted sialic acid binding protein that is expressed in the CNS following damage to the blood-brain barrier (Perry et al., 1992), demonstrated that these cells were activated microglia/macrophage ([Figure 42](#)). The microglia/macrophages survived well in the culture system and were present, together with differentiated OPCs, after seven days *in vitro*.

Since I was unable to separate the adult #72 OPCs from the microglia it became imperative that the wild type OPCs, against which the #72 OPCs were to be

compared, were cultured in the same environment. To achieve this, I isolated normal adult OPCs from  $\beta$ -actin-GFP expressing mice and combined them with the OPC/microglial mix derived from the adult #72 mice. Thus, I was able to distinguish the normal from the mutant cells on the basis of GFP expression.

#### **4.4.1.2 Adult #72 OPCs showed an impaired development compared to the wild type OPCs *in vitro***

Adult OPCs from the -P120 corpus callosum survived and differentiated *in vitro*. After seven days in culture #72 cell processes appeared shorter and showed reduced branching compared to the wild type cells. I measured the length of all processes branching from the cell body on phase contrast images taken from cells that stained for O4. The mean total process length per cell after seven days *in vitro* was significantly ( $p < 0.05$ ) reduced in the #72 homozygote cells compared to the wild type cells ([Figure 43](#)).

To test if this impairment in differentiation of adult #72 OPCs was related solely to their genotype, I next determined whether neonatal #72 OPCs behaved similarly.

#### **4.4.1.3 Neonatal #72 and wild type OPCs were morphologically indistinguishable after 7 days *in vitro***

Co-cultures containing neonatal GFP positive wild type and non-GFP positive #72 homozygote OPCs were established. The isolated neonatal normal and #72 OPCs developed similarly during seven days *in vitro* ([Figure 44](#)). The average of the total process length per cell obtained from two separate experiments showed no significant difference ( $p = 0.44$ ) between the two genotypes.

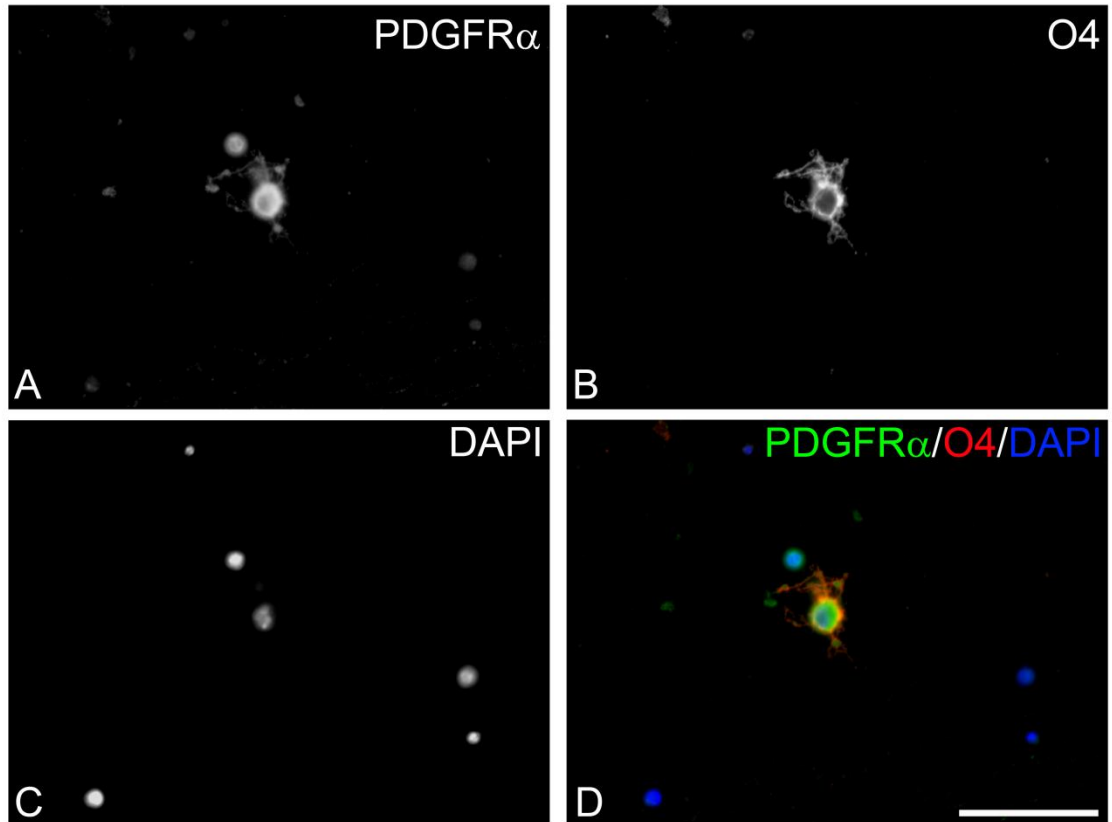


**Figure 41. OPCs were successfully isolated from adult corpus callosum using a Percoll<sup>®</sup> gradient technique.**

Micrographs of cultured cells isolated from adult corpus callosum at 1 day in vitro using antibody against PDGFR $\alpha$  and O4 to identify OPCs. During the early stages of differentiation, OPCs co-express PDGFR $\alpha$  (A) and the surface marker O4 (B). DAPI was used to identify the cell nucleus (C). After one day in vitro, multiple, PDGFR $\alpha$  and O4 positive cells were present (D). This suggests that the purified cells are OPCs (x400, scale bar 50 $\mu$ m).

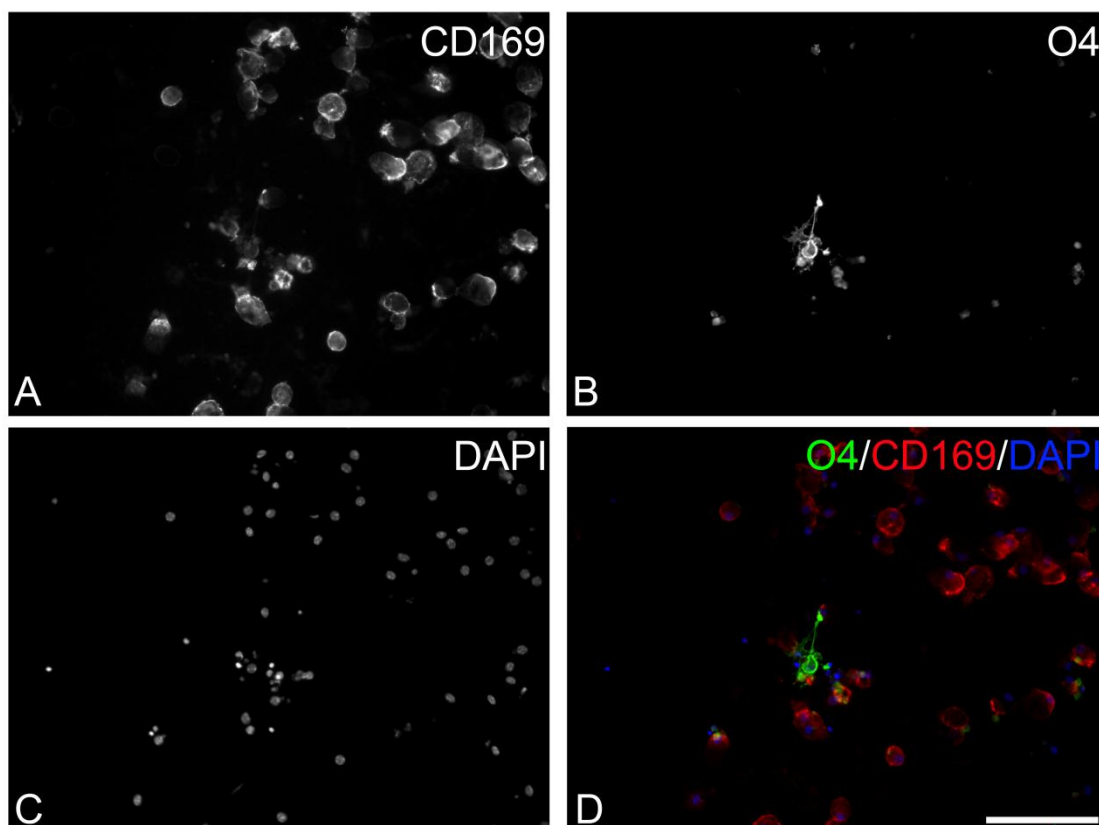


**Figure 42. Microglial/macrophage contamination could not be prevented when using the Percoll<sup>®</sup> gradient protocol to purify adult #72 homozygote OPCs.**

Micrograph of a cell culture using only cells isolated from adult #72 homozygote corpus callosum. Antibody against CD169 was used to identify activated microglia/macrophages and antibody against O4 was used to identify cells from the oligodendroglial lineage. It was not possible to exclude activated microglial/macrophage cells (A) when using the Percoll<sup>®</sup> gradient protocol. Both microglia/macrophages and OPCs were present after seven days in vitro (B). DAPI was used to identify the cell nuclei (C). The two cell types were growing in close proximity to each other (D, x200, scale bar 100 $\mu$ m).

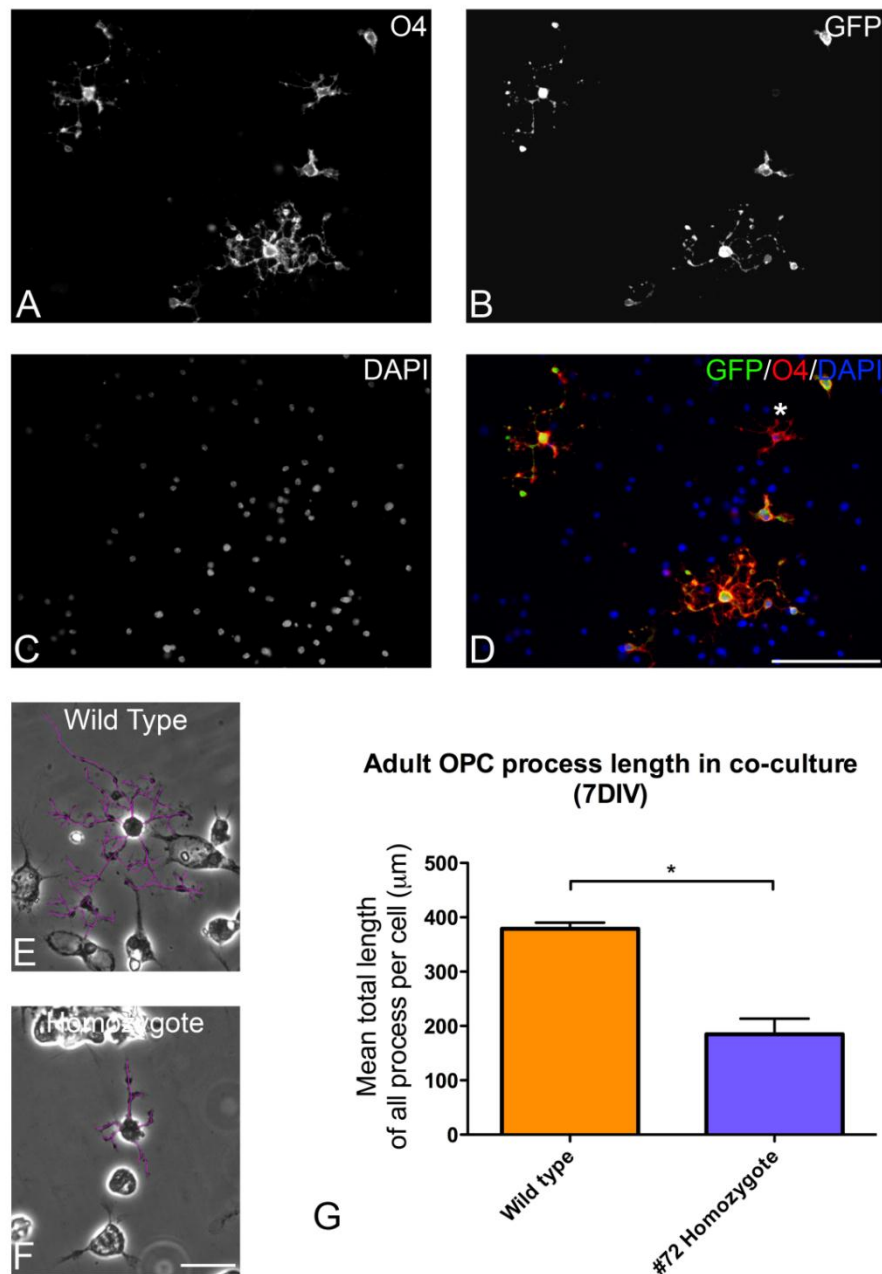


**Figure 43. The cell process length of adult #72 homozygote OPCs was significantly reduced when compared to the co-cultured wild type OPCs.**

Micrographs of co-cultured adult #72 and wild type to the Plp1 gene, GFP expressing cells after seven days in vitro. O4 was used to identify cells of oligodendroglial origin (A). The presence of GFP (B) was used to differentiate between the wild type and #72 homozygote cells (D, asterisk), of which the latter lack GFP (A - D, x200, scale bar 100μm). Phase contrast images were used to quantify the process length per cell as previously described (E, F, x200, digitally magnified, scale bar 50μm). The adult #72 homozygote cells appeared morphologically different (F) compared to the wild type (E) and had a significantly reduced mean total cellular process length per cell after seven days in vitro when compared to the wild type cells (G, \*: p<0.05). The graph shows the mean total length of all processes per OPC (+ s.e.m.); each experiment was repeated 3 times.

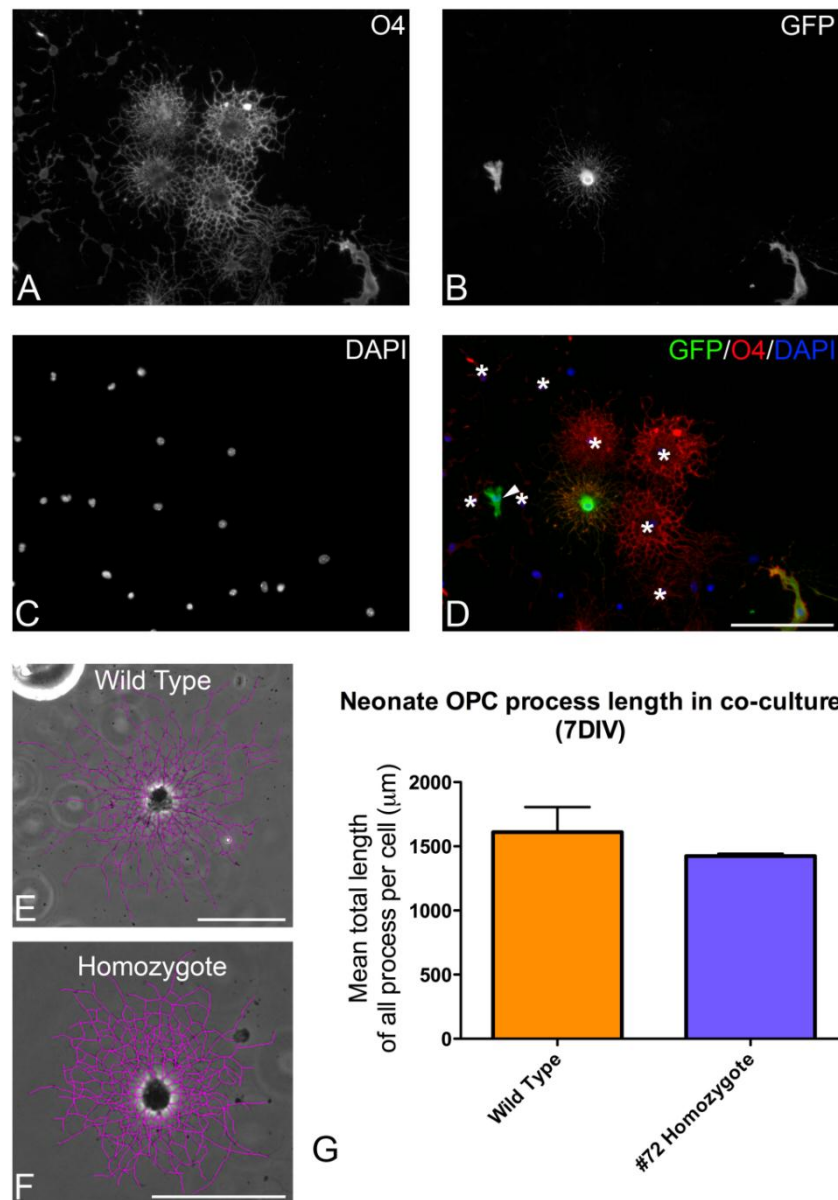


**Figure 44. The mean total process length of neonatal #72 and wild type OPCs was not significantly different after 7 days in vitro.**

Micrographs of co-cultured neonatal wild type to the Plp1 gene (green) and #72 OPCs at 7 DIV. The surface marker O4 (A) was used to confirm that the cells were from the oligodendroglial lineage. The presence of cytoplasmic green fluorescent protein (B) indicated that the cells were of wild type origin. DAPI was used to label the nuclei (C). The merged image was used to distinguish between wild type and #72 homozygote (asterisk) OPCs, in which GFP was absent (D, x200, scale bar 100μm). Very rarely, astrocytes (arrowhead) were present in the cultures. After identifying the genotype of the differentiating OPCs, phase contrast images were used to measure, in a semi-automated manner, the total process length per cell (E, F, x200, digitally magnified, scale bar 50μm). There was no significant ( $p=0.44$ ) difference in total process length between the neonate #72 homozygote OPCs and wild type cells (G) after 7 days in vitro. The graph shows the mean total length of all processes per OPC (+ s.e.m.); each experiment was repeated 3 times.

#### **4.4.2 Evaluating the cell extrinsic compartment: Cell transplantation into demyelinated corpus callosum**

The results from the *in vitro* experiment suggest that adult #72 OPCs are impaired in their differentiation compared to wild type cells. To determine if their environment is permissive for myelination, I transplanted myelination competent cells into the adult #72 mouse corpus callosum.

##### **4.4.2.1 Advanced demyelination and a marked microglial/astroglial response was present in the #72 homozygote corpus callosum at P100 before transplantation**

In Chapter 3, I quantified cellular changes in the #72 corpus callosum at P40, 60, 90 and 120. Before transplanting cells into the P100 corpus callosum, I confirmed by immunostaining, that the environment was similar to that at P120. The PLP and MBP staining showed a loss of myelin integrity. There was an increase in microglia, which was accompanied by microglial activation and an astroglial response. NG2 positive cells were abundantly present ([Figure 45](#)).

##### **4.4.2.2 The transplanted neurospheres were viable and showed multipotency *in vitro***

To evaluate the viability and the differentiation potential of transplanted neurospheres, surplus cells remaining at the end of the transplantation procedure were plated onto poly-L-lysine coated coverslips. Neurosphere-derived cells used in the transplant study developed within three days *in vitro* into O4, MBP and PLP/DM20 positive cells proving the viability and the differentiation potential of the neurospheres. Cultured neurospheres also developed into GFAP+ astrocytes and occasionally also into neurons, identified by the neuronal nuclear marker NeuN ([Figure 46](#)), confirming the multipotency of the neurospheres *in vitro*, as described by others (Zhang et al., 1998; Mokry et al., 2005).

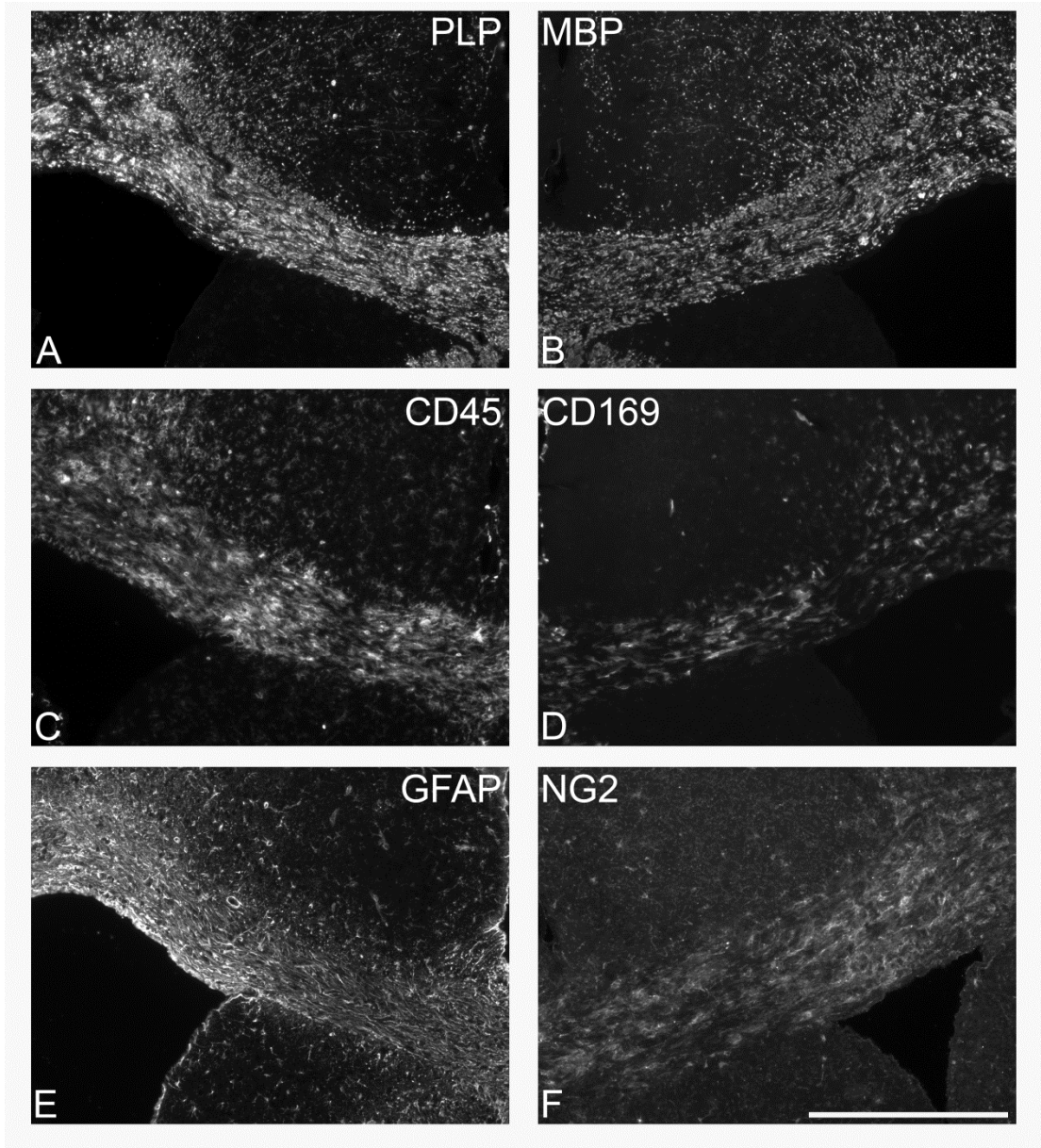


**Figure 45. Pronounced changes in myelin integrity and astroglial, microglial and OPC populations were present in the #72 mouse corpus callosum at P100.**

Micrographs of #72 corpus callosum at P100 using antibody against MBP, PLP/DM20, CD45, CD169, GFAP and NG2 to characterise the environmental changes. Myelin integrity was severely compromised, as shown using immunohistochemistry against myelin proteins PLP/DM20 (A) and MBP (B). There was also an apparent microglial (C) and astroglial (D) cell response. A proportion of microglia/macrophage cells expressed CD169 (E) a macrophage restricted sialic acid binding protein. At the same time there were abundant NG2 positive (F) cells in the corpus callosum (x100, scale bar 400µm).

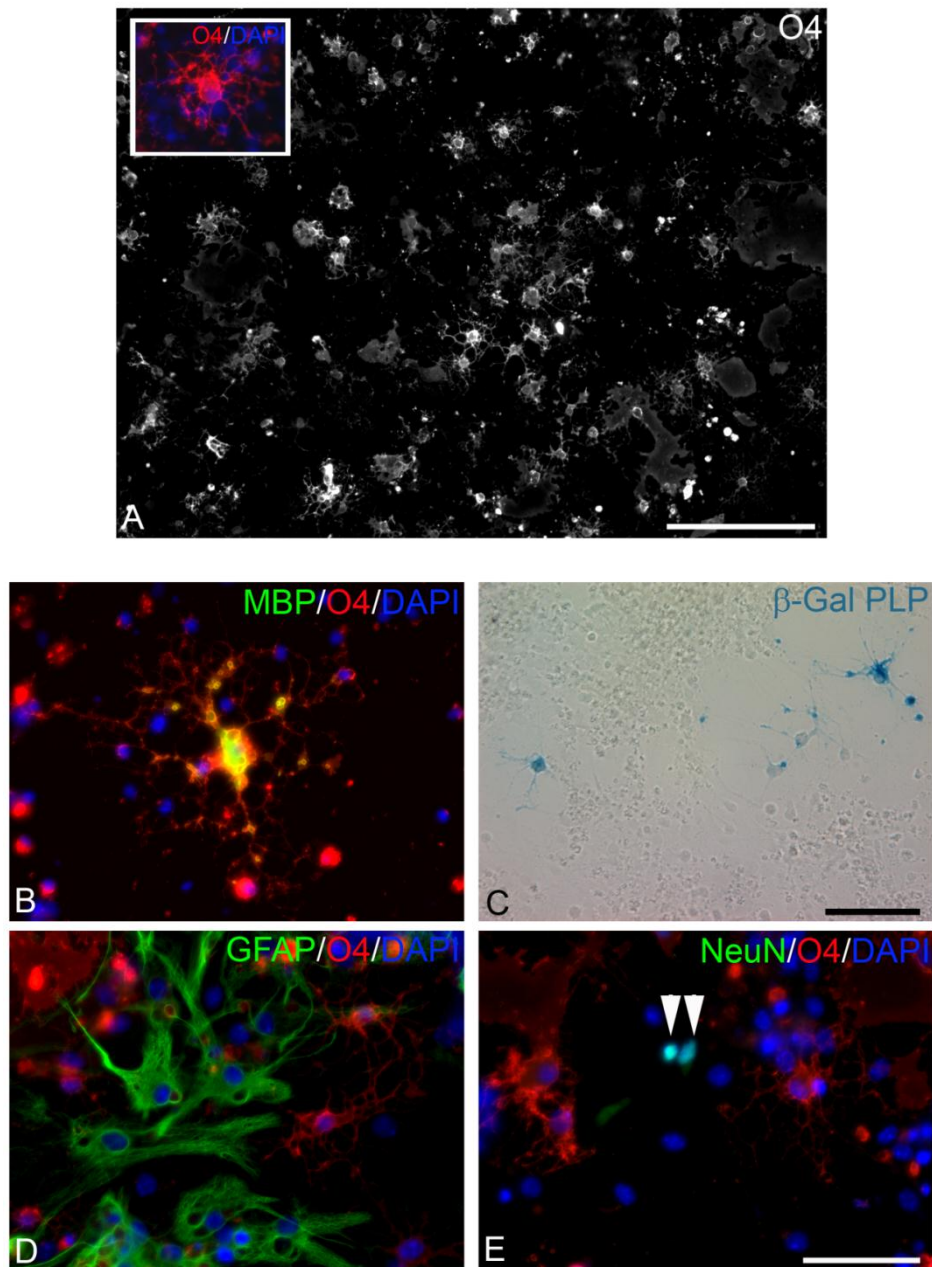


**Figure 46. LacZ transgene expressing neurospheres are multipotent and develop into oligodendrocytes, astrocytes and neurons in vitro.**

Micrographs of coverslips with cultured surplus neurospheres after transplantation for three days in vitro. Antibody to O4, MBP, GFAP and NeuN were used to identify the multipotency of transplanted cells in vitro. X-Gal staining was used to visualise PLP/DM20 expression ( $\beta$ -galactosidase generates enzymatically the blue appearing 5-bromo-4-chloro-3-indolyl  $\beta$ -D-galactoside product after X-gal treatment). After 3 days in vitro a relatively high density of O4 positive cells was present (A, x200, scale bar 200 $\mu$ m, insert, x400), some of which expressed MBP (B, x400) and PLP/DM20 (C, x200, scale bar 100 $\mu$ m). This showed the capacity of the transplanted neurospheres to differentiate into oligodendroglia. However, the neurospheres also differentiated into GFAP expressing astrocytes (D, x400) and even into a few neurons (arrowheads) expressing NeuN (E, x400, scale bar 50 $\mu$ m) when plated in differentiating media.

#### **4.4.2.3 Transplanted neurospheres survived for 14 days in the adult #72 homozygote corpus callosum**

To assess the influence of the OPC extrinsic compartment on remyelination failure in the #72 homozygote mouse, wild type neurospheres expressing GFP or carrying a *Plp1 LacZ* fusion gene were introduced, together, into the demyelinated corpus callosum of #72 homozygote mice at P100.

Fourteen days after transplantation, GFP and  $\beta$ -galactosidase positive transplanted cells were present within the #72 homozygote mouse corpus callosum. Transplanted cells were observed in close proximity to the needle track and also up to approximately 1.2mm distal from the injection site ([Figure 47](#)).

#### **4.4.2.4 Axons in the demyelinated #72 homozygote mouse corpus callosum are myelination competent**

On high power images of the transplant region,  $\beta$ -galactosidase positive cells showed a morphology which resembled myelin sheath producing oligodendrocytes. Most of the GFP positive cells appeared similar to the  $\beta$ -galactosidase positive oligodendroglia. Co-labelling with GFP and MBP (the latter a relatively late marker of oligodendroglial differentiation and myelin compaction) indicated that transplanted GFP positive neurospheres had differentiated into ensheathing/myelinating oligodendrocytes ([Figure 47](#)).

To test if the transplanted cells formed a compact myelin sheath around axons, I examined resin section of areas containing transplanted cells in the corpus callosum. On the resin sections thin, ring like structures were seen around axons in the area where cells had been transplanted ([Figure 48](#)). The relative abundance of ring like structures (arrows in A) became obvious when compared to a non-transplanted region of the corpus callosum from the same animal, where only a few similar structures were present (arrows in B).

Electron microscopy was used to evaluate the ultrastructure of the myelin sheath in the transplanted corpus callosum. The corpus callosum treated with transplanted cells was compared to an untreated corpus callosum and showed an increased presence of myelinated axons. Ultrastructural evaluation of the myelin sheath showed a normal myelin sheath with an inner tongue, and normal appearing major dense and intraperiod lines ([Figure 49](#)).

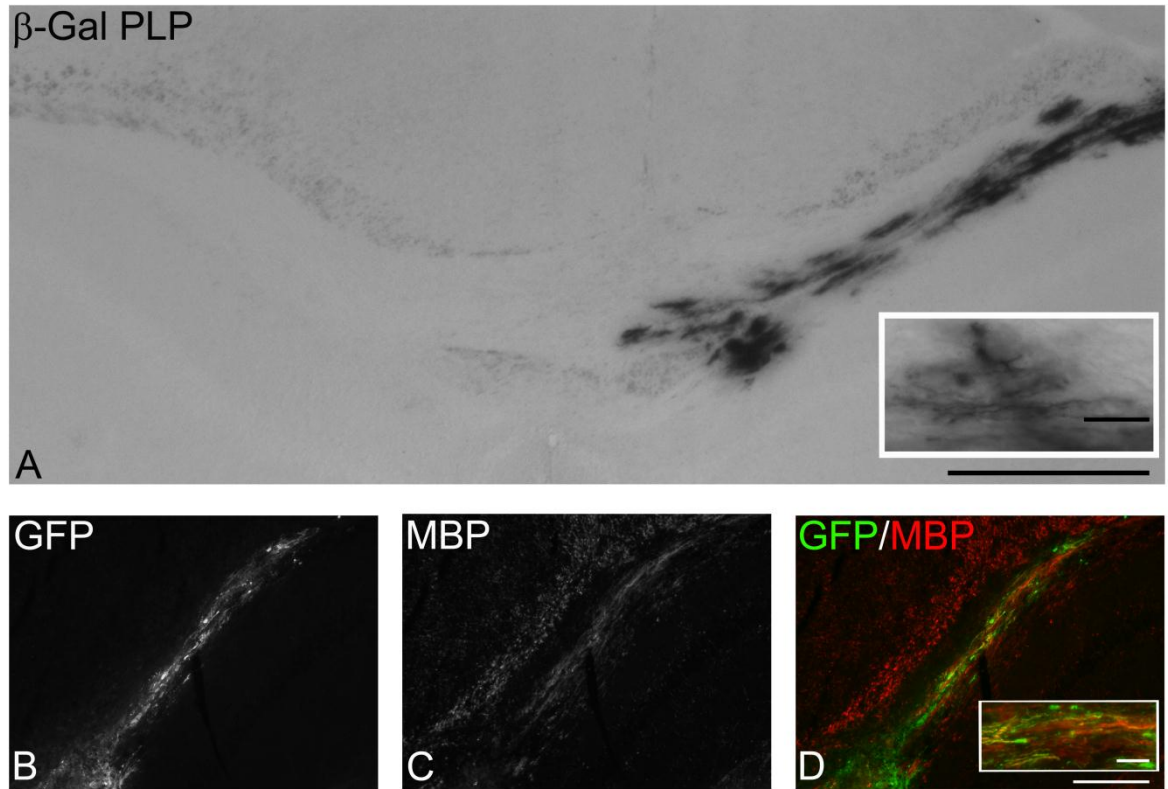


**Figure 47. Transplanted neurospheres survived and (re)myelinated axons in the adult chronically demyelinated #72 homozygote corpus callosum.**

Micrographs of the corpus callosum of an adult #72 homozygote mouse 14 days after transplantation, using antibodies to MBP and GFP. X-gal treatment was used to visualise PLP/DM20 expression. Transplanted neurospheres differentiated into (re)myelinating oligodendrocytes in the adult #72 homozygote mouse. The transplanted neurospheres differentiated into Plp1 expressing oligodendrocytes indicated by cells turning blue after X-gal treatment (A, x40, scale bar 400µm, insert in A, x400, scale bar 20µm). The X-gal positive cells formed myelin sheath-like structures (insert in A, x400, scale bar 20µm). Co-expression of MBP on the GFP positive myelin-like structures confirmed that the transplanted cells formed myelinating oligodendrocytes (B, C, D, x100, scale bar 200µm, insert in D, x400, scale bar 20µm).

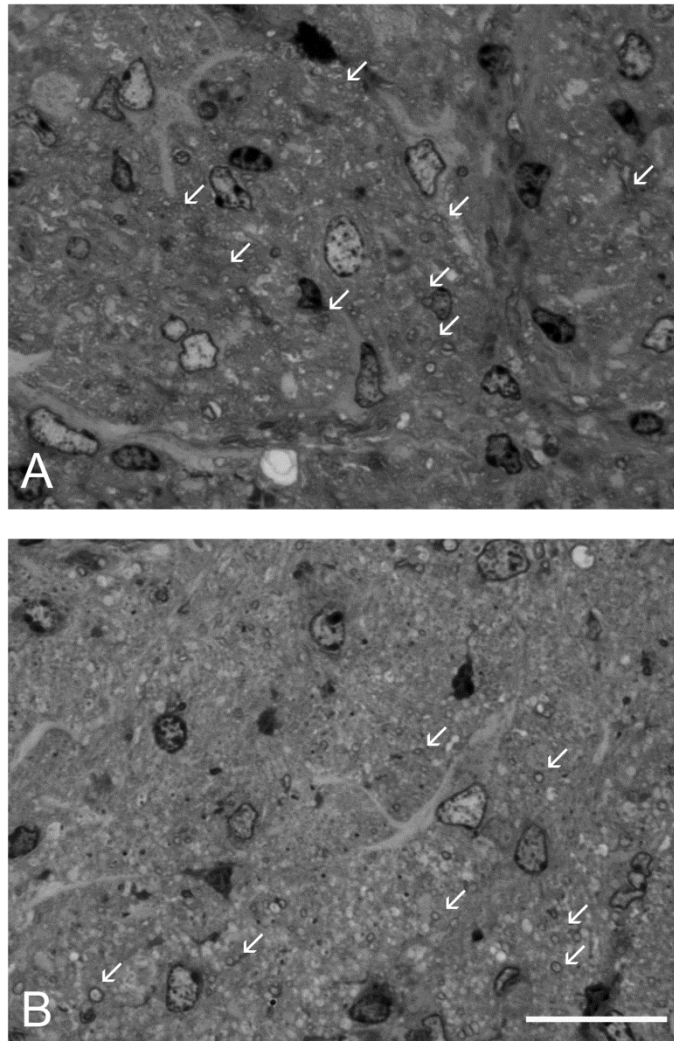


**Figure 48. Neurospheres formed myelin sheaths after transplantation into the adult #72 corpus callosum.**

Micrograph of methylene blue/azur II sections from a #72 homozygote mouse 14 days after injection of neurospheres. On the methylene blue/azur II stained, 1 $\mu$ m thick resin sections, ring like structures resembling myelin sheaths were identified. When comparing a transplanted #72 homozygote mouse corpus callosum (A) with an untreated corpus callosum (B), more myelin sheaths (arrows in A) were present in the transplanted corpus callosum than in the untreated corpus callosum (arrows in B) (x1000, scale bar 20 $\mu$ m).

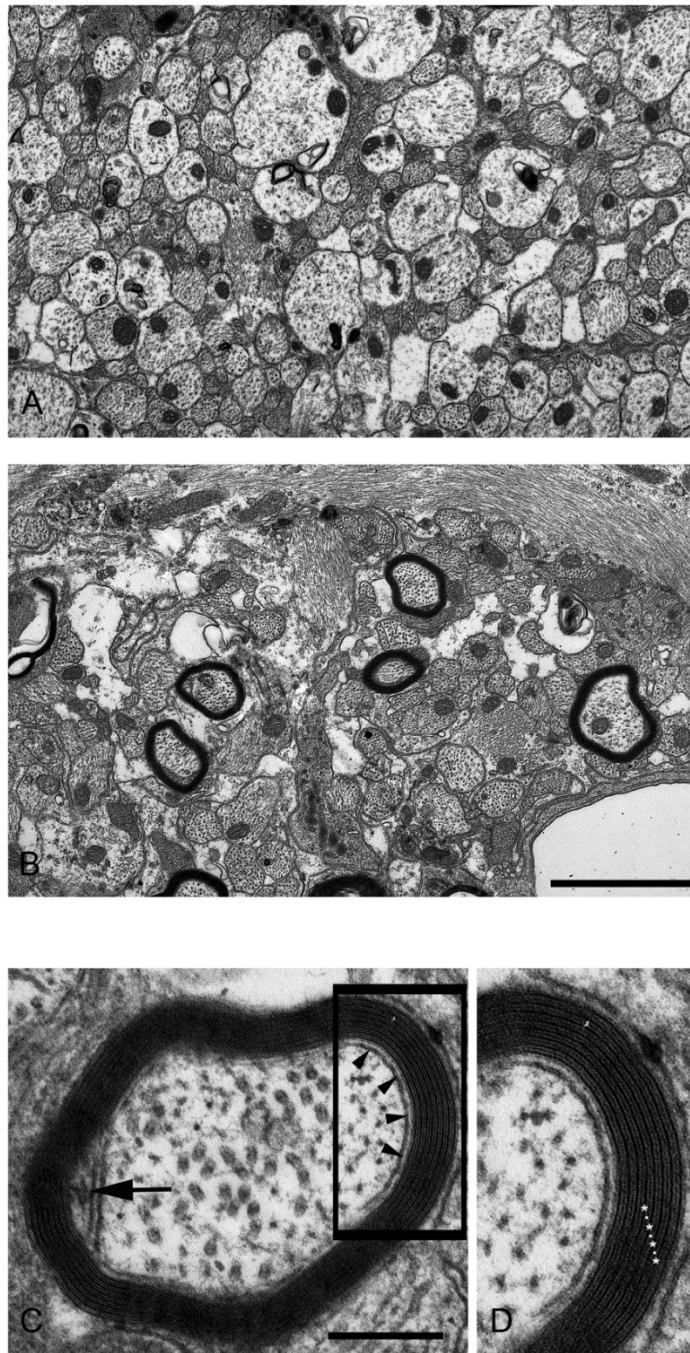


**Figure 49. Formation of normal compact myelin sheaths 14 days after neurosphere transplantation into #72 homozygote corpus callosum.**

EM micrographs from areas of neurosphere transplantation in the #72 homozygote corpus callosum 14 days after transplantation. To illustrate the changes after neurosphere transplantation an untreated #72 corpus callosum, which was almost completely demyelinated at P120 (A, x8000) was compared to the transplanted region of the corpus callosum (B, x8000, scale bar 2 $\mu$ m). After transplanting neurospheres into the demyelinated region, axons became (re)myelinated by an ultrastructural normal myelin sheath (B, x8000, C, D, x50000, scale bar 250nm) with normal appearing inner tongue (arrow in C) and periaxonal space (arrowheads C) and its characteristic major dense (asterisks in D) and intraperiod (dots in D) lines.

#### 4.4.2.5 Transplanted neurospheres differentiated into astroglial cells

These results suggest that the axons in the adult #72 corpus callosum are permissive for myelination. However neonatal neurospheres differentiate into cell types other than oligodendrocytes and it was important to determine if other neurosphere derived cells populations were produced, that could potentially alter the environment.

In the transplanted region, some of the neurospheres differentiated into stellar shaped cells, resembling astrocytes. The identity of the cells was confirmed by double immunohistochemical staining with antibodies to GFP and the astrocytic marker, GFAP ([Figure 50](#)).

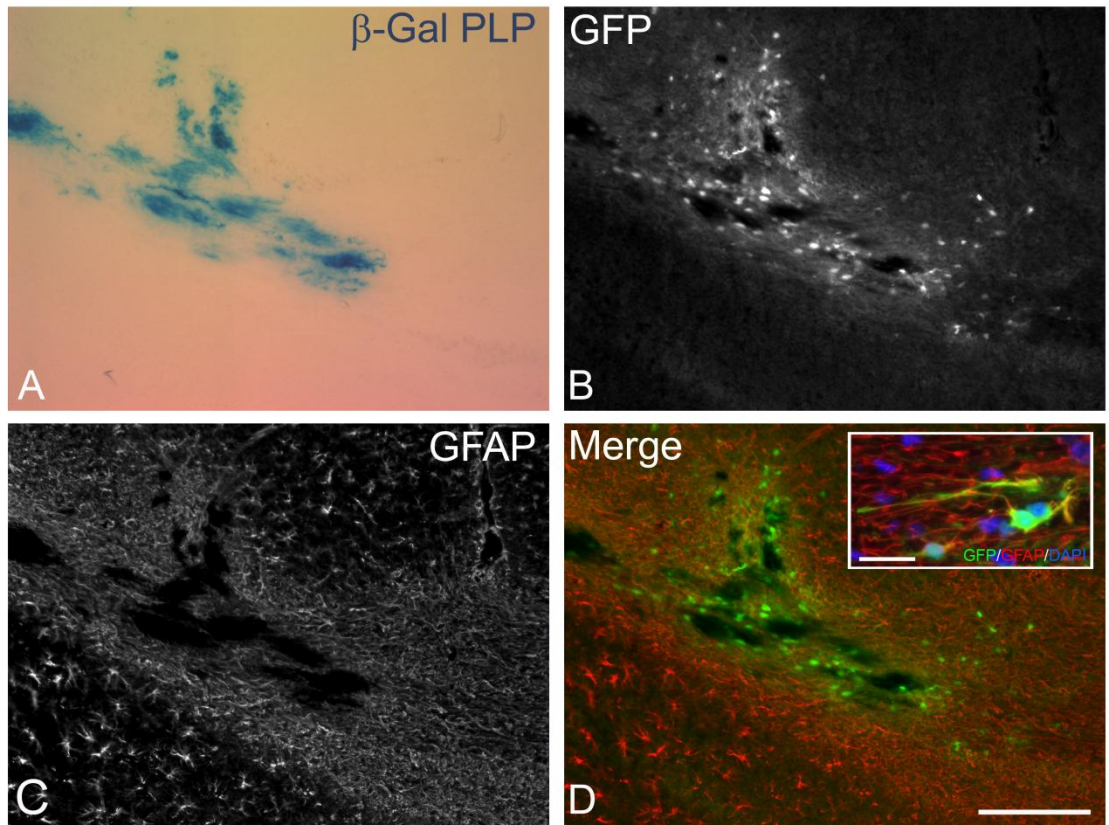


**Figure 50. Transplanted neurospheres also differentiated into astroglia.**

Micrographs of a #72 homozygote corpus callosum after X-Gal treatment to visualise the  $\beta$ -galactosidase positive transplanted cells. The transplanted neurospheres also developed into astrocytes reflecting their multipotent capacity in vivo. After transplantation of neurospheres into the demyelinated #72 homozygote corpus callosum there were not only Plp1 expressing cells (A, x100) but also a subset of the GFP+ (B) transplanted cells, which had differentiated into astrocytes (C, D, x100, scale bar 200 $\mu$ m; insert, x400, scale bar 20 $\mu$ m).

#### 4.4.3 Long term survival and integration of transplanted wild type neurospheres after neonatal cell transplantation into CNS parenchyma

Besides addressing the basic questions posed at the start of this Chapter, the results of these experiments suggest that transplanted cells could potentially be used therapeutically to restore myelin in the adult CNS. However, the literature has shown that widespread myelination of the adult CNS is virtually impossible to achieve through focal transplantation of cells, principally because the transplanted cells are relatively slow in populating the adult CNS, failing to reach the pro (re)myelinating environment of acute lesions in time and therefore fail to initiate remyelination in the demyelinated region (Blakemore et al., 2002). Additionally, migration through normal tissue has been shown to be less effective than through lesioned tissue (Franklin et al., 1996) and finally the presence of dysfunctional OPCs within the demyelinated region may inhibit the population by transplanted cells (Chari et al., 2003). The advantage of transplanting multipotent cells in the new-born has been shown to be more effective for wide spread distribution and integration of the transplanted cells in the CNS (Learish et al., 1999; Windrem et al., 2008). With this in mind, I asked if transplantation of neurospheres into the brain of new-born #72 mice would provide proof-of-principle of the potential for cell transplantation to treat PMD. Previous transplant studies, mainly from the Duncan laboratory, have focussed on models of PMD due to point or missense mutations ((Duncan et al., 1988; Zhang and Duncan, 2000; Zhang et al., 2003) and a recent study by (Windrem et al., 2008) achieved a complete replacement of CNS oligodendroglia after neonatal injection of human glial progenitor cells in *shiverer* mice. However the potential of cell transplantation to treat PMD due to gene duplication has not previously been tested. The main difference in PMD models caused by mild overexpression of *Plp1* gene is that early post natal OPCs are relatively healthy and the initial myelination of the CNS is virtually normal, unlike in the missense mutations where virtually no myelin is formed in the first place. Therefore the competition between transplanted cells and relatively healthy endogenous OPCs may lead to a less effective establishment of transplanted cells.

At 7, 14, 35, 80 and 120 days post transplantation, two male mice were sacrificed and the brain was evaluated for donor cell survival, integration and ensheathment/myelin formation. Macroscopically, extensive regions of  $\beta$ -galactosidase positive cells in white and grey matter were found from P35 to P120. At P35 cells of transplant origin were mainly present in major white matter tracts. At P120 patches of X-gal staining were found in the corpus callosum, anterior commissure, thalamus, hypothalamus, optic chiasm and hippocampus. At P14, the first  $\beta$ -galactosidase positive cells with myelin-like structures could be seen using light microscopy. With time the areas of transplanted cells forming myelin-like structures in white matter tracts increased, showing that the transplanted cells had survived, migrated after focal injection to various white matter tracts in the cerebrum, and successfully integrated and ensheathed/myelinated axons in the host brain parenchyma ([Figure 51](#)).

To see if the transplanted cells formed a normal myelin sheath EM was used to evaluate the myelin morphology. A substantial amount of myelinated axons were found in the transplant integrated white matter at P120 when comparing areas of successful integration of transplanted cells to areas without integration of transplanted cells in the same mouse. The myelin sheath appeared morphologically normal although some myelin sheaths appeared thicker than others and occasionally redundant myelin was observed ([Figure 52](#)).

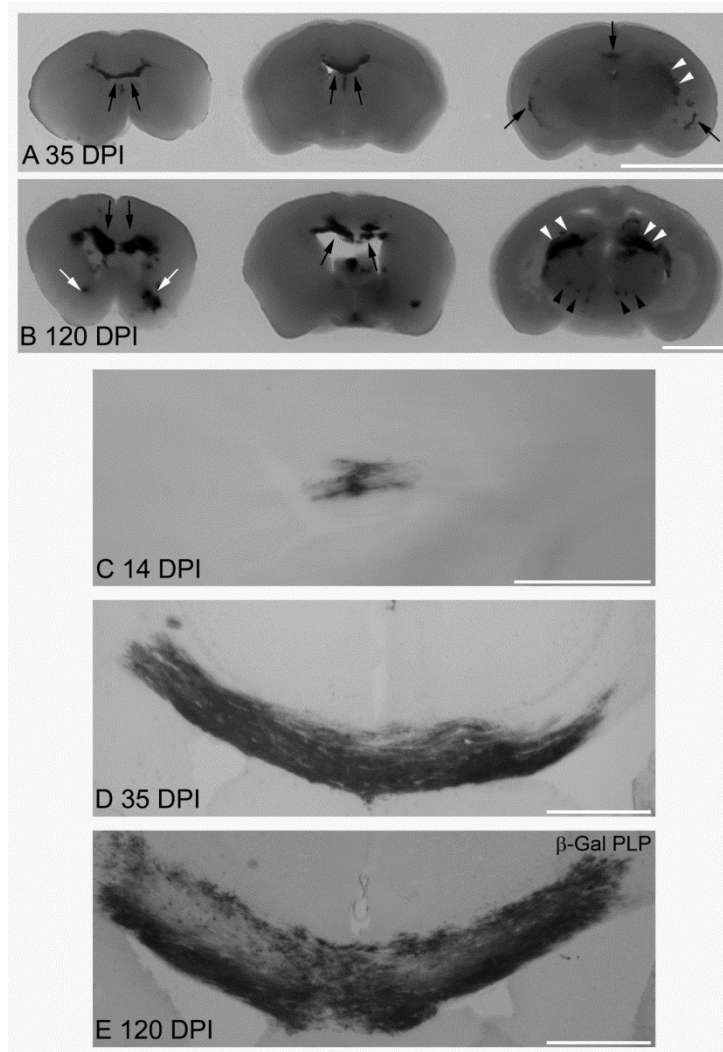


**Figure 51. Successful integration, ensheathment/myelination and long term survival of neurospheres after intracerebral transplantation into neonatal #72 homozygote mice.**

Photographs of 2mm thick brain tissue slices taken from mice at 14, 35 and 120 days after transplantation of neurospheres harbouring the Plp1/LacZ transgene into neonatal brain parenchyma. At 35 (A) and 120 (B, scale bar 5mm) days post injection (DPI) the areas containing myelin of donor cell origin was made visible after X-Gal treatment, which stained cells and the myelin sheath expressing Plp1 gene promoted  $\beta$ -galactosidase blue. In general, LacZ expressing transplant derived cells occurred in clusters. Myelin-like sheaths of transplant origin were detected from 14 DPI (C, x100, scale bar 200 $\mu$ m). The transplanted neurospheres had not only integrated into various regions such as the corpus callosum (black arrow), anterior commissure (white arrow), thalamus (black arrowhead) and hippocampal regions (white arrowhead) but had also differentiated into Plp1 expressing oligodendrocytes, which formed myelin sheath-like structures, presumably around axons. Transplanted donor cells were present at 14 (C), 35 (D, x40 scale bar 400 $\mu$ m), 80 (data not shown) and 120 (E, x40, scale bar 400 $\mu$ m) DPI, suggesting that the transplanted cells survived and differentiated into myelin synthesising oligodendrocytes, which were stably integrated up until 120 DPI, without immunosuppression.

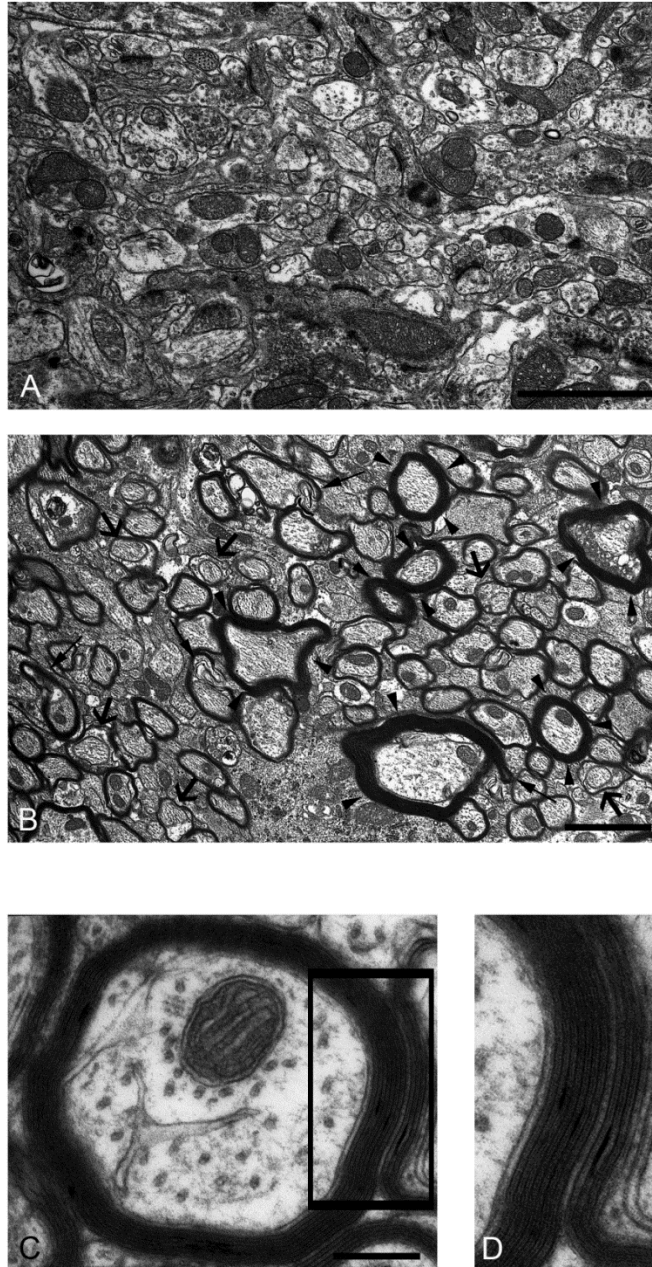


**Figure 52. A large amount of transplant-derived myelin is present in regions of the adult #72 mouse corpus callosum after transplantation of neurospheres into the neonatal brain.**

EM micrographs of a transplanted #72 corpus callosum 120 days post injection, in which transplant-derived myelin is absent (A, x5000) compared to an area in which transplant-derived myelin is present (B, x5000, scale bar 2 $\mu$ m). At this age, the areas of corpus callosum where cell transplants did not integrate are virtually devoid of myelin sheaths, confirming that the myelin that is present is likely to be derived from the transplanted cells. The myelin appears relatively normal (C, D x40000, scale bar 250nm), although some redundant myelin is present (arrows head) and some sheaths appear thicker (filled arrow) or thinner (empty arrow) than normal.

#### **4.4.3.1 Early post natally injected donor cells locally ameliorate the white matter microglial response**

To investigate if the changes in the local environment are mainly a response to demyelination I also investigated the effect of the neonatal cell transplantation on the local environment at 120 DPI. In regions where the transplanted cells had formed extensive myelin the cell density was visibly reduced ([Figure 53](#)). This was primarily due to the fact that the leukocyte population, labelled with an antibody recognising CD45, appeared reduced in areas containing large amounts of transplant-derived myelin ([Figure 54](#)).

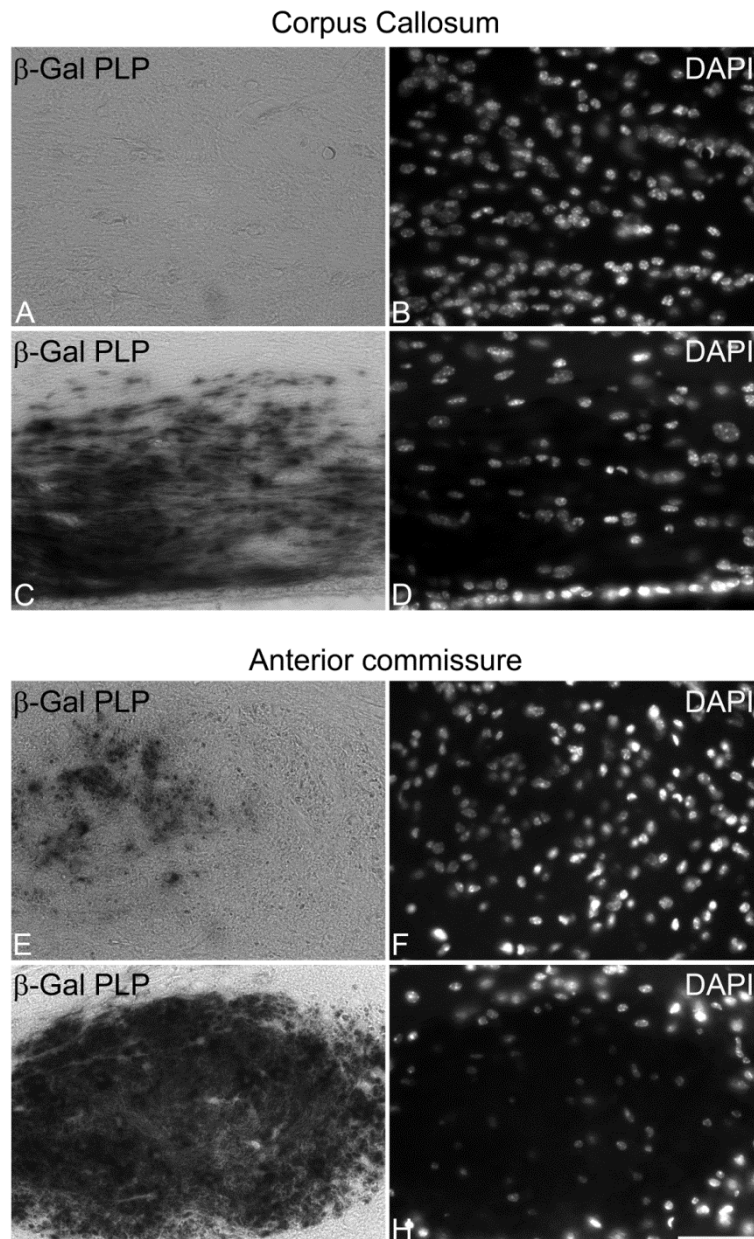


**Figure 53. The cell density appeared normal in white matter regions where donor cells populated and myelinated the white matter.**

Micrographs from two prominent white matter tract regions, the corpus callosum (A - D) and the rostral part of the anterior commissure (E - H, x400, scale bar 50 $\mu$ m), from #72 homozygote mice 120 days after neonatal implantation of transgenic neurospheres containing a *LacZ Plp1* fusion gene. The myelin, which was produced by transplanted cells, stained blue (5-bromo-4-chloro-3-indolyl  $\beta$ -D-galactoside) after X-Gal treatment, due to the incorporation of the PLP/ $\beta$ -galactosidase fusion protein into the myelin sheath. Using DAPI as a nuclear stain, there were obvious differences between regions where there was extensive myelin formation of transplant origin compared to a similar region with only a few or no myelin sheaths from transplanted cells. When comparing the areas without (B) or with only few (F) transplanted cells there was a visible reduction of cell nuclear density in the anterior commissure (D) and in the corpus callosum (H) when myelinating oligodendrocytes of transplant origin were present.

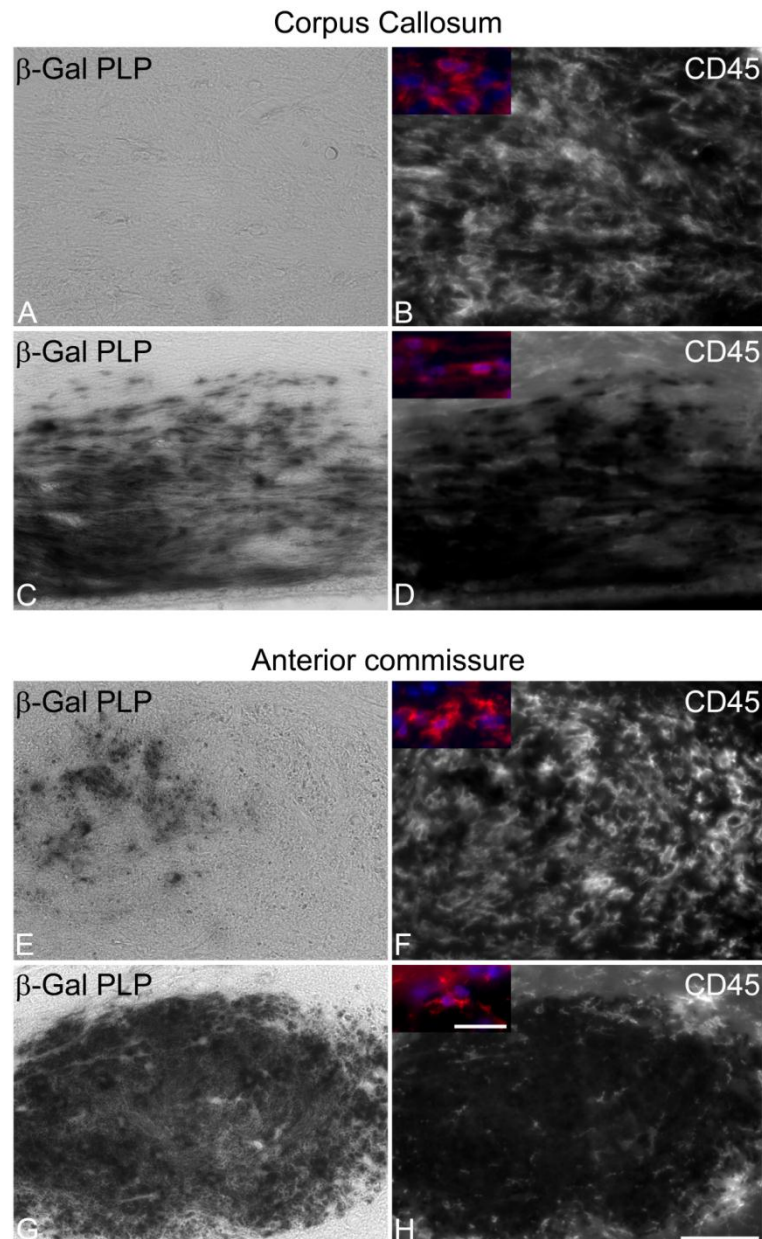


**Figure 54. The inflammatory response was reduced in white matter regions if the #72 CNS was populated by transplanted, Plp1 expressing oligodendroglia.**

Micrographs from two prominent white matter tract regions, the corpus callosum (A - D) and the rostral part of the anterior commissure (E - H, x400, scale bar 50µm), from #72 homozygote mice 120 days after neonatal implantation of transgenic neurospheres containing a *LacZ Plp1* fusion gene. A marked microglial response was present in regions containing none or only a few donor cells (A, B, E, F). This was in contrast to regions where many myelinating donor cells were present (C, D, G, H, x400, scale bar 50µm). In the myelinated regions, the microglia appeared normal. This suggested that the previously observed reduction of cell nuclei in regions where extensive amounts of myelin of donor cell origin were synthesised was mainly due to a reduction of CD45 positive leukocytes. Note that the 5-bromo-4-chloro-3-indolyl β-D-galactoside appeared dark when using the red spectra in immunofluorescence microscopy.

## 4.5 Discussion

In this study I assessed the role of the OPC intrinsic and the OPC extrinsic compartments in remyelination failure in the #72 mouse corpus callosum, using cell culture and cell transplantation techniques. The *in vitro* and *in vivo* results suggest that there is mainly an intrinsically mediated impairment in OPC function contributing to the remyelination failure. The reduced cell development of OPCs appears to be age related, as neonatally derived #72 OPCs developed comparable to wild type cells *in vitro*. The *in vivo* evaluation of the OPC extrinsic compartment by using neurosphere cell transplants showed that the axons are permissive for remyelination in the adult #72 corpus callosum.

This suggests that the OPC differentiation block and the remyelination failure, which has been observed in adult #72 mouse *in situ* is most likely cell intrinsically mediated.

The development of an age dependent OPC differentiation block mediated by cell intrinsic abnormalities results in a limited or even absent endogenous remyelination response. Whether endogenous remyelination can be stimulated in this model is questionable and the benefit is doubtful since differentiating OPCs would still harbour the gene defect, which is known to lead to unstable myelin sheaths. This raises the question of whether it would not be more beneficial to patients suffering from PMD caused by gene duplication to consider early replacement of endogenous OPCs with genetically normal glial progenitor cells, rather than to initiate treatment during the stage of progressive demyelination. By transplanting neurospheres, which are wild type to the *Plp1* gene, I provided proof-of-principle for the potential of cell transplantation into the neonate as a therapy for PMD caused by gene duplication.

### 4.5.1 Impaired OPC differentiation is age dependent in #72 mouse

Here I attempted to assess the differentiation potential of adult #72 OPCs, compared to normal age-matched OPCs, in the absence of confounding environmental factors, using cell culture. However, using an established protocol

to isolate OPCs, I was unable to obtain pure OPCs without contaminating microglia/macrophages. To eliminate the contaminating cells, I attempted to enrich for OPCs using a magnetic bead separation method. However, the cell yield was prohibitively low and the cells became severely damaged during the purification procedure and did not survive *in vitro*. Furthermore the total cell yield obtained per experiment using the Percoll gradient separation was maximally 600000 cells and was considered too low for FACS sorting of OPCs and microglia/macrophages.

Since the contaminating microglia/macrophages from the demyelinated #72 corpus callosum could potentially influence the differentiation potential of the OPCs, it was imperative that the normal OPCs and the #72 OPCs were cultured under the same conditions. In order to be able to distinguish the two genotypes, the normal OPCs were generated from mice expressing GFP under the  $\beta$ -actin promoter, rendering the cells green.

Under these conditions, adult #72 homozygote OPCs had a reduced process outgrowth compared to adult wild type OPCs. In contrast, #72 OPCs derived from neonates differentiated similarly to wild type OPCs, suggesting that the genotype of the cells alone is not responsible for the impaired differentiation. Rather, factors specific to the adult #72 OPCs, seem to play a role in impairing the process growth. Assuming this is also true *in vivo*, the impaired morphological development would be predicted to lead to a delayed or reduced development of a myelin sheath. Axonal glial interactions, for example as mediated through NRG1-III (Brinkmann et al., 2008), are important for the induction of remyelination in the CNS but appear not to be the sole required component. Instead the remyelination process is also influenced by a complex interaction of different secreted myelin inducing signals such as insulin growth factor 1 (Carson et al., 1993), apotransferrin (Marta et al., 2003) and astrocyte leukaemia inhibitory factor (Ishibashi et al., 2006;Nave, 2010a). The time window, where the remyelination process is positively influenced after the demyelination, is thought to be limited and something as simple as a delay in OPC differentiation has been shown to be sufficient to impair the remyelination process (Fancy et al., 2009). With slow OPC differentiation and growth, as might be the case in the #72 adult OPCs, which leads to a prolonged delay of the

remyelination process by delayed axonal-glia interactions, the extracellular myelination permissive environment might change to a more restrictive one, which would additionally contribute to an OPC differentiation block (reviewed in Fancy et al., 2010).

To find an explanation for the abnormal *in vitro* growth of differentiating OPCs, it may be relevant that the DM20 transcript and protein is expressed in pre-myelinating oligodendrocytes *in vitro* (Yamada et al., 1999) and in a subset of murine spinal cord OPCs (Dickinson et al., 1996) before active myelination takes place. In the *Plp1* gene overexpressing mice, both PLP and DM20 will be overexpressed. Although the published results are from normal embryonic cells and observed *in vivo* during embryonic development up till P20, the results may be extrapolated to explain the differentiation block in adult #72 homozygote OPCs. If chronic abnormal overexpression of *Dm20* into adulthood is present in #72 OPCs, a low grade accumulation of DM20 may occur with time. This low grade accumulation could potentially stress cells, leading to an inhibitory effect on adult OPC differentiation during the demyelinating process. Further evidence that overexpression of DM20 alone can cause late onset myelin impairment is derived from a mouse model where overexpression of *Dm20* only has been shown to induce a slowly progressing demyelinating phenotype, which developed over 8 months (Mastronardi et al., 1993) suggesting that accumulation of DM20 as a minimum impairs myelin integrity and, over time, potentially the capacity for remyelination. However, DM20 expression in non myelinating cells has only been demonstrated in the spinal cord and around the ventricular zone between E12 and E14 (Yu et al., 1994) and it is questionable if DM20 is expressed in OPCs at all and if DM20 plays a role in the #72 mouse model.

An age dependent derangement of intracellular pathways may be responsible for the differentiation block of OPCs. Histone deacetylase (HDACs) induced deacetylation of remyelination promoter regions is an important step in the regulation of remyelination. With age the regeneration in white matter generally becomes altered, amongst other mechanisms by a reduction in the HDAC activity, leading to impaired remyelination (Shen et al., 2008). Alteration of HDAC1 and/or HDAC2 has been shown to lead to  $\beta$ -catenin stabilisation, a pivotal part of the canonical Wnt pathway, which resulted in blocked OPC

differentiation (Ye et al., 2009). The canonical Wnt pathway has been investigated in Chapter 3 and abnormal prolonged activation had not been observed. However, the apparent normal development of neonate OPCs in my *in vitro* experiment still underlines an age dependent component leading to an OPC differentiation block.

This is in contrast to the similar study by (Ma et al., 2006) where they stated that “The ability of oligodendrocytes from older *Plp1* gene overexpressing transgenic animals to produce a myelin membrane-like structure was not impaired when cultured *in vitro*, which indicates that the lack of remyelination is not simply caused by changes in the intrinsic properties of the oligodendrocytes.” Nevertheless, this study is inconclusive and while Ma et al. reported the characteristics of adult OPCs in the brain or in isolated form of the 4e-PLP model, there is no evidence in the literature (including publications cited by Ma) to show that the brain is demyelinated and that a remyelination failure occurs in the 4e-PLP model.

Another study by (Karim et al., 2010) however, showed that the development of oligodendrocytes derived from P5 #72 mouse spinal cord developed significantly less membranous sheaths compared to the wild type cells in cultures. The observed differences were reversible by applying siRNA to suppress PLP overexpression *in vitro* (Karim et al., 2010). In my study I did not see any difference in development of #72 and wild type neonatal brain derived OPCs. However it is difficult to compare the study from (Karim et al., 2010) with my experiment because firstly they used a different cell isolation protocol, where a mixed population of OPCs and young oligodendrocytes were cultured. This is in comparison to my study where only OPCs, which will develop differently from young oligodendrocytes, were cultured. Secondly they cultured only spinal cord derived cells, which is in contrast to my study, where I only cultured cerebral derived OPCs, which are known to have a different developmental background (Kessaris et al., 2006). Thirdly in my study the significant effect occurred only in adult OPCs and (Karim et al., 2010) did not investigate adult cells.

PLP expression is present in isolated OPCs after 7DIV (data not shown) and, due to the primary genetic defect leading to the overexpression of PLP, may

interfere with the differentiation phase eventually being responsible for the impaired development in #72 OPCs. On the other hand PLP expression starts after the OPC has differentiated into an oligodendrocyte and it shows that the OPCs can differentiate *in vitro* under ideal conditions which may lead to the reduced cell growth. However PLP expression is also present in the neonatally derived OPCs after 7DIV and these cells developed similarly compared to the wild type. Again an age dependent component is probably involved in the development of impaired differentiation.

Finally the ability of adult #72 to differentiate into PLP expressing oligodendrocytes *in vivo* also suggest that with age changes in the cell extrinsic component may also contribute to the OPC differentiation block.

#### **4.5.2 The adult #72 homozygote corpus callosum is permissive for (re)myelination when neurospheres are transplanted.**

Transplanted multipotent cells from the neuroglial lineage have been shown to be capable of restoring demyelinated areas in young and adult genetically altered mouse models of dysmyelination, including the myelin deficient (*md*) rat (Learish et al., 1999;Brustle et al., 1999) and the *shiverer* mouse (Warrington et al., 1993;Nistor et al., 2005;Windrem et al., 2008). The myelination capacity and the effect after intravenous and intracranial injection of adult neurospheres in chronic EAE mouse models have also been evaluated (Pluchino et al., 2003;Einstein et al., 2006). However, the permissiveness for remyelination in the #72 homozygote mouse model has never been investigated and I used the known (re)myelinating potential of neurospheres in this study to evaluate the role of the cell extrinsic compartment on remyelination failure in the #72 homozygote mouse. I also decided to use neurospheres for this study, because like rat OPCs, but in contrast to mouse OPCs, they can be generated in large numbers (Kondo and Duncan, 2009)

In my study I showed that neurospheres derived from neonatal wild type mice transplanted into demyelinated corpus callosum survive, integrate and locally (re)myelinate the #72 homozygote CNS. Electron microscopy was used to confirm

that the newly generated oligodendrocytes formed compact myelin sheaths. I was unable to confirm that the sheaths that were imaged by EM were derived from the LacZ expressing cells, because the X-gal staining could not be discerned by EM. However, since demyelination was virtually complete at this age, the relative abundance of sheaths in the transplanted regions suggested that they were derived from the transplanted cells.

Considering the short time given for the transplanted neurospheres to differentiate and remyelinate, the local remyelination process appears to be relatively effective in the #72 homozygote corpus callosum after transplantation. This finding suggests that the OPC extrinsic compartment is, to a certain degree, permissive for remyelination. The results show that the axons are capable of being (re)myelinated. The transplants survived and remyelinated in an area with a marked activated microglial/macrophage population, many of which expressed sialoadhesin. Sialoadhesin positive microglia/macrophages have been shown to contribute to demyelination in another *Plp1* gene overexpressing transgenic mouse model (#66) (Ip et al., 2007), possibly through the recruitment of pathogenically relevant CD8+ve T cells. In my study the microglia/macrophages population seemed not to interfere with the transplanted cells, at least within an intermediate timeframe (14 days).

With regard to remyelination failure, the influence of activated microglia on OPCs is controversial. A study using cell culture and tissue slice culture suggested that the activation of microglia supports OPC proliferation (Filipovic and Zecevic, 2005). However this was an *in vitro* study and the proliferation of OPCs is not indicative that differentiation and remyelination will eventually take place. On the other hand it has been observed that after suppressing the microglial response in a dysmyelinating rat model using minocycline *in vivo*, more effective remyelination after neuronal stem cell transplantation took place, suggesting that activation of microglia inhibits the remyelination process after transplantation (Zhang et al., 2003). But then again a more recent study by the same group showed that genetic depletion of microglia/macrophages worsens disease severity in a mouse model of globoid cell leukodystrophy (Kondo et al., 2011). In general, microglial/macrophage responses (Kotter et al., 2001;Kotter et al., 2005) and acute inflammation (Foote and Blakemore,

2005a;Setzu et al., 2006).have been shown to promote OPC differentiation and remyelination

It is important to keep in mind that after cell transplantation, an acute inflammation will result, additional to the existing chronic inflammation. This will cause considerable change in the OPC extrinsic environment and could potentially shift the inhibitory environment into a permissive, supportive environment. It has been shown that an acute lesion induced on top of a chronic inflammatory demyelinated lesion has a promoting effect for implanted neuronal stem cells to develop into myelinating oligodendrocytes (Foote and Blakemore, 2005a). It may well be that in my study the cells were only capable of remyelinating the demyelinated area because of the change in environment caused by external manipulation. A certain capacity of immunomodulation has also been attributed to neonatal neurospheres themselves after implantation into acute and chronic EAE mice (Einstein et al., 2006;Einstein et al., 2003).

By using GFP expressing neurospheres, I was able to show that the transplanted cells differentiated into astrocytes, as well as into oligodendrocytes. Astrocytes are known to influence myelination either positively by secreting for example IGF-1 (Liu et al., 1994) or CNTF (Albrecht et al., 2003) or negatively by secreting semaphorin 3 (Syed et al., 2011;Williams et al., 2007a) or hyaluronan (Back et al., 2005; reviewed by Williams et al., 2007b). The bivalent role of the astrocyte is also influenced by their functional status, where activated astrocytes are considered to promote remyelination and reactive astrocytes to inhibit the remyelination process (reviewed in Nash et al., 2011). Therefore the neurosphere derived astrocytes could also influence the remyelination potential of the environment and since the astrocytes of neurosphere origin are in close physical relationship to the transplanted OPCs, a locally confined supportive environment could be the reason for the observed focal remyelination.

It is possible that some of the newly formed myelin sheath originated from endogenous OPCs that acquired remyelination competence in the altered environment. Nevertheless, if there was a response by the endogenous OPC population then it did not seem to be extensive, since most of the MBP positive sheath-like structures were also GFP positive, confirming that they were derived

from cells of transplant origin. Taking the findings from the cell intrinsic evaluation of the *in vitro* experiment into consideration, the adult #72 homozygote OPCs seemed in general to be impaired in their differentiation into oligodendrocytes.

A more parsimonious view, but one that cannot be completely discounted, is that failed remyelination could also be due to the short life span of the #72 homozygote mice. It may be that remyelination is just about to begin effectively. However since none of the mice during this study period had survived longer than 135 days it is difficult to say if this is the case. An answer to this unsolved question may be found when looking at the #72 homozygote optic nerve, where two pathologically distinct regions can be identified at P120 (Edgar et al., 2010). The retinal region, which seems to be demyelinated earlier than the rest of the optic nerve turns into a non-inflammatory, chronic demyelinated region where OPCs are still present (shown [in Chapter 5 Evaluation of advanced diffusion weighted magnetic resonance imaging as a molecular probe to distinguish between acute and chronic demyelination in the optic nerve of the #72 mouse](#)). The chiasmal region shows a high degree of demyelination but is also filled with activated microglia (as seen in the Chapter 5 and in Edgar et al., 2010) which is believed to be a less advanced stage of the disease process. Given the presence of an acute inflamed demyelinating region and a chronic “silent” demyelinated region, the pathology in the #72 homozygote seems to evolve towards a chronic demyelinating disease.

#### 4.5.3 Early post natal transplanted gene wild type neurospheres integrate and form a stable myelinating cell population in the #72 CNS - a potential treatment for PMD

Duplication of the X-linked *PLP1* gene is the most common cause of PMD. In the absence of a treatment for PMD, the replacement of genetically defective oligodendrocytes with intact ones through cell transplantation represents a potential therapeutic approach. PMD spans a broad clinical spectrum, ranging from congenital forms associated with an almost complete lack of CNS myelin to milder forms with nearly normal numbers of, but structurally defective, myelin sheaths. For cell transplantation to bring about functional recovery in PMD, transplanted cells would have to produce and maintain widespread myelination of the CNS. While previous studies have shown that transplanted cells can form large amounts of myelin in murine (Hammang et al., 1997; Learish et al., 1999) and canine (Archer et al., 1997; Milward et al., 1997) models of the most severe forms of the disease, studies to test the feasibility of this approach in animal models of milder (but still profoundly disabling forms) are lacking. Here I showed that the transplantation of neural stem cells at multiple sites, into the brain of new-born *Plp1* gene overexpressing mice led to the production and maintenance of CNS myelin in competition with the myelination competent, but defective, endogenous cells.

I showed, using X-gal staining and electron microscopy that the transplanted neurospheres differentiated into myelin forming oligodendrocytes that populated diverse white matter tracts in the forebrain. Transplant cell derived sheaths were not evident in P7 brains by X-gal staining, but could be detected by P14. Given that increasing volumes of myelin were present with time after transplantation, it seems most likely that at least some of the myelin that was present at P120 had been generated much earlier. Thus, I tentatively concluded that, unlike the endogenous myelin, the transplant derived myelin does not undergo degradation.

The X-Gal staining, however, turns the cell in vicinity of intracellular  $\beta$ -galactosidase blue. This process causes unexpected difficulties, when using the

tissue for immunofluorescence microscopy. The blue product (if present in high concentration) obliterates the epifluorescent signal, as seen in my study. This effect on epifluorescent microscopy renders the image difficult to interpret. A simple and effective way to solve this problem is to avoid using the X-Gal technique and to visualise intracellular  $\beta$ -galactosidase by using normal antibody labelling technique.

Since myelin degradation in the *Plp1* overexpressers has been shown to be related to the presence of sialoadhesin positive microglia/macrophages (Ip et al., 2007), I examined the relationship between microglial/macrophage cell density and transplant myelin. Given the previously described pathological changes involving the activation of microglia in the #72 homozygote mouse corpus callosum, it is of interest that the neonatally transplanted cells appear to interact locally with the environment. In areas, where myelin originated mainly from transplanted cells, the cell density was visible lower than in areas containing no or only a few myelin forming transplanted cells. Regions where a substantial amount of transplanted cells turned into a stable, myelin forming population at P120 seemed to have a less severe microglial response, suggesting that the intact transplants don't elicit the microglial response, or when looking at this finding the other way round, the progressive breakdown of the abnormal #72 homozygote mouse myelin most likely fuels the microglial response, starting a negative spiral of increased demyelination and probably impaired remyelination.

The distribution cells derived from the neonatal transplanted neurospheres demonstrates that the transplanted cells migrate into white and grey matter. Why the transplants grow in a patchy pattern cannot be explained at this stage. However when looking at other studies, similar patterns have been observed (Archer et al., 1997; Learish et al., 1999; Windrem et al., 2004; Yandava et al., 1999) and a competition between the endogenous and transplanted cells probably occurs during development, where the successful population finally establishes locally, possibly as a result of clonal expansion (Edgar et al., 2002).

Most experiments involving neuronal stem cell transplantation into murine neonates were either of shorter duration (Learish et al., 1999; Webber et al.,

2009;Yandava et al., 1999), in normal animals (Learish et al., 1999), in immunocompromised animals (Windrem et al., 2008) or in *shiverer* mice, where severe dysmyelination is already present during development (Nistor et al., 2005;Windrem et al., 2004;Windrem et al., 2008;Yandava et al., 1999).

The long term survival of cells without immunosuppression is of interest. As others have shown in different models of dysmyelination (Windrem et al., 2004;Archer et al., 1997) the absence of graft rejection is probably due to perinatal toleration of the injected cells (Windrem et al., 2004;Ridge et al., 1996). This shows that at least in mice and dogs, neuronal stem cells can be introduced into the neonate CNS parenchyma without the necessity of immunosuppression. This finding could be of importance for humans suffering from severe PMD, where neonatal injection of neuronal stem cells is FDA approved (<http://www.stemcellsinc.com/Therapeutic-Programs/PMD.htm>).

## 4.6 Conclusion

I have shown that an OPC intrinsic impairment is most likely the cause of the remyelination failure in the #72 homozygote mouse. Based on *in vitro* and *in vivo* data the adult OPCs seem to be impaired in differentiation, which causes the OPCs to be blocked in a premyelinating state, failing to initiate the remyelination process. The *in vivo* experiments have shown that the cell extrinsic compartment seems to be permissive for a certain degree of remyelination, or at least that the axons are not inhibiting myelination after implantation with normal neurospheres derived from young mice. However, I cannot exclude the possibility that the environment becomes permissive to myelination due to the effect of the transplantation itself.

I have also shown that the neurospheres derived from young animals integrate, myelinate and persist without immunosuppression in the #72 homozygote mouse brain, either after neonatal or adult injection. In particular, the data obtained from neonatal transplantation of stem cells is of practical interest. Overexpression of the *PLP1* gene is the most frequent genetic aberration leading to PMD in humans (Sistermans et al., 1998) and the #72 mouse is a valid model of

this disease. Post natal injection of stem cells has been approved in patients with PMD and is a potential treatment option. The results show the potential of early stem cell injection to compete and integrate into #72 homozygote CNS tissue, with stable long term myelin formation. With this observed finding in mind, transplantation of neuronal stem cells may ameliorate or even result in the rescue of the PMD phenotype in some human patients.

## **5 Evaluation of advanced diffusion weighted magnetic resonance imaging as a molecular probe to distinguish between acute and chronic demyelination in the optic nerve of the #72 mouse**

### **5.1 Introduction**

In Chapter 3 and 4 I showed that the #72 mouse develops a progressive demyelination with failed remyelination. A previous study (Edgar et al., 2010) of the optic nerve of this model demonstrated a progressive demyelination that resulted in the development of two spatially separate regions, a chronic demyelinated region without inflammation and an acute inflamed demyelinated region. MRI has facilitated the detection and distribution of CNS pathologies *in vivo* (Ciumas et al., 2008; Fox, 2008; Guttmann et al., 1995; Inglese et al., 2005b; Inglese et al., 2005a). However, the specificity is still low and identification of lesion type often remains speculative. New MRI techniques, such as diffusion weighted MRI, which aims to serve as a molecular probe, have been developed but remain poorly understood. The #72 mouse brain has previously been analysed using diffusion weighted MRI (DW MRI) (Ruest et al., 2011), showing that DW MRI is a valuable tool for detecting widespread white matter changes in relation to myelin integrity. I speculated that the #72 mouse optic nerve, with its clear anatomical features and its spatially defined histopathology (Edgar et al., 2010), would make an ideal model to evaluate the capability of modified DW MRI sequences to distinguish white matter lesion types.

#### **5.1.1 The impact of conventional magnetic resonance imaging in diagnosing central nervous system white matter changes**

Historically, the diagnosis and monitoring of progression of demyelinating lesions *in vivo* has been difficult. In order to investigate lesion development, surgical procedures to obtain serial biopsy samples from CNS tissue were necessary.

However, the invasive nature of this procedure meant that disease progression was altered (complicating evaluation of disease development). Additionally, the surgical procedures were associated with detrimental effects on the animal/patient. The full distribution and extent of the pathology could previously only be assessed at the point of necropsy.

With progress in the development of advanced imaging modalities, including magnetic resonance imaging (MRI), *in vivo* evaluation and monitoring of white matter lesions dispersed over the whole CNS, has become possible. In the case of multiple sclerosis, MRI has improved the accuracy of diagnosing, localising and monitoring the course and extent of white matter pathology (reviewed in Ciumas et al., 2008;Inglese et al., 2005b). Repeated MRI allows mapping of lesion distribution and reveals temporal changes in lesion size and location (Guttmann et al., 1995; reviewed in Ciumas et al., 2008). One major weakness of conventional MRI sequences in the characterisation of white matter pathology is the low sensitivity to distinguish lesion types, in particular between areas of acute active inflammation with ongoing demyelination and inactive, chronic demyelination (Bitsch et al., 2001; reviewed in Inglese et al., 2005b).

### **5.1.2 The use of diffusion weighted imaging of central nervous system white and grey matter in the research and clinical settings**

The provision of a modality capable of distinguishing active inflammation with ongoing demyelination from inactive, chronic demyelination would have a major impact on monitoring disease development, response to treatment and accurate determination of the long-term prognosis for the affected patient. It may also provide greater insight into myelination dynamics that lead to the failure of remyelination observed in experimental demyelinating models and in MS.

One modality that might permit differentiation of lesion types is diffusion weighted imaging (DWI). DWI sequences measure the movement of water molecules within tissues (Basser et al., 1994; reviewed in Basser and Oezarslan E, 2009). The diffusion of water molecules refers to the natural phenomenon of random thermal motion that all molecules at temperatures above zero degrees

Kelvin undergo; also referred to as Brownian motion (reviewed in Mori and Zhang, 2006). In liquids, individual molecules can move freely, with the diffusion coefficient depending on molecular size, viscosity and temperature of the media (reviewed in Beaulieu, 2002;Mori and Zhang, 2006). In tissue such as the white matter, the degree and direction of diffusion of water molecules is restricted by the tissue microstructure (Moseley et al., 1990a;Turner et al., 1990). Intracellular structures, cell membranes and tissue properties (including cell type, density, size and integrity, as well as extracellular matrix) all influence water diffusivity (reviewed in Beaulieu, 2009).

The sensitivity of DWI in detecting changes in water diffusion due to pathological processes in the CNS means that DWI is being increasingly used in clinical applications (Warach et al., 1995;Larsson et al., 1992; reviewed in Goldberg-Zimring et al., 2005). One example is in the early detection of cerebral ischemia: while standard sequences still appear normal during the pre-acute stage, pathological changes are usually already apparent in DWI (Mintorovitch et al., 1991;Moseley et al., 1990b;Warach et al., 1995). Following white matter ischemia, DWI differentiates cytotoxic oedema, which is present soon after the ischaemic event, and vasogenic oedema, which is present at a later stage (Ebisu et al., 1993). DWI is also more sensitive in detecting white matter lesions than standard T2 weighted magnetic resonance sequences, as demonstrated in a monkey model of experimental autoimmune encephalitis (Heide et al., 1993).

### **5.1.3 Diffusion tensor imaging and its application in investigating central nervous system white matter physiology and pathology**

In order to measure diffusion, diffusion sensitising gradients are applied to a pulsed gradient spin echo (PGSE) sequence (reviewed in Beaulieu, 2002). In “standard” diffusion weighted imaging (DWI) the diffusion sensitising gradients are applied along a single direction, sensitising the signal to diffusion only along that direction. Two gradient pulses separated by a defined time and a gradient strength of a defined duration are applied to the scan area. These adjustable parameters are part of the *b*-value, which is a diffusion sensitising factor (reviewed in Basser and Oezarslan E, 2009). The attenuation of the signal

measured after applying the sequence is caused by diffusion of the ‘labelled’ water molecules (Norris, 2001).

The  $b$ -value is defined as follows:

Equation 1: 
$$b = (\gamma G \delta)^2 \left( \Delta - \frac{\delta}{3} \right)$$

$\gamma$  is the magnetogyric ratio (depends on the nucleus used e.g.  $^1\text{H}$ ),  $G$  is the gradient strength,  $\delta$  is the duration of the applied gradient and  $\Delta$  is the time between the two gradient pulses (called the observation time).

Diffusion can be measured in any direction using a linear combination of the X, Y and Z gradients (Basser et al., 1994; reviewed in Jones, 2009). This directional application of the gradient is also used in diffusion tensor imaging (DTI), a modification of DWI (Basser et al., 1994; reviewed in Jones, 2009). Using the assumption that there is a Gaussian diffusion process and that the signal decay occurs mono-exponentially as a direct result of water molecule diffusion, DTI requires diffusions to be measured along a minimum of 6 directions. In DTI, diffusion in each direction is measured using a PGSE pulse sequence with two different  $b$ -values, usually 0 and  $\sim 1000 \text{ s/mm}^2$ . This allows the calculation of diffusion and diffusivity in any direction of interest (reviewed in Jones, 2009).

Quantification of diffusion directionality, which is the basis of DTI, is possible because diffusion can be anisotropic or isotropic, depending on the microstructure of tissue (Doran et al., 1990; Moseley et al., 1990a). Anisotropy arises when the water molecule movement is more restricted in certain directions than others (Doran et al., 1990; LeBihan D. et al., 1993; Moseley et al., 1990a; reviewed in Beaulieu, 2002; Mori and Zhang, 2006). Faster diffusion in certain directions compared to others results in a specific directionality of bulk water molecule movement in tissue, which can be expressed in terms of an ellipsoid. In contrast, isotropic diffusion is present when water diffusion is equal in all directions, and can be expressed in terms of a sphere (reviewed in Beaulieu, 2002; Mori and Zhang, 2006). As mentioned before, water diffusivity can be measured in different directions, allowing determination of the direction of the largest versus the mid-range versus the lowest principal diffusivity. The

higher the anisotropy of tissue, the simpler it is to determine the main directionality of diffusion by means of DTI (reviewed in Mori and Zhang, 2006). High anisotropy is particularly evident in tissue such as the CNS white matter (reviewed in Beaulieu, 2002), which comprises parallel arrays of nerve fibres ([Figure 55](#)).

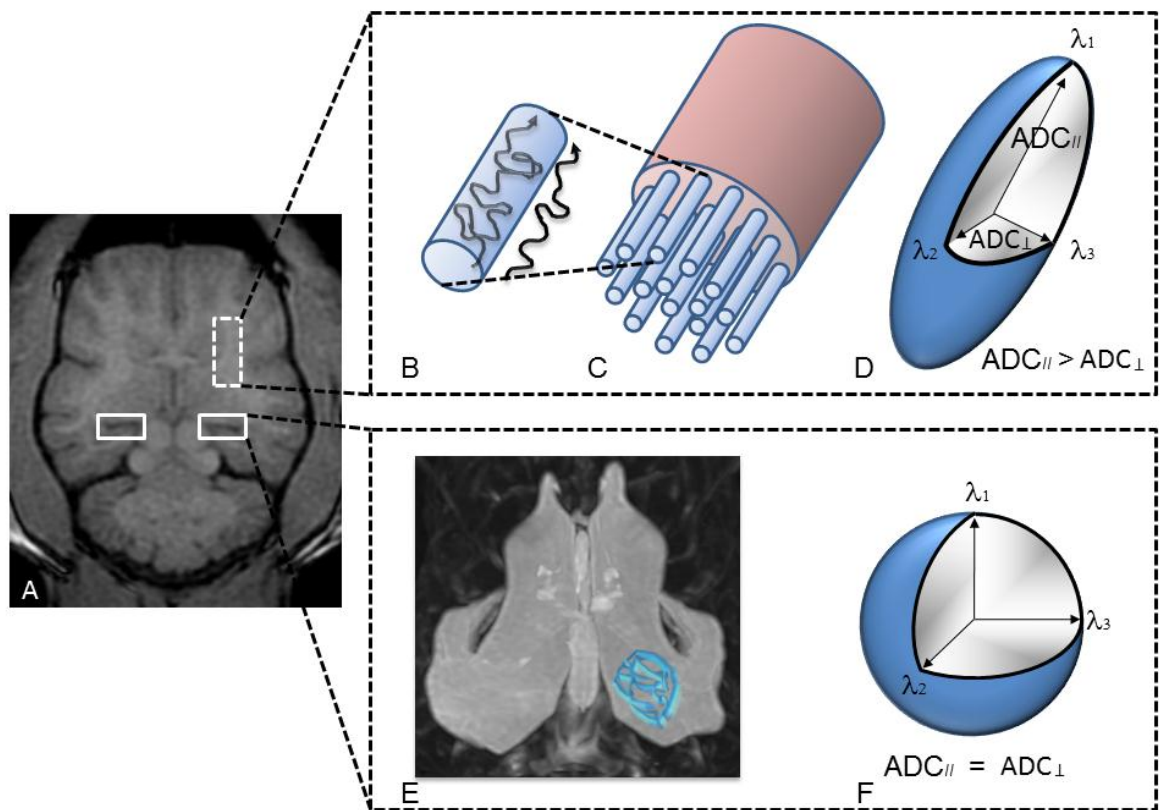


**Figure 55. Examples of anisotropic and isotropic diffusion.**

Dorsal view of a 3D fast spoiled gradient echo image of a cat brain (A). White matter tracts such as the internal capsule (rectangle with dotted lines) are composed of dense axonal bundles. The strict anatomical organisation of nerve fibers guides the bulk diffusion along a main direction, which is the basis of anisotropic diffusion in white matter (B, C). Anisotropic diffusion is expressed in form of a diffusion ellipsoid (D). The diffusion ellipsoid reflects the difference between the parallel ( $ADC_{||}$  or  $\lambda_1$ ) and perpendicular ( $ADC_{\perp}$  or  $\lambda_2$  and  $\lambda_3$ ) diffusion in relation to the neural fibers, showing that diffusion is faster in the parallel than perpendicular direction to the nerve fibers ( $ADC_{||} > ADC_{\perp}$ ). An example of isotropic diffusion in the CNS is found in the ventricular system (rectangles with solid lines in A; E; three dimensional reconstruction of the ventricular system in a dog), which contains cerebrospinal fluid (CSF), a virtually acellular fluid with low protein content. In the CSF filled ventricular system, diffusion similar in all directions, and can be expressed in terms of a sphere. (F,  $ADC_{||} = ADC_{\perp}$ ). Adapted from (Beaulieu, 2009).

Studies aimed at understanding the tissue correlates of the DTI parameters have shown that axons, with the axonal membrane as the main barrier, are the main contributors to anisotropy (reviewed in Beaulieu, 2002;Beaulieu, 2009). The influence of intra-axonal structures on diffusion is considered to be insignificant (Beaulieu and Allen, 1994;Ono et al., 1995;Gulani et al., 2001;Mori and Zhang, 2006). Furthermore, correlative studies in dysmyelinating and demyelinating mouse models such as *shiverer* (Nair et al., 2005;Song et al., 2002), *jimpy* (Ono et al., 1995;Harsan et al., 2007), the transgenic *olig-TTK* mouse (Harsan et al., 2006) or lysolecithin induced demyelination models (Xie et al., 2010) have shown that myelin sheaths have a modulatory effect on diffusion anisotropy. Consequently DTI sequences can be used to identify pathological changes in myelin, which interfere with the normal diffusion of water along white matter tracts (reviewed in Barkovich, 2000;Laule et al., 2007). For example, it has been shown that demyelination is associated with increased radial (perpendicular to the axons) diffusivity (Song et al., 2002;Song et al., 2005) and axonopathy with reduced axial (parallel to the axons) diffusivity (Budde et al., 2008). Interestingly remyelination reverses the changes in radial diffusivity (Harsan et al., 2006).

The potential influence on diffusion measures of other white matter components such as of astrocytes, microglia, trafficking immune cells and OPCs has often been neglected. However, recent studies investigating the role of extra-axonal factors on diffusion parameters have shown that these cells also influence diffusion (Harsan et al., 2007;Xie et al., 2010;Ruest et al., 2011), albeit to a considerably lesser extent than the nerve fibres themselves.

#### **5.1.4 Multiexponential signal decay - an opportunity to differentiate between inflammation with acute demyelination and chronic silent demyelination?**

In DWI, the diffusion of water molecules (i.e. H nuclei) results in signal attenuation, which can be directly related to diffusion rate. The higher the diffusion rate the more pronounced is the signal decay (Westbrook et al., 2005;Jones, 2009). Generally, diffusion is considered to produce

monoexponential signal decay. However, a number of studies have shown that there is non-monoexponential signal decay if the DWI sequence is extended by applying multiple increasing  $b$ -values, extending up to  $40000 \text{ s/mm}^2$  (Stanisz et al., 1997; Clark and LeBihan D., 2000; Ronen et al., 2006). The origin of biexponential, or even triexponential (Assaf and Cohen, 1998) signal decay is not fully understood and various models have been investigated and proposed.

Some groups have suggested that biexponential decay is the result of microstructures restricting or hindering diffusion in characteristic ways (Stanisz et al., 1997; Pfeuffer et al., 1999). If this is assumed to be the case then multiexponential diffusion decay can be analysed by dividing the data into two or more independent monoexponential diffusion components, each representing a distinct micro anatomical entity within the tissue. In white matter these micro anatomical entities have been classified as the intracellular space versus the extracellular space, or more specifically, the intraaxonal space versus the extra axonal space including the myelin sheath (reviewed in C. Beaulieu, 2002).

Others state that the compartmentalisation into slow and fast diffusion does not sufficiently explain the presence of biexponential signal decay (Niendorf et al., 1996; Schwarcz et al., 2004). It has been suggested that different binding states of water molecules to protein fragments or conformational changes in proteins after injury may also contribute to the presence of the biexponential signal decay phenomenon (Schwarcz et al., 2004).

Demyelinating lesions in MS patients possess the capacity to remyelinate, even after long term disease (Patani et al., 2007; Patrikios et al., 2006). However, some chronically demyelinated regions fail to remyelinate (Chang et al., 2002). Axonal loss, which is considered to be the major contributor to permanent disability (Kornek et al., 2000; Bjartmar and Trapp, 2003; Bjartmar et al., 2003), is associated with chronic demyelination, highlighting the importance of preventing the development of chronic lesions. If a method such as DWI with multiple increasing  $b$ -values is capable of identifying lesion type non-invasively, this would substantially improve the diagnostic accuracy, inform the most suitable treatment and allow accurate determination of the long term prognosis.

I hypothesised that using multiple increasing  $b$ -values might increase the sensitivity of DWI to differentiate between different pathological states such as inflammation and demyelination versus chronic demyelination without inflammation. If true, then this technique may become particularly useful as a molecular probe for diagnosing different stages of inflammatory demyelinating white matter disease. In particular, in MS where it could help to distinguish chronic, silent demyelination and active inflamed demyelination.

#### **5.1.5 The #72 mouse optic nerve as a model system in which to assess the potential of DWI to distinguish complete demyelination from inflammatory demyelination**

Anatomically the optic nerve comprises a region of parallel axons with a defined supporting cell population. In terms of the application of DWI, the unidirectionality of optic nerve axons allows the reduction of the full diffusion tensor (as used in DTI) to two directions; parallel and perpendicular to the fibres (Tu et al., 2010). The adult #72 mouse optic nerve displays a highly reproducible persistent demyelination in the rostral segment and active demyelination with inflammation in the caudal segment (Edgar et al., 2010). The predictable lesion progression in the optic nerve of the #72 mouse creates an ideal model with which to test the hypothesis that applying multiple increasing  $b$ -values to the DWI sequence can increase the sensitivity of DWI to distinguish lesion types within nerve fibre tracts.

## 5.2 The aims of the chapter

- 1.) To establish a protocol for the preparation of isolated optic nerves for high resolution DWI of CNS white matter
- 2.) To apply DWI with multiple increasing  $b$ -values to normal, completely demyelinated and actively demyelinating optic nerve regions
- 3.) To undertake a detailed histological examination of the regions of interest of the scanned nerves for comparison with the DWI data
- 4.) To assess whether DWI with increasing  $b$ -values is more sensitive than conventional DWI using two  $b$ -values, to distinguish active demyelination from complete demyelination

## 5.3 Material and Methods

### 5.3.1 Breeding and identification of homozygote #72 mice

*Plp1* overexpressing #72 transgenic mice were generated and genotyped as described in [Chapter 2.2 Mouse breeding](#). Optic nerves from homozygote #72 and wild type mice were used.

### 5.3.2 Coil and sample holder design for mouse optic nerve DWI

#### 5.3.2.1 Coil design

Commercially available coils did not meet the requirements for scanning the small diameter of the mouse optic nerves (diameter of approximately 300 $\mu$ m each). A purpose built coil, designed and built by William Holmes and Jim McMullen was used. The coil was of a transmit/receive solenoid design, directly connected to the standard scanner electronics. In order to avoid metal related artefacts the metal part was the coil itself, for which magnetic susceptibility matched wire was used. Acrylic glass was used for the front part of the coil

([Figure 56](#)). To prevent the sample from moving during the scan, an adjustable acrylic screw was placed beneath the coil. The acrylic screw was also used to adjust the position of the samples vertically within the coil (one revolution = 1 mm movement).

### 5.3.2.2 Sample holder design

The sample holder was designed to allow three pairs of optic nerves to be imaged simultaneously. The orientation of the nerves within the sample tube was critical because diffusion was to be measured in two directions only. The sample itself had to be confined in order to avoid motion during the scan. Additionally, the samples had to be surrounded by fluid, in order to prevent them from drying out, as this would lead to irreversible tissue damage and interfere with diffusion of H<sub>2</sub>O molecules. Therefore the sample holder had to fulfil certain criteria: it had to be small in diameter to avoid movement of the optic nerve, linear, waterproof and ideally made of plastic to avoid interference with the magnetic field. A commercially available plastic tube commonly used for microinfusion in rats fulfilled all the requirements. The tube was readily available, made of plastic and had an intraluminal diameter of 500µm. Two centimetre long sections of tubing were cut to act as sample holders. These were mounted on a steel needle (0.5 x 20mm) and were left overnight on a hot plate (60°C) to straighten. A bundle of seven tubes were glued together using nail varnish to form a cylinder, which fitted tightly into a larger plastic tube. The larger tube was used as a template to define the coil diameter when the coil was built and therefore fitted securely inside the coil ([Figure 57](#)).

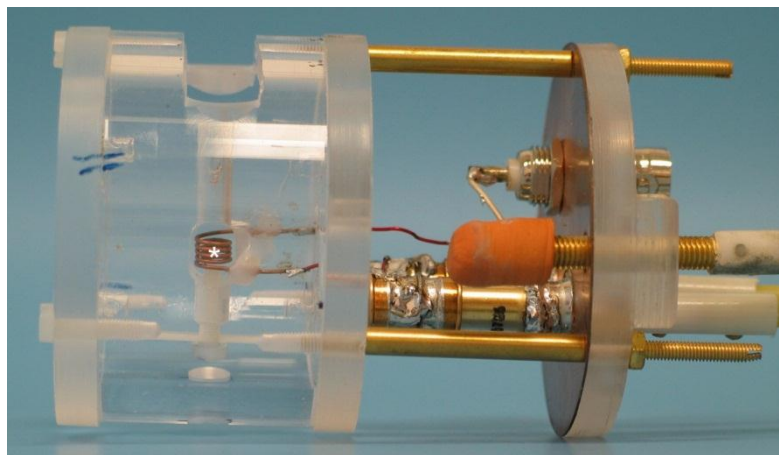


**Figure 56. Image of the purpose built transmit/receive coil.**

The scanning part of the coil, with a diameter of 4mm is marked with an asterisk. Acrylic glass was used in close proximity to the coil to avoid artefact generation. An acrylic screw (arrow) just below the coil region was used to adjust the location of the samples, and to immobilise the samples, which were placed vertically inside the coil.

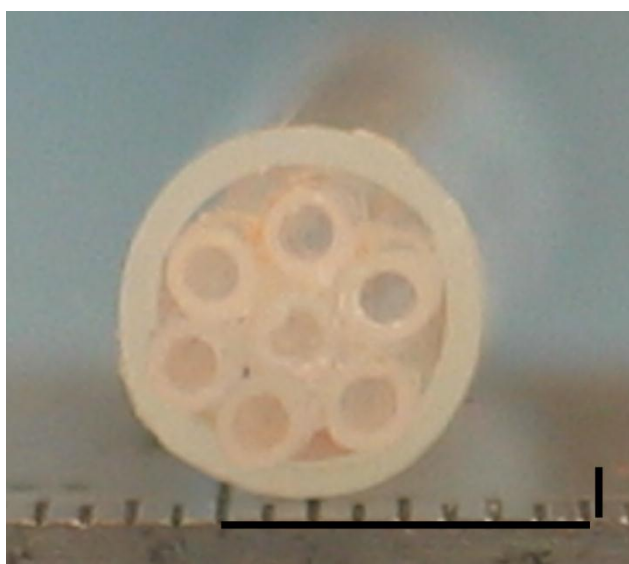


**Figure 57. Image of the optic nerve sample holder used for the diffusion weighted imaging experiment.**

Seven plastic microtubes with an inner diameter of 500 $\mu$ m, each assigned to hold one optic nerve and one to contain PBS/Multihance, were glued together using clear nail varnish. The cylinder of seven tubes was then fitted tightly into a larger sample tube with a 4mm outer diameter. The large tube was used as a template for determining the diameter of the transmit/receive coil and therefore fitted securely inside the coil (horizontal line 4mm, vertical line 0.5mm).

### 5.3.3 Preparation of optic nerves for DW MRI scan

Twelve #72 mice and six wild type mice were euthanized in a CO<sub>2</sub> chamber. Intracardiac perfusion of 0.85% saline (20ml) followed by 4% paraformaldehyde (PF, 20ml) was performed, as described in [Chapter 2.6 Tissue sampling and processing](#), for optimal tissue fixation. Immediately after perfusion, both optic nerves were dissected, leaving the eyes, the optic nerves, the chiasm and a part of the optic tract as one intact unit. The optic nerves were freed of surrounding tissue as thoroughly as possible. The optic nerves were separated from each other longitudinally at the chiasm leaving two intact single optic nerves with chiasm and optic tract. After removing the lens and retina the optic nerve was pinned down at the sclera and at the optic tract on a wax board, without applying tension, to straighten the nerve. The pinned nerves were then transferred into 4% paraformaldehyde for another six hours. Since paraformaldehyde may interfere with diffusion (Kim et al., 2009; Shepherd et al., 2009; Sun et al., 2003), extensive washing of the tissue was performed to remove all free paraformaldehyde from the tissue. After the fixation period the nerves were transferred into PBS for 24 hours at 4°C. To enhance the MR signal the PBS solution was subsequently incubated in a 2.5mM solution of gadobenate dimeglumine (MultiHance®, Bracco, 0.5M containing 334mg/ml gadobenic acid) in PBS (250µl MultiHance®/50ml PBS) for 6 days at 4°C.

On the day of the scan the nerves were removed from the wax board, submerged in a MultiHance®/PBS bath and microsurgical threads (SurgiPro® II 7-0, polypropylene, monofilament, Surgalloy) were sutured to the sclera. Each nerve was then pulled through a designated plastic microtube filled with MultiHance®/PBS solution. The optic nerves were aligned with each other longitudinally, under magnification, using the scleral-optic nerve junction as a landmark. Six microtubes were filled with three optic nerve pairs. The seventh tube containing MultiHance®/PBS only, served as a control. While still submerged in solution, the barrel containing the samples was transferred into the large sample holder ([Figure 58](#)). Once the barrel was in place the sample holder was sealed using Blu-Tack® ([Figure 59](#)). The alignment of the nerves was

verified under high magnification and a mark was placed on the holder at 1 mm and 4mm caudal to the scleral-nerve junction, using graph paper as a ruler.

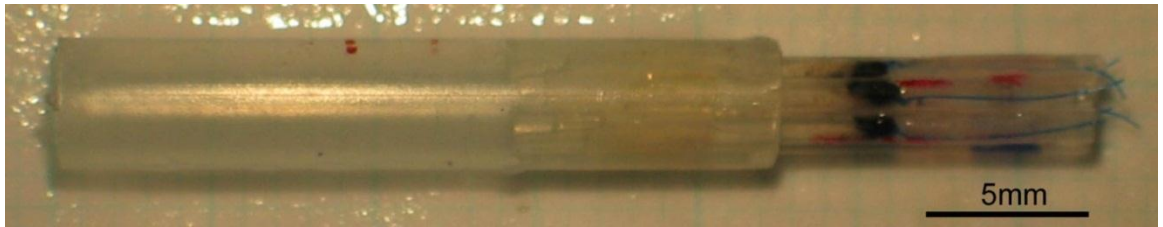


**Figure 58.** Image of the sample holder filled with seven microtubes, each containing one optic nerve or just PBS/Multihance.

Seven plastic microtubes were merged together to form a cylinder containing a total of 3 pairs of optic nerves and one empty tube filled with Multihance®/PBS. Microsurgical sutures (blue) were attached to the sclera (arrow) to facilitate placement of each optic nerve in its designated microtube.

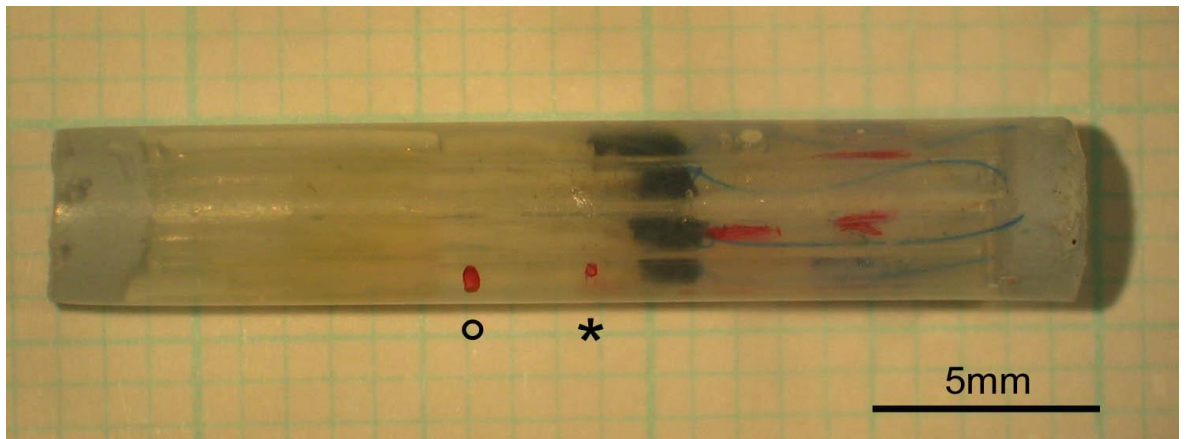


**Figure 59.** Image of a sealed sample holder containing optic nerves ready to be placed into the coil for scanning.

The large sample tube was filled with Multihance®/PBS to prevent the tissue from drying out during the scan procedure. The tube was sealed with Blu-Tack® at both ends. The scan region, which was positioned in the middle of the coil was 1mm (asterisk) and 4mm (o) distal to the scleral-optic nerve attachment. The regions were identified under magnification using graph paper and the external tube was marked with a permanent marker.

### 5.3.4 Instrumentation

The MR images were acquired on a 7 Tesla Bruker Biospin Biospec 70/30 MRI system with a micro imaging gradient insert (model BG-6) and 100-A gradient amplifiers. The gradient system provides linear magnetic field gradient pulses up to 1000mT/m.

### 5.3.5 Scan protocol

A three dimensional pilot image was acquired. As the region of interest was physically positioned in the middle of the RF coil, the centre of the scan field was in the middle region of the pilot image. The imaging slice was manually positioned to be perpendicular to the axis of the optic nerve using the pilot image. In the pulse program the diffusion sensitising gradients were defined to be parallel and perpendicular to the imaging slice, thus avoiding the need for manual adjustments to the coil placement.

The DW MRI of the optic nerves was acquired by performing a spin echo DTI with a spin echo imaging sequence (TR/TE of 500ms/24.35ms, 4 NEX). Since the directionality of the nerve fibres is known a full tensor was not required (Tu et al., 2010). Diffusion gradient pulses were instead applied along three diffusion directions, one parallel and two perpendicular directions in relation to the axonal fibre orientation. Sixteen increasing  $b$ -values were applied along each gradient directions (94.6, 270.7, 492.3, 708.9, 922.9, 1135.3, 1661.5, 2183.6, 2703.1, 3220.8, 3737, 4252.1, 4766.3, 5279.7, 5792.4, 6304.6 s/mm<sup>2</sup>). Gradient pulse timing was fixed at  $\delta = 4$ ms and  $\Delta = 16$ ms. The slice thickness was 1mm. The matrix of the scan region was 62 x 62, with a 65 $\mu$ m x 65 $\mu$ m resolution per voxel. In each sample, a water phantom was scanned simultaneously with the optic nerve samples. All scans were performed at room temperature (20°C). The diffusivity of water at room temperature is known and the water sample served as a control.

### 5.3.6 Processing and analysis of DWI data

The DWI raw data was extracted using ImageJ®. The data was further processed in MatLab®, where curve fitting, diffusion coefficient and fractional anisotropy were calculated.

### 5.3.7 Conventional analysis of the data using two $b$ -values only

The diffusion coefficient  $D$  of water molecule can be calculated based on the signal in spin echo sequences which is derived from proton density (PD),  $T_1$  and  $T_2$  relaxation time using this simplified formula (Stejskal and Tanner, 1965; Mori and Zhang, 2006)

$$\text{Equation 2} \quad S = PD(1 - e^{-TR/T_1})e^{-TE/T_2}e^{-bD}$$

$$\text{Equation 3} \quad S = S_0e^{-bD}$$

In diffusion experiment using two  $b$ -values:

$$\text{Equation 4} \quad S_1 = S_0e^{-b_1D}$$

$$\text{Equation 5} \quad S_2 = S_0e^{-b_2D}$$

$$\text{Equation 6} \quad \frac{S_2}{S_1} = e^{-(b_2-b_1)D}$$

$$\text{Equation 7} \quad D = -\frac{\ln\left(\frac{S_2}{S_1}\right)}{(b_2-b_1)} \quad (\text{Mori and Zhang, 2006})$$

Based on Equation 7 the apparent diffusion coefficient for  $ADC_{//}$  and  $ADC_{\perp}$  is calculated. When working with only two  $b$ -values in an assumingly monoexponential diffusion decay experiment, the optimal  $b$ -values are in general considered to be for  $b_1$  close to 0 and for  $b_2$  between 900 and 1200  $s/mm^2$  (Jones, 2009). In this case we used for  $b_1$  94.6  $s/mm^2$  and for  $b_2$  1135.3  $s/mm^2$  to calculate  $ADC_{//}$  and  $b_1$  68.4  $s/mm^2$  and  $b_2$  1018.4  $s/mm^2$  to calculate  $ADC_{\perp}$ .

The fractional anisotropy (FA) is a numeric value that provides an indication of the “directionality” of diffusion in tissue. Values lie between 0 (isotropic diffusion) and 1 (completely anisotropic diffusion, in one direction).

FA is calculated from the parallel and perpendicular apparent diffusion coefficient ADC or, when applying the full tensor, from the three eigenvalues  $\lambda_1$ ,  $\lambda_2$ ,  $\lambda_3$ . In our case, where the fibre orientation is known,  $ADC_{\parallel}$  is  $\lambda_1$  and  $ADC_{\perp}$  is  $\lambda_2$  and  $\lambda_3$ .

$$\text{Equation 8} \quad FA = \frac{\sqrt{3}}{\sqrt{2}} \frac{\sqrt{(\lambda_1 - \langle \lambda \rangle)^2 (\lambda_2 - \langle \lambda \rangle)^2 (\lambda_3 - \langle \lambda \rangle)^2}}{\sqrt{\lambda_1^2 + \lambda_2^2 + \lambda_3^2}} \quad (\text{Jones, 2009})$$

where

$$\text{Equation 9} \quad \langle \lambda \rangle = \frac{\lambda_1 + \lambda_2 + \lambda_3}{3}$$

this is also the mean diffusivity  $\langle D \rangle$ , a measurement of diffusion without considering directionality (Beaulieu, 2009).

$$\text{Equation 10} \quad \langle D \rangle = \frac{ADC_{\parallel} + ADC_{\perp} + ADC_{\perp}}{3}$$

### 5.3.8 Analysis of the data using multiple increasing $b$ -values

The data was further analysed by fitting the signal attenuation with biexponential fitting routine-using the following formula:

$$\text{Equation 11} \quad \frac{S(g)}{S_0} = \alpha \exp(-\gamma^2 g^2 \delta^2 D_1 (\Delta - \delta/3)) + \beta \exp(-\gamma^2 g^2 \delta^2 D_2 (\Delta - \delta/3))$$

$$\text{Equation 12} \quad E(b) = \alpha e^{-D_1 b} + \beta e^{-D_2 b}$$

$S(g)/S_0$  or  $E(b)$  is the signal intensity change,  $\alpha$  is the contribution of the fast portion from the total signal decay,  $\beta$  is the contribution of the slow portion from the total signal decay,  $\gamma$  is the magnetogyric ratio of  $^1\text{H}$ ,  $g$  is the gradient strength,  $\delta$  is the length of duration of the applied gradient and  $\Delta$  is the time

between the two gradient pulses.  $D_1$  is the diffusion coefficient of the fast diffusion and  $D_2$  is the coefficient of the slow diffusion component. The  $b$ -value is defined as described in Equation 1. The fast diffusion ( $D_1$ ) and the slow diffusion ( $D_2$ ) as well as the contribution of fast diffusion ( $\alpha$ ) and slow diffusion ( $\beta$ ) on total diffusion can be calculated using Equation 12 ([Figure 60](#)).

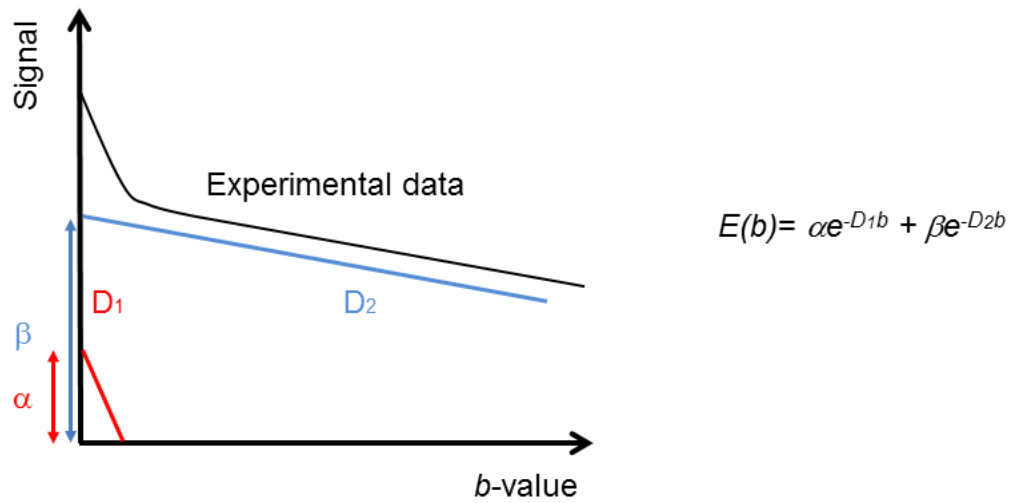


**Figure 60.** Illustration of the two components identified after applying the curve fitting routine on the signal decay curve obtained from multiple increasing *b*-values.

Using Equations 11 and 12 for curve fitting allowed the differentiation between two different components, a fast diffusion component (*D*1) and a slow diffusion component (*D*2), where the slope of the components, expressed as red and blue lines, displays the different diffusivities. Additional data were generated by calculating the contribution of each diffusion component, in percentage, relative to the total diffusion process.

### 5.3.9 Tissue sampling for histological examination

Immediately following the scan, the optic nerves were sectioned into three parts. The first part included the sclera and the retinal portion of the optic nerve, extending 1.5mm caudally from the optic disc. The second and third parts consisted of 1.5mm long segments, starting 1.5 and 3mm, respectively, from the optic disc. The first and the third parts (equivalent to the two scan regions) were frozen as described in Chapter 2. Ten  $\mu\text{m}$  thick transverse sections were cut on a cryostat and mounted on APES coated slides. Serial sections, spanning 1mm through the nerve, were collected on 10 slides (consecutive sections were mounted on consecutively numbered slides). Each slide contained up to 10 sections, each one sectioned at a distance of  $100\mu\text{m}$  from the previous one. These sections were used for immunofluorescence. The middle part each nerve was cut in half and processed for electron microscopic evaluation as described in [Chapter 2 Material and Methods](#). Sample processing, immunohistochemistry and EM procedures are described in [Chapter 2.7.3 Electron microscopy](#).

### 5.3.10 Primary antibodies for characterisation of cell types in the optic nerve

The following antibodies were used to identify specific cell populations: adenomatous polyposis coli (APC) to identify mature oligodendrocytes, chondroitin sulphate proteoglycan (NG2) to identify oligodendrocyte precursor cells, glial fibrillary acidic protein (GFAP) to identify astrocytes and CD45 to identify the microglial/macrophage/leukocytic population. For dilutions and suppliers, see [Table 2](#).

### 5.3.11 Secondary antibodies

Secondary FITC labelled antibodies were used to visualise primary antibody binding. Anti-mouse IgG1 for APC, anti-rabbit IgG for NG2, anti-mouse IgG1 for GFAP and anti-rat IgG for CD45. For dilutions and suppliers, see [Table 3](#).

### 5.3.12 Quantification of cell densities

A minimum of 6 sections, each 90 $\mu\text{m}$  apart from the previous, were analysed for cell quantification. Micrographs were opened in Image ProPlus 6.0 software and an area of interest (AOI: 28060.45 $\mu\text{m}^2$ ) was applied manually onto each image. To calculate total cell density, semi-automated quantification of DAPI stained nuclei, applying a signal threshold value between 5 and 200, was obtained from an AOI of 9983.98 $\mu\text{m}^2$ . All cells, which were fully or partially located in the AOI, except cells touching the southern and the western borders of the AOI, were counted. Cell density per  $\text{mm}^2$  was calculated based on counts from a minimum of 6 AOIs. A similar procedure was used to quantify densities of specific cell types, but in this case, the immuno-labelled cells with a DAPI nucleus were identified and quantified manually.

### 5.3.13 Statistics

For both DW MRI and histological analyses, a two tailed, paired t-test was used to compare retinal and chiasmal regions of wild type or #72 optic nerves. Comparisons between genotypes were made using an unpaired two tailed t-test. No corrections for multiple comparisons were made. All statistical analyses were done using GraphPad Prism® 5.

## 5.4 Results

An initial scan of 6 wild type nerves was undertaken in order to test the reproducibility of the protocol and the stability of the device. Once optimised, 18 optic nerves of sex and age matched control (wild type) and #72 nerves were scanned. DW MRI data was obtained from 16 increasing  $b$ -values ranging from 94.6 to 6304.4  $\text{s}/\text{mm}^2$ .

Initially the DW MRI data generated from the analysis of 2  $b$ -values was extracted from the complete dataset  $b$ -values ( $b_1 = 94.6 \text{ s}/\text{mm}^2$ ;  $b_2 = 1135.3 \text{ s}/\text{mm}^2$ ), was analysed. These results are summarised in Table 5 and Table 6. The

complete dataset (i.e. using all  $b$ -values) was then used to unveil fast and slow diffusion components. The results are summarised in [Table 7](#), [Table 8](#), [Table 9](#), [Table 10](#), [Table 11](#), [Table 12](#).

#### **5.4.1 Good signal quality was obtained from the scanned optic nerves**

The signal obtained from the optic nerves during the scan in the sample holder was stable and a good signal to noise ratio of 25 : 1 was achieved ([Figure 61](#)). The data were used to measure diffusion parallel and perpendicular to the orientation of the optic nerve fibres.

#### **5.4.2 Analysis of the data using two $b$ -values**

##### **5.4.2.1 Fractional anisotropy was reduced in the #72 optic nerves**

The fractional anisotropy (FA), a measure of diffusion directionality, was calculated using Equation 8 from the data generated using two  $b$ -values. There was a significant reduction in FA in both the retinal and chiasmal regions of the #72 optic nerves compared to the same regions in the wild type nerves ([Figure 62](#), [Table 5](#)). There was also a significant reduction in FA in the chiasmal region compared to the retinal region in #72 nerves ([Figure 62](#), [Table 6](#)).

##### **5.4.2.2 Mean diffusivity increased with demyelination**

Mean diffusion, calculated using Equation 10, was significantly increased in both retinal and chiasmal regions of the #72 nerves, compared to the same regions in the wild type nerves ([Figure 63](#)). Furthermore, although diffusion was similar in both regions of wild type nerves, it was significantly greater in the retinal region than in the chiasmal region of the #72 nerves ([Figure 63](#)).

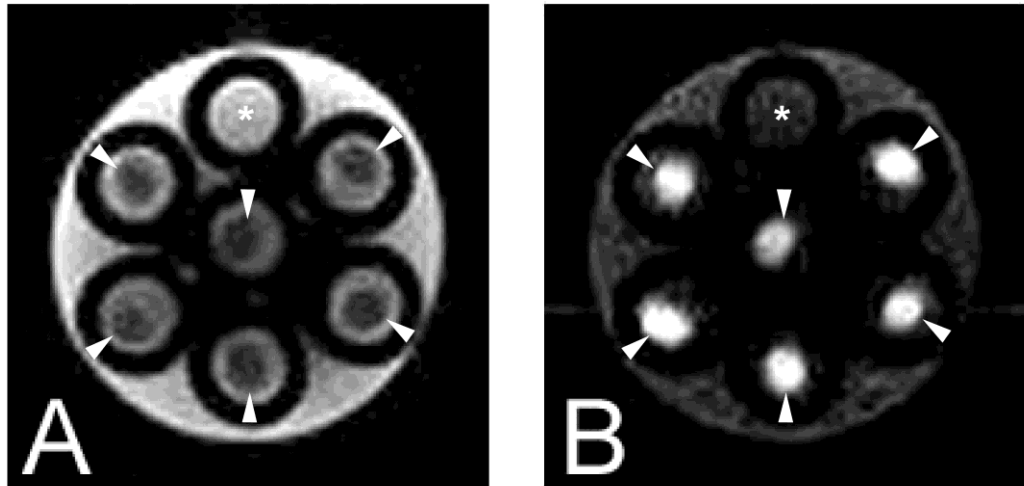


**Figure 61. Good signal to noise ratio was achieved with the purpose built coil.**

Representative examples of two diffusion weighted (DW) images obtained at a  $b$ -value of 94.6 (A) and 1135.3 (B)  $s/mm^2$  along the parallel direction in relation to the orientation of the optic nerve fibers. Depending on the quantity of the  $b$ -value the optic nerves can be identified as grey (arrowheads in A) or white (arrowheads in B), circular objects.  $H_2O$  served as a control (asterisk in A & B). The slower the diffusion, the more  $1H$  protons remain in the scan region, generating the bright signal in the object at high  $b$ -values. A quadrate region of interest was chosen in the middle of the optic nerve with an area composed of  $2 \times 2$  voxels resulting in a measured area of  $130\mu m \times 130\mu m \times 1000\mu m$ .

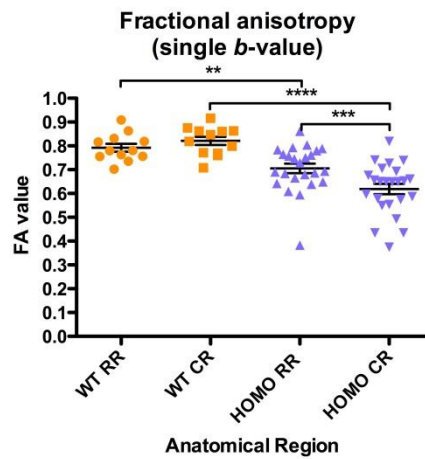


**Figure 62. Fractional anisotropy was reduced in both #72 optic nerve regions, compared to wild type.**

Graph representing the mean fractional anisotropy (FA) values (+ s.e.m.) in the two scanned regions of wild type and #72 optic nerves using two b-values  $b_1=94.6 \text{ s/mm}^2$ ;  $b_2=1135.3 \text{ s/mm}^2$ . There was a significant decrease in FA in both regions of the #72 optic nerve compared to the same regions in the wild type. There was also a significant decrease in FA in the chiasmal region compared to the retinal region of the #72 optic nerves. Wild type: N=12, #72: N=24; WT RR: wild type retinal region. WT CR: wild type chiasmal region. Homo RR: #72 retinal region. Homo CR: #72 chiasmal region. Stars indicate p values: \*\*p < 0.01. \*\*\*p < 0.001; \*\*\*\*p < 0.0001.

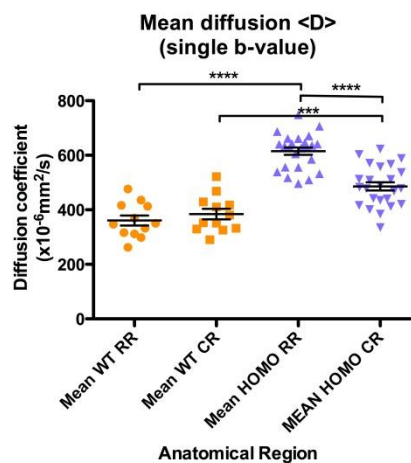


**Figure 63. Mean diffusion was increased in the #72 mouse optic nerve.**

Graph representing the mean apparent diffusion coefficient (+ s.e.m.) in wild type and #72 optic nerves obtained using two b-values  $b_1=94.6 \text{ s/mm}^2$ ;  $b_2=1135.3 \text{ s/mm}^2$ . The mean diffusion was significantly higher in the retinal and chiasmal regions of the #72 nerves compared to the same regions in the wild type nerve. Within the #72 nerve, the mean diffusion was significantly higher in the retinal region than in the chiasmal region. WT RR: wild type retinal region. Wild type: N=12, #72: N=24; WT CR: wild type chiasmal region. Homo RR: #72 retinal region. Homo CR: #72 chiasmal region. Stars indicate p values: \*\*p < 0.01; \*\*\*p < 0.001; \*\*\*\*p < 0.0001.

#### 5.4.2.3 Changes in the parallel apparent diffusion coefficient ( $ADC_{//}$ ) and perpendicular apparent diffusion coefficient ( $ADC_{\perp}$ ) in the #72 nerve

To calculate  $ADC_{//}$  and  $ADC_{\perp}$ , Equation 7 was used (Jones, 2009).  $ADC_{\perp}$  was significantly increased in both the retinal and chiasmal regions of the #72 nerves compared to the corresponding regions in the wild type nerves ([Figure 64](#), [Table 5](#), [Table 6](#)). In contrast,  $ADC_{//}$  was significantly increased in only the retinal region of the #72 nerve compared to (i) the same region in the wild type nerve and (ii) to the chiasmal region of the #72 nerve. Conversely, in the wild type nerve,  $ADC_{//}$  was slightly, but significantly, higher in the chiasmal region than in the retinal region. ([Figure 65](#), [Table 5](#), [Table 6](#)).

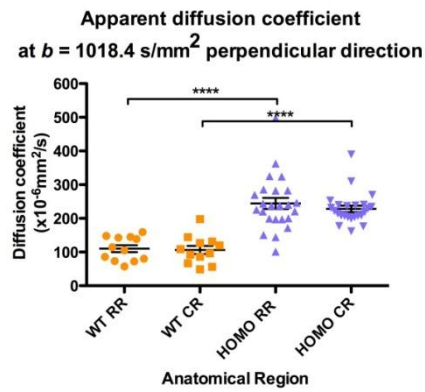


**Figure 64. Perpendicular apparent diffusion coefficient was increased in the #72 optic nerve.**

Graph presenting the mean values (+ s.e.m.) of the perpendicular apparent diffusion coefficient ( $\text{ADC}_{\perp}$ ) taken from the two scanned regions in the wild type and the #72 optic nerves using two b-values  $b_1=68.4 \text{ s/mm}^2$ ;  $b_2=1018.4 \text{ s/mm}^2$ . There was a highly significant increase in  $\text{ADC}_{\perp}$  in both regions of the demyelinated #72 optic nerve compared to the same regions in the wild type. Wild type: N=12, #72: N=24; WT RR: wild type retinal region. WT CR: wild type chiasmal region. Homo RR: #72 retinal region. Homo CR: #72 chiasmal region. Stars indicate p value: \*\*\*\*p < 0.0001.

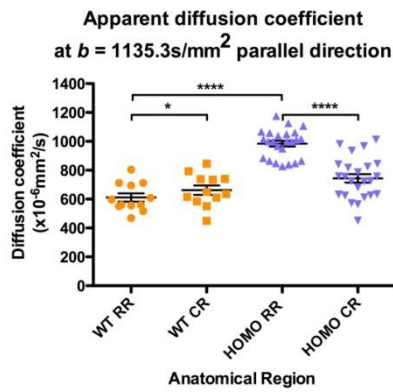


**Figure 65. Parallel apparent diffusion coefficient was increased in the retinal, but not the chiasmal region of the #72 nerve, compared to wild type.**

Graph presenting the mean values (+ s.e.m.) of the parallel apparent diffusion coefficients ( $ADC_{//}$ ) in the retinal and chiasmal regions of the wild type and #72 optic nerves using two  $b$ -values  $b_1=94.6 \text{ s/mm}^2$ ;  $b_2=1135.3 \text{ s/mm}^2$ . There was a significant increase in parallel diffusion in the #72 retinal region compared to the same region in the wild type nerve. There was also a significant increase in  $ADC_{//}$  in the #72 retinal region compared to the #72 chiasmal region. In contrast, in the wild type nerve,  $ADC_{//}$  was very slightly, but significantly, higher in the chiasmal region compared to the retinal region. Wild type: N=12, #72: N=24; WT RR: wild type retinal region. WT CR: wild type chiasmal region. Homo RR: #72 retinal region. Homo CR: #72 chiasmal region. Stars indicate p values: \*p < 0.05; \*\*\*\*p < 0.0001.

In summary,  $ADC_{\perp}$  was significantly increased in the #72 optic nerves compared to the wild type. This contributed to the decreased FA values and to the increased mean diffusion. A significant increase in  $ADC_{\parallel}$  in the #72 retinal region was also present when compared to the wild type and the #72 chiasmal region. Results are summarised in [Table 5](#) and [Table 6](#).

### **5.4.3 Analysis of the data using multiple increasing $b$ -values**

#### **5.4.3.1 A biexponential signal decay became apparent in the optic nerve when applying multiple increasing $b$ -values**

I hypothesised that the application of multiple increasing  $b$ -values would increase the sensitivity of DWI to detect differences between white matter lesions. Therefore, in the following sections, the entire data set generated using 16  $b$ -values was analysed. Signal decay curves were created, by plotting signal intensity as a function of  $b$ -value, for both parallel and perpendicular diffusion gradient directions. Signal decay deviated from mono-exponential behaviour (Figure 66) in both wild type and #72 nerves.

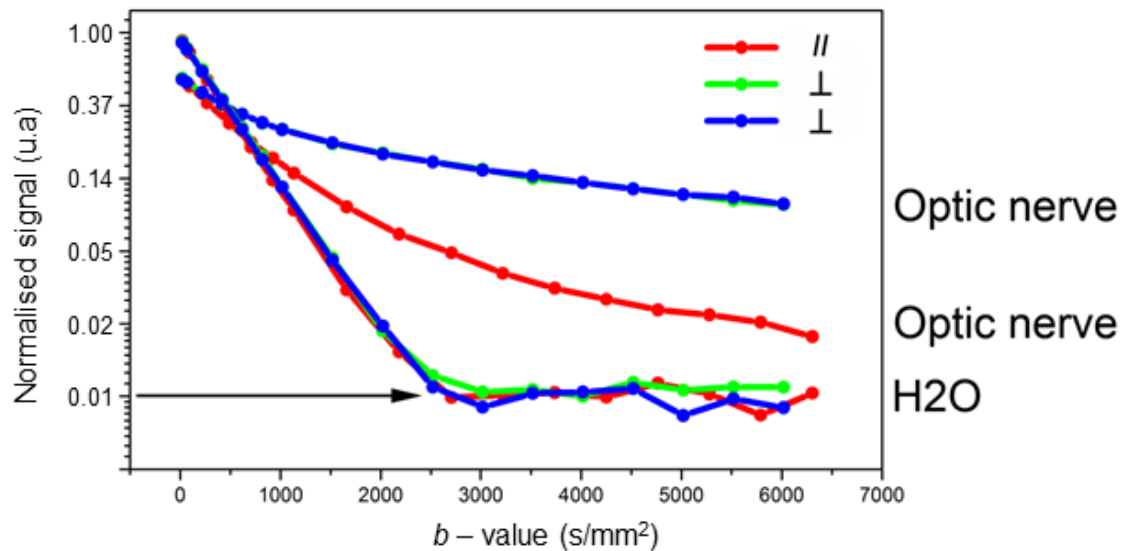


**Figure 66. Biexponential signal decay became apparent with increasing  $b$ -values.**

Signal decay curves obtained from a scanned optic nerve and from H<sub>2</sub>O, in the parallel ( $//$ , red line) and perpendicular ( $\perp$ , green and blue lines) directions (in relation to optic nerve fibers). The signal changes were plotted on a natural logarithmic scale in relation to the  $b$ -value. Biexponential signal decay was present in optic nerves suggesting the presence of two different diffusion components; a fast and a slow. In the parallel diffusion direction (red line), the slow diffusion component only became visible at higher  $b$ -values, suggesting that this information was lost when using  $b$ -values only up to 1500 s/mm<sup>2</sup>. Water, in which diffusion was unrestricted, showed a monoexponential characteristic and served as a negative control. The noise level (arrow) did not interfere with the parallel and perpendicular DWI measurement in the optic nerve.

#### 5.4.3.2 Fast and slow diffusion were altered in #72 nerves compared to wild type

Curve fitting using Equation 11 was applied in order to obtain information regarding fast and slow diffusion components of CNS water.

The perpendicular and parallel diffusion within the fast and slow components were calculated using Equation 12 and the results are summarised in [Table 7](#), [Table 8](#), [Table 9](#), [Table 10](#), [Table 11](#) and [Table 12](#). Although perpendicular fast diffusion ( $D_{1\perp}$ ) was similar in wild type and #72 nerves, there was a significant increase in the slow diffusion ( $D_{2\perp}$ ) in both retinal and chiasmal regions of the #72 optic nerves compared to the corresponding regions in the wild type ([Figure 67](#)).

Small, but significant differences between samples were found in fast parallel diffusion ( $D_{1\parallel}$ ).  $D_{1\parallel}$  was slightly, but significantly increased in retinal and reduced in chiasmal regions of the #72 nerves compared to the wild type nerves.  $D_{1\parallel}$  was significantly higher in the retinal region of the #72 nerve than in the chiasmal region. More marked differences were found in slow parallel diffusion ( $D_{2\parallel}$ ).  $D_{2\parallel}$  was significantly increased in both retinal and chiasmal regions of the #72 nerves compared to that in the corresponding regions of the wild type nerves and was also markedly higher in the retinal region of the #72 nerve than in the chiasmal region ([Figure 68](#)).

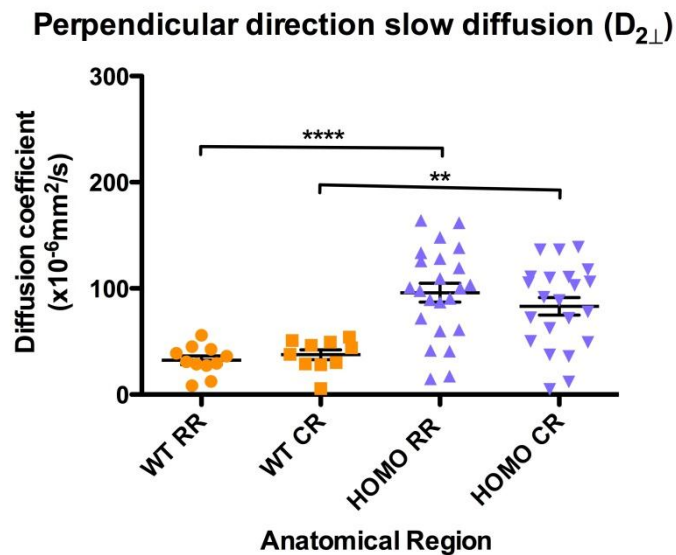
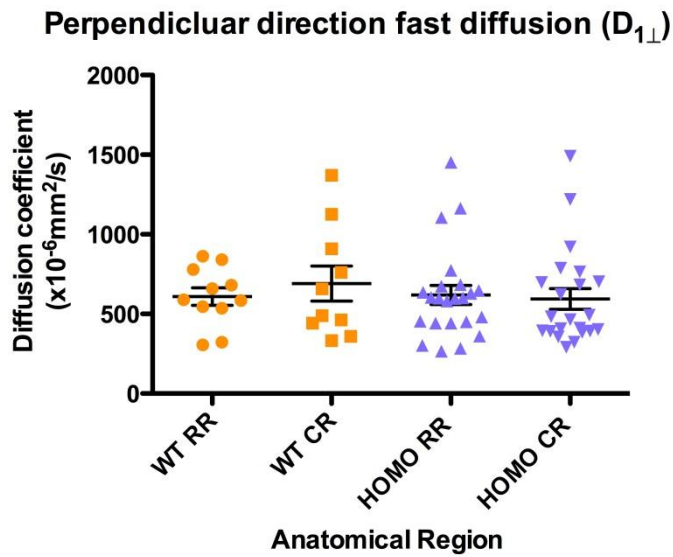


**Figure 67. Perpendicular slow diffusion was increased in #72 nerves compared to wild type.**

Graph displaying the means ( $\pm$ s.e.m) of the fast ( $D_{1\perp}$ ) and slow ( $D_{2\perp}$ ) perpendicular diffusion in wild type and #72 optic nerves.  $D_{2\perp}$  was significantly increased in both regions of the #72 nerves compared to the corresponding regions in wild type nerves. WT RR: wild type retinal region.

Wild type: N=12, #72: N=24; WT CR: wild type chiasmal region. Homo RR: #72 retinal region. Homo CR: #72 chiasmal region. Stars indicate p values: \*\*p < 0.01; \*\*\*\*p < 0.0001.

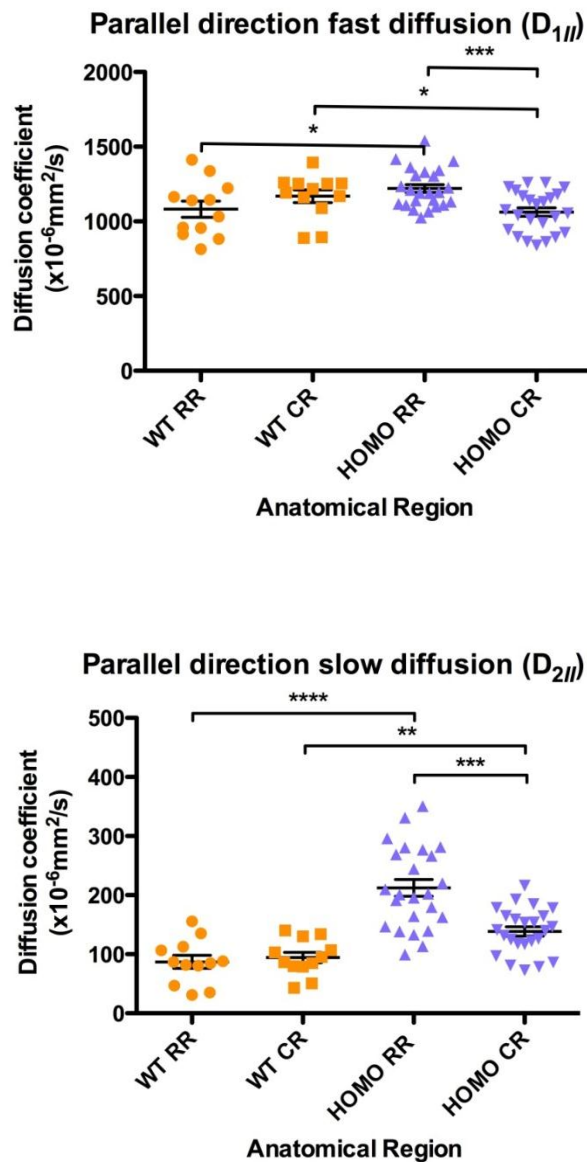


**Figure 68. Parallel slow diffusion was increased in the #72 nerve compared to wild type.**

Graph displaying the means ( $\pm$ s.e.m) of the fast ( $D_{1||}$ ) and slow ( $D_{2||}$ ) perpendicular diffusion in wild type and #72 optic nerves. Small, but significant, changes in  $D_{1||}$  were detected in #72 nerves compared to wild type. More pronounced changes were observed in  $D_{2||}$ , which was markedly and significantly increased in #72 nerves compared to wild type, particularly in the retinal region of the nerve, where it was almost 3 times the corresponding wild type value. WT RR: wild type retinal region. Wild type: N=12, #72: N=24; WT CR: wild type chiasmatal region. Homo RR: #72 retinal region. Homo CR: #72 chiasmatal region. Stars indicate p values: \*p < 0.05; \*\*p < 0.01. \*\*\*p < 0.001; \*\*\*\*p < 0.0001.

#### 5.4.3.3 The contribution of the fast diffusion component to the total diffusion was increased in #72 optic nerves

With alteration in white matter, changes in diffusivity might not just be restricted to changes within the two components of fast and slow diffusion, but the relative contribution of the fast ( $\alpha$ ) and slow ( $\beta$ ) components could also change. Particularly where the measured diffusivity itself remained unchanged, pathological changes could potentially still be detected by determining changes in the contribution of the slow and fast diffusion components, independent from the diffusion rate.

The contribution of the fast diffusion to total diffusion was significantly increased in retinal and chiasmal portions of the #72 mouse optic nerve compared to the wild type mouse optic nerve in both the parallel and perpendicular orientation ([Figure 69](#)). Conversely, the opposite, was true for the slow diffusion contribution. Results are summarised in [Table 7](#) and [Table 8](#).

Within the #72 nerve, the contribution of the parallel fast diffusion to the total diffusion was significantly greater in the retinal region than in the chiasmal region. Since ( $\alpha + \beta = 100\%$ ), the contribution of slow diffusion, reflects the opposite changes.

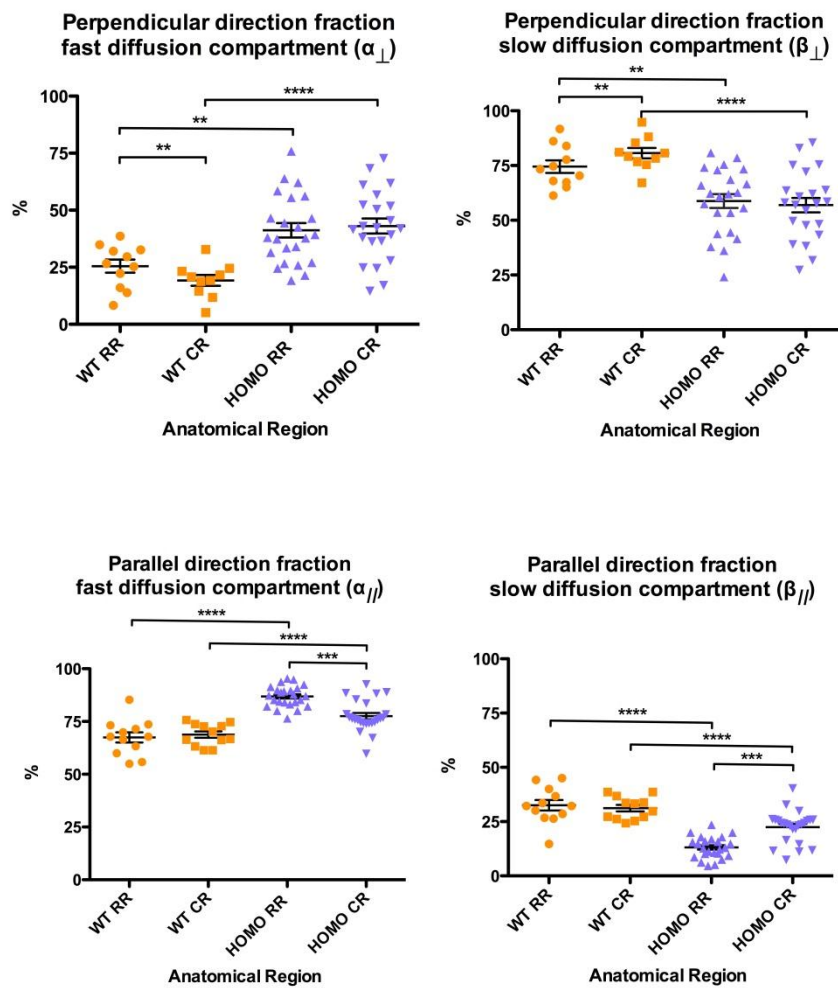


**Figure 69.** The contribution of fast diffusion ( $\alpha$ ) was increased in the #72 optic nerve.

Graphs representing mean (+ s.e.m) percentage contribution of fast or slow diffusion to total diffusion. A significant increase in the contribution of the perpendicular and parallel fast diffusion component ( $\alpha$ ) was present in the #72 nerve compared to the wild type nerve. Within the #72 nerve,  $\alpha$  was significantly elevated in the retinal region compared to the chiasmal region, in the parallel direction. The contribution of the slow diffusion component ( $\beta$ ) consequently demonstrated the same, but inverted changes. Wild type: N=12, #72: N=24; WT RR: wild type retinal region. WT CR: wild type chiasmal region. Homo RR: #72 retinal region. Homo CR: #72 chiasmal region. Stars indicate p values: \*\*p < 0.01. \*\*\*p < 0.001; \*\*\*\*p < 0.0001.

#### **5.4.4 Histological examination of optic nerves confirmed the spatially distinct regions of silent demyelination and active inflammatory demyelination in the scanned regions of #72 mouse optic nerves**

##### **5.4.4.1 Virtually complete demyelination was present in the #72 optic nerve**

Electron microscopic evaluation showed a virtually complete demyelination in the tissue immediately adjacent to the two scan regions, the retinal and the chiasmal portion of the #72 optic nerve. The demyelination appeared similar in both regions, which was in agreement with previously published results (Edgar et al., 2010). The wild type optic nerve appeared highly myelinated as expected at P120 ([Figure 70](#)).

##### **5.4.4.2 Marked increase in cell density in the chiasmal part of the #72 mouse optic nerve**

Quantification of DAPI stained nuclei showed a significant increase in total cell density in the chiasmal portion of the #72 optic nerve, compared to both the corresponding region of the wild type nerve and to the retinal region of the #72 nerve ([Figure 71](#)).

##### **5.4.4.3 Inflammatory cells contributed to the increased cell density in the #72 mouse optic nerve chiasmal region**

Immunohistochemical staining with an antibody to CD45, a pan-leukocyte marker, revealed a marked increase in numbers of CD45 +ve cells in the chiasmal region of the #72 nerve. Quantification of CD45 +ve cell density confirmed that the chiasmal region of the #72 nerve contained significantly more cells than the same region of the wild type nerve. In contrast, CD45 +ve cell density in the retinal region of the #72 nerve was slightly, but significantly, reduced compared to wild type ([Figure 72](#)).

#### **5.4.4.4 An astrocytic response was pronounced in the #72 mouse optic nerve**

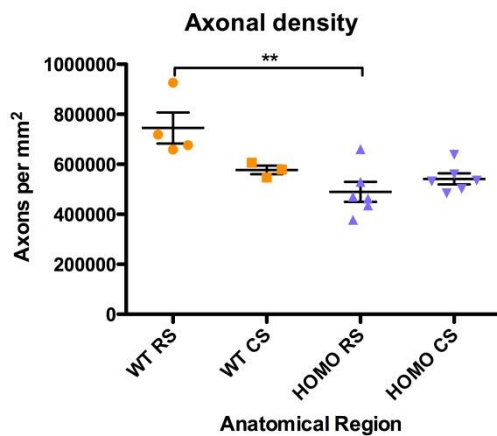
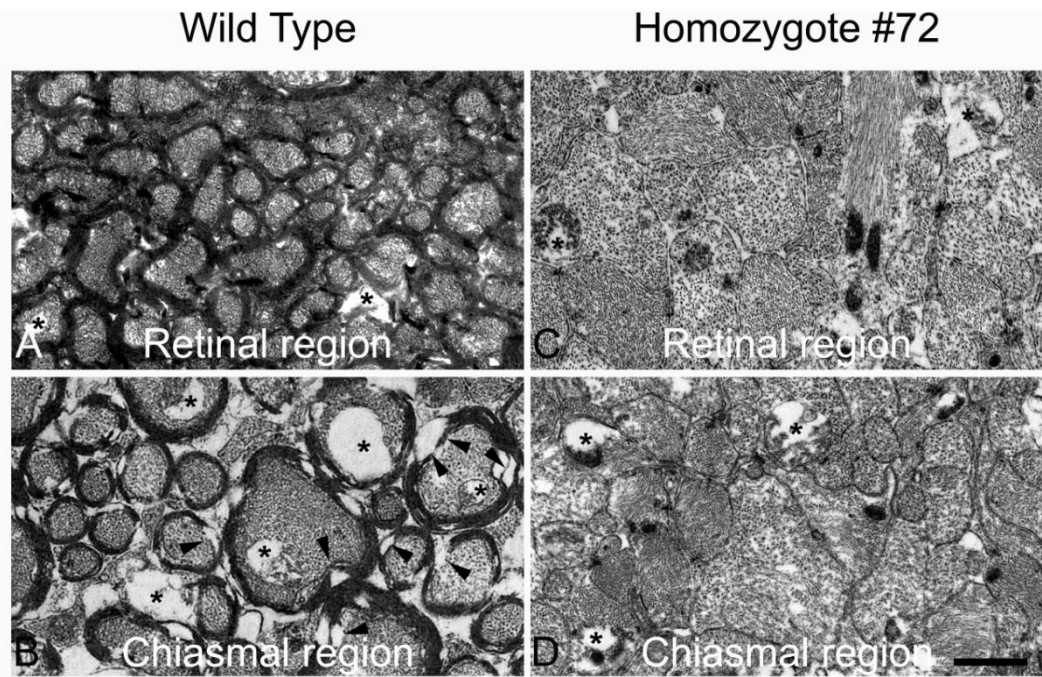
To examine the status of astrocytes, optic nerve sections were stained with an antibody to GFAP. In both regions of the #72 mouse optic nerve there was a significant increase in the area occupied by GFAP +ve astrocytic processes compared to the same regions of the wild type nerve. The extent of GFAP immunoreactivity was similar in retinal and chiasmal regions of the #72 nerve. ([Figure 73](#)).

#### **5.4.4.5 Oligodendrocyte densities were mildly reduced in the #72 mouse optic nerve**

An antibody to APC (clone CC1) was used to identify mature oligodendrocytes. Oligodendroglial density was significantly reduced in the #72 optic nerve, compared to the wild type nerve. The #72 retinal section demonstrated the lowest oligodendrocyte cell density ([Figure 74](#)). However, despite that fact that the #72 nerve was virtually completely demyelinated a remarkable number of mature oligodendrocytes were still present.

#### **5.4.4.6 Oligodendrocyte precursor cells were present in the #72 mouse optic nerve**

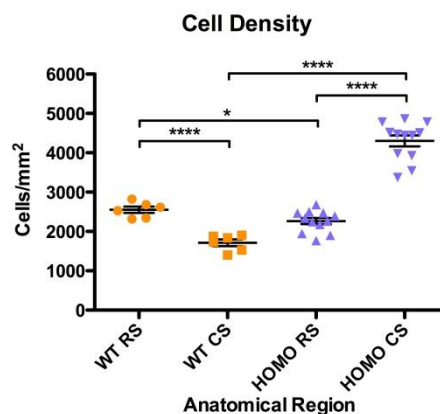
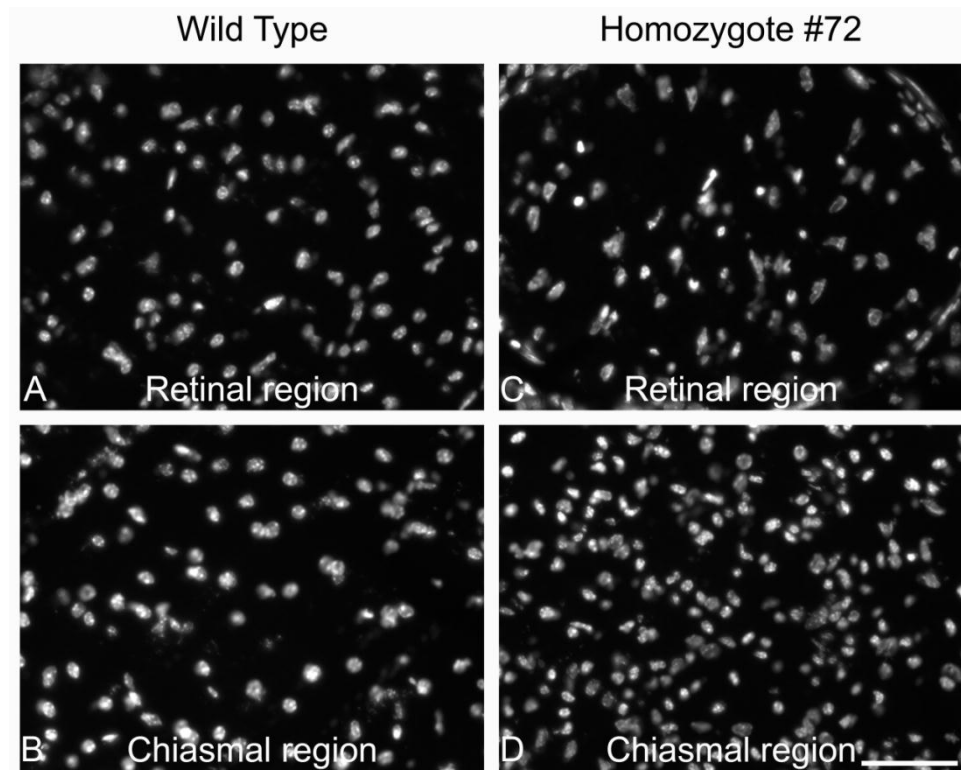
To examine OPCs, an antibody to NG2 was used. Although completely demyelinated the #72 optic nerve contained NG2 positive cells, the density of which was significantly increased in the chiasmal region of the #72 optic nerve, compared to the same region in the wild type nerve ([Figure 75](#)). Since NG2 is not completely OPC specific and may bind to a subset of microglial cells, the increase in NG2 cell density may not only represent an increase in OPCs.



E

**Figure 70. The #72 mouse optic nerve was almost completely demyelinated at P120.**

Electron micrographs of wild type (A, B) and #72 (C, D) retinal and chiasmal optic nerve regions. The wild type optic nerve was highly myelinated in both sections (A, B). This was in contrast to the #72 optic nerve, where there was a complete absence of myelin in both regions (C, D, x6700, scale bar 2 $\mu$ m). Artefacts, such as mitochondrial swellings (asterisk), were probably due to suboptimal fixation for EM processing. Graph of mean axonal density (+s.e.m) showed that axonal density was significantly decreased in the retinal region of the #72 optic nerves compared to same region in the wild type (E). No such difference was found between #72 and wild type nerves in the chiasmal region. Wild type: N=3, #72: N=5; WT RR: wild type retinal region. WT CR: wild type chiasmal region. Homo RR: #72 retinal region. Homo CR: #72 chiasmal region. Stars indicate p values: \*\*p < 0.01.



E

**Figure 71. Cell density was markedly increased in the #72 chiasmal section of optic nerve.**

Micrographs of DAPI-stained 10µm-thick transverse sections of retinal and chiasmal regions of P120 #72 and wild type mouse optic nerves (A - D, x400, scale bar 50µm). A marked increase in cellular density was seen in the #72 chiasmal region of optic nerve (D). Graph of mean cell density (+ s.e.m.) in retinal and chiasmal regions of wild type and #72 optic nerve (E). The cell density was significantly increased in the #72 chiasmal region compared to the corresponding region in the wild type and also compared to the retinal region of the #72 nerve. Conversely, cell density was very slightly, but significantly, reduced in the retinal region of the #72 nerve compared to the same region in the wild type nerve. Wild type: N=6, #72: N=12; WT RR: wild type retinal region. WT CR: wild type chiasmal region. Homo RR: #72 retinal region. Homo CR: #72 chiasmal region. Stars indicate p values: \*p < 0.05; \*\*\*\*p < 0.0001.

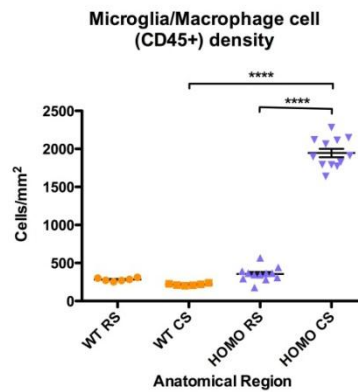
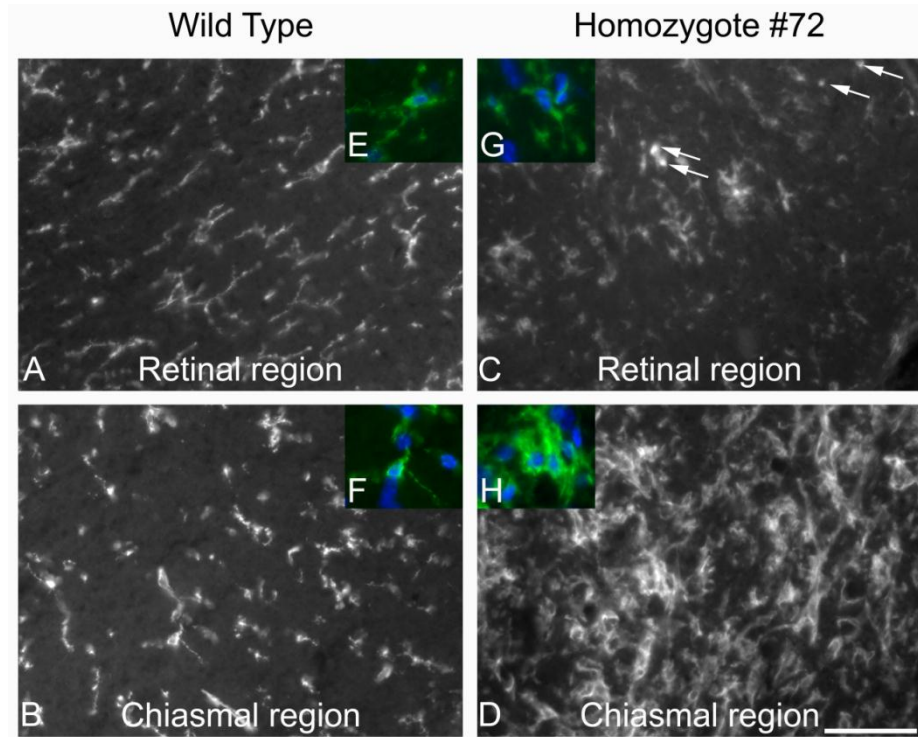


**Figure 72.** The density of CD45 +ve microglia/macrophages was increased in the chiasmal portion of the #72 mouse optic nerve.

Micrographs of CD45-stained 10µm-thick transverse sections of retinal and chiasmal regions of P120 #72 and wild type mouse optic nerves (A - D, x400, scale bar 50µm). Lipofuscin granules were prominent in the #72 mouse nerve and were seen as fluorescent granules in C (arrows). The processes of the CD45+ cells in the #72 chiasmal region (H) appeared thickened compared to those in the wild type (E, F) and the #72 retinal region (G), suggesting that the cells were ‘activated’. Graph showing the mean (+s.e.m.) CD45 +ve cell density in retinal and chiasmal regions of wild type and #72 nerves (I). The density of CD45 +ve cells was significantly increased in the #72 nerve compared to the wild type, most markedly so in the chiasmal region, in which there was an approximately 10 fold increase in cell density compared to the control. WT RR: wild type retinal region. Wild type: N=6, #72: N=12; WT CR: wild type chiasmal region. Homo RR: #72 retinal region. Homo CR: #72 chiasmal region. Stars indicate p values: \*\*\*\*p < 0.0001.

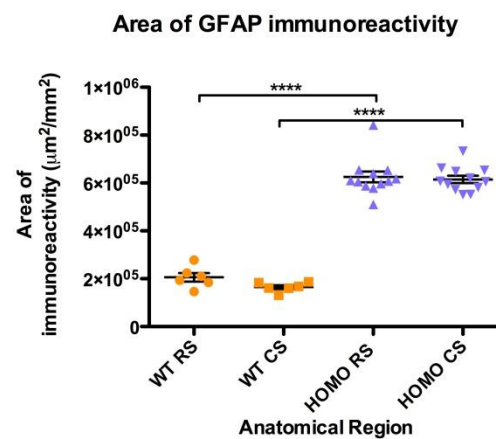
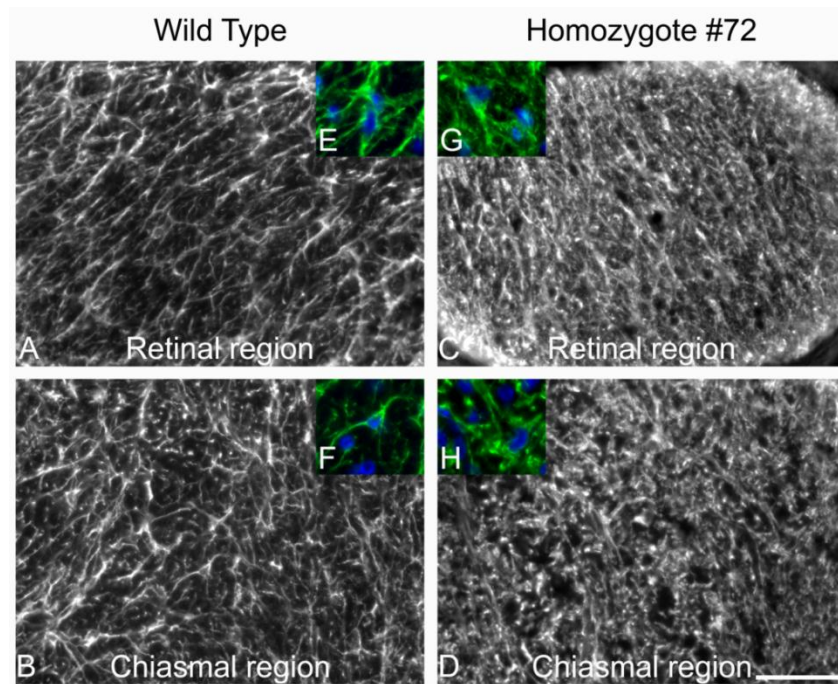


**Figure 73. The #72 mouse optic nerve was characterised by a marked astrocytosis.**

Micrographs of GFAP-stained 10µm-thick transverse sections of retinal and chiasmal regions of P120 wild type and #72 mouse optic nerves (A - D, x400, scale bar: 50µm). Astrocytes appeared more numerous and processes appeared enlarged in the #72 (G, H) compared to the wild type optic nerve (E, F). Graph showing the mean area (+s.e.m.) occupied by GFAP immunoreactivity in retinal and chiasmal regions of wild type and #72 optic nerves (I). The area occupied by GFAP immunoreactivity was significantly increased in both regions of the #72 optic nerve compared to the same regions in the wild type nerve. There was no significant difference between the two regions of the #72 mouse optic nerve. Wild type: N=6, #72: N=12; WT RR: wild type retinal region. WT CR: wild type chiasmal region. Homo RR: #72 retinal region. Homo CR: #72 chiasmal region. Stars indicate p values: \*\*\*\*p < 0.0001.

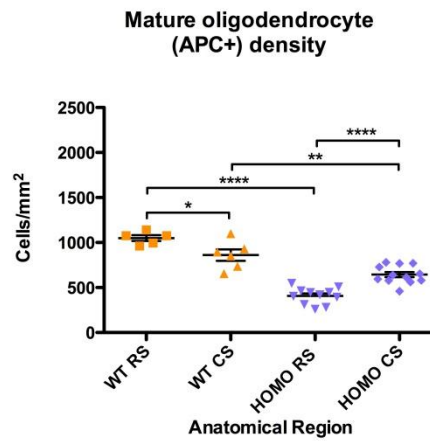
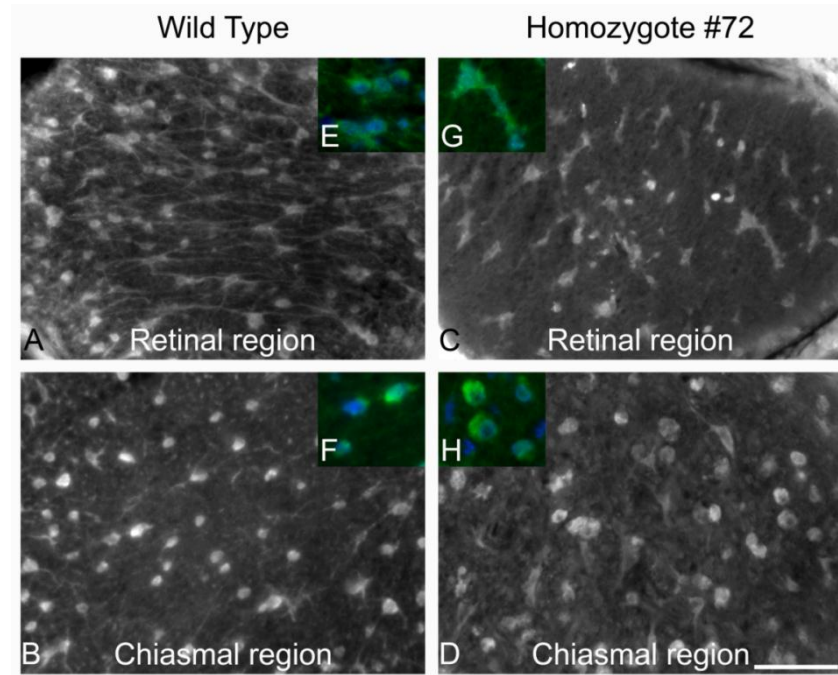


**Figure 74. Mature oligodendrocyte cell density was reduced in #72 mouse optic nerve.**

Micrographs of APC-stained 10µm-thick transverse sections of retinal and chiasmal regions of P120 wild type and #72 mouse optic nerves (A - H, x400, scale bar 50µm). (I) Graph showing the mean density (+s.e.m.) of APC +ve cells in retinal and chiasmal regions of wild type and #72 optic nerves. Oligodendrocyte cell density was significantly reduced in the #72 optic nerve compared to the wild type optic nerve, most markedly in the retinal region. Wild type: N=6, #72: N=12; WT RR: wild type retinal region. WT CR: wild type chiasmal region. Homo RR: #72 retinal region. Homo CR: #72 chiasmal region. Stars indicate p values: \*p < 0.05; \*\*p < 0.01; \*\*\*\*p < 0.0001.

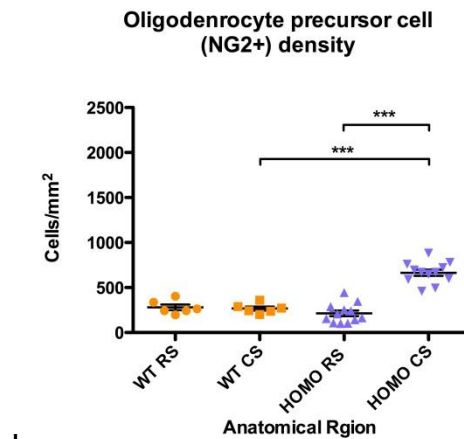
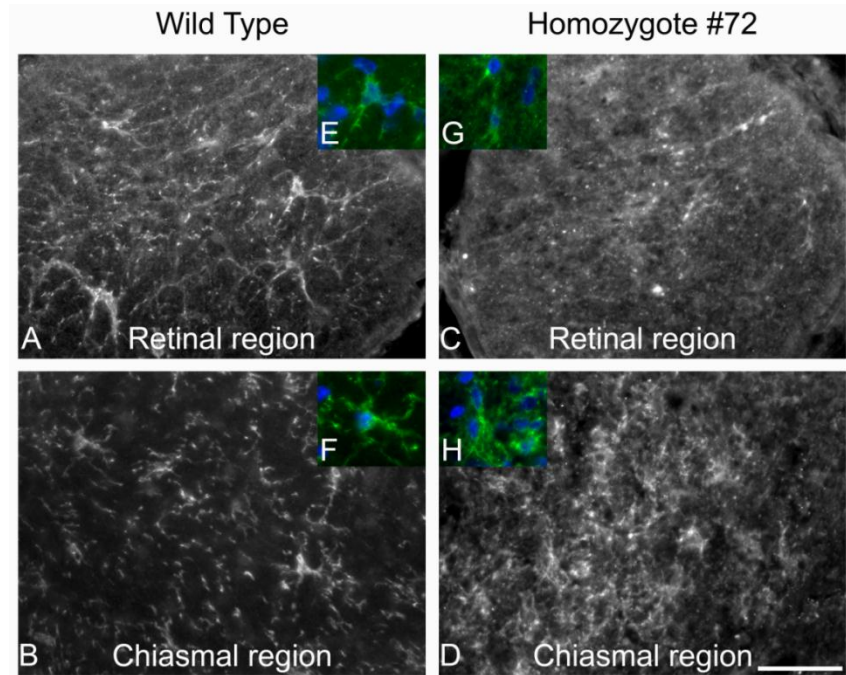


**Figure 75. Oligodendrocyte precursor cell density was elevated in the inflamed demyelinated chiasmal region of #72 optic nerve.**

Micrographs of retinal and chiasmal regions of P120 wild type and #72 mouse optic nerves (A - D, x400, scale bar 50µm) using NG2 as a marker for OPCs. The morphology of the NG2+ cells appeared similar in both wild type regions (E, F) and in the #72 retinal region (G), whereas cell processes appeared more prominent in the inflamed and demyelinated #72 chiasmal region (H). Graph showing the mean density (+s.e.m.) of NG2 +ve cells in retinal and chiasmal regions of wild type and #72 optic nerves (I). The NG2+ cell density was significantly increased in the #72 chiasmal region of the optic nerve compared to the corresponding region of the wild type nerve and to the retinal regions of the #72 nerve. Wild type: N=6, #72: N=12; WT RR: wild type retinal region. WT CR: wild type chiasmal region. Homo RR: #72 retinal region. Homo CR: #72 chiasmal region. Stars indicate p values: \*\*\*p < 0.001.

In quantifying axonal and cellular densities, I confirmed and extended previous work (Edgar et al., 2010) which showed that at P120, the optic nerve of the #72 mouse comprises a rostral, completely demyelinated, non-inflamed region and a caudal, demyelinating, inflamed region. Tables summarising the DWI data in relation to the histological findings are presented in [Table 1](#), [Table 2](#), [Table 3](#), [Table 4](#) and [Table 5](#).

	Myelin	Inflam- mation	ADC <sub>∥</sub> x10 <sup>-6</sup> mm <sup>2</sup> /s	ΔADC <sub>∥</sub> (%)	ADC <sub>⊥</sub> x10 <sup>-6</sup> mm <sup>2</sup> /s	ΔADC <sub>⊥</sub> (%)	MD x10 <sup>-6</sup> mm <sup>2</sup> /s	FA	ΔFA (%)
WT RR	Yes	No	611.56 (±28.43)	+60.9	110.08 (±10.31)	+120.6	278.4 (±41.22)	0.79 (±0.02)	-10
#72 RR	No	No	984.12 (±20.14)		244.42 (±16.53)		496.3 (±42.98)	0.71 (±0.02)	
WT CR	Yes	No	662.01 (±32.22)	+12.3	106.23 (±12.06)	+115	290.1 (±45.94)	0.82 (±0.02)	-24
#72 CR	No	Yes	743.58 (±29.19)		228.35 (±9.46)		401.8 (±30.56)	0.62 (±0.02)	

**Table 5. Summary of diffusion parameters, calculated from two *b*-values only.**

(94.6 and 1135.3 s/mm<sup>2</sup> in the parallel direction and 68.4 and 1118.4 s/mm<sup>2</sup> in the perpendicular direction). ADC<sub>∥</sub> and ADC<sub>⊥</sub> are mean values of all optic nerves measured in this study. Standard error of mean (s.e.m.) is in brackets below the values. Wild type: N=12, #72: N=24.

	Myelin	Inflam- mation	ADC <sub>∥</sub> x10 <sup>-6</sup> mm <sup>2</sup> /s	ΔADC <sub>∥</sub> (%)	ADC <sub>⊥</sub> x10 <sup>-6</sup> mm <sup>2</sup> /s	ΔADC <sub>⊥</sub> (%)	MD x10 <sup>-6</sup> mm <sup>2</sup> /s	FA	ΔFA (%)
#72 RR	No	No	984.12 (±20.14)	-24.4	244.42 (±16.53)	-6.6	496.3 (±42.98)	0.71 (±0.02)	-12.7
#72 CR	No	Yes	743.58 (±29.19)		228.35 (±9.46)		401.8 (±30.56)	0.62 (±0.02)	

**Table 6. Summary of #72 diffusion parameters calculated from two *b*-values only.**

Standard error of mean (s.e.m.) is in brackets below the mean value. Wild type: N=12, #72: N=24.

	Myelin	Inflam- mation	D <sub>1⊥</sub> x10 <sup>-6</sup> mm <sup>2</sup> /s	ΔD <sub>1⊥</sub> (%)	D <sub>2⊥</sub> x10 <sup>-6</sup> mm <sup>2</sup> /s	ΔD <sub>2⊥</sub> (%)
WT ret	Yes	No	609.4 (±55.49)	+1.5	32.29 (±4.16)	+197.12
#72 ret	No	No	618.7 (±59.71)		95.94 (±8.85)	
WT ch	Yes	No	690.8 (±110.4)	-13.94	37.53 (±4.66)	+121.53
#72 ch	No	Yes	594.5 (±64.71)		83.14 (±8.35)	

**Table 7. Summary of the mean perpendicular fast (D<sub>1⊥</sub>) and slow (D<sub>2⊥</sub>) diffusion values including the percentage of diffusion changes (ΔD<sub>1⊥</sub> and ΔD<sub>2⊥</sub>) between the wild type and the #72 optic nerves.**

Standard error of mean (s.e.m.) is in brackets below the mean value.–Wild type: N=12, #72: N=24.

	Myelin	Inflam- mation	D <sub>1⊥</sub> x10 <sup>-6</sup> mm <sup>2</sup> /s	ΔD <sub>1⊥</sub> (%)	D <sub>2⊥</sub> x10 <sup>-6</sup> mm <sup>2</sup> /s	ΔD <sub>2⊥</sub> (%)
#72 ret	No	No	618.7 (±59.71)	-3.9	95.94 (±8.85)	-13.3
#72 ch	No	Yes	594.5 (±64.71)		83.14 (±8.35)	

**Table 8. Summary of the mean perpendicular fast (D<sub>1⊥</sub>) and slow (D<sub>2⊥</sub>) diffusion values in #72 optic nerves.**

Standard error of mean (s.e.m.) is in brackets below the mean value. Wild type: N=12, #72: N=24.

	Myelin	Inflam- mation	$D_{1  }$ $\times 10^{-6} \text{mm}^2/\text{s}$	$\Delta D_{1  }$ (%)	$D_{2  }$ $\times 10^{-6} \text{mm}^2/\text{s}$	$\Delta D_{2  }$ (%)
WT ret	Yes	No	1082 ( $\pm 53.72$ )	+12.8	87.08 ( $\pm 10.86$ )	+143.8
#72 ret	No	No	1220 ( $\pm 26.63$ )		212.3 ( $\pm 14.23$ )	
WT ch	Yes	No	1169 ( $\pm 42.89$ )	-9.1	92.42 ( $\pm 8.831$ )	+50
#72 ch	No	Yes	1062 ( $\pm 27.93$ )		138.6 ( $\pm 7.84$ )	

**Table 9.** Summary of the mean parallel fast ( $D_{1||}$ ) and slow ( $D_{2||}$ ) diffusion values including the percentage of diffusion changes ( $\Delta D_{1||}$  and  $\Delta D_{2||}$ ) between the wild type and the #72 optic nerves.

Standard error of mean (s.e.m.) is in brackets below the mean value. Wild type: N=12, #72: N=24.

	Myelin	Inflam- mation	$D_{1  }$ $\times 10^{-6} \text{mm}^2/\text{s}$	$\Delta D_{1  }$ (%)	$D_{2  }$ $\times 10^{-6} \text{mm}^2/\text{s}$	$\Delta D_{2  }$ (%)
#72 ret	No	No	1220 ( $\pm 26.63$ )	-13	212.3 ( $\pm 14.23$ )	-34.7
#72 ch	No	Yes	1062 ( $\pm 27.93$ )		138.6 ( $\pm 7.84$ )	

**Table 10.** Summary of the mean perpendicular fast ( $D_{1||}$ ) and slow ( $D_{2||}$ ) diffusion values in #72 optic nerves.

Standard error of mean (s.e.m.) is in brackets below the mean value. Wild type: N=12, #72: N=24.

	Myelin	Inflam- mation	$\alpha_{\perp}$ (%)	$\beta_{\perp}$ (%)	$\Delta_{\perp}$ (%)	$\alpha_{\parallel}$ (%)	$\beta_{\parallel}$ (%)	$\Delta_{\parallel}$ (%)
WT RR	Yes	No	25 ( $\pm 3$ )	75 ( $\pm 3$ )	$\pm 16$	68 ( $\pm 2$ )	32 ( $\pm 2$ )	$\pm 19$
#72 RR	No	No	41 ( $\pm 3$ )	59 ( $\pm 3$ )		87 ( $\pm 1$ )	13 ( $\pm 1$ )	
WT CR	Yes	No	19 ( $\pm 2$ )	81 ( $\pm 2$ )	$\pm 24$	69 ( $\pm 2$ )	31 ( $\pm 2$ )	$\pm 9$
#72 CR	No	Yes	43 ( $\pm 3$ )	57 ( $\pm 3$ )		78 ( $\pm 2$ )	22 ( $\pm 2$ )	

**Table 11. Summary of the contribution of fast and slow diffusion (in %) in the perpendicular and parallel direction.**

Standard error of mean (s.e.m.) is in brackets below the value. In the perpendicular direction the slow diffusion ( $\beta_{\perp}$ ) is the main type of diffusion. This is in contrast to the parallel direction, where the fast diffusion ( $\alpha_{\parallel}$ ) is the prominent type of diffusion. Wild type: N=12, #72: N=24.

	Myelin	Inflam- mation	$\alpha_{\perp}$ (%)	$\beta_{\perp}$ (%)	$\Delta_{\perp}$ (%)	$\alpha_{\parallel}$ (%)	$\beta_{\parallel}$ (%)	$\Delta_{\parallel}$ (%)
#72 RR	No	No	41 ( $\pm 3$ )	59 ( $\pm 3$ )	$\pm 3.9$	87 ( $\pm 1$ )	13 ( $\pm 1$ )	$\pm 30.8$
#72 CR	No	Yes	43 ( $\pm 3$ )	57 ( $\pm 3$ )		78 ( $\pm 2$ )	22 ( $\pm 2$ )	

**Table 12. Summary of the contribution of fast and slow diffusion (in %) in the #72 optic nerves.**

Standard error of mean (s.e.m.) is in brackets below the value. Wild type: N=12, #72: N=24.

## 5.5 Discussion

In this study I took advantage of the simple anatomy and stereotypic pattern of demyelination and inflammation in the #72 mouse optic nerve to assess the sensitivity of high resolution DW MRI and DW MRI with increasing  $b$ -values, to distinguish complete demyelination from inflammatory demyelination.

The purpose built coil and sampling container proved useful for the application of DW MRI to fixed and excised mouse optic nerves. Preliminary studies were undertaken to show that nerves could be accurately positioned within the coil and that results of multiple scans of wild type nerves showed that the technique provided highly reproducible data. Despite the fact that such high resolution scanning is currently not feasible *in vivo*, the data demonstrate proof-of-principle of the potential of high resolution DW MRI with multiple increasing  $b$ -values to distinguish between different types of white matter lesions.

I showed that both conventional DW MRI and DW MRI with increasing  $b$ -values detected differences in diffusion parameters in the #72 nerves compared to wild type as well as between rostral and caudal regions of the #72 nerves. Histological analyses confirmed that the #72 nerve comprised a rostral, completely demyelinated region and a caudal, inflammatory demyelinating region. The demyelinated nerve was also characterised by a marked astrocytosis and contained both mature oligodendrocytes and NG2 +ve cells. Assessment of axonal integrity proved difficult due to tissue fixation being suboptimal for EM evaluation. The use of multiple increasing  $b$ -values proved to be more sensitive than conventional two  $b$ -value DW MRI in detecting the diffusion changes between inflammatory and non-inflammatory demyelination. In the standard approach the diffusion changes between the non-inflammatory and the inflammatory demyelinated region in percentages were -24.4 % in the  $ADC_{||}$  direction and -6.6 % in the  $ADC_{\perp}$  compared to the slow diffusion changes measured with multiple  $b$ -values where the changes were -34.7 % in the  $D2_{||}$  direction and -13.3 % in the  $D2_{\perp}$  direction ([Table 6](#) versus [Table 8](#) and [Table 10](#)).

### **5.5.1 Distinct changes in parallel and perpendicular fast and slow diffusion become apparent**

Using DW MRI with increasing  $b$ -values, similar changes as in standard DW MRI of the #72 nerve compared to wild type nerve and also between the two regions of the #72 nerve were found. These changes were most marked in the slow diffusion component ( $D_{2\parallel}$  and  $D_{2\perp}$ ). Only very minor changes were evident in the fast parallel diffusion component ( $D_{1\parallel}$ ) and no changes were observed in fast perpendicular diffusion component ( $D_{1\perp}$ ). Thus the slow diffusion component appeared more sensitive to the histological changes in optic nerves. Changes in the slow diffusion component were more pronounced compared with changes observed using only two  $b$ -values but did not reveal more specific information in regard of diffusivity changes related to histological background.

### **5.5.2 The basis of anisotropic diffusion and the relation of diffusion changes to white matter disease**

The strictly organised arrangement of axons is believed to be the main contributor to the anisotropic diffusion of water molecules in white matter (reviewed in Beaulieu, 2002;Beaulieu, 2009) The organised fibre tract structure forms the basis for the ability of diffusion tensor imaging to detect and trace nerve fibre bundles (Moseley et al., 1990a). However, studies correlating DTI parameters with histological measures have further demonstrated its value as a tool for assessing white matter integrity (Budde et al., 2008;Harsan et al., 2006;Harsan et al., 2008;Song et al., 2002;Song et al., 2005). Indeed, a number of studies, particularly from the Song laboratory at Washington University St. Louis, Missouri USA, have provided evidence that pathological changes in specific white matter elements can be deduced from calculation of the diffusion coefficient perpendicular and parallel to the nerve fibre bundles.

For example, it has been shown that dys- or demyelination increases the perpendicular diffusion coefficient and reduces fractional anisotropy (Song et al., 2002;Song et al., 2005). Remyelination reverses the changes, emphasising the influence of the myelin sheath on perpendicular diffusivity (Harsan et al.,

2006). Axonal pathology on the other hand has been shown in several studies, to correlate with reduced parallel diffusion and also leads to decreased FA and MD values (Budde et al., 2008; Budde et al., 2009; DeBoy et al., 2007; Feng et al., 2009; Kim et al., 2006).

However most of the correlative DTI studies have only examined the status of myelin and axons and failed to take account of other white matter elements. Therefore the possibility that changes in the density and morphology of other cell types could influence the DTI measures has largely been neglected. Recent studies have shown an increased parallel diffusion in the presence of mild axonal pathology after demyelination (Harsan et al., 2007; Ruest et al., 2011) and yet others have shown a temporal reduction of parallel and perpendicular diffusion in the presence of mild axonal pathology, with a return to initial values despite more severe axonal damage after demyelination (Xie et al., 2010).

While the increase in perpendicular (radial) diffusion is generally accepted to be related to demyelination and may be altered by cell density (Xie et al., 2010), the increase in parallel (axial) diffusion in the presence of mild axonal injury (Harsan et al., 2007; Ruest et al., 2011) is more difficult to explain. One study (Harsan et al., 2007) suggested that the increase in astrocytes, which was present in the *jimpy* mouse model of PMD, correlated with increased parallel diffusion, whereas a different study (Ruest et al., 2011) suggested that a combination of increased axonal density and astrocytosis could contribute.

Nevertheless, all of the three more comprehensive studies (Harsan et al., 2007; Ruest et al., 2011; Xie et al., 2010) show that, especially for parallel diffusivity, there is at the moment no clear explanation for the observed diffusion changes. Tissue and cellular changes besides demyelination and axonopathy are most likely responsible for the variation in results reported in the literature.

### 5.5.3 Changes in “conventional” DW MRI parameters distinguish lesion types in the optic nerve

#### 5.5.3.1 Fractional anisotropy and mean diffusion changes in #72 optic nerve

I found that fractional anisotropy, which is a measure of diffusion directionality, was reduced in the #72 optic nerve compared to the wild type. This has also been shown in other studies (Harsan et al., 2006;Ono et al., 1995) where a significant reduction of FA values has been found following demyelination (Harsan et al., 2006;Ono et al., 1995; reviewed in Beaulieu, 2009).

FA provides a measure of the relationship between parallel and perpendicular diffusion, such that it is highest (closest to one) when diffusion in one particular direction is markedly greater than in another and lowest (closest to zero) when diffusion in all directions is of similar magnitude (Equation 8). Generally, a reduction in FA in white matter is associated with either a reduction in diffusion in the parallel direction or an increase in diffusion in the perpendicular direction (reviewed in Beaulieu, 2002;Beaulieu, 2009).

In contrast, in the current study, a reduction FA was associated with increases in both parallel and perpendicular diffusion. This can be explained by the fact that the increase in the perpendicular diffusion in the #72 mouse nerves was relatively greater than the increase in the parallel direction ([Table 5](#)).

With respect to whether DWI could distinguish complete demyelination from inflammatory demyelination, FA was also significantly reduced in the inflamed region of the #72 nerve compared to the non-inflamed region (see Table 6).

Examination of perpendicular and parallel diffusions (of which FA is a function) showed that this was due to a disproportionately high parallel diffusion in the non-inflamed nerve ([Table 5](#)). This was somewhat surprising because increased parallel diffusion is not commonly observed in relation to demyelination, although it has been recently described (Harsan et al., 2007;Ruest et al., 2011).

A significant increase in mean diffusivity (MD) in the #72 optic nerve was most pronounced in the retinal region. This reflects the observed increase in both parallel and perpendicular diffusion in the #72 optic nerve. Again, loss of myelin causes an increase in MD (reviewed in Beaulieu, 2009)

#### **5.5.3.2 Perpendicular diffusion changes were associated with the loss of myelin integrity**

Although significantly different to the wild type, there were no significant changes in the perpendicular diffusion between the retinal and the chiasmal region of the #72 optic nerve. This implies that the differences (compared to wild type) are probably mainly caused by demyelination, the extent of which was similar in both regions. This is in agreement with other studies (Harsan et al., 2006; Harsan et al., 2008; Klawiter et al., 2011; Nair et al., 2005; Ruest et al., 2011; Song et al., 2002; Song et al., 2005; Xie et al., 2010). Surprisingly, the inflammation in the chiasmal section of #72 optic nerves did not seem to alter perpendicular diffusion. This was somewhat unexpected, since increased cell density has been suggested to decrease perpendicular diffusion (Xie et al., 2010).

Diffusion in tissue, which is a combination of intracellular as well as extracellular diffusion, is considered to be mainly restricted by the cell membrane (Beaulieu, 2009). Since axons, which are believed to be the main structure influencing diffusion, are densely packed (in the current study at least 500,000 axons  $\text{mm}^{-2}$ ), the perpendicular diffusing water molecule will be confronted with a minimum of one cell membrane within the average distance of an axonal diameter, which in the optic nerve is around  $1\mu\text{m}$  (Edgar et al., 2010). A decrease in axonal density, which may be caused by enlargement of the extra-axonal space, could also lead to facilitated extra-axonal perpendicular diffusion. There was a reduced axonal density in the #72 optic nerve when compared to the wild type retinal region which may explain the prominent increase.

So why should an increase in cell density not affect perpendicular diffusion? Given the size of microglia, which in the non-activated state is approximately 10

- 20µm and considerably larger after activation, the cell is 10 - 20 times larger than the average axonal cross-section. If the assumption is correct that the cell membrane is the main barrier to diffusion (Beaulieu, 2009) the distance between two cell membranes of a microglial cell would be 10 - 20µm. This is in contrast to the axons, where on average every 1µm at least one cell membrane occurs. Additional cell membranes from inflammatory cells would only add one more obstacle every tenth to twentieth axon and only minimally influence perpendicular diffusion. Therefore, the perpendicular diffusion is most likely governed by the density of axonal membrane and, since most of the axons are myelinated in the optic nerve (Edgar et al., 2010), modified by myelin sheath.

In contrast to the finding of the current study, (Xie et al., 2010) suggested that inflammation reduces perpendicular diffusion. However, in their model (in contrast to the model used in my study) the corpus callosum was not completely demyelinated at the time point where elevated microglial cell density was observed by (Xie et al, 2010). The remaining intact myelin sheaths could potentially still influence the diffusion. Therefore it is questionable if the reduced perpendicular diffusion observed by (Xie et al., 2010) is due to increased cell density or if the remaining intact myelin sheaths are still numerous enough to prevent perpendicular diffusion to increase.

#### **5.5.3.3 Diffusion parallel to optic nerve fibres is altered in association with loss of myelin integrity and changes in cell density**

The marked increase in parallel diffusivity, especially in the non-inflamed demyelinated retinal region was unexpected. Only a small number of studies have recently demonstrated increased parallel diffusion in models of dys- and demyelinated tissue, with relatively mild axonal changes and increased axonal density (Ruest et al., 2011; Harsan et al., 2007).

In the parallel diffusion direction, water molecules diffuse in and along axons, where virtually no membranes other than myelin restrict diffusion. With demyelination, a component of the extra-axonal diffusion barrier will disappear and could facilitate the extra-axonal diffusion alongside axons, resulting in an

increase in bulk parallel diffusion as was observed when comparing the #72 with the wild type nerve. However, in the presence of inflammation, multiple cell membranes could potentially restrict the previously relatively unrestricted extra-axonal parallel diffusion and reduce the bulk parallel diffusivity, leading to the differences in parallel diffusion observed in the #72 chiasmal region compared to the #72 retinal region.

From an intraaxonal point of view, changes in extra-axonal structures will most likely have little if any impact on intraaxonal diffusion. However, studies have shown that with axonal swellings or transection of axons, parallel diffusion is reduced (Budde et al., 2008; Budde et al., 2009). The presence of axonal swellings in the chiasmal region of the #72 optic nerve has been described in the previous study by (Edgar et al., 2010). Despite the relatively low number of axonal swellings, the difference between the retinal and the chiasmal #72 optic nerve may reflect this.

Since the ultrastructural evaluation of the #72 optic nerve showed a similar degree of demyelination in both regions accompanied by only mild axonal changes (Edgar et al., 2010) and unaltered axonal numbers, other histopathological changes besides demyelination and axonal pathology may influence additionally parallel diffusion (diffusion #72 retinal region > chiasmal region, Table 5). Along the entire optic nerve there is a marked astrogliosis. Astrocytes have been proposed to alter diffusion values in both parallel and perpendicular direction (Harsan et al., 2007). Two proposals have been made: that hypertrophic astrocytic processes align along axons and facilitate intracellular diffusion parallel to the axons (Skoff, 1976) and an increase in aquaporin 4, a transmembranous water channel expressed on astrocytes, facilitate fast transmembranous water transport (reviewed in Nicchia et al., 2004; Harsan et al., 2007). Whereas the astrogliosis in the #72 mouse nerve may explain an increase in parallel and also in the perpendicular diffusivity compared to the wild type, the parallel diffusion differences within the #72 optic nerve appears not to be influenced by the astroglial population, since the astrogliosis is similar in the retinal region compared to the chiasmal region.

Finally the study by (Ruest et al., 2011) also demonstrated an increase in perpendicular and parallel diffusivity in #72 corpus callosum at P120. These results are in agreement to the findings of the current study. Additionally when comparing the histological data from (Ruest et al., 2011) to Chapter 3 and the chiasmal region of #72 optic nerve, all three regions appears histologically similar.

#### **5.5.4 Multiexponential signal decay becomes apparent after applying multiple increasing high $b$ -values to the DWI**

The DTI sequences normally uses two  $b$ -values,  $b \sim 0$  and  $b \sim 1000 \text{ s/mm}^2$ . By applying multiple increasing  $b$ -values to the sequence, the signal decay versus  $b$ -value becomes multiexponential. It is believed that different types of water diffusion within the tissue are responsible for the generation of the multiexponential signal decay (reviewed in Beaulieu, 2002). The distinct types of diffusion detected using multiple increasing high  $b$ -values are believed to be influenced by various micro anatomical structures such as microtubules, cells nuclei, cell membranes and myelin sheaths (reviewed in Beaulieu, 2002). Therefore, potentially novel information about tissue architecture, which is excluded in scans only using  $b$  - value up to  $1500 \text{ s/mm}^2$ , may come to light.

In the current study, where I extended the diffusion experiment by applying multiple increasing  $b$ -values, particular diffusion aberrations were detected when compared to standard monoexponential analysis. By applying multiple  $b$ -values ranging from  $68.4$  to  $6304.6 \text{ s/mm}^2$  to the parallel and perpendicular DWI sequence in relation to the optic nerve fibres, a non-monoexponential signal decay became apparent. This finding was consistent with findings in other DWI studies of white matter, using a similar range of  $b$ -values, in which the signal decay curve appears to change around the  $b$ -value of  $2000 \text{ s/mm}^2$  (Mulkern et al., 2000; Ronen et al., 2006).

#### **5.5.4.1 Biexponential analysis of the signal decay curve allowed the distinction of a fast and slow diffusion component**

Analysis of the signal decay curve in this study showed that curve fitting was accurate when using a biexponential fitting routine. The biexponential characteristic of the curve allowed separation of the data into two distinct diffusion components, a fast and a slow diffusion component. The fast diffusion component is assumed to be mainly under axonal influence whereas the slow diffusion component is assumed to be influenced by extra-axonal structures such as myelin sheaths and glial cells (reviewed in Beaulieu and Allen, 1994; Beaulieu, 2002).

#### **5.5.4.2 The slow diffusion components were sensitive to detect histopathological changes in demyelinated optic nerve**

When comparing the percental changes of  $ADC_{\perp}$  and  $ADC_{\parallel}$  between the two regions in the #72 optic nerve ([Table 2](#)) with the percental changes in the slow diffusion compartment in both  $\perp$  and  $\parallel$  direction ([Table 8](#) and [Table 10](#)), a clear augmentation of the diffusion changes were detected. This shows the clear advantage of the high resolution DW MRI with multiple  $b$ -values to enhance the sensitivity to detect specific histopathological changes such as inflammation besides demyelination.

#### **5.5.4.3 The fast and slow diffusion components provided information beyond diffusion rate**

The distinction of two different components also allowed the analysis of diffusion changes not only by differences in diffusion but also by changes in diffusion characteristics. The contribution of fast ( $\alpha$ ) and slow ( $\beta$ ) diffusion components to overall diffusion showed that in the perpendicular direction the slow diffusion ( $\beta_{\perp}$ ) and in the parallel direction the fast diffusion ( $\alpha_{\parallel}$ ) were most prominent  $\alpha_{\perp}$  and  $\alpha_{\parallel}$  were significantly increased in the homozygote optic nerve compared to the wild type, suggesting that the contribution of the fast diffusion

is increased after demyelination. The increase in  $\alpha$  was more significantly elevated in the non-inflamed retinal region compared to the inflamed chiasmal region, demonstrating that inflammatory cells could influence diffusion characteristics. The calculation of  $\alpha$  and  $\beta$  provided further information about tissue related changes in diffusion characteristics, because  $D_{1\perp}$  was similar in wild type and #72 optic nerves but still there were significant changes in the diffusion characteristics. By calculating  $\alpha$  and  $\beta$  additional information about diffusion changes were gained, which was especially of importance when diffusivity within each component remained unchanged.

The general increase in  $\alpha$  in both directions in the #72 mouse nerves may also provide an explanation why “standard” DW MRI also detects the changes caused by demyelination and inflammation. Standard DW MRI values are a mixture of slow and fast diffusion. If changes in contribution of the fast or slow diffusion component occur within the range of a b-value of  $1500 \text{ s/mm}^2$ , the changes will also be detected in standard DW MRI as it appeared to be in my study.

I used the Student’s t-test in this experiment, since the plan was not to compare all measurements with each other. Therefore, in order not to run inappropriate comparisons, I separately compared the results from the two different sections within the same optic nerve and the results from the same section between wild type and #72 optic nerve (see [5.3.13 Statistics](#)). Multiple comparison tests, however, which are more conservative tests with less probability of making a type I error, would have been more appropriate for this experiment. The use of one way ANOVA with post-hoc tests (e.g. Bonferroni’s multiple comparison test) may have been a better choice to analyse this experiment. In my opinion, however, using the one way ANOVA with multiple comparisons would not have made any changes in the results and interpretation of this experiment.

## 5.6 Conclusion

I have shown in this study specific diffusion parameter changes in both “classical” and modified DW MRI experiment, linked to demyelination and inflammation in the optic nerve. The potential of DW MRI to distinguish between two crucial lesion types in demyelinating disease, namely acute inflammatory demyelination and chronic silent demyelination was demonstrated.

However, the DW MRI parameter differences were relatively small and unless specific numerical values can be assigned to specific white matter lesion type, it will remain difficult to distinguish lesion types *in vivo* in the absence of a comparator.

The biexponential signal decay allowed me to analyse two distinct diffusion components, the slow and the fast diffusion component. In this study I demonstrated that demyelination was associated with an increase in the slow diffusion coefficient parallel and perpendicular to the optic nerve fibre tracts. Demyelination without inflammation appeared to further increase the parallel slow diffusion coefficient suggesting that inflammation had a modulatory effect on slow diffusion along the parallel direction. Furthermore the changes in the contribution of fast and slow diffusion probably signify a general effect on diffusion characteristics after demyelination and inflammation.

These new findings are important in context with *in vivo* diagnosis and monitoring of demyelinating diseases. I have shown, that standard diffusion weighted imaging distinguishes normal and demyelinated white matter lesions (confirming the results published by other investigators). I also showed that it is possible to distinguish between demyelination accompanied by inflammation and chronic demyelination when high resolution DWI is used. Using multiple increasing *b*-values, I showed that diffusion changes could mainly be attributed to the slow diffusion component. Using this method, the presumptive extra-axonal influence especially on slow parallel diffusion became more apparent, demonstrating DWI with multiple *b*-values is a sensitive molecular probe capable of exploring changes in the extra-axonal space. However there are still some

technical issues restricting the DWI MRI with multiple increasing *b*-values to be used in clinical settings.

Considering the results from the current study, “standard” DW MRI also differentiates distinct lesion types, and may be used in clinical settings as an *in vivo* tool to identify white matter lesion type.

The possibility to distinguish these two specific white matter lesion types may be of importance for the MS research community and patients suffering from MS in giving the opportunity to diagnose demyelination non-invasively *in vivo*, to monitor lesion development more accurately, to assess therapeutic success and allow accurate determination of the long term prognosis.

## 6 Final discussion and future experiments

Data presented in this study provided insight into the development of intracranial demyelination and remyelination failure in the homozygous *Plp1* gene overexpressing mouse, line #72. The study demonstrated that, following initial myelination, there follows spontaneously, a progressive, non-remitting demyelination that eventually leads to a virtually complete absence of myelin sheaths.

*In vitro* and *in vivo* studies (i.e. what was done in [Chapter 3 The development of the phenotype and pathology of the homozygote #72 corpus callosum](#) and [Chapter 4 An evaluation of cell intrinsic and cell extrinsic factors that contribute to remyelination failure](#)) were undertaken to evaluate the role of OPC intrinsic and OPC extrinsic factors in the pathogenesis. The data provided evidence that remyelination failure may be due to an age related impairment of differentiation of OPCs. This, in line with evidence that increasing age plays a major role in diminishing the efficacy of the repair process (Shen et al., 2008) suggests that final OPC differentiation during the complex remyelination process is probably the most vulnerable step. Despite the fact that exogenous, neonatal derived neurospheres were able to myelinate axons in the adult #72 mouse brain, factors were present in demyelinated CNS that have previously been shown to be inhibitory to remyelination. Therefore a combination of OPC intrinsic and extrinsic factors is most likely leading to remyelination failure in the adult #72.

The transplantation of multipotent neurospheres into neonates provided evidence that early introduction of these cells has the potential to replace the endogenous, genetically defective oligodendroglia during post natal development, to form normal myelin sheath around axons and to stably integrate into the CNS, possibly indefinitely. These findings would support the development of an approved therapeutic strategy to rescue or ameliorate severe forms of PMD by neonatal neuronal stem cell application into the CNS.

The results presented also showed that the #72 mouse with its highly reproducible and stereotypic optic nerve pathology with a spatially distinct

inflamed demyelinated region and a non-inflamed demyelinated region is valuable as a model to evaluate the potential of novel DW MRI techniques to function as a molecular probe, able to distinguish white matter changes. The aim of this section is to bring together results from the phenotypic study, the evaluation of the OPC intrinsic and extrinsic compartments, the cell transplant and the DW MRI study in order to suggest future work and discuss some of the points raised in the thesis.

## 6.1 The #72 mouse as a model for chronic demyelination

Although complete demyelination was present in the #72 mouse at the end stage of the disease and coincided with clinical signs, OPCs were still present. The lesion development in #72 mice is comparable, in some respects, to the situation described in chronic demyelinated MS lesions, where, despite the presence of OPCs, remyelination fails (Chang et al., 2002). Nevertheless, although *Plp1* is not expressed in OPCs they still harbour the genetic defect, which may also have an effect on normal OPC function. The failed remyelination is thought to lead to a progressive axonal loss, which is considered to be the primary reason underlying permanent disability in MS patients (Bjartmar and Trapp, 2003).

There is a growing interest in investigating OPC response in relation to the remyelination process, mainly with the aim to find possible ways to enhance the myelin repair mechanism and to prevent the development of irreversible axonal damage. However, animal models with chronic demyelination are relatively rare. Chronic EAE models have been described but require manipulation of the immune system to induce disease (Swanborg, 1995). Also it is difficult to evaluate the direct effect of therapeutic interventions on OPCs in EAE models, because putative effects could be mediated through a treatment related immuno-modulatory effect and not by direct enhancement of OPC proliferation and differentiation.

This point of view was taken into consideration in a recent study by (Huang et al., 2011) investigating the remyelination enhancing effect of systemically applied retinoic acid, a metabolite of vitamin A. The investigators argued

against the use of the EAE model because of potential modulatory effects of the therapeutic substance on the immune mediated process.

Furthermore any remyelination enhancing therapies investigated in a systemically induced chronic demyelination using a toxin as for example cuprizone (Torkildsen et al., 2008) must also be interpreted with caution, since chronic intoxication may also have not only adverse effects on oligodendrocytes but also on all other cells in the CNS.

Bearing in mind the caveat that OPCs in the #72 mouse harbour a genetic abnormality, data presented in this thesis suggest the chronically demyelinated (as defined earlier) #72 mouse may represent a useful tool for testing myelin enhancing therapies. With respect to this aspiration, this model has a number of strengths. First, demyelination occurs spontaneously, obviating surgical or immunological intervention. Secondly, the background in which the reparative process should take place is less complex than in the EAE model, making the interpretation more straightforward. Thirdly, the stereotypic temporal and spatial progression of demyelination in this model facilitates the assessment of effect.

## **6.2 *In vitro* systems to investigate cell intrinsic pathways**

The integrity of the OPC is an important prerequisite for successful repair and any disturbance to OPC intrinsic properties could result in remyelination failure. Although it has been shown that *Plp1* gene overexpression in oligodendrocytes leads to a sequestration of PLP to endosomes, lysosomes and autophagosomes, which results in an impaired intracellular transport of myelin proteins to the myelin sheath, the effect on OPCs is not understood (Karim et al., 2007; Karim et al., 2010). PLP/DM20 has not been identified in adult OPCs to date, but there is evidence that OPCs transiently express *Dm20* mRNA and DM20 protein during embryonic development and it has been suggested that DM20 plays a role in normal glial development (Dickinson et al., 1996). Interestingly, overexpression of DM20 leads to late onset CNS demyelination with astrocytosis and a lymphocytic infiltration (Mastronardi et al., 1993) similar to the pathology seen

in adult hemizygote #72 mice (Anderson et al., 1998). In the #72 mouse *Dm20* will most likely also be overexpressed. It is not known if adult #72 OPCs express DM20, which could potentially impair adult cell function. Clarification of the role of DM20 may render novel information in the development of *Plp1* gene overexpression mediated adult demyelination pathology.

*In vitro* studies provide an elegant way to address questions regarding cell intrinsic properties, in the absence of confounding extrinsic (environmental) factors. One confounding factor in the cell culture experiment that I performed was contamination by microglia. Although a co-culture system was utilised, where wild type and #72 adult OPCs were exposed to the same environment, microglia might secrete substances such as free radicals to which the #72 OPCs could potentially be more susceptible than the wild type. The magnetic cell sorter technique, as described in (Windrem et al., 2008), could provide a relatively simple solution to avoid unwanted cell contamination. However, adult OPCs are relatively sparse and my initial attempts to use a magnetic cell sorting system failed. For the same reason, FACS sorting of adult, corpus callosum derived OPCs is impractical.

Most of the published work on cultured OPCs used neonatal animals as a source (Dietrich et al., 2006;Huang et al., 2011;Pang et al., 2005;Syed et al., 2008). The OPC yield from neonatal mouse is considerably higher than from the adult. If a higher yield of adult OPCs could be obtained, experiments involving immunoprecipitation, western blot quantification and protein turnover could potentially provide more detailed information about protein-protein interaction and protein integrity during OPC differentiation. Also, after successful purification of sufficient number of OPCs *in vitro*, microarrays (DNA, RNA, protein and cytokine arrays) could be applied to screen for candidate molecules that could explain the OPC differentiation block observed in the #72 mouse.

The results of this study should help inform hypotheses regarding putative OPC intrinsic factors that could influence remyelination failure in the #72 mouse. Candidates identified using microarray could then be *verified* using a cell culture model of myelination such as a myelinating culture (Thomson et al., 2006) or a brain tissue culture system (Zhang et al., 2011). These systems can be

manipulated (i) pharmacologically (ii) using RNA interference and (iii) by transfection, to examine the consequence for myelination and/or remyelination of the up- or down-regulation of specific gene products, providing a relatively inexpensive, high-throughput screen.

Recently the regulatory role of specific microRNA during (re)myelination, miR-219 and miR-338, by suppressing OPC differentiation inhibitors, has shown a further cell intrinsic (re)myelination control mechanism (Zhao et al., 2010). The role of microRNA in *Plp1* gene overexpression has not been elucidated so far and would definitively be warranted to be further explored in the #72 mouse.

More insight into the OPC function may be gained from culture of brain slices (Zhang et al., 2011). The advantage of tissue culture compared to cell culture is the inclusion of the OPC extrinsic compartment including oligodendrocytes, axons, astroglia and microglia. Tissue culture also allows the possibility to evaluate myelination and monitor remyelination after demyelination and may provide the opportunity to test remyelination enhancing substances. I obtained preliminary results from #72 brain slice cultures containing the corpus callosum and the brain stem (data not shown). The development of corpus callosum slices was satisfactory but some unexpected axonal damage appeared after lysolecithin induced demyelination, making the interpretation of (re)myelination difficult. However, complement induced demyelination appeared to be more successful (in collaboration with Dr. Ariel Arthur from the Linington lab, University of Glasgow) and may offer an opportunity to evaluate the remyelination dynamics and capacity on #72 brain slices. A further advantage of tissue culture is the high throughput of relatively large quantities of tissue which can be used for morphometric analysis or for microarray screening before, during and after demyelination.

A major drawback with the culture technique is that so far adult brain slices do not survive in culture for prolonged periods and the method appears only to work when using neonatal tissue. In my case neonatal tissue does not mimic the chronically demyelinated CNS and results obtained in context with the remyelination process in slice culture may not be extrapolated to the adult situation *in vivo*.

## 6.3 Evaluation of OPC extrinsic changes in relation to remyelination failure

### 6.3.1 The role of the microglial/macrophage response in the pathogenesis of remyelination failure in the #72 mouse

The role of the profound microglial/macrophage response in the #72 mouse is also of interest in the development of the demyelination and remyelination failure pathology.

The role of the inflammatory response in myelination and remyelination is in general controversial. There is evidence that acute inflammation is beneficial for the remyelination process (Foote and Blakemore, 2005a). On the other hand, excessive inflammation most likely generates a hostile environment for cells to survive. In the adult and neonate #72 the inflammation appeared not to injure transplanted neuronal stem cells, despite the fact that the inflammatory response probably contributes to the progression of demyelination, as demonstrated in another *Plp1* overexpressing line (Ip et al., 2006; Ip et al., 2007).

The intravenous application of neuronal stem cells may represent an alternative, less invasive way to promote repair (Pluchino et al., 2003). On the other hand even this approach renders difficulties in interpretation since another study has shown an indirect disease modulating effect in EAE without tissue integration of the systemically applied stem cells (Einstein et al., 2006). Just recently the beneficial effect of macrophages in globoid cell leukodystrophy was demonstrated (Kondo et al., 2011) and further experiments aimed directly at reducing the inflammatory response, using for example corticosteroid or minocycline, may also help to determine if the inflammation in the #72 corpus callosum promotes or inhibits (re)myelination.

### 6.3.2 The extracellular matrix - impact on myelin repair and beyond

It is possible that accumulation of hyaluronan contributes to the remyelination failure in the #72 mouse. Further evaluation of the role of hyaluronan in the #72 corpus callosum needs to be addressed by for example quantitative measurement of hyaluronan using western blot techniques and a metabolic and secretory assessment of the astrocytic population, the cell population predominantly responsible for hyaluronan synthesis in the CNS. The effect of hyaluronan on remyelination inhibition could also be evaluated *in vivo* by injecting hyaluronidase into the adult #72 corpus callosum with subsequent evaluation of the (re)myelination response. The entire group of glycosaminoglycans are of interest, especially chondroitin sulphate proteoglycan, which has been shown to interfere with axonal regeneration after trauma (Massey et al., 2006; Garcia-Alias et al., 2009). ABC chondroitinase, which breaks down glycosaminoglycans, enhanced axonal growth leading to improved recovery if applied in combination with task specific rehabilitation exercises (Wang et al., 2011). Since trauma not only causes axonal damage, but also damages the myelin sheath, it may be of interest to evaluate the extent, and the clinical impact, of myelin repair following trauma. Based on the negative influence of hyaluronan on myelin sheath repair, it may also be of interest to investigate if hyaluronan has a negative impact on axonal regeneration after trauma.

### 6.4 Axonal pathology as a consequence of *Plp1* gene overexpression

Data from this study and a previous study by (Edgar et al., 2010) demonstrated a progressive development of axonal swellings in the #72 mouse. In the optic nerve it has been shown that the presence of axonal swellings correlated with the microglial/macrophage response. This also seems to be the case in the corpus callosum, where an increasing microglial/macrophage response was accompanied by the presence of axonal swellings. In the optic nerve, it has been

demonstrated that some of these swellings occur on otherwise intact axons (Edgar et al., 2011).

In the study by (Edgar et al., 2010) there was virtually no axonal pathology present in the chronic demyelinated retinal region of the optic nerve. This is in contrast to MS lesions where a progressive axonal degeneration due to long term demyelination is believed to be the main cause of permanent disability after demyelination. Interestingly activation of microglia has been suggested to mediate axonal pathology in EAE, with the main evidence for this being a reduction in axonal injury in mice treated with minocycline (Howell et al., 2010). Treating the #72 mice with minocycline could render further insight into the development of axonal pathology in relation to microglial activation associated with spontaneous demyelination. However, reducing the inflammatory cell response would most likely also lead to reduced demyelination, which could lead to a decrease in axonal damage. This makes it difficult to dissect the single components possibly involved in axonal pathology.

## **6.5 The use of stem cells in long term myelin repair**

This study demonstrated the proof-of-concept that early intracranial transplantation of multipotent neuronal stem cells potentially can replace the defective endogenous oligodendrocyte population. While I showed that neurospheres survive, integrate, myelinate and form an apparently stable population of oligodendrocytes after transplantation into neonate #72 mouse brains, the procedure did not rescue the phenotype despite the quite remarkable sizes of these patches of remyelination. Also the fate of transplanted cells other than myelin forming oligodendrocytes, which is unknown at present, could provide more insight into the distribution of the transplanted cells and to monitor if the transplanted cells also replace the genetically defective OPC population in the subventricular zone. One possible method to address this would be to transplant neuronal stem cells permanently expressing a fluorescent marker (such as GFP) into neonate mice. The fate of the transplanted cells could be characterised after constructing a #72 chimera, in particular to investigate if the transplanted cells produce a continuous OPC niche in the CNS.

## 6.6 Diffusion weighted imaging in myelin disorders

DW MRI is increasingly being used to evaluate white matter changes *in vivo*, non-invasively (Budde et al., 2009;Harsan et al., 2006;Harsan et al., 2008;Song et al., 2002;Song et al., 2005). The modification of DW MRI by adding multiple increasing *b*-values, as in this study, showed that it enhances the sensitivity to detect demyelination and inflammation. Using multiple increasing *b*-values may therefore improve the diagnostic accuracy of DW MRI for the detection of specific white matter lesions. An experiment using multiple higher *b*-values has recently been performed in shaking pups *in vivo* (Wu et al., 2011). Although the study did not investigate the pathological changes as detailed and not the same diffusion parameters were calculated as I did, Wu et al. showed that from a technical point of view, DW MRI with multiple increasing *b*-values is possible *in vivo*. A further step would involve the performance of similar experiments *in vivo* in order to verify the changes seen in my experiment using fixed tissue and in order to rule out any fixation related influence.

At the moment I have not evaluated the role of axonal changes in DW MRI with multiple increasing high *b*-values in detail. To further analyse the influence of changes in axonal integrity on diffusion, the experiments undertaken in this study could be repeated in wild type and #72 mice, subsequent to optic nerve crush.

## 6.7 The use of demyelinating models in investigating psychiatric disorders

Changes in myelin integrity recently demonstrated in psychiatric disorders such as schizophrenia, point to a potential central role of myelin integrity and distribution in the development of these diseases (reviewed in Davis et al., 2003). Schizophrenia is a severe psychiatric disorder where an impaired connectivity between brain regions is regarded as the main abnormality (reviewed in Davis et al., 2003). Interestingly, in certain demyelinating disorders, such as metachromatic leukodystrophy (MLD) and to a much lesser

extent multiple sclerosis (MS), patients may also develop schizophrenic-like symptoms (reviewed in Davis et al., 2003), emphasising the role of myelin in cognitive (dys)function.

Two month old heterozygote 4e mice (another *Plp1* overexpressing line), where mild demyelination of major white matter tracts in the spinal cord, brainstem and corpus callosum was present, were reported to develop schizophrenic-like behavioural changes (Tanaka et al., 2009). The increased awareness of the myelin related changes in the pathogenesis of schizophrenia, and the need for models involving spontaneous demyelination in order to study these disorders, means that the #72 model may also be useful for studying the influence of spontaneous demyelination on schizophrenic-like symptoms.

## 6.8 Summary

In short, the *Plp1* gene overexpressing #72 mouse, a model of PMD, is useful for future investigation into the development and treatment of chronic demyelination and remyelination failure. Novel stem cell transplantation strategies for white matter diseases that progress into debilitating chronic demyelination can furthermore be evaluated using the #72 model. Additionally the #72 model has raised relevant questions about the influence of *Plp1* gene overexpression on adult OPC function and integrity. Due to the endogenous mediated microglial changes, the model also allows us to investigate the role of microglial activation in demyelination and remyelination pathology and on the effect on axonal integrity. This study has also shown that standard and modified DW MRI with multiple *b*-values may serve as a molecular probe to evaluate myelin pathology and may become an important technique in diagnostic imaging to distinguish lesion type in MS.

## 7 Appendix

### 7.1 Fixatives

#### 7.1.1 Periodate lysine paraformaldehyde

Preparation of ingredients for 1000ml of PLP fixative

Buffered lysine solution:

13.7g lysine monohydrate in 375ml distilled water

1.8g sodium hydrogen phosphate in 100ml distilled water

Mix the two solutions to give 475ml buffer, pH7.4

10% paraformaldehyde:

20g paraformaldehyde in 250ml distilled water

Heat to 65°C

Add a few drops of 1M NaOH until solution clears

Allow to cool under running water

Filter solution

The two solutions can be stored at 4°C separately overnight if necessary.

Immediately before use of PLP fixative, the two solutions were mixed and made up to a final volume of 1 litre using 0.1M phosphate buffer. 2.14g sodium periodate was added and allowed to dissolve. Ready PLP fix cannot be stored overnight.

#### 7.1.2 4% Paraformaldehyde in PBS

For 500ml of fixative

25 g paraformaldehyde made up to 500 ml with PBS

Heat to 65°C

Add a few drops of 5m NaOH until solution clears

Cool solution under running water

Filter solution

Store at 4°C

### 7.1.3 Karnovsky's modified fixative (paraformaldehyde / glutaraldehyde 4% / 5%)

Preparation of ingredients for 500ml of fixative

8% paraformaldehyde

20g paraformaldehyde in 250ml distilled water

Heat to 65°C

Add a few drops of 1M NaOH until solution clears

Cool solution under running water

Filter solution

0.08M cacodylate buffer

17.1224g sodium cacodylate in 1 litre of distilled water

Adjust pH to 7.2

25% glutaraldehyde

For 500ml Karnovsky's modified fixative mix

250ml 8% paraformaldehyde

100ml 25% glutaraldehyde

150ml 0.08M cacodylate buffer

250mg Calcium chloride

Filter the solution, adjust to pH 7.2 and store at 4°C

## 7.2 Tissue Processing

### 7.2.1 Resin processing

Perfusion fixed tissue was passed through the following protocol before embedding in resin:

Vial	Solution	Time	Temp	Comments
1	Na-cacodylate buffer <sup>1</sup>	50 min	4°C	
2	1% Osmium tetroxide (OsO <sub>4</sub> ) in cacodylate buffer	2 hrs.	Room Temperature (RT)	toxic, add vial just shortly before needed, remove after use & pour into corn oil
3	Na-cacodylate buffer	30 min	RT	
4	50% Ethanol	5 min	RT	
5	50% Ethanol	10 min	RT	
6	70% Ethanol	5 min	RT	
7	70% Ethanol	10 min	RT	
8	80% Ethanol	5 min	RT	
9	80% Ethanol	10 min	RT	
10	90% Ethanol	5 min	RT	
11	90% Ethanol	10 min	RT	
12	100% Ethanol	5 min	RT	add vial just shortly before needed, fill to 20ml (evaporation )

Vial	Solution	Time	Temp	Comments
13	100% Ethanol	10 min	RT	add vial just shortly before needed, fill to 20ml (evaporation)
14	Propylene oxide	15 min	RT	add vial just shortly before needed, fill to 20ml (evaporation)
15	Propylene oxide	15 min	RT	add vial just shortly before needed, fill to 20ml (evaporation)
16	1:2 araldite <sup>2</sup> :propylene oxide change to fresh vial same slot 1:1 araldite:propylene oxide	13 hrs. & 6 hrs.	RT	
17	2:1 araldite:propylene oxide	18 hrs.	RT	
18	araldite	4 hrs. 15 min	RT	

After the procedure, processed tissue samples were placed in resin filled silicon moulds and left to polymerise for 24 hours at 60°C.

<sup>1</sup>Isotonic cacodylate buffer

16.05g sodium cacodylate

3.8g sodium chloride

0.055g      calcium chloride

0.102g      magnesium chloride

Dissolve in 1 litre distilled water and adjust pH to 7.2

## <sup>2</sup>Araldite Resin

30g	araldite (CY212)	resin
25.2g	dodecanyl succinic anhydride	hardener
1.2ml	2,4,6-tri-diethylaminomethyl-phenol	accelerator
1.0ml	di-butyl phthalate	plasticiser

## 7.3 Staining protocols

### 7.3.1 Immunohistochemistry using methanol for cell membrane penetration

1	PBS	10 min	RT
2	Methanol -20 °C	10 min	freezer
3	PBS	10 min	RT
4	block with PBS containing 10% normal goat serum	1 hr.	RT
5	remove excess and apply primary antibody in PBS/10% NGS	12 hrs.	fridge
6	PBS x3	3x10 min	RT
7	apply secondary antibody in PBS/10% NGS	1 hr.	RT
8	PBS x3	3x10 min	RT
9	DAPI in PBS (1:1500)	1 min	RT
10	PBS	5 min	RT
11	running water	5 min	RT
12	coverslip with glycine in PBS		RT

### 7.3.2 Immunohistochemistry using Triton-X 100 for cell membrane penetration

1	PBS	10 min	RT
2	block with PBS containing 10% normal goat serum and 0.5% Triton-X 100	1 hr.	RT
3	remove excess and apply primary antibody in PBS/10% NGS 0.5% Triton-X	12 hrs.	Fridge
4	PBS x3	3x10 min	RT
5	apply secondary antibody in PBS/10% NGS and 0.5% Triton-X	1 hr.	RT
6	PBS x3	3x10 min	RT
7	DAPI in PBS (1:1500)	1 min	RT
8	PBS	5 min	RT
9	running water	5 min	RT
10	cover with coverslip containing glycine in PBS		RT

### 7.3.3 X-gal staining

Either freshly perfused and cryoprotected 1mm thick brain samples or 10 and 20µm thick mounted cryosections were post fixed for 10 minutes on ice in 4% paraformaldehyde. The samples were then washed twice for 10 minutes on ice using fresh 2mM MgCl<sub>2</sub>/PBS solution followed by a 10 minute treatment with a

detergent solution containing 1mM MgCl<sub>2</sub> (Sigma), 0.01% sodium desoxycholate (Sigma) 0.02% NP40. The samples were then immersed or covered for three hours at room temperature with the X-gal staining solution containing 20mM K<sub>3</sub>Fe(CN)<sub>6</sub>, 20mM K<sub>4</sub>Fe(CN)<sub>6</sub> 3H<sub>2</sub>O, 2mM MgCl<sub>2</sub>, 0.01% sodium desoxycholate, 0.02% NP40 and X-gal at a final concentration of 1 mg/ml in PBS pH 7.4. Finally the samples were washed three times for 10 minutes in PBS and once in water for five minutes

### 7.3.4 Staining for electron microscopy

1	saturated uranyl acetate in 50% ethanol	15 min	RT
2	50% ethanol	Rinse	RT
3	50% ethanol	Rinse	RT
4	distilled water	Rinse	RT
5	distilled water	Rinse	RT
6	air dry		
7	Reynolds's lead citrate <sup>1</sup> (Sodium hydroxide moistened chamber)	10 min	RT
8	1M sodium hydroxide	Rinse	RT
9	1M sodium hydroxide	Rinse	RT
10	1M sodium hydroxide	Rinse	RT
11	distilled water	several rinses	RT

<sup>1</sup>Reynold's lead citrate (1.2mM lead citrate, 1.8mM sodium citrate, pH12) 1.33g lead citrate dissolved in 15ml distilled water for 1 min. Shake vigorously 1.76g

sodium citrate dissolved in 15ml distilled water for 1 min. Shake vigorously. Combine the solutions and equilibrate over 30 minutes with occasional shaking. Clear with 1M NaOH. Make up a final volume of 50ml adding distilled water.

## **7.4 Staining solutions**

### **7.4.1 Methylene blue / azur II**

1% methylene blue

1% azur II

1% borax

In distilled water. Filter before use.

## **7.5 Media for cell culture**

### **7.5.1 Differentiation media with insulin (50 ml)**

48.85 ml DMEM (Gibco 31885-023) containing 2.5 ml Penicillin/ Streptomycin (Gibco, 15070-022) per 500ml DMEM

0.583 ml 30% glucose (Sigma, G-7021)

0.25ml of 10 $\mu$ M hydrocortisone (Sigma, H-0396)

0.25 ml N1 mix

1 ml insulin (human, recombinant, Sigma I-2767)

50 $\mu$ l biotin (Sigma, B-4501)

### **7.5.2 N1 mix (25ml)**

In PBS with a final concentration of

1 mg/ml transferrin (Sigma, T-2252)

16.11 mg/ml putrescine (Sigma, P-7505)

4 $\mu$ M progesterone (Sigma P-0130)

6 $\mu$ M selenium (Sigma, S-9133)

### 7.5.3 Neurosphere media (50 ml)

250 ml NS medium contains

38 ml sterile distilled water

5 ml 10x DMEM/F12 (GIBCO, 21700-026)

5 ml N1 mix

1 ml 30% Glucose

0.75ml 7.5% NaHCO<sub>3</sub> (Sigma, S-5761)

0.25ml 1M HEPES (Sigma, H-9136)

0.5ml L-Glutamine (Gibco, 25030-081)

0.5ml Penicilline/Streptomycine

0.125ml 4% bovine serum albumin (Sigma, A-3059).

## 8 Abbreviations

APC:	Adenomatous polyposis coli
ATP:	Adenosine Triphosphate
BDNF:	Brain derived neurotrophic factor
bHLH:	Basic helix-loop-helix
BrdU:	5-bromo-2-deoxyuridine
cAMP:	Cyclic adenosine monophosphate
CASPR:	Contactin associated protein
CDK:	Cyclin-dependent kinase
CFP:	Cyan fluorescence protein
CNP:	2'-3'-cyclic nucleotide-3'-phosphodiesterase
CNS:	Central Nervous System
CO <sub>2</sub> :	Carbon dioxide
D2:	Deiodinase 2
DAPI:	4'-6-diamidino-2-phenylindol
DMEM:	Dulbecco's modified Eagle's medium
DNA:	Deoxyribonucleic acid
DNase:	Deoxyribonuclease
DTI:	Diffusion Tensor Imaging
DW MRI:	Diffusion weighted MRI
EAE:	Experimental autoimmune encephalitis
EGF:	Epidermal growth factor
EM:	Electron Microscopy
FGF:	Fibroblast growth factor
FISH:	Fluorescence <i>in situ</i> hybridisation
FITC:	Fluorescein isothiocyanate
GalC:	Galactocerebrosides
GFAP:	Glial fibrillary acidic protein
GFP:	Green fluorescence protein
Golli-MBP:	Gene of oligodendrocyte lineage myelin basic protein
HABP:	Hyaluronan binding protein
HDAC:	Histone deacetylase
HIFBS:	Heat inactivated foetal bovine serum
HMW:	High molecular weight

IGF-1:	Insulin growth factor 1
IGFBP-2:	Insulin-like growth factor binding protein 2
IGFR-1:	Insulin-like growth factor receptor 1
IL6:	Interleukin 6
iNOS:	Inducible nitric oxide synthase
IPL:	Intraperiod line
LINGO1:	Leucine rich repeat and Ig domain containing 1
LMW:	Low molecular weight
MAG:	Myelin associated protein
MBP:	Myelin basic protein
md rat:	Myelin deficient rat
MDL:	Major dense line
MHCII:	Major histocompatibility complex II
microRNA:	Micro ribonucleic acid
MOBP:	Myelin associated oligodendrocytic basic protein
MOG:	Myelin/oligodendrocyte protein
MRI:	Magnetic Resonance Imaging
mRNA:	Messenger ribonucleic acid
MRS:	Magnetic resonance spectroscopy
MS:	Multiple Sclerosis
MTC:	Monocarboxylase transporters
MTI:	Magnetisation transfer imaging
NAA:	N-acetylaspartate
NF155:	Neurofascin 155
NG2:	Neuronal/glial 2
NGS:	Normal goat serum
NO <sub>2</sub> :	Nitrogen dioxide
NRG1:	Neuregulin 1
NRG1-III:	Neuregulin 1 - III
NS:	Neurosphere
NTIS :	Non-thyroidal illness syndrome
O <sub>2</sub> :	Oxygen
OCT:	Optimal cutting temperature compound
Olig1:	Oligodendrocyte transcription factor 1
Olig2:	Oligodendrocyte transcription factor 2

OMpg:	Oligodendrocyte myelin glycoprotein
OPC:	Oligodendrocyte Precursor Cell
OSP:	Oligodendrocyte specific protein
P120:	120 days post-partum
PBS:	Phosphate buffered saline
PDGF:	Platelet derived growth factor
PDGFR $\alpha$ :	Platelet derived growth factor receptor $\alpha$
PLP fixative:	Periodate - lysine - paraformaldehyde
PLP/DM20:	Proteolipidprotein
Plp1 gene:	Proteolipidprotein 1 gene (mouse)
<i>PLP1</i> :	Proteolipidprotein gene 1 (human)
PMD:	Pelizaesus - Merzbacher - Disease
PNS:	Peripheral Nervous System
PSA NCAM:	Polisialylated acid form of neuronal cell adhesion molecule
r.p.m:	Rounds per minute
Rb:	Retinoblastoma
SPG2:	X-linked hereditary spastic paraplegia
T3:	Thriiodothyronine
T4:	Thyroxin
Tcf4:	Transcription factor 4
TGF- $\beta$ :	Transforming growth factor $\beta$
TGFB-1:	Transforming growth factor $\beta$ 1
Thy1:	Thymocyte differentiation antigen 1
TLR-2:	Toll-like receptor 2
TMEV:	Theiler's murine encephalomyelitis virus
TNF $\alpha$ :	Tumour necrosis factor $\alpha$
TRH:	Thyroid releasing hormone
UPR:	Unfolded protein response
UV:	Ultra violet
X-ALD:	X-linked adrenoleukodystrophy

## 9 Reference list

Abbott NJ (2002) Astrocyte-endothelial interactions and blood-brain barrier permeability. *J Anat* 200:629-638.

Agrawal D, Hawk R, Avila RL, Inouye H, Kirschner DA (2009) Internodal myelination during development quantitated using X-ray diffraction. *J Struct Biol* 168:521-526.

Agrawal SM, Yong VW (2007) Immunopathogenesis of multiple sclerosis. *Int Rev Neurobiol* 79:99-126.

Albrecht PJ, Murtie JC, Ness JK, Redwine JM, Enterline JR, Armstrong RC, Levison SW (2003) Astrocytes produce CNTF during the remyelination phase of viral-induced spinal cord demyelination to stimulate FGF-2 production. *Neurobiol Dis* 13:89-101.

Alexander AL, Lee JE, Lazar M, Field AS (2007) Diffusion tensor imaging of the brain. *Neurotherapeutics* 4:316-329.

Al-Saktawi K, McLaughlin M, Klugmann M, Schneider A, Barrie JA, McCulloch MC, Montague P, Kirkham D, Nave KA, Griffiths IR (2003) Genetic background determines phenotypic severity of the Plp rumpshaker mutation. *J Neurosci Res* 72:12-24.

Amos LA, Amos WB (1987) Cytoplasmic transport in axons. *J Cell Sci* 87 ( Pt 1):1-2.

Anderson TJ, Klugmann M, Thomson CE, Schneider A, Readhead C, Nave KA, Griffiths IR (1999) Distinct phenotypes associated with increasing dosage of the PLP gene: implications for CMT1A due to PMP22 gene duplication. *Ann N Y Acad Sci* 883:234-246.

Anderson TJ, Schneider A, Barrie JA, Klugmann M, McCulloch MC, Kirkham D, Kyriakides E, Nave KA, Griffiths IR (1998) Late-onset neurodegeneration in mice with increased dosage of the proteolipid protein gene. *J Comp Neurol* 394:506-519.

Archer DR, Cuddon PA, Lipsitz D, Duncan ID (1997) Myelination of the canine central nervous system by glial cell transplantation: a model for repair of human myelin disease. *Nat Med* 3:54-59.

Arnett HA, Fancy SPJ, Alberta JA, Zhao C, Plant SR, Kaing S, Raine CS, Rowitch DH, Franklin RJM, Stiles CD (2004) bHLH Transcription Factor Olig1 Is Required to Repair Demyelinated Lesions in the CNS. *Science* 306:2111-2115.

Arnett HA, Mason J, Marino M, Suzuki K, Matsushima GK, Ting JP (2001) TNF alpha promotes proliferation of oligodendrocyte progenitors and remyelination. *Nat Neurosci* 4:1116-1122.

Arnett HA, Wang Y, Matsushima GK, Suzuki K, Ting JP (2003) Functional genomic analysis of remyelination reveals importance of inflammation in oligodendrocyte regeneration. *J Neurosci* 23:9824-9832.

Assaf Y, Cohen Y (1998) Non-mono-exponential attenuation of water and N-acetyl aspartate signals due to diffusion in brain tissue. *J Magn Reson* 131:69-85.

Ayers MM, Hazelwood LJ, Catmull DV, Wang D, McKormack Q, Bernard CC, Orian JM (2004) Early glial responses in murine models of multiple sclerosis. *Neurochem Int* 45:409-419.

Baas D, Bourbeau D, Sarlieve LL, Ittel ME, Dussault JH, Puymirat J (1997) Oligodendrocyte maturation and progenitor cell proliferation are independently regulated by thyroid hormone. *Glia* 19:324-332.

Back SA, Tuohy TM, Chen H, Wallingford N, Craig A, Struve J, Luo NL, Banine F, Liu Y, Chang A, Trapp BD, Bebo BF, Jr., Rao MS, Sherman LS (2005) Hyaluronan accumulates in demyelinated lesions and inhibits oligodendrocyte progenitor maturation. *Nat Med* 11:966-972.

Baer AS, Syed YA, Kang SU, Mitteregger D, Vig R, French-Constant C, Franklin RJ, Altmann F, Lubec G, Kotter MR (2009) Myelin-mediated inhibition of oligodendrocyte precursor differentiation can be overcome by pharmacological modulation of Fyn-RhoA and protein kinase C signalling. *Brain* 132:465-481

Barkovich AJ (2000) Concepts of myelin and myelination in neuroradiology. *AJNR Am J Neuroradiol* 21:1099-1109.

- Barres BA, Raff MC (1993) Proliferation of oligodendrocyte precursor cells depends on electrical activity in axons. *Nature* 361:258-260.
- Basser PJ, Mattiello J, LeBihan D (1994) MR diffusion tensor spectroscopy and imaging. *Biophys J* 66:259-267.
- Basser PJ, Mattiello J, LeBihan D (1994) MR diffusion tensor spectroscopy and imaging. *Biophys J* 66:259-267.
- Basser PJ, Oezarlan E (2009) Introduction into Diffusion MR. In: *Diffusion MRI* (Johansen-Berg H, Behrens TEJ, eds), pp 3-11. Academic Press.
- Basser PJ, Pierpaoli C (1996) Microstructural and physiological features of tissues elucidated by quantitative-diffusion-tensor MRI. *J Magn Reson B* 111:209-219.
- Bates JM, St Germain DL, Galton VA (1999) Expression profiles of the three iodothyronine deiodinases, D1, D2, and D3, in the developing rat. *Endocrinology* 140:844-851.
- Beaulieu C (2002) The basis of anisotropic water diffusion in the nervous system - a technical review. *NMR Biomed* 15:435-455.
- Beaulieu C (2009) The biological basis of diffusion anisotropy. In: *Diffusion MRI* (Johansen-Berg H, Behrens TEJ, eds), pp 105-126. Academic Press.
- Beaulieu C, Allen PS (1994) Determinants of anisotropic water diffusion in nerves. *Magn Reson Med* 31:394-400.
- Bhat RV, Axt KJ, Fosnaugh JS, Smith KJ, Johnson KA, Hill DE, Kinzler KW, Baraban JM (1996) Expression of the APC tumor suppressor protein in oligodendroglia. *Glia* 17:169-174.
- Biffi A, Aubourg P, Cartier N (2011) Gene therapy for leukodystrophies. *Hum Mol Genet* 20:R42-R53.
- Bignami A, Eng LF, Dahl D, Uyeda CT (1972) Localization of the glial fibrillary acidic protein in astrocytes by immunofluorescence. *Brain Res* 43:429-435.
- Billings-Gagliardi S, Kirschner DA, Nadon NL, DiBenedetto LM, Karthigasan J, Lane P, Pearsall GB, Wolf MK (1995) Jimpy 4J: a new X-linked mouse mutation producing severe CNS hypomyelination. *Dev Neurosci* 17:300-310.

Bitsch A, Kuhlmann T, Stadelmann C, Lassmann H, Lucchinetti C, Bruck W (2001) A longitudinal MRI study of histopathologically defined hypointense multiple sclerosis lesions. *Ann Neurol* 49:793-796.

Bizzozero OA, Lees MB (1999) Fatty acid composition of myelin proteolipid protein during vertebrate evolution. *Neurochem Res* 24:269-274.

Bjartmar C, Trapp BD (2001) Axonal and neuronal degeneration in multiple sclerosis: mechanisms and functional consequences. *Curr Opin Neurol* 14:271-278.

Bjartmar C, Trapp BD (2003) Axonal degeneration and progressive neurologic disability in multiple sclerosis. *Neurotox Res* 5:157-164.

Bjartmar C, Wujek JR, Trapp BD (2003) Axonal loss in the pathology of MS: consequences for understanding the progressive phase of the disease. *J Neurol Sci* 206:165-171.

Blakemore WF (1974) Remyelination of the superior cerebellar peduncle in old mice following demyelination induced by cuprizone. *J Neurol Sci* 22:121-126.

Blakemore WF (1982) Ethidium bromide induced demyelination in the spinal cord of the cat. *Neuropathol Appl Neurobiol* 8:365-375.

Blakemore WF, Chari DM, Gilson JM, Crang AJ (2002) Modelling large areas of demyelination in the rat reveals the potential and possible limitations of transplanted glial cells for remyelination in the CNS. *Glia* 38:155-168.

Blakemore WF, Gilson JA, Crang AJ (2003) The presence of astrocytes in areas of demyelination influences remyelination following transplantation of oligodendrocyte progenitors. *Experimental Neurology* 184:955-963.

Blaschuk KL, French-Constant C (1998) Developmental neurobiology: notch is tops in the developing brain. *Curr Biol* 8:R334-R337.

Blumenfeld H (2002) *Neuroanatomy through clinical cases*. Sinauer Associates.

Boelen A, Kwakkel J, Alkemade A, Renckens R, Kaptein E, Kuiper G, Wiersinga WM, Visser TJ (2005) Induction of type 3 deiodinase activity in inflammatory cells of mice with chronic local inflammation. *Endocrinology* 146:5128-5134.

Boelen A, Mikita J, Boiziau C, Chassande O, Fliers E, Petry KG (2009) Type 3 deiodinase expression in inflammatory spinal cord lesions in rat experimental autoimmune encephalomyelitis. *Thyroid* 19:1401-1406.

Boison D, Bussow H, D'Urso D, Muller HW, Stoffel W (1995) Adhesive properties of proteolipid protein are responsible for the compaction of CNS myelin sheaths. *J Neurosci* 15:5502-5513.

Boison D, Stoffel W (1989) Myelin-deficient rat: a point mutation in exon III (A----C, Thr75----Pro) of the myelin proteolipid protein causes dysmyelination and oligodendrocyte death. *EMBO J* 8:3295-3302.

Bongarzone ER, Campagnoni CW, Kampf K, Jacobs EC, Handley VW, Schonmann V, Campagnoni AT (1999) Identification of a new exon in the myelin proteolipid protein gene encoding novel protein isoforms that are restricted to the somata of oligodendrocytes and neurons. *J Neurosci* 19:8349-8357.

Bosio A, Binczek E, Haupt WF, Stoffel W (1998) Composition and biophysical properties of myelin lipid define the neurological defects in galactocerebroside- and sulfatide-deficient mice. *J neurochem* 70:308-315.

Brady ST, Witt AS, Kirkpatrick LL, de Waegh SM, Readhead C, Tu PH, Lee VM (1999) Formation of compact myelin is required for maturation of the axonal cytoskeleton. *J Neurosci* 19:7278-7288.

Bridge KE, Berg N, Adalbert R, Babetto E, Dias T, Spillantini MG, Ribchester RR, Coleman MP (2009) Late onset distal axonal swelling in YFP-H transgenic mice. *Neurobiol Aging* 30:309-321.

Brinkmann BG, Agarwal A, Sereda MW, Garratt AN, Muller T, Wende H, Stassart RM, Nawaz S, Humml C, Velanac V, Radyushkin K, Goebbels S, Fischer TM, Franklin RJ, Lai C, Ehrenreich H, Birchmeier C, Schwab MH, Nave KA (2008) Neuregulin-1/ErbB signaling serves distinct functions in myelination of the peripheral and central nervous system. *Neuron* 59:581-595.

Bronstein JM, Micevych PE, Chen K (1997) Oligodendrocyte-specific protein (OSP) is a major component of CNS myelin. *J Neurosci Res* 50:713-720.

Brustle O, Jones KN, Learish RD, Karram K, Choudhary K, Wiestler OD, Duncan ID, McKay RD (1999) Embryonic stem cell-derived glial precursors: a source of myelinating transplants. *Science* 285:754-756.

Budde MD, Kim JH, Liang HF, Russell JH, Cross AH, Song SK (2008) Axonal injury detected by in vivo diffusion tensor imaging correlates with neurological disability in a mouse model of multiple sclerosis. *NMR Biomed* 21:589-597.

Budde MD, Xie M, Cross AH, Song SK (2009) Axial diffusivity is the primary correlate of axonal injury in the experimental autoimmune encephalomyelitis spinal cord: a quantitative pixelwise analysis. *J Neurosci* 29:2805-2813.

Butt AM, Duncan A, Berry M (1994) Astrocyte associations with nodes of Ranvier: ultrastructural analysis of HRP-filled astrocytes in the mouse optic nerve. *J Neurocytol* 23:486-499.

Butt AM, Duncan A, Hornby MF, Kirvell SL, Hunter A, Levine JM, Berry M (1999) Cells expressing the NG2 antigen contact nodes of Ranvier in adult CNS white matter. *Glia* 26:84-91.

Cailloux F, Gauthier-Barichard F, Mimault C, Isabelle V, Courtois V, Giraud G, Dastugue B, Boespflug-Tanguy O (2000) Genotype-phenotype correlation in inherited brain myelination defects due to proteolipid protein gene mutations. *Eur J Hum Genet* 8:837-845.

Camara J, Wang Z, Nunes-Fonseca C, Friedman HC, Grove M, Sherman DL, Komiyama NH, Grant SG, Brophy PJ, Peterson A, ffrench-Constant C (2009) Integrin-mediated axoglial interactions initiate myelination in the central nervous system. *J Cell Biol* 185:699-712.

Cambi F, Kamholz J (1994) Transcriptional regulation of the rat PLP promoter in primary cultures of oligodendrocytes. *Neurochem Res* 19:1055-1060.

Campagnoni AT, Skoff RP (2001) The pathobiology of myelin mutants reveal novel biological functions of the MBP and PLP genes. *Brain Pathol* 11:74-91.

Campagnoni CW, Garbay B, Micevych P, Pribyl T, Kampf K, Handley VW, Campagnoni AT (1992) DM20 mRNA splice product of the myelin proteolipid protein gene is expressed in the murine heart. *J Neurosci Res* 33:148-155.

Caroni P (1997) Overexpression of growth-associated proteins in the neurons of adult transgenic mice. *J Neurosci Methods* 71:3-9.

Caroni P (1997) Overexpression of growth-associated proteins in the neurons of adult transgenic mice. *J Neurosci Methods* 71:3-9.

Carson MJ, Behringer RR, Brinster RL, McMorris FA (1993) Insulin-like growth factor I increases brain growth and central nervous system myelination in transgenic mice. *Neuron* 10:729-740.

Cartier N, et al. (2009) Hematopoietic stem cell gene therapy with a lentiviral vector in X-linked adrenoleukodystrophy. *Science* 326:818-823.

Casaccia-Bonnet P, Liu A (2003) Relationship between cell cycle molecules and onset of oligodendrocyte differentiation. *J Neurosci Res* 72:1-11.

Cerghet M, Bessert DA, Nave KA, Skoff RP (2001) Differential expression of apoptotic markers in jimpy and in Plp overexpressors: evidence for different apoptotic pathways. *J Neurocytol* 30:841-855.

Chalfie M, Tu Y, Euskirchen G, Ward WW, Prasher DC (1994) Green fluorescent protein as a marker for gene expression. *Science* 263:802-805.

Chang A, Tourtellotte WW, Rudick R, Trapp BD (2002) Premyelinating oligodendrocytes in chronic lesions of multiple sclerosis. *N Engl J Med* 346:165-173.

Chari DM, Huang WL, Blakemore WF (2003) Dysfunctional oligodendrocyte progenitor cell (OPC) populations may inhibit repopulation of OPC depleted tissue. *J Neurosci Res* 73:787-793.

Charles P, Hernandez MP, Stankoff B, Aigrot MS, Colin C, Rougon G, Zalc B, Lubetzki C (2000) Negative regulation of central nervous system myelination by polysialylated-neural cell adhesion molecule. *Proc Natl Acad Sci U S A* 97:7585-7590.

Charles P, Reynolds R, Seilhean D, Rougon G, Aigrot MS, Niezgodka A, Zalc B, Lubetzki C (2002) Re-expression of PSA-NCAM by demyelinated axons: an inhibitor of remyelination in multiple sclerosis? *Brain* 125:1972-1979.

- Chow E, Mottahedeh J, Prins M, Ridder W, Nusinowitz S, Bronstein JM (2005) Disrupted compaction of CNS myelin in an OSP/Claudin-11 and PLP/DM20 double knockout mouse. *Mol Cell Neurosci* 29:405-413.
- Ciomas C, Montavont A, Ryvlin P (2008) Magnetic resonance imaging in clinical trials. *Curr Opin Neurol* 21:431-436.
- Clark CA, LeBihan D. (2000) Water diffusion compartmentation and anisotropy at high b values in the human brain. *Magn Reson Med* 44:852-859.
- Coetzee T, Fujita N, Dupree J, Shi R, Blight A, Suzuki K, Suzuki K, Popko B (1996) Myelination in the absence of galactocerebroside and sulfatide: normal structure with abnormal function and regional instability. *Cell* 86:209-219.
- Coffman RL (1982) Surface antigen expression and immunoglobulin gene rearrangement during mouse pre-B cell development. *Immunol Rev* 69:5-23.
- Coffman RL (1982) Surface antigen expression and immunoglobulin gene rearrangement during mouse pre-B cell development. *Immunol Rev* 69:5-23.
- Colman DR, Kreibich G, Frey AB, Sabatini DD (1982) Synthesis and incorporation of myelin polypeptides into CNS myelin. *JCB* 95:598-608.
- Coman I, Barbin G, Charles P, Zalc B, Lubetzki C (2005) Axonal signals in central nervous system myelination, demyelination and remyelination. *J Neurol Sci* 233:67-71.
- Cook JL, Irias-Donaghey S, Deininger PL (1992) Regulation of rodent myelin proteolipid protein gene expression. *Neurosci Lett* 137:56-60.
- Dal Canto MC, Melvold RW, Kim BS, Miller SD (1995) Two models of multiple sclerosis: experimental allergic encephalomyelitis (EAE) and Theiler's murine encephalomyelitis virus (TMEV) infection. A pathological and immunological comparison. *Microsc Res Tech* 32:215-229.
- Davis KL, Stewart DG, Friedman JI, Buchsbaum M, Harvey PD, Hof PR, Buxbaum J, Haroutunian V (2003) White matter changes in schizophrenia: evidence for myelin-related dysfunction. *Arch Gen Psychiatry* 60:443-456.

Dawson MR, Polito A, Levine JM, Reynolds R (2003) NG2-expressing glial progenitor cells: an abundant and widespread population of cycling cells in the adult rat CNS. *Mol Cell Neurosci* 24:476-488.

DeBoy CA, Zhang J, Dike S, Shats I, Jones M, Reich DS, Mori S, Nguyen T, Rothstein B, Miller RH, Griffin JT, Kerr DA, Calabresi PA (2007) High resolution diffusion tensor imaging of axonal damage in focal inflammatory and demyelinating lesions in rat spinal cord. *Brain* 130:2199-2210.

Denault JB, Salvesen GS (2002) Caspases: keys in the ignition of cell death. *Chem Rev* 102:4489-4500.

Denault JB, Salvesen GS (2002) Caspases: keys in the ignition of cell death. *Chem Rev* 102:4489-4500.

Diaz RS, Monreal J, Lucas M (1990) Calcium movements mediated by proteolipid protein and nucleotides in liposomes prepared with the endogenous lipids from brain white matter. *J Neurochem* 55:1304-1309.

Dickinson PJ, Fanarraga ML, Griffiths IR, Barrie JM, Kyriakides E, Montague P (1996) Oligodendrocyte progenitors in the embryonic spinal cord express DM-20. *Neuropathol Appl Neurobiol* 22:188-198.

Diehl HJ, Schaich M, Budzinski RM, Stoffel W (1986) Individual exons encode the integral membrane domains of human myelin proteolipid protein. *Proc Natl Acad Sci U S A* 83:9807-9811.

Dietrich J, Han R, Yang Y, Mayer-Proschel M, Noble M (2006) CNS progenitor cells and oligodendrocytes are targets of chemotherapeutic agents in vitro and in vivo. *J Biol* 5:22.

D'Intino G, Lorenzini L, Fernandez M, Taglioni A, Perretta G, Del VG, Villoslada P, Giardino L, Calza L (2011) T3 administration ameliorates the demyelination/remyelination ratio in a non-human primate model of multiple sclerosis by correcting tissue hypothyroidism. *J Neuroendocrinol*.

Doherty P, Cohen J, Walsh FS (1990) Neurite outgrowth in response to transfected N-CAM changes during development and is modulated by polysialic acid. *Neuron* 5:209-219.

Doran M, Hajnal JV, Van BN, King MD, Young IR, Bydder GM (1990) Normal and abnormal white matter tracts shown by MR imaging using directional diffusion weighted sequences. *J Comput Assist Tomogr* 14:865-873.

Duffner PK, Caviness VS, Jr., Erbe RW, Patterson MC, Schultz KR, Wenger DA, Whitley C (2009) The long-term outcomes of presymptomatic infants transplanted for Krabbe disease: report of the workshop held on July 11 and 12, 2008, Holiday Valley, New York. *Genet Med* 11:450-454.

Duncan ID, Brower A, Kondo Y, Curlee JF, Jr., Schultz RD (2009) Extensive remyelination of the CNS leads to functional recovery. *Proc Natl Acad Sci U S A* 106:6832-6836.

Duncan ID, Hammang JP, Jackson KF, Wood PM, Bunge RP, Langford L (1988) Transplantation of oligodendrocytes and Schwann cells into the spinal cord of the myelin-deficient rat. *J Neurocytol* 17:351-360.

Duncan ID, Hammang JP, Trapp BD (1987) Abnormal compact myelin in the myelin-deficient rat: absence of proteolipid protein correlates with a defect in the intraperiod line. *Proc Natl Acad Sci U S A* 84:6287-6291.

Dutta R, Trapp BD (2011) Mechanisms of neuronal dysfunction and degeneration in multiple sclerosis. *Prog Neurobiol* 93:1-12.

Dyer CA, Benjamins JA (1988) Antibody to galactocerebroside alters organization of oligodendroglial membrane sheets in culture. *J Neurosci* 8:4307-4318.

Dyer CA, Benjamins JA (1990) Glycolipids and transmembrane signaling: antibodies to galactocerebroside cause an influx of calcium in oligodendrocytes. *JCB* 111:625-633.

Ebisu T, Naruse S, Horikawa Y, Ueda S, Tanaka C, Uto M, Umeda M, Higuchi T (1993) Discrimination between different types of white matter edema with diffusion-weighted MR imaging. *J Magn Reson Imaging* 3:863-868.

Edgar JM, Anderson TJ, Dickinson PJ, Barrie JA, McCulloch MC, Nave KA, Griffiths IR (2002) Survival of, and competition between, oligodendrocytes expressing different alleles of the *Plp* gene. *JCB* 158:719-729.

Edgar JM, Garbern J (2004) The myelinated axon is dependent on the myelinating cell for support and maintenance: molecules involved. *J Neurosci Res* 76:593-598.

Edgar JM, Griffiths IR (2009) White Matter Structure: A Microscopist's View. In: *Diffusion MRI* (Johansen-Berg H, Behrens TEJ, eds), pp 75-103. Academic Press.

Edgar JM, McCulloch MC, Montague P, Brown AM, Thilemann S, Pratola L, Gruenenfelder FI, Griffiths IR, Nave KA (2010) Demyelination and axonal preservation in a transgenic mouse model of Pelizaeus-Merzbacher disease. *EMBO Mol Med* 2:42-50.

Edgar JM, McLaughlin M, Barrie JA, McCulloch MC, Garbern J, Griffiths IR (2004a) Age-related axonal and myelin changes in the rumpshaker mutation of the *Plp* gene. *Acta Neuropathol* 107:331-335.

Edgar JM, McLaughlin M, Werner HB, McCulloch MC, Barrie JA, Brown A, Faichney AB, Snaidero N, Nave KA, Griffiths IR (2009) Early ultrastructural defects of axons and axon-glia junctions in mice lacking expression of *Cnp1*. *Glia* 57:1815-1824.

Edgar JM, McLaughlin M, Yool D, Zhang SC, Fowler JH, Montague P, Barrie JA, McCulloch MC, Duncan ID, Garbern J, Nave KA, Griffiths IR (2004b) Oligodendroglial modulation of fast axonal transport in a mouse model of hereditary spastic paraplegia. *Jcb* 166:121-131.

Einstein O, Grigoriadis N, Mizrachi-Kol R, Reinhartz E, Polyzoidou E, Lavon I, Milonas I, Karussis D, Abramsky O, Ben-Hur T (2006) Transplanted neural precursor cells reduce brain inflammation to attenuate chronic experimental autoimmune encephalomyelitis. *Exp Neurol* 198:275-284.

Einstein O, Karussis D, Grigoriadis N, Mizrachi-Kol R, Reinhartz E, Abramsky O, Ben-Hur T (2003) Intraventricular transplantation of neural precursor cell spheres attenuates acute experimental allergic encephalomyelitis. *Mol Cell Neurosci* 24:1074-1082.

Emery B (2010a) Regulation of oligodendrocyte differentiation and myelination. *Science* 330:779-782.

Emery B (2010b) Transcriptional and post-transcriptional control of CNS myelination. *Curr Opin Neurobiol* 20:601-607.

Eng LF, Vanderhaeghen JJ, Bignami A, Gerstl B (1971) An acidic protein isolated from fibrous astrocytes. *Brain Res* 28:351-354.

Fanarraga ML, Griffiths IR, McCulloch MC, Barrie JA, Kennedy PG, Brophy PJ (1992) Rumpshaker: an X-linked mutation causing hypomyelination: developmental differences in myelination and glial cells between the optic nerve and spinal cord. *Glia* 5:161-170.

Fancy SP, Baranzini SE, Zhao C, Yuk DI, Irvine KA, Kaing S, Sanai N, Franklin RJ, Rowitch DH (2009) Dysregulation of the Wnt pathway inhibits timely myelination and remyelination in the mammalian CNS. *Genes Dev* 23:1571-1585.

Fancy SP, Harrington EP, Yuen TJ, Silbereis JC, Zhao C, Baranzini SE, Bruce CC, Otero JJ, Huang EJ, Nusse R, Franklin RJ, Rowitch DH (2011) Axin2 as regulatory and therapeutic target in newborn brain injury and remyelination. *Nat Neurosci*.

Fancy SP, Kotter MR, Harrington EP, Huang JK, Zhao C, Rowitch DH, Franklin RJ (2010) Overcoming remyelination failure in multiple sclerosis and other myelin disorders. *Exp Neurol* 225:18-23.

Fancy SP, Zhao C, Franklin RJ (2004) Increased expression of Nkx2.2 and Olig2 identifies reactive oligodendrocyte progenitor cells responding to demyelination in the adult CNS. *Mol Cell Neurosci* 27:247-254.

Feng GP, Mellor RH, Bernstein M, Keller-Peck C, Nguyen QT, Wallace M, Nerbonne JM, Lichtman JW, Sanes JR (2000) Imaging neuronal subsets in transgenic mice expressing multiple spectral variants of GFP. *Neuron* 28:41-51.

Feng S, Hong Y, Zhou Z, Jinsong Z, Xiaofeng D, Zaizhong W, Yali G, Ying L, Yingjuan C, Yi H (2009) Monitoring of acute axonal injury in the swine spinal cord with EAE by diffusion tensor imaging. *J Magn Reson Imaging* 30:277-285.

Figley CR, Stroman PW (2011) The role(s) of astrocytes and astrocyte activity in neurometabolism, neurovascular coupling, and the production of functional neuroimaging signals. *Eur J Neurosci* 33:577-588.

Filipovic R, Zecevic N (2005) Interaction between microglia and oligodendrocyte cell progenitors involves Golgi proteins. *Ann N Y Acad Sci* 1048:166-174.

Finzsch M, Stolt CC, Lommes P, Wegner M (2008) Sox9 and Sox10 influence survival and migration of oligodendrocyte precursors in the spinal cord by regulating PDGF receptor alpha expression. *Development* 135:637-646.

Flores AI, Narayanan SP, Morse EN, Shick HE, Yin X, Kidd G, Avila RL, Kirschner DA, Macklin WB (2008) Constitutively active Akt induces enhanced myelination in the CNS. *J Neurosci* 28:7174-7183.

Foote AK, Blakemore WF (2005a) Inflammation stimulates remyelination in areas of chronic demyelination. *Brain* 128:528-539.

Foote AK, Blakemore WF (2005b) Repopulation of oligodendrocyte progenitor cell depleted tissue in a model of chronic demyelination. *Neuropathol Appl Neurobiol* 31:105-114.

Fox RJ (2008) Picturing multiple sclerosis: conventional and diffusion tensor imaging. *Semin Neurol* 28:453-466.

Frankenhaeuser B (1952) Saltatory conduction in myelinated nerve fibres. *J Physiol* 118:107-112.

Franklin RJ (2002) Why does remyelination fail in multiple sclerosis? *Nat Rev Neurosci* 3:705-714.

Franklin RJ, Bayley SA, Blakemore WF (1996) Transplanted CG4 cells (an oligodendrocyte progenitor cell line) survive, migrate, and contribute to repair of areas of demyelination in X-irradiated and damaged spinal cord but not in normal spinal cord. *Exp Neurol* 137:263-276.

Franklin RJ, Crang AJ, Blakemore WF (1991) Transplanted type-1 astrocytes facilitate repair of demyelinating lesions by host oligodendrocytes in adult rat spinal cord. *J Neurocytol* 20:420-430.

Franklin RJ, ffrench-Constant C (2008) Remyelination in the CNS: from biology to therapy. *Nat Rev Neurosci* 9:839-855.

Fressinaud C (2005) Repeated injuries dramatically affect cells of the oligodendrocyte lineage: effects of PDGF and NT-3 in vitro. *Glia* 49:555-566.

Friede RL, Samorajski T (1970) Axon caliber related to neurofilaments and microtubules in sciatic nerve fibers of rats and mice. *Anat Rec* 167:379-387.

Frohlich N, Nagy B, Hovhannisyan A, Kukley M (2011) Fate of neuron-glia synapses during proliferation and differentiation of NG2 cells. *J Anat* 219:18-32.

Fruttiger M, Montag D, Schachner M, Martini R (1995) Crucial role for the myelin-associated glycoprotein in the maintenance of axon-myelin integrity. *Eur J Neurosci* 7:511-515.

Fry JM, Weissbarth S, Lehrer GM, Bornstein MB (1974) Cerebroside antibody inhibits sulfatide synthesis and myelination and demyelinate in cord tissue cultures. *Science* 183:540-542.

Fujiwara K (1994) Mouse hepatitis virus. In: *Virus infections of rodents and langomorphs* (Osterhaus ADME, ed), pp 249-257. Amsterdam: Elsevier Science.

Fukuhara Y, Li XK, Kitazawa Y, Inagaki M, Matsuoka K, Kosuga M, Kosaki R, Shimazaki T, Endo H, Umezawa A, Okano H, Takahashi T, Okuyama T (2006) Histopathological and behavioral improvement of murine mucopolysaccharidosis type VII by intracerebral transplantation of neural stem cells. *Mol Ther* 13:548-555.

Fulton D, Paez PM, Campagnoni AT (2010) The multiple roles of myelin protein genes during the development of the oligodendrocyte. *ASN Neuro* 2:e00027.

Galiano MR, Andrieux A, Deloulme JC, Bosc C, Schweitzer A, Job D, Hallak ME (2006) Myelin basic protein functions as a microtubule stabilizing protein in differentiated oligodendrocytes. *J Neurosci Res* 84:534-541.

Galton VA (2005) The roles of the iodothyronine deiodinases in mammalian development. *Thyroid* 15:823-834.

Garbern J, Cambi F, Shy M, Kamholz J (1999) The molecular pathogenesis of Pelizaeus-Merzbacher disease. *Arch Neurol* 56:1210-1214.

Garbern JY (2007) Pelizaeus-Merzbacher disease: Genetic and cellular pathogenesis. *Cell Mol Life Sci* 64:50-65.

Garbern JY, Yool DA, Moore GJ, Wilds IB, Faulk MW, Klugmann M, Nave KA, Siermans EA, van der Knaap MS, Bird TD, Shy ME, Kamholz JA, Griffiths IR

(2002) Patients lacking the major CNS myelin protein, proteolipid protein 1, develop length-dependent axonal degeneration in the absence of demyelination and inflammation. *Brain* 125:551-561.

Garcia-Alias G, Barkhuysen S, Buckle M, Fawcett JW (2009) Chondroitinase ABC treatment opens a window of opportunity for task-specific rehabilitation. *Nat Neurosci* 12:1145-1151.

Gencic S, Abuelo D, Ambler M, Hudson LD (1989) Pelizaeus-Merzbacher disease: an X-linked neurologic disorder of myelin metabolism with a novel mutation in the gene encoding proteolipid protein. *Am J Hum Genet* 45:435-442.

Gencic S, Hudson LD (1990) Conservative amino acid substitution in the myelin proteolipid protein of jimpymsd mice. *J Neurosci* 10:117-124.

Genoud S, Lappe-Siefke C, Goebbels S, Radtke F, Aguet M, Scherer SS, Suter U, Nave KA, Mantei N (2002) Notch1 control of oligodendrocyte differentiation in the spinal cord. *JCB* 158:709-718.

Gieselmann V (2008) Metachromatic leukodystrophy: genetics, pathogenesis and therapeutic options. *Acta Paediatr Suppl* 97:15-21.

Goldberg-Zimring D, Mewes AU, Maddah M, Warfield SK (2005) Diffusion tensor magnetic resonance imaging in multiple sclerosis. *J Neuroimaging* 15:68S-81S.

Goldschmidt T, Antel J, König FB, Brück W, Kuhlmann T (2009) Remyelination capacity of the MS brain decreases with disease chronicity. *Neurology* 72:1914-1921.

Gow A, Friedrich VL, Jr., Lazzarini RA (1994) Intracellular transport and sorting of the oligodendrocyte transmembrane proteolipid protein. *J Neurosci Res* 37:563-573.

Gow A, Southwood CM, Lazzarini RA (1998) Disrupted proteolipid protein trafficking results in oligodendrocyte apoptosis in an animal model of Pelizaeus-Merzbacher disease. *J Cell Biol* 140:925-934.

Gow A, Southwood CM, Li JS, Pariali M, Riordan GP, Brodie SE, Danias J, Bronstein JM, Kachar B, Lazzarini RA (1999) CNS myelin and Sertoli cell tight junction strands are absent in *Osp/claudin-11* null mice. *Cell* 99:649-659.

Grant P, Pant HC (2000) Neurofilament protein synthesis and phosphorylation. *J Neurocytol* 29:843-872.

Grant P, Pant HC (2000) Neurofilament protein synthesis and phosphorylation. *J Neurocytol* 29:843-872.

Gravel M, Peterson J, Yong VW, Kottis V, Trapp B, Braun PE (1996) Overexpression of 2',3'-cyclic nucleotide 3'-phosphodiesterase in transgenic mice alters oligodendrocyte development and produces aberrant myelination. *Mol Cell Neurosci* 7:453-466.

Gravel M, Robert F, Kottis V, Gallouzi IE, Pelletier J, Braun PE (2009) 2',3'-Cyclic nucleotide 3'-phosphodiesterase: a novel RNA-binding protein that inhibits protein synthesis. *J Neurosci Res* 87:1069-1079.

Griffiths I, Klugmann M, Anderson T, Yool D, Thomson C, Schwab MH, Schneider A, Zimmermann F, McCulloch M, Nadon N, Nave KA (1998) Axonal swellings and degeneration in mice lacking the major proteolipid of myelin. *Science* 280:1610-1613.

Griffiths IR, Montague P, Dickinson P (1995a) The proteolipid protein gene. *Neuropathol Appl Neurobiol* 21:85-96.

Griffiths IR, Schneider A, Anderson J, Nave KA (1995b) Transgenic and natural mouse models of proteolipid protein (PLP)-related dysmyelination and demyelination. *Brain Pathol* 5:275-281.

Griffiths IR, Scott I, McCulloch MC, Barrie JA, McPhilemy K, Cattanach BM (1990) Rumpshaker mouse: a new X-linked mutation affecting myelination: evidence for a defect in PLP expression. *J Neurocytol* 19:273-283.

Gruenenfelder FI, Thomson G, Penderis J, Edgar JM (2011) Axon-glia interaction in the CNS: what we have learned from mouse models of Pelizaeus-Merzbacher disease. *J Anat* 219:33-43.

Gulani V, Webb AG, Duncan ID, Lauterbur PC (2001) Apparent diffusion tensor measurements in myelin-deficient rat spinal cords. *Magn Reson Med* 45:191-195.

Guttmann CR, Ahn SS, Hsu L, Kikinis R, Jolesz FA (1995) The evolution of multiple sclerosis lesions on serial MR. *AJNR Am J Neuroradiol* 16:1481-1491.

Hall SM (1972) The effect of injections of lysophosphatidyl choline into white matter of the adult mouse spinal cord. *J Cell Sci* 10:535-546.

Hammang JP, Archer DR, Duncan ID (1997) Myelination following transplantation of EGF-responsive neural stem cells into a myelin-deficient environment. *Exp Neurol* 147:84-95.

Hanisch UK, Kettenmann H (2007) Microglia: active sensor and versatile effector cells in the normal and pathologic brain. *Nat Neurosci* 10:1387-1394.

Harsan LA, Paul D, Schnell S, Kreher BW, Hennig J, Staiger JF, von ED (2010) In vivo diffusion tensor magnetic resonance imaging and fiber tracking of the mouse brain. *NMR Biomed* 23:884-896.

Harsan LA, Poulet P, Guignard B, Parizel N, Skoff RP, Ghandour MS (2007) Astrocytic hypertrophy in dysmyelination influences the diffusion anisotropy of white matter. *J Neurosci Res* 85:935-944.

Harsan LA, Poulet P, Guignard B, Steibel J, Parizel N, de Sousa PL, Boehm N, Grucker D, Ghandour MS (2006) Brain dysmyelination and recovery assessment by noninvasive in vivo diffusion tensor magnetic resonance imaging. *J Neurosci Res* 83:392-402.

Harsan LA, Steibel J, Zaremba A, Agin A, Sapin R, Poulet P, Guignard B, Parizel N, Grucker D, Boehm N, Miller RH, Ghandour MS (2008) Recovery from chronic demyelination by thyroid hormone therapy: myelinogenesis induction and assessment by diffusion tensor magnetic resonance imaging. *J Neurosci* 28:14189-14201.

Heide AC, Richards TL, Alvord EC, Jr., Peterson J, Rose LM (1993) Diffusion imaging of experimental allergic encephalomyelitis. *Magn Reson Med* 29:478-484.

Herwig A, Ross AW, Nilaweera KN, Morgan PJ, Barrett P (2008) Hypothalamic thyroid hormone in energy balance regulation. *Obes Facts* 1:71-79.

Highley JR, Esiri MM, McDonald B, Cortina-Borja M, Herron BM, Crow TJ (1999) The size and fibre composition of the corpus callosum with respect to gender and schizophrenia: a post-mortem study. *Brain* 122 ( Pt 1):99-110.

- Hildebrand C, Hahn R (1978) Relation between myelin sheath thickness and axon size in spinal cord white matter of some vertebrate species. *J Neurol Sci* 38:421-434.
- Hildebrand C, Mohseni S (2005) The structure of myelinated axons in the CNS. In: *Multiple Sclerosis as a Neuronal Disease* (Waxman SG, ed), pp 1-28. San Diego: Elsevier Academic Press.
- Hildebrand C, Remahl S, Persson H, Bjartmar C (1993) Myelinated nerve fibres in the CNS. *Prog Neurobiol* 40:319-384.
- Hildebrand C, Waxman SG (1984) Postnatal differentiation of rat optic nerve fibers: electron microscopic observations on the development of nodes of Ranvier and axoglial relations. *J Comp Neurol* 224:25-37.
- Hodes ME, Blank CA, Pratt VM, Morales J, Napier J, Dlouhy SR (1997) Nonsense mutation in exon 3 of the proteolipid protein gene (PLP) in a family with an unusual form of Pelizaeus-Merzbacher disease. *Am J Med Genet* 69:121-125.
- Hodes ME, DeMyer WE, Pratt VM, Edwards MK, Dlouhy SR (1995) Girl with signs of Pelizaeus-Merzbacher disease heterozygous for a mutation in exon 2 of the proteolipid protein gene. *Am J Med Genet* 55:397-401.
- Horsfield MA (2005) Magnetization transfer imaging in multiple sclerosis. *J Neuroimaging* 15:58S-67S.
- Howell OW, Rundle JL, Garg A, Komada M, Brophy PJ, Reynolds R (2010) Activated microglia mediate axoglial disruption that contributes to axonal injury in multiple sclerosis. *J Neuropathol Exp Neurol* 69:1017-1033.
- Huang JK, Jarjour AA, Nait OB, Kerninon C, Williams A, Krezel W, Kagechika H, Bauer J, Zhao C, Evercooren AB, Chambon P, ffrench-Constant C, Franklin RJ (2011) Retinoid X receptor gamma signaling accelerates CNS remyelination. *Nat Neurosci* 14:45-53.
- Huang SA (2005) Physiology and pathophysiology of type 3 deiodinase in humans. *Thyroid* 15:875-881.

Hudson LD, Garbern JY, Kamholz JA (2004) Pelizaeus-Merzbacher disease. In: Myelin biology and disorders (Lazzarini RA, Griffin JW, Lassmann H, Nave K-A, Miller RH, Trapp BD, eds), pp 867-885. Amsterdam: Elsevier.

Hudson LD, Puckett C, Berndt J, Chan J, Gencic S (1989) Mutation of the proteolipid protein gene PLP in a human X chromosome-linked myelin disorder. *Proc Natl Acad Sci U S A* 86:8128-8131.

Huntington ND, Tarlinton DM (2004) CD45: direct and indirect government of immune regulation. *Immunol Lett* 94:167-174.

Ikawa M, Kominami K, Yoshimura Y, Tanaka K, Nishimune Y, Okabe M (1995) Green fluorescent protein as a marker in transgenic mice. *Development, Growth and Differentiation* 37:455-459.

Ikonen E (2008) Cellular cholesterol trafficking and compartmentalization. *Nat Rev Mol Cell Biol* 9:125-138.

Inglese M, Benedetti B, Filippi M (2005a) The relation between MRI measures of inflammation and neurodegeneration in multiple sclerosis. *J Neurol Sci* 233:15-19.

Inglese M, Grossman RI, Filippi M (2005b) Magnetic resonance imaging monitoring of multiple sclerosis lesion evolution. *J Neuroimaging* 15:225-295.

Inoue K, Osaka H, Imaizumi K, Nezu A, Takanashi J, Arai J, Murayama K, Ono J, Kikawa Y, Mito T, Shaffer LG, Lupski JR (1999) Proteolipid protein gene duplications causing Pelizaeus-Merzbacher disease: molecular mechanism and phenotypic manifestations. *Ann Neurol* 45:624-632.

Inoue K, Osaka H, Sugiyama N, Kawanishi C, Onishi H, Nezu A, Kimura K, Yamada Y, Kosaka K (1996a) A duplicated PLP gene causing Pelizaeus-Merzbacher disease detected by comparative multiplex PCR. *Am J Hum Genet* 59:32-39.

Inoue Y, Kagawa T, Matsumura Y, Ikenaka K, Mikoshiba K (1996b) Cell death of oligodendrocytes or demyelination induced by overexpression of proteolipid protein depending on expressed gene dosage. *Neurosci Res* 25:161-172.

Ip CW, Kroner A, Bendszus M, Leder C, Kobsar I, Fischer S, Wiendl H, Nave KA, Martini R (2006) Immune cells contribute to myelin degeneration and

axonopathic changes in mice overexpressing proteolipid protein in oligodendrocytes. *J Neurosci* 26:8206-8216.

Ip CW, Kroner A, Crocker PR, Nave K-A, Martini R (2007) Sialoadhesin deficiency ameliorates myelin degeneration and axonopathic changes in the CNS of PLP overexpressing mice. *Neurobiology of Disease* 25:105-111.

Ishibashi T, Dakin KA, Stevens B, Lee PR, Kozlov SV, Stewart CL, Fields RD (2006) Astrocytes promote myelination in response to electrical impulses. *Neuron* 49:823-832.

Jahn O, Tenzer S, Werner HB (2009) Myelin proteomics: molecular anatomy of an insulating sheath. *mol neurobiol* 40:55-72.

Johnson AB, Brenner M (2003) Alexander's disease: clinical, pathologic, and genetic features. *J Child Neurol* 18:625-632.

Johnson RS, Roder JC, Riordan JR (1995) Over-expression of the DM-20 myelin proteolipid causes central nervous system demyelination in transgenic mice. *j neurochem* 64:967-976.

Jones DK (2009) Gaussian modeling of the diffusion signal. In: *Diffusion MRI* (Johansen-Berg H, Behrens TEJ, eds), pp 37-54. Academic Press.

Kagawa T, Ikenaka K, Inoue Y, Kuriyama S, Tsujii T, Nakao J, Nakajima K, Aruga J, Okano H, Mikoshiba K (1994) Glial cell degeneration and hypomyelination caused by overexpression of myelin proteolipid protein gene. *Neuron* 13:427-442.

Karim SA, Barrie JA, McCulloch MC, Montague P, Edgar JM, Iden DL, Anderson TJ, Nave KA, Griffiths IR, McLaughlin M (2010) PLP/DM20 expression and turnover in a transgenic mouse model of Pelizaeus-Merzbacher disease. *Glia* 58:1727-1738.

Karim SA, Barrie JA, McCulloch MC, Montague P, Edgar JM, Kirkham D, Anderson TJ, Nave KA, Griffiths IR, McLaughlin M (2007) PLP overexpression perturbs myelin protein composition and myelination in a mouse model of Pelizaeus-Merzbacher disease. *Glia* 55:341-351.

Kassmann CM, Lappe-Siefke C, Baes M, Brugger B, Mildner A, Werner HB, Natt O, Michaelis T, Prinz M, Frahm J, Nave KA (2007) Axonal loss and

neuroinflammation caused by peroxisome-deficient oligodendrocytes. *Nat Genet* 39:969-976.

Keirstead HS, Blakemore WF (1997) Identification of post-mitotic oligodendrocytes incapable of remyelination within the demyelinated adult spinal cord. *J Neuropathol Exp Neurol* 56:1191-1201.

Kessarlis N, Fogarty M, Iannarelli P, Grist M, Wegner M, Richardson WD (2006) Competing waves of oligodendrocytes in the forebrain and postnatal elimination of an embryonic lineage. *Nat Neurosci* 9:173-179.

Kim JH, Budde MD, Liang HF, Klein RS, Russell JH, Cross AH, Song SK (2006) Detecting axon damage in spinal cord from a mouse model of multiple sclerosis. *Neurobiol Dis* 21:626-632.

Kim TH, Zollinger L, Shi XF, Rose J, Jeong EK (2009) Diffusion tensor imaging of ex vivo cervical spinal cord specimens: the immediate and long-term effects of fixation on diffusivity. *Anat Rec (Hoboken)* 292:234-241.

Kitada M, Rowitch DH (2006) Transcription factor co-expression patterns indicate heterogeneity of oligodendroglial subpopulations in adult spinal cord. *Glia* 54:35-46.

Klawiter EC, Schmidt RE, Trinkaus K, Liang HF, Budde MD, Naismith RT, Song SK, Cross AH, Benzinger TL (2011) Radial diffusivity predicts demyelination in ex vivo multiple sclerosis spinal cords. *Neuroimage* 55:1454-1460.

Klugmann M, Schwab MH, Puhlhofer A, Schneider A, Zimmermann F, Griffiths IR, Nave KA (1997) Assembly of CNS myelin in the absence of proteolipid protein. *Neuron* 18:59-70.

Koeppen AH, Robitaille Y (2002) Pelizaeus-Merzbacher disease. *J Neuropathol Exp Neurol* 61:747-759.

Kohler W (2010) Leukodystrophies with late disease onset: an update. *Curr Opin Neurol* 23:234-241.

Kollias G, Spanopoulou E, Grosveld F, Ritter M, Beech J, Morris R (1987) Differential regulation of a Thy-1 gene in transgenic mice. *Proc Natl Acad Sci U S A* 84:1492-1496.

Kondo Y, Adams JM, Vanier MT, Duncan ID (2011) Macrophages counteract demyelination in a mouse model of globoid cell leukodystrophy. *J Neurosci* 31:3610-3624.

Kondo Y, Duncan ID (2009) Transplantation of oligodendrocyte progenitor cells in animal models of leukodystrophies. *Methods Mol Biol* 549:175-185.

Kornek B, Storch MK, Weissert R, Wallstroem E, Stefferl A, Olsson T, Linington C, Schmidbauer M, Lassmann H (2000) Multiple sclerosis and chronic autoimmune encephalomyelitis: a comparative quantitative study of axonal injury in active, inactive, and remyelinated lesions. *Am J Pathol* 157:267-276.

Korniyuchuk E, Dempster JM, O'Connor E, Alexander JS, Kelley RE, Kenner M, Menon U, Misra V, Hoque R, Gonzalez-Toledo E, Schwendimann RN, Smith S, Minagar A (2007) Evolving therapies for multiple sclerosis. *Int Rev Neurobiol* 79:571-588.

Kosaras B, Kirschner DA (1990) Radial component of CNS myelin: junctional subunit structure and supramolecular assembly. *J Neurocytol* 19:187-199.

Kotter MR, Li WW, Zhao C, Franklin RJ (2006) Myelin impairs CNS remyelination by inhibiting oligodendrocyte precursor cell differentiation. *J Neurosci* 26:328-332.

Kotter MR, Setzu A, Sim FJ, Van RN, Franklin RJ (2001) Macrophage depletion impairs oligodendrocyte remyelination following lysolecithin-induced demyelination. *Glia* 35:204-212.

Kotter MR, Zhao C, Van RN, Franklin RJ (2005) Macrophage-depletion induced impairment of experimental CNS remyelination is associated with a reduced oligodendrocyte progenitor cell response and altered growth factor expression. *Neurobiol Dis* 18:166-175.

Kubista M, Akerman B, Norden B (1987) Characterization of interaction between DNA and 4',6-diamidino-2-phenylindole by optical spectroscopy. *Biochemistry* 26:4545-4553.

Kuhlmann T, Miron V, Cui Q, Wegner C, Antel J, Bruck W (2008) Differentiation block of oligodendroglial progenitor cells as a cause for remyelination failure in chronic multiple sclerosis. *Brain* 131:1749-1758.

Kuspert M, Hammer A, Bosl MR, Wegner M (2011) Olig2 regulates Sox10 expression in oligodendrocyte precursors through an evolutionary conserved distal enhancer. *Nucleic Acids Res* 39:1280-1293.

Lappe-Siefke C, Goebbels S, Gravel M, Nicksch E, Lee J, Braun PE, Griffiths IR, Nave K-A (2003) Disruption of the *CNP* gene uncouples oligodendroglial functions in axonal support and myelination. *Nat Genet* 33:366-374.

Larsson HB, Thomsen C, Frederiksen J, Stubgaard M, Henriksen O (1992) In vivo magnetic resonance diffusion measurement in the brain of patients with multiple sclerosis. *Magn Reson Imaging* 10:7-12.

Laule C, Vavasour IM, Kolind SH, Li DK, Traboulsee TL, Moore GR, Mackay AL (2007) Magnetic resonance imaging of myelin. *Neurotherapeutics* 4:460-484.

Laursen LS, Chan CW, French-Constant C (2009) An integrin-contactin complex regulates CNS myelination by differential Fyn phosphorylation. *J Neurosci* 29:9174-9185.

Learish RD, Brustle O, Zhang SC, Duncan ID (1999) Intraventricular transplantation of oligodendrocyte progenitors into a fetal myelin mutant results in widespread formation of myelin. *Ann Neurol* 46:716-722.

LeBihan D., Turner R, Douek P (1993) Is water diffusion restricted in human brain white matter? An echo-planar NMR imaging study. *Neuroreport* 4:887-890.

Lee MK, Cleveland DW (1994) Neurofilament function and dysfunction: involvement in axonal growth and neuronal disease. *Curr Opin Cell Biol* 6:34-40.

Lee MK, Cleveland DW (1994) Neurofilament function and dysfunction: involvement in axonal growth and neuronal disease. *Curr Opin Cell Biol* 6:34-40.

Levine JM, Reynolds R, Fawcett JW (2001) The oligodendrocyte precursor cell in health and disease. *trends neurosci* 24:39-47.

Levine SM, Wong D, Macklin WB (1990) Developmental expression of proteolipid protein and DM20 mRNAs and proteins in the rat brain. *Dev Neurosci* 12:235-250.

Lipton HL, Rozhon EJ, Bandyopadhyay P (1994) Picorna Infections. (Osterhaus ADME, ed), pp 373-385. Amsterdam: Elsevier Science BV.

- Liu X, Yao DL, Bondy CA, Brenner M, Hudson LD, Zhou J, Webster HD (1994) Astrocytes express insulin-like growth factor-I (IGF-I) and its binding protein, IGFBP-2, during demyelination induced by experimental autoimmune encephalomyelitis. *Mol Cell Neurosci* 5:418-430.
- Looney GA, Elberger AJ (1986) Myelination of the corpus callosum in the cat: time course, topography, and functional implications. *J Comp Neurol* 248:336-347.
- Lu QR, Sun T, Zhu Z, Ma N, Garcia M, Stiles CD, Rowitch DH (2002) Common developmental requirement for Olig function indicates a motor neuron/oligodendrocyte connection. *Cell* 109:75-86.
- Lublin F (2005) History of modern multiple sclerosis therapy. *J Neurol* 252 Suppl 3:iii3-iii9.
- Ma J, Matsumoto M, Tanaka KF, Takebayashi H, Ikenaka K (2006) An animal model for late onset chronic demyelination disease caused by failed terminal differentiation of oligodendrocytes. *Neuron Glia Biol* 2:81-91.
- MacFadyen J, Savage K, Wienke D, Isacke CM (2007) Endosialin is expressed on stromal fibroblasts and CNS pericytes in mouse embryos and is downregulated during development. *Gene Expr Patterns* 7:363-369.
- Macklin WB, Campagnoni CW, Deininger PL, Gardinier MV (1987) Structure and expression of the mouse myelin proteolipid protein gene. *J Neurosci Res* 18:383-394.
- Maire CL, Buchet D, Kerninon C, Deboux C, Baron-Van EA, Nait-Oumesmar B (2009) Directing human neural stem/precursor cells into oligodendrocytes by overexpression of Olig2 transcription factor. *J Neurosci Res* 87:3438-3446.
- Maire CL, Wegener A, Kerninon C, Nait OB (2010) Gain-of-function of Olig transcription factors enhances oligodendrogenesis and myelination. *Stem Cells* 28:1611-1622.
- Marcus J, Dupree JL, Popko B (2002) Myelin-associated glycoprotein and myelin galactolipids stabilize developing axo-glial interactions. *JCB* 156:567-577.

- Marta CB, Paez P, Lopez M, Pellegrino d, I, Soto EF, Pasquini JM (2003) Morphological changes of myelin sheaths in rats intracranially injected with apotransferrin. *Neurochem Res* 28:101-110.
- Massaro AR (2002) The role of NCAM in remyelination. *Neurol Sci* 22:429-435.
- Massaro AR, Sbriccoli A, Tonali P (2002) Reactive astrocytes within the acute plaques of multiple sclerosis are PSA-NCAM positive. *Neurol Sci* 23:255-256.
- Massey JM, Hubscher CH, Wagoner MR, Decker JA, Amps J, Silver J, Onifer SM (2006) Chondroitinase ABC digestion of the perineuronal net promotes functional collateral sprouting in the cuneate nucleus after cervical spinal cord injury. *J Neurosci* 26:4406-4414.
- Mastronardi FG, Ackerley CA, Arsenault L, Roots BI, Moscarello MA (1993) Demyelination in a transgenic mouse: a model for multiple sclerosis. *J Neurosci Res* 36:315-324.
- Matsumoto H, Kumon Y, Watanabe H, Ohnishi T, Shudou M, Chuai M, Imai Y, Takahashi H, Tanaka J (2008) Accumulation of macrophage-like cells expressing NG2 proteoglycan and Iba1 in ischemic core of rat brain after transient middle cerebral artery occlusion. *J Cereb Blood Flow Metab* 28:149-163.
- Mattei MG, Alliel PM, Dautigny A, Passage E, Pham-Dinh D, Mattei JF, Jolles P (1986) The gene encoding for the major brain proteolipid (PLP) maps on the q-22 band of the human X chromosome. *Hum Genet* 72:352-353.
- McKerracher L, David S, Jackson DL, Kottis V, Dunn RJ, Braun PE (1994) Identification of myelin-associated glycoprotein as a major myelin-derived inhibitor of neurite growth. *Neuron* 13:805-811.
- McLaughlin M, Karim SA, Montague P, Barrie JA, Kirkham D, Griffiths IR, Edgar JM (2007) Genetic background influences UPR but not PLP processing in the rumpshaker model of PMD/SPG2. *Neurochem Res* 32:167-176.
- McLean IW, Nakane PK (1974) Periodate-lysine-paraformaldehyde fixative. A new fixation for immunoelectron microscopy. *J Histochem Cytochem* 22:1077-1083.

Meijering E, Jacob M, Sarria JC, Steiner P, Hirling H, Unser M (2004) Design and validation of a tool for neurite tracing and analysis in fluorescence microscopy images. *Cytometry A* 58:167-176.

Merson TD, Binder MD, Kilpatrick TJ (2010) Role of cytokines as mediators and regulators of microglial activity in inflammatory demyelination of the CNS. *Neuromolecular Med* 12:99-132.

Mi S, Lee X, Hu Y, Ji B, Shao Z, Yang W, Huang G, Walus L, Rhodes K, Gong BJ, Miller RH, Pepinsky RB (2011) Death receptor 6 negatively regulates oligodendrocyte survival, maturation and myelination. *Nat Med* 17:816-821.

Mi S, Miller RH, Lee X, Scott ML, Shulag-Morskaya S, Shao Z, Chang J, Thill G, Levesque M, Zhang M, Hession C, Sah D, Trapp B, He Z, Jung V, McCoy JM, Pepinsky RB (2005) LINGO-1 negatively regulates myelination by oligodendrocytes. *Nat Neurosci* 8:745-751.

Michailov GV, Sereda MW, Brinkmann BG, Fischer TM, Haug B, Birchmeier C, Role L, Lai C, Schwab MH, Nave KA (2004) Axonal neuregulin-1 regulates myelin sheath thickness. *Science* 304:700-703.

Miller BA, Crum JM, Tovar CA, Ferguson AR, Bresnahan JC, Beattie MS (2007) Developmental stage of oligodendrocytes determines their response to activated microglia in vitro. *J Neuroinflammation* 4:28.

Miller RH (2002) Regulation of oligodendrocyte development in the vertebrate CNS. *Prog Neurobiol* 67:451-467.

Milward EA, Lundberg CG, Ge B, Lipsitz D, Zhao M, Duncan ID (1997) Isolation and transplantation of multipotential populations of epidermal growth factor-responsive, neural progenitor cells from the canine brain. *J Neurosci Res* 50:862-871.

Mimault C, Giraud G, Courtois V, Cailloux F, Boire JY, Dastugue B, Boespflug-Tanguy O (1999) Proteolipoprotein gene analysis in 82 patients with sporadic Pelizaeus-Merzbacher Disease: duplications, the major cause of the disease, originate more frequently in male germ cells, but point mutations do not. The Clinical European Network on Brain Demyelinating Disease. *Am J Hum Genet* 65:360-369.

Mintorovitch J, Moseley ME, Chileuitt L, Shimizu H, Cohen Y, Weinstein PR (1991) Comparison of diffusion- and T2-weighted MRI for the early detection of cerebral ischemia and reperfusion in rats. *Magn Reson Med* 18:39-50.

Miron VE, Kuhlmann T, Antel JP (2011) Cells of the oligodendroglial lineage, myelination, and remyelination. *Biochim Biophys Acta* 1812:184-193.

Mobius W, Patzig J, Nave KA, Werner HB (2008) Phylogeny of proteolipid proteins: divergence, constraints, and the evolution of novel functions in myelination and neuroprotection. *Neuron Glia Biol* 4:111-127.

Mokry J, Karbanova J, Filip S (2005) Differentiation potential of murine neural stem cells in vitro and after transplantation. *Transplant Proc* 37:268-272.

Moore CS, Abdullah SL, Brown A, Arulpragasam A, Crocker SJ (2011a) How factors secreted from astrocytes impact myelin repair. *J Neurosci Res* 89:13-21.

Moore CS, Milner R, Nishiyama A, Frausto RF, Serwanski DR, Pagarigan RR, Whitton JL, Miller RH, Crocker SJ (2011b) Astrocytic tissue inhibitor of metalloproteinase-1 (TIMP-1) promotes oligodendrocyte differentiation and enhances CNS myelination. *J Neurosci* 31:6247-6254.

Morell P, Jurevics H (1996) Origin of cholesterol in myelin. *Neurochem Res* 21:463-470.

Mori S, Zhang J (2006) Principles of diffusion tensor imaging and its applications to basic neuroscience research. *Neuron* 51:527-539.

Moseley ME, Cohen Y, Kucharczyk J, Mintorovitch J, Asgari HS, Wendland MF, Tsuruda J, Norman D (1990a) Diffusion-weighted MR imaging of anisotropic water diffusion in cat central nervous system. *Radiology* 176:439-445.

Moseley ME, Cohen Y, Mintorovitch J, Chileuitt L, Shimizu H, Kucharczyk J, Wendland MF, Weinstein PR (1990b) Early detection of regional cerebral ischemia in cats: comparison of diffusion- and T2-weighted MRI and spectroscopy. *Magn Reson Med* 14:330-346.

Moser HW, Raymond GV, Dubey P (2005) Adrenoleukodystrophy: new approaches to a neurodegenerative disease. *JAMA* 294:3131-3134.

Mothe AJ, Tator CH (2008) Transplanted neural stem/progenitor cells generate myelinating oligodendrocytes and Schwann cells in spinal cord demyelination and dysmyelination. *Exp Neurol* 213:176-190.

Mulkern RV, Zengingonul HP, Robertson RL, Bogner P, Zou KH, Gudbjartsson H, Guttman CR, Holtzman D, Kyriakos W, Jolesz FA, Maier SE (2000) Multi-component apparent diffusion coefficients in human brain: relationship to spin-lattice relaxation. *Magn Reson Med* 44:292-300.

Nadon NL, Arnheiter H, Hudson LD (1994) A combination of PLP and DM20 transgenes promotes partial myelination in the jimpy mouse. *J Neurochem* 63:822-833.

Nadon NL, Duncan ID (1995) Gene expression and oligodendrocyte development in the myelin deficient rat. *J Neurosci Res* 41:96-104.

Nadon NL, Duncan ID (1996) Molecular analysis of glial cell development in the canine 'shaking pup' mutant. *Dev Neurosci* 18:174-184.

Nadon NL, Duncan ID, Hudson LD (1990) A point mutation in the proteolipid protein gene of the 'shaking pup' interrupts oligodendrocyte development. *Development* 110:529-537.

Nagy JI, Li X, Rempel J, Stelmack G, Patel D, Staines WA, Yasumura T, Rash JE (2001) Connexin26 in adult rodent central nervous system: demonstration at astrocytic gap junctions and colocalization with connexin30 and connexin43. *J Comp Neurol* 441:302-323.

Nair G, Tanahashi Y, Low HP, Billings-Gagliardi S, Schwartz WJ, Duong TQ (2005) Myelination and long diffusion times alter diffusion-tensor-imaging contrast in myelin-deficient shiverer mice. *Neuroimage* 28:165-174.

Nakahara J, Kanekura K, Nawa M, Aiso S, Suzuki N (2009) Abnormal expression of TIP30 and arrested nucleocytoplasmic transport within oligodendrocyte precursor cells in multiple sclerosis. *J Clin Invest* 119:169-181.

Nash B, Ioannidou K, Barnett SC (2011) Astrocyte phenotypes and their relationship to myelination. *J Anat* 219:44-52.

Nave KA (2010a) Myelination and support of axonal integrity by glia. *Nature* 468:244-252.

Nave KA (2010b) Myelination and the trophic support of long axons. *Nat Rev Neurosci* 11:275-283.

Nave KA, Bloom FE, Milner RJ (1987a) A single nucleotide difference in the gene for myelin proteolipid protein defines the jimpy mutation in mouse. *J Neurochem* 49:1873-1877.

Nave KA, Lai C, Bloom FE, Milner RJ (1987b) Splice site selection in the proteolipid protein (PLP) gene transcript and primary structure of the DM-20 protein of central nervous system myelin. *Proc Natl Acad Sci U S A* 84:5665-5669.

Neumann H, Kotter MR, Franklin RJ (2009) Debris clearance by microglia: an essential link between degeneration and regeneration. *Brain* 132:288-295.

Nicchia GP, Nico B, Camassa LM, Mola MG, Loh N, Dermietzel R, Spray DC, Svelto M, Frigeri A (2004) The role of aquaporin-4 in the blood-brain barrier development and integrity: studies in animal and cell culture models. *Neuroscience* 129:935-945.

Niendorf T, Dijkhuizen RM, Norris DG, van Lookeren CM, Nicolay K (1996) Biexponential diffusion attenuation in various states of brain tissue: implications for diffusion-weighted imaging. *Magn Reson Med* 36:847-857.

Nishiyama A, Komitova M, Suzuki R, Zhu X (2009) Polydendrocytes (NG2 cells): multifunctional cells with lineage plasticity. *Nat Rev Neurosci* 10:9-22.

Nistor GI, Totoiu MO, Haque N, Carpenter MK, Keirstead HS (2005) Human embryonic stem cells differentiate into oligodendrocytes in high purity and myelinate after spinal cord transplantation. *Glia* 49:385-396.

Norris DG (2001) The effects of microscopic tissue parameters on the diffusion weighted magnetic resonance imaging experiment. *NMR Biomed* 14:77-93.

Norton WT (1984) Recent advances in myelin biochemistry. *Ann N Y Acad Sci* 436:5-10.

Norton WT, Aquino DA, Hozumi I, Chiu FC, Brosnan CF (1992) Quantitative aspects of reactive gliosis: a review. *Neurochem Res* 17:877-885.

- Norton WT, Cammer W (1984) Isolation and characterization of myelin. In: Myelin (Morell P, ed), pp 147-195. Plenum Press, New York and London.
- Noseworthy JH, Lucchinetti C, Rodriguez M, Weinshenker BG (2000) Multiple sclerosis. *N Engl J Med* 343:938-952.
- O'Connor LT, Goetz BD, Kwiecien JM, Delaney KH, Fletch AL, Duncan ID (1999) Insertion of a retrotransposon in Mbp disrupts mRNA splicing and myelination in a new mutant rat. *J Neurosci* 19:3404-3413.
- Okabe M, Ikawa M, Kominami K, Nakanishi T, Nishimune Y (1997) 'Green mice' as a source of ubiquitous green cells. *FEBS Lett* 407:313-319.
- Olivares R, Montiel J, Aboitiz F (2001) Species differences and similarities in the fine structure of the mammalian corpus callosum. *Brain Behav Evol* 57:98-105.
- Ono J, Harada K, Takahashi M, Maeda M, Ikenaka K, Sakurai K, Sakai N, Kagawa T, Fritz-Zieroth B, Nagai T, . (1995) Differentiation between dysmyelination and demyelination using magnetic resonance diffusional anisotropy. *Brain Res* 671:141-148.
- Othman A, Frim DM, Polak P, Vujcic S, Arnason BG, Boullerne AI (2011) Olig1 is expressed in human oligodendrocytes during maturation and regeneration. *Glia* 59:914-926.
- Ozaki HS, Wahlsten D (1998) Timing and origin of the first cortical axons to project through the corpus callosum and the subsequent emergence of callosal projection cells in mouse. *J Comp Neurol* 400:197-206.
- Pang Y, Cai Z, Rhodes PG (2005) Effect of tumor necrosis factor-alpha on developing optic nerve oligodendrocytes in culture. *J Neurosci Res* 80:226-234.
- Papanicolaou DA (2000) Euthyroid Sick Syndrome and the role of cytokines. *Rev Endocr Metab Disord* 1:43-48.
- Patani R, Balaratnam M, Vora A, Reynolds R (2007) Remyelination can be extensive in multiple sclerosis despite a long disease course. *Neuropathol Appl Neurobiol* 33:277-287.

Patrikios P, Stadelmann C, Kutzelnigg A, Rauschka H, Schmidbauer M, Laursen H, Sorensen PS, Bruck W, Lucchinetti C, Lassmann H (2006) Remyelination is extensive in a subset of multiple sclerosis patients. *Brain* 129:3165-3172.

Paxinos G, Franklin KBJ (2001) *Mouse Brain in Stereotaxic Coordinates*. Elsevier.

Pearsall GB, Nadon NL, Wolf MK, Billings-Gagliardi S (1997) Jimpy-4J mouse has a missense mutation in exon 2 of the Plp gene. *Dev Neurosci* 19:337-341.

Penderis J, Shields SA, Franklin RJ (2003) Impaired remyelination and depletion of oligodendrocyte progenitors does not occur following repeated episodes of focal demyelination in the rat central nervous system. *Brain* 126:1382-1391.

Perry VH, Crocker PR, Gordon S (1992) The blood-brain barrier regulates the expression of a macrophage sialic acid-binding receptor on microglia. *J Cell Sci* 101 ( Pt 1):201-207.

Peru RL, Mandrycky N, Nait-Oumesmar B, Lu QR (2008) Paving the axonal highway: from stem cells to myelin repair. *Stem Cell Rev* 4:304-318.

Petzold A (2005) Neurofilament phosphoforms: surrogate markers for axonal injury, degeneration and loss. *J Neurol Sci* 233:183-198.

Pfeiffer SE, Warrington AE, Bansal R (1993) The oligodendrocyte and its many cellular processes. *Trends Cell Biol* 3:191-197.

Pfeuffer J, Provencher SW, Gruetter R (1999) Water diffusion in rat brain in vivo as detected at very large b values is multicompartmental. *MAGMA* 8:98-108.

Piaton G, Gould RM, Lubetzki C (2010) Axon-oligodendrocyte interactions during developmental myelination, demyelination and repair. *J Neurochem* 114:1243-1260.

Pluchino S, Quattrini A, Brambilla E, Gritti A, Salani G, Dina G, Galli R, Del CU, Amadio S, Bergami A, Furlan R, Comi G, Vescovi AL, Martino G (2003) Injection of adult neurospheres induces recovery in a chronic model of multiple sclerosis. *Nature* 422:688-694.

Pohl HB, Porcheri C, Mueggler T, Bachmann LC, Martino G, Riethmacher D, Franklin RJ, Rudin M, Suter U (2011) Genetically induced adult oligodendrocyte

cell death is associated with poor myelin clearance, reduced remyelination, and axonal damage. *J Neurosci* 31:1069-1080.

Popovic N, Schubart A, Goetz BD, Zhang SC, Linington C, Duncan ID (2002) Inhibition of autoimmune encephalomyelitis by a tetracycline. *Ann Neurol* 51:215-223.

Pringle NP, Mudhar HS, Collarini EJ, Richardson WD (1992) PDGF receptors in the rat CNS: during late neurogenesis, PDGF alpha-receptor expression appears to be restricted to glial cells of the oligodendrocyte lineage. *Development* 115:535-551.

Puckett C, Hudson L, Ono K, Friedrich V, Benecke J, Dubois-Dalcq M, Lazzarini RA (1987) Myelin-specific proteolipid protein is expressed in myelinating Schwann cells but is not incorporated into myelin sheaths. *J Neurosci Res* 18:511-518.

Raskind WH, Williams CA, Hudson LD, Bird TD (1991) Complete deletion of the proteolipid protein gene (PLP) in a family with X-linked Pelizaeus-Merzbacher disease. *Am J Hum Genet* 49:1355-1360.

Readhead C, Hood L (1990) The dysmyelinating mouse mutations shiverer (shi) and myelin deficient (shimld). *Behav Genet* 20:213-234.

Readhead C, Schneider A, Griffiths I, Nave KA (1994) Premature arrest of myelin formation in transgenic mice with increased proteolipid protein gene dosage. *Neuron* 12:583-595.

Ridge JP, Fuchs EJ, Matzinger P (1996) Neonatal tolerance revisited: turning on newborn T cells with dendritic cells. *Science* 271:1723-1726.

Ronen I, Moeller S, Ugurbil K, Kim DS (2006) Investigation of multicomponent diffusion in cat brain using a combined MTC-DWI approach. *Magn Reson Imaging* 24:425-431.

Rosenbluth J (2009) Multiple functions of the paranodal junction of myelinated nerve fibers. *J Neurosci Res* 87:3250-3258.

Rosenbluth J, Liu Z, Guo D, Schiff R (1994) Inhibition of CNS myelin development in vivo by implantation of anti-GalC hybridoma cells. *J Neurocytol* 23:699-707.

Ruest T, Holmes WM, Barrie JA, Griffiths IR, Anderson TJ, Dewar D, Edgar JM (2011) High-resolution diffusion tensor imaging of fixed brain in a mouse model of Pelizaeus-Merzbacher disease: comparison with quantitative measures of white matter pathology, (in press).

Rusakov DA, Zheng K, Henneberger C (2011) Astrocytes as Regulators of Synaptic Function: A Quest for the Ca<sup>2+</sup> Master Key. *Neuroscientist*.

Rushton WA (1951) A theory of the effects of fibre size in medullated nerve. *J Physiol* 115:101-122.

Saher G, Brugger B, Lappe-Siefke C, Mobius W, Tozawa R, Wehr MC, Wieland F, Ishibashi S, Nave KA (2005) High cholesterol level is essential for myelin membrane growth. *Nat Neurosci* 8:468-475.

Saher G, Quintes S, Nave KA (2011) Cholesterol: a novel regulatory role in myelin formation. *Neuroscientist* 17:79-93.

Salzer JL (2003) Polarized domains of myelinated axons. *Neuron* 40:297-318.

Sarret C, Combes P, Micheau P, Gelot A, Boespflug-Tanguy O, Vaurs-Barriere C (2010) Novel neuronal proteolipid protein isoforms encoded by the human myelin proteolipid protein 1 gene. *Neuroscience* 166:522-538.

Schiffmann R, Boespflug-Tanguy O (2001) An update on the leukodystrophies. *Curr Opin Neurol* 14:789-794.

Schiffmann R, van der Knaap MS (2004) The latest on leukodystrophies. *Curr Opin Neurol* 17:187-192.

Schirmer L, Antel JP, Bruck W, Stadelmann C (2010) Axonal Loss and Neurofilament Phosphorylation Changes Accompany Lesion Development and Clinical Progression in Multiple Sclerosis. *Brain Pathol*.

Schmahmann JD, Smith EE, Eichler FS, Filley CM (2008) Cerebral white matter: neuroanatomy, clinical neurology, and neurobehavioral correlates. *Ann N Y Acad Sci* 1142:266-309.

Schnaar RL, Lopez PH (2009) Myelin-associated glycoprotein and its axonal receptors. *J Neurosci Res* 87:3267-3276.

Schneider A, Montague P, Griffiths I, Fanarraga M, Kennedy P, Brophy P, Nave KA (1992) Uncoupling of hypomyelination and glial cell death by a mutation in the proteolipid protein gene. *Nature* 358:758-761.

Schnitzer J, Schachner M (1982) Cell type specificity of a neural cell surface antigen recognized by the monoclonal antibody A2B5. *Cell Tissue Res* 224:625-636.

Scholz J, Klein MC, Behrens TE, Johansen-Berg H (2009) Training induces changes in white-matter architecture. *Nat Neurosci* 12:1370-1371.

Schwarcz A, Bogner P, Meric P, Correze JL, Berente Z, Pal J, Gallyas F, Doczi T, Gillet B, Beloeil JC (2004) The existence of biexponential signal decay in magnetic resonance diffusion-weighted imaging appears to be independent of compartmentalization. *Magn Reson Med* 51:278-285.

Seitelberger F (1995) Neuropathology and genetics of Pelizaeus-Merzbacher disease. *Brain Pathol* 5:267-273.

Selmaj K, Raine CS (1988) Tumor necrosis factor mediates myelin damage in organotypic cultures of nervous tissue. *Ann N Y Acad Sci* 540:568-570.

Setzu A, ffrench-Constant C, Franklin RJM (2004) CNS axons retain their competence for myelination throughout life. *Glia* 45:307-311.

Setzu A, Lathia JD, Zhao C, Wells K, Rao MS, ffrench-Constant C, Franklin RJ (2006) Inflammation stimulates myelination by transplanted oligodendrocyte precursor cells. *Glia* 54:297-303.

Shen S, Casaccia-Bonnel P (2008) Post-translational modifications of nucleosomal histones in oligodendrocyte lineage cells in development and disease. *J Mol Neurosci* 35:13-22.

Shen S, Liu A, Li J, Wolubah C, Casaccia-Bonnel P (2008) Epigenetic memory loss in aging oligodendrocytes in the corpus callosum. *Neurobiol Aging* 29:452-463.

Shen S, Sandoval J, Swiss VA, Li J, Dupree J, Franklin RJ, Casaccia-Bonnel P (2008) Age-dependent epigenetic control of differentiation inhibitors is critical for remyelination efficiency. *Nat Neurosci* 11:1024-1034.

Shepherd TM, Thelwall PE, Stanisz GJ, Blackband SJ (2009) Aldehyde fixative solutions alter the water relaxation and diffusion properties of nervous tissue. *Magn Reson Med* 62:26-34.

Sim FJ, Zhao C, Penderis J, Franklin RJ (2002) The age-related decrease in CNS remyelination efficiency is attributable to an impairment of both oligodendrocyte progenitor recruitment and differentiation. *J Neurosci* 22:2451-2459.

Simons K, Ikonen E (1997) Functional rafts in cell membranes. *Nature* 387:569-572.

Simons M, Kramer EM, Macchi P, Rathke-Hartlieb S, Trotter J, Nave KA, Schulz JB (2002) Overexpression of the myelin proteolipid protein leads to accumulation of cholesterol and proteolipid protein in endosomes/lysosomes: implications for Pelizaeus-Merzbacher disease. *Jcb* 157:327-336.

Simons M, Kramer EM, Thiele C, Stoffel W, Trotter J (2000) Assembly of myelin by association of proteolipid protein with cholesterol- and galactosylceramide-rich membrane domains. *Jcb* 151:143-154.

Sistermans EA, de Coo RF, De Wijs IJ, Van Oost BA (1998) Duplication of the proteolipid protein gene is the major cause of Pelizaeus-Merzbacher disease. *Neurology* 50:1749-1754.

Skoff RP (1976) Myelin deficit in the Jimpy mouse may be due to cellular abnormalities in astroglia. *Nature* 264:560-562.

Skoff RP (1995) Programmed cell death in the dysmyelinating mutants. *Brain Pathol* 5:283-288.

Sloane JA, Batt C, Ma Y, Harris ZM, Trapp B, Vartanian T (2010) Hyaluronan blocks oligodendrocyte progenitor maturation and remyelination through TLR2. *Proc Natl Acad Sci U S A* 107:11555-11560.

Sofroniew MV, Vinters HV (2010) Astrocytes: biology and pathology. *Acta Neuropathol* 119:7-35.

- Sommer I, Schachner M (1981) Monoclonal antibodies (O1 to O4) to oligodendrocyte cell surfaces: an immunocytological study in the central nervous system. *Dev Biol* 83:311-327.
- Song SK, Sun SW, Ramsbottom MJ, Chang C, Russell J, Cross AH (2002) Demyelination revealed through MRI as increased radial (but unchanged axial) diffusion of water. *Neuroimage* 17:1429-1436.
- Song SK, Yoshino J, Le TQ, Lin SJ, Sun SW, Cross AH, Armstrong RC (2005) Demyelination increases radial diffusivity in corpus callosum of mouse brain. *Neuroimage* 26:132-140.
- Sorg BA, Smith MM, Campagnoni AT (1987) Developmental expression of the myelin proteolipid protein and basic protein mRNAs in normal and dysmyelinating mutant mice. *J Neurochem* 49:1146-1154.
- Southwood CM, Garbern J, Jiang W, Gow A (2002) The unfolded protein response modulates disease severity in Pelizaeus-Merzbacher disease. *Neuron* 36:585-596.
- Spassky N, Goujet-Zalc C, Parmantier E, Olivier C, Martinez S, Ivanova A, Ikenaka K, Macklin W, Cerruti I, Zalc B, Thomas JL (1998) Multiple restricted origin of oligodendrocytes. *J Neurosci* 18:8331-8343.
- Stanisz GJ, Szafer A, Wright GA, Henkelman RM (1997) An analytical model of restricted diffusion in bovine optic nerve. *Magn Reson Med* 37:103-111.
- Stejskal EO, Tanner JE (1965) Spin diffusion measurement: spin echoes in the presence of a time-dependent field gradient. *The Journal of Chemical Physics* 42:288-292.
- Stidworthy MF, Genoud S, Li WW, Leone DP, Mantei N, Suter U, Franklin RJ (2004) Notch1 and Jagged1 are expressed after CNS demyelination, but are not a major rate-determining factor during remyelination. *Brain* 127:1928-1941.
- Stolt CC, Rehberg S, Ader M, Lommès P, Riethmacher D, Schachner M, Bartsch U, Wegner M (2002) Terminal differentiation of myelin-forming oligodendrocytes depends on the transcription factor Sox10. *Genes Dev* 16:165-170.
- Sturrock RR (1980) Myelination of the mouse corpus callosum. *Neuropathol Appl Neurobiol* 6:415-420.

Su Z, Yuan Y, Chen J, Zhu Y, Qiu Y, Zhu F, Huang A, He C (2011) Reactive Astrocytes Inhibit the Survival and Differentiation of Oligodendrocyte Precursor Cells by Secreted TNF-alpha. *J Neurotrauma*.

Sun SW, Neil JJ, Song SK (2003) Relative indices of water diffusion anisotropy are equivalent in live and formalin-fixed mouse brains. *Magn Reson Med* 50:743-748.

Swanborg RH (1995) Experimental autoimmune encephalomyelitis in rodents as a model for human demyelinating disease. *Clin Immunol Immunopathol* 77:4-13.

Syed YA, Baer AS, Lubec G, Hoeger H, Widhalm G, Kotter MR (2008) Inhibition of oligodendrocyte precursor cell differentiation by myelin-associated proteins. *Neurosurg Focus* 24:E5.

Syed YA, Hand E, Mobius W, Zhao C, Hofer M, Nave KA, Kotter MR (2011) Inhibition of CNS remyelination by the presence of semaphorin 3A. *J Neurosci* 31:3719-3728.

Tanaka H, Ma J, Tanaka KF, Takao K, Komada M, Tanda K, Suzuki A, Ishibashi T, Baba H, Isa T, Shigemoto R, Ono K, Miyakawa T, Ikenaka K (2009) Mice with altered myelin proteolipid protein gene expression display cognitive deficits accompanied by abnormal neuron-glia interactions and decreased conduction velocities. *J Neurosci* 29:8363-8371.

Tatar CL, Appikatla S, Bessert DA, Paintlia AS, Singh I, Skoff RP (2010) Increased Plp1 gene expression leads to massive microglial cell activation and inflammation throughout the brain. *ASN Neuro* 2.

Taveggia C, Feltri ML, Wrabetz L (2010) Signals to promote myelin formation and repair. *Nat Rev Neurol* 6:276-287.

Taveggia C, Thaker P, Petrylak A, Caporaso GL, Toews A, Falls DL, Einheber S, Salzer JL (2008) Type III neuregulin-1 promotes oligodendrocyte myelination. *Glia* 56:284-293.

Thomson CE, Hunter AM, Griffiths IR, Edgar JM, McCulloch MC (2006) Murine spinal cord explants: a model for evaluating axonal growth and myelination in vitro. *J Neurosci Res* 84:1703-1715.

Thomson CE, Montague P, Jung M, Nave KA, Griffiths IR (1997) Phenotypic severity of murine Plp mutants reflects in vivo and in vitro variations in transport of PLP isoproteins. *Glia* 20:322-332.

Torkildsen O, Brunborg LA, Myhr KM, Bo L (2008) The cuprizone model for demyelination. *Acta Neurol Scand Suppl* 188:72-76.

Tosic M, Dolivo M, Domanska-Janik K, Matthieu JM (1994) Paralytic tremor (pt): a new allele of the proteolipid protein gene in rabbits. *J Neurochem* 63:2210-2216.

Trapp BD, Nave KA (2008) Multiple sclerosis: an immune or neurodegenerative disorder? *Annu Rev Neurosci* 31:247-269.

Trapp BD, Peterson J, Ransohoff RM, Rudick R, Mork S, Bo L (1998) Axonal transection in the lesions of multiple sclerosis. *N Engl J Med* 338:278-285.

Trofatter JA, Dlouhy SR, DeMyer W, Conneally PM, Hodes ME (1989) Pelizaeus-Merzbacher disease: tight linkage to proteolipid protein gene exon variant. *Proc Natl Acad Sci U S A* 86:9427-9430.

Truett GE, Heeger P, Mynatt RL, Truett AA, Walker JA, Warman ML (2000) Preparation of PCR-quality mouse genomic DNA with hot sodium hydroxide and tris (HotSHOT). *BioTechniques* 29:52, 54.

Tsoukas CD, Landgraf B, Bentin J, Lamberti JF, Carson DA, Vaughan JH (1987) Structural and functional characteristics of the CD3 (T3) molecular complex on human thymocytes. *J Immunol* 138:3885-3890.

Tu TW, Kim JH, Wang J, Song SK (2010) Full tensor diffusion imaging is not required to assess the white-matter integrity in mouse contusion spinal cord injury. *J Neurotrauma* 27:253-262.

Turner R, Le BD, Maier J, Vavrek R, Hedges LK, Pekar J (1990) Echo-planar imaging of intravoxel incoherent motion. *Radiology* 177:407-414.

Ullian EM, Sapperstein SK, Christopherson KS, Barres BA (2001) Control of synapse number by glia. *Science* 291:657-661.

Vaurs-Barriere C, Deville M, Sarret C, Giraud G, Des P, V, Prats-Vinas JM, De MG, Dan B, Brady AF, Boespflug-Tanguy O, Touraine R (2009) Pelizaeus-Merzbacher-

Like disease presentation of MCT8 mutated male subjects. *Ann Neurol* 65:114-118.

Vela JM, Dalmau I, Gonzalez B, Castellano B (1996) The microglial reaction in spinal cords of jimpy mice is related to apoptotic oligodendrocytes. *Brain Res* 712:134-142.

Verity AN, Campagnoni AT (1988) Regional expression of myelin protein genes in the developing mouse brain: in situ hybridization studies. *J Neurosci Res* 21:238-248.

Vidal M, Morris R, Grosveld F, Spanopoulou E (1990) Tissue-specific control elements of the Thy-1 gene. *EMBO J* 9:833-840.

Vidal M, Morris R, Grosveld F, Spanopoulou E (1990) Tissue-specific control elements of the Thy-1 gene. *EMBO J* 9:833-840.

Visser WE, Friesema EC, Visser TJ (2011) Minireview: thyroid hormone transporters: the knowns and the unknowns. *Mol Endocrinol* 25:1-14.

Voskuhl RR (1998) Myelin protein expression in lymphoid tissues: implications for peripheral tolerance. *Immunol Rev* 164:81-92.

Walter L, Neumann H (2009) Role of microglia in neuronal degeneration and regeneration. *Semin Immunopathol* 31:513-525.

Wang C, Pralong WF, Schulz MF, Rougon G, Aubry JM, Pagliusi S, Robert A, Kiss JZ (1996) Functional N-methyl-D-aspartate receptors in O-2A glial precursor cells: a critical role in regulating polysialic acid-neural cell adhesion molecule expression and cell migration. *JCB* 135:1565-1581.

Wang D, Ichiyama RM, Zhao R, Andrews MR, Fawcett JW (2011) Chondroitinase combined with rehabilitation promotes recovery of forelimb function in rats with chronic spinal cord injury. *J Neurosci* 31:9332-9344.

Wang S, Sdrulla AD, diSibio G, Bush G, Nofziger D, Hicks C, Weinmaster G, Barres BA (1998) Notch receptor activation inhibits oligodendrocyte differentiation. *Neuron* 21:63-75.

Warach S, Gaa J, Siewert B, Wielopolski P, Edelman RR (1995) Acute human stroke studied by whole brain echo planar diffusion-weighted magnetic resonance imaging. *Ann Neurol* 37:231-241.

Warrington AE, Barbarese E, Pfeiffer SE (1993) Differential myelinogenic capacity of specific developmental stages of the oligodendrocyte lineage upon transplantation into hypomyelinating hosts. *J Neurosci Res* 34:1-13.

Webber DJ, van BM, Chandran S (2009) Neuroprotective effect of oligodendrocyte precursor cell transplantation in a long-term model of periventricular leukomalacia. *Am J Pathol* 175:2332-2342.

Werner HB, Kuhlmann K, Shen S, Uecker M, Schardt A, Dimova K, Orfaniotou F, Dhaunchak A, Brinkmann BG, Mobius W, Guarente L, Casaccia-Bonnel P, Jahn O, Nave KA (2007) Proteolipid protein is required for transport of sirtuin 2 into CNS myelin. *J Neurosci* 27:7717-7730.

Westbrook C, Kaut Roth C, Talbot J (2005) *MRI in Practice*. Blackwell Publishing.

Wight PA, Duchala CS, Readhead C, Macklin WB (1993) A myelin proteolipid protein-LacZ fusion protein is developmentally regulated and targeted to the myelin membrane in transgenic mice. *JCB* 123:443-454.

Williams A, Piaton G, Aigrot MS, Belhadi A, Theaudin M, Petermann F, Thomas JL, Zalc B, Lubetzki C (2007a) Semaphorin 3A and 3F: key players in myelin repair in multiple sclerosis? *Brain* 130:2554-2565.

Williams A, Piaton G, Lubetzki C (2007b) Astrocytes--friends or foes in multiple sclerosis? *Glia* 55:1300-1312.

Windrem MS, Nunes MC, Rashbaum WK, Schwartz TH, Goodman RA, McKhann G, Roy NS, Goldman SA (2004) Fetal and adult human oligodendrocyte progenitor cell isolates myelinate the congenitally dysmyelinated brain. *Nat Med* 10:93-97.

Windrem MS, Schanz SJ, Guo M, Tian GF, Washco V, Stanwood N, Rasband M, Roy NS, Nedergaard M, Havton LA, Wang S, Goldman SA (2008) Neonatal chimerization with human glial progenitor cells can both remyelinate and rescue the otherwise lethally hypomyelinated shiverer mouse. *Cell Stem Cell* 2:553-565.

- Wolswijk G (1998) Chronic stage multiple sclerosis lesions contain a relatively quiescent population of oligodendrocyte precursor cells. *J Neurosci* 18:601-609.
- Woodruff RH, Franklin RJ (1999) Demyelination and remyelination of the caudal cerebellar peduncle of adult rats following stereotaxic injections of lysolecithin, ethidium bromide, and complement/anti-galactocerebroside: a comparative study. *Glia* 25:216-228.
- Woodward K, Kendall E, Vetrie D, Malcolm S (1998) Pelizaeus-Merzbacher disease: identification of Xq22 proteolipid-protein duplications and characterization of breakpoints by interphase FISH. *Am J Hum Genet* 63:207-217.
- Woodward KJ (2008) The molecular and cellular defects underlying Pelizaeus-Merzbacher disease. *Expert Rev Mol Med* 10:e14.
- Wu YC, Field AS, Duncan ID, Samsonov AA, Kondo Y, Tudorascu D, Alexander AL (2011) High b-value and diffusion tensor imaging in a canine model of dysmyelination and brain maturation. *Neuroimage*.
- Xie M, Tobin JE, Budde MD, Chen CI, Trinkaus K, Cross AH, McDaniel DP, Song SK, Armstrong RC (2010) Rostrocaudal analysis of corpus callosum demyelination and axon damage across disease stages refines diffusion tensor imaging correlations with pathological features. *J Neuropathol Exp Neurol* 69:704-716.
- Xin M, Yue T, Ma Z, Wu FF, Gow A, Lu QR (2005) Myelinogenesis and axonal recognition by oligodendrocytes in brain are uncoupled in Olig1-null mice. *J Neurosci* 25:1354-1365.
- Yamada M, Ivanova A, Yamaguchi Y, Lees MB, Ikenaka K (1999) Proteolipid protein gene product can be secreted and exhibit biological activity during early development. *J Neurosci* 19:2143-2151.
- Yandava BD, Billingham LL, Snyder EY (1999) "Global" cell replacement is feasible via neural stem cell transplantation: evidence from the dysmyelinated shiverer mouse brain. *Proc Natl Acad Sci U S A* 96:7029-7034.
- Ye F, Chen Y, Hoang T, Montgomery RL, Zhao XH, Bu H, Hu T, Taketo MM, van Es JH, Clevers H, Hsieh J, Bassel-Duby R, Olson EN, Lu QR (2009) HDAC1 and HDAC2 regulate oligodendrocyte differentiation by disrupting the beta-catenin-TCF interaction. *Nat Neurosci* 12:829-838.

Yool DA (2000) Phenotypic analysis of the *Plp*-deficient mouse. pp 1-223. University of Glasgow, UK.

Yool DA, Edgar JM, Montague P, Malcolm S (2000) The proteolipid protein gene and myelin disorders in man and animal models. *Hum Mol Genet* 9:987-992.

Yu WP, Collarini EJ, Pringle NP, Richardson WD (1994) Embryonic expression of myelin genes: evidence for a focal source of oligodendrocyte precursors in the ventricular zone of the neural tube. *Neuron* 12:1353-1362.

Zalc B, Fields RD (2000) Do Action Potentials Regulate Myelination? *Neuroscientist* 6:5-13.

Zarei M, Johansen-Berg H, Smith S, Ciccarelli O, Thompson AJ, Matthews PM (2006) Functional anatomy of interhemispheric cortical connections in the human brain. *J Anat* 209:311-320.

Zawadzka M, Rivers LE, Fancy SP, Zhao C, Tripathi R, Jamen F, Young K, Goncharevich A, Pohl H, Rizzi M, Rowitch DH, Kessaris N, Suter U, Richardson WD, Franklin RJ (2010) CNS-resident glial progenitor/stem cells produce Schwann cells as well as oligodendrocytes during repair of CNS demyelination. *Cell Stem Cell* 6:578-590.

Zhang H, Jarjour AA, Boyd A, Williams A (2011) Central nervous system remyelination in culture - A tool for multiple sclerosis research. *Exp Neurol* 230:138-148.

Zhang SC, Duncan ID (2000) Remyelination and restoration of axonal function by glial cell transplantation. *Prog Brain Res* 127:515-533.

Zhang SC, Goetz BD, Duncan ID (2003) Suppression of activated microglia promotes survival and function of transplanted oligodendroglial progenitors. *Glia* 41:191-198.

Zhang SC, Lundberg C, Lipsitz D, O'Connor LT, Duncan ID (1998) Generation of oligodendroglial progenitors from neural stem cells. *J Neurocytol* 27:475-489.

Zhao X, He X, Han X, Yu Y, Ye F, Chen Y, Hoang T, Xu X, Mi QS, Xin M, Wang F, Appel B, Lu QR (2010) MicroRNA-mediated control of oligodendrocyte differentiation. *Neuron* 65:612-626.

Zhu X, Bergles DE, Nishiyama A (2008a) NG2 cells generate both oligodendrocytes and gray matter astrocytes. *Development* 135:145-157.

Zhu X, Hill RA, Nishiyama A (2008b) NG2 cells generate oligodendrocytes and gray matter astrocytes in the spinal cord. *Neuron Glia Biol* 4:19-26.

Ziskin JL, Nishiyama A, Rubio M, Fukaya M, Bergles DE (2007) Vesicular release of glutamate from unmyelinated axons in white matter. *Nat Neurosci* 10:321-330.

Zivadinov R, Cox JL (2007) Neuroimaging in multiple sclerosis. *Int Rev Neurobiol* 79:449-474.